In Vivo FLIM-FRET Imaging of Pharmacodynamics and Disease Progression in Mouse Cancer Models

Max Nobis (B.Sc, M.Sc)

Thesis submitted to the University of Glasgow for the degree of Doctor of Philosophy

September 2015

Beatson Institute for Cancer Research

College of Medical, Veterinary and Life Science (MVLS)

Abstract

Förster resonance energy transfer (FRET) imaging with a combination of multiphoton and fluorescence lifetime measurements (FLIM) analysis allows for accurate, spatially resolved and live monitoring of protein activity in cells. Here, I used this approach to look at the spatial and temporal monitoring of drug efficacy and clearance *in vitro* and *in vivo.*

First, the utility of a Src biosensor in the context of KPC ($Kras^{G12D}$ and $p53^{R172H}$) driven pancreatic cancer cells was used to monitor pharmacodynamics of Src inhibition by dasatinib treatment. This revealed spatial regulation of Src activity in 3D organotypic invasion assays and in the primary tumour. There, Src activity was differentially regulated at the invasive border and in relation to the local vasculature. Temporal treatment monitoring was further explored as well as the application of optical imaging windows. This demonstrated the utility of FLIM-FRET imaging in the tracking of drug treatment responses as well as innate protein signaling *in vivo*.

Using transgenic FRET reporter mice for the small GTPases Rac-1 and RhoA further allowed for the tracking of the pharmacodynamics of Rac-1 and RhoA inhibition *in vitro* and *in vivo* in polyoma middle T antigen (PyMT) mammary carcinoma model and the KPC model of pancreatic cancer in mice. Moreover, the activity of both GTPases was examined in the ErbB2-driven mammary tumour model, as well as during the different cancer progression stages of all three tumour models.

Rac-1 activity was finally shown to be linked to mTRAIL expression in KPC cells *in vitro* and *in vivo* by FLIM-FRET imaging. The Rac-1 GEF P-Rex1 was also shown to be a key driver in regulating Rac-1 activity in the PyMT, ErbB2 and KPC model as determined by the use of the P-Rex1 KO mouse.

Publications arising from this work

Susanto O, Muinonen-Martin A.J, **Nobis M**, Insall RH
Visualizing cancer cell chemotaxis and invasion in 2D
Chemotaxis: Methods and Protocols (*in press*)

von Karstedt S, Conti A, **Nobis M**, Montinaro A, Hartwig T, Lemke J, Legler K, Annewanter F, Campbell AD, Taraborrelli L, Grosse-Wilde A, Coy JF, El-Bahrawy MA, Bergmann F, Koschny R, Werner J, Ganten TM, Schweiger T, Hoetzenecker K, Kenessey I, Hegedüs B, Bergmann M, Hauser C, Egberts JH, Becker T, Röcken C, Kalthoff H, Trauzold A, Anderson KI, Sansom OJ, Walczak H. **Cancer cell-autonomous TRAIL-R signaling promotes KRAS-driven cancer progression, invasion, and metastasis.**
Cancer Cell. 2015 Apr 13;27(4):561-73

Nobis M, McGhee EJ, Herrmann D, Magenau A, Morton JP, Anderson KI, Timpson P. **Monitoring the dynamics of Src activity in response to anti-invasive dasatinib treatment at a subcellular level using dual intravital imaging.**
Cell Adhesion & Migration. 2014 Jul ;8(5):478-86

Johnsson AK*, Dai Y*, **Nobis M**, Baker MJ, McGhee EJ, Walker S, Schwarz JP, Kadir S, Morton JP, Myant KB, Huels DJ, Segonds-Pichon A, Sansom OJ, Anderson KI, Timpson P, Welch HC. **The Rac-FRET mouse reveals tight spatiotemporal control of Rac activity in primary cells and tissues.**
Cell Reports. 2014 Mar 27;6(6):1153-64

Nobis M, Carragher NO, McGhee EJ, Morton JP, Sansom OJ, Anderson KI, Timpson P. **Advanced intravital subcellular imaging reveals vital three-dimensional signalling events driving cancer cell behaviour and drug responses in live tissue.**
FEBS Journal. 2013 Nov;280(21):5177-97

Nobis M, McGhee EJ, Morton JP, Schwarz JP, Karim SA, Quinn J, Edward M, Campbell AD, McGarry LC, Evans TR, Brunton VG, Frame MC, Carragher NO, Wang Y, Sansom OJ, Timpson P, Anderson KI. **Intravital FLIM-FRET imaging reveals dasatinib-induced spatial control of src in pancreatic cancer.**
Cancer Research. 2013 Aug 1;73(15):4674-86

Timpson P, McGhee EJ, Erami Z, **Nobis M**, Quinn JA, Edward M, Anderson KI. **Organotypic collagen I assay: a malleable platform to assess cell behaviour in a 3-dimensional context.**
Journal of Visual Experiments. 2011 Oct 13;(56):e3089

* denotes equal contribution of authors

Table of Contents

List of Figures

List of Tables

List of accompanying material

Nobis M, McGhee EJ, Morton JP, Schwarz JP, Karim SA, Quinn J, Edward M, Campbell AD, McGarry LC, Evans TR, Brunton VG, Frame MC, Carragher NO, Wang Y, Sansom OJ, Timpson P, Anderson KI. **Intravital FLIM-FRET imaging reveals dasatinib-induced spatial control of src in pancreatic cancer.**
Cancer Research. 2013 Aug 1;73(15):4674-86

Nobis M, Carragher NO, McGhee EJ, Morton JP, Sansom OJ, Anderson KI, Timpson P. **Advanced intravital subcellular imaging reveals vital three-dimensional signalling events driving cancer cell behaviour and drug responses in live tissue.**
FEBS Journal. 2013 Nov;280(21):5177-97

Nobis M, McGhee EJ, Herrmann D, Magenau A, Morton JP, Anderson KI, Timpson P. **Monitoring the dynamics of Src activity in response to anti-invasive dasatinib treatment at a subcellular level using dual intravital imaging.**
Cell Adhesion & Migration. 2014 Jul ;8(5):478-86

Acknowledgements

I would like to thank a great many people for being supportive and indispensible for the duration of my PhD studies.

My supervisor Prof. Kurt Anderson I would like to thank for letting me spend the last almost 5 years in his lab, taking me in as an intern and letting me go on to do my PhD work. His unwavering moral and technical support throughout, helpful discussions and feedback have taught me a great deal and I am beyond grateful. Furthermore, I would like to thank Dr. Paul Timpson for his support, crazy ideas and guidance at the beginning of my PhD. I owe much of the outcome of this thesis to his input and start-up and deeply appreciate it.

I further want to thank my advisor Prof. Owen Sansom for his positive feedback, ideas and referrals that sparked great collaborations.

I would also like to thank lab members past and present, Agata, Shereen, Kirsty, Ross, Meg and Zahra for creating a wonderful atmosphere in which to do research and their support. I would especially like to thank Juliana, for not only being a great friend but also a great teacher in all things molecular biology related. I am moreover grateful for the help the BAIR team, especially Ewan for bearing with me through all multiphoton crises, Margaret for wonderful training and support on all other microscopy systems, David for great help with Omero and any IT problem I faced and Tom for helping come to grips with FACS. I am also very grateful for the Machesky and Insall labs for a great many coffee breaks and untold amounts of cake. It has been a great pleasure working with and alongside you all.

Moreover, I am very grateful for the staff of the Beatson Institute, be it Central Services, IT, Stores, Histology, Molecular Biology and last but not least the Animal Unit, without whom I would never have been able to achieve as much as I have in

terms of quantity, but most importantly quality of the research I was allowed to undertake.

On a personal note, I would like to thank my friends Hannah and Janis for getting me all the way to Scotland and to stay, chats, dinners, parties and so much more. Further I would like to thank my friends Elena, Steve and Sarah for great company throughout the PhD and shared suffering and of course drinks. Especially Elena I would like to thank for getting me through the write-up phase with many a wine and helpful discussion.

I would further like to thank my family for their continued support and love, my Mum, Dad, Michael, Grit, my little sister Eva, my big siblings Svenia, Annika and Jan and of course all my grandparents for always being there.

Finally and most of all I would like to thank my partner Valters for his love, support and a great deal more. I would like to dedicate my thesis to him, my family and friends.

Author’s Declaration

I, Max Nobis, declare that I am the sole author of this thesis. The work presented here is entirely my own, unless otherwise stated.

Max Nobis

Abbreviations

2D – two-dimensional
3D – three-dimensional
Abl – Abelson murine leukemia viral oncogene homolog 1
ADM – Acinar-ductal metaplasia
ADP – Adenosine diphosphate
AIW – Abdominal imaging window
Akt – Protein kinase B
Arp2/3 - Actin-related protein-2/3
Bcr – Breakpoint cluster region
Brk – Breast tumour kinase
c-KIT – v-kit Hardy-Zuckerman 4 feline sarcoma viral oncogene homolog
c-Src – Cellular Src
Cadherin – Calcium-dependent adhesion
CAG – CMV early enhancer/chicken β actin
cAMP - 3',5'-cyclic adenosine monophosphate
Cas – CRK-associated substrate
Cav – Caveolin
CCK – Cholecystokinin
Cdc42 – Cell division control protein 42 homolog
Cdk – Cyclin-dependent kinase
CFP – Cyan fluorescent protein
CIW – Cutaneous imaging window
CSK – c-Src tyrosine kinase
CXCR – C-X-C chemokine receptor
CXCR2SM – C-X-C chemokine receptor 2 small molecule inhibitor
DC – Dendritic cell
DCIS – Ductal carcinoma *in situ*
DH – Dbl-homology
DMEM – Dulbecco's Modified Eagle Medium
DNA – Deoxyribonucleic acid
DRF – Diaphanous-related formin
ECFP – Enhanced Cyan Fluorescent Protein
ECL – Enhanced chemiluminescence
ECM – Extracellular matrix
EDTA - Ethylenediaminetetraacetic acid
EGF – Epidermal growth factor
EGFP – Enhanced green fluorescent protein
EGFR – Epidermal growth factor receptor
EMT – Epithelial mesenchymal transition
EphA2 – Ephrin A2
ER – Estrogen receptor
ERK – Extracellular signal-regulated kinase
ERRα – Estrogen-related receptorα
FAK – Focal adhesion kinase
FBS – Fetal bovine serum
FLARE – Fluorescent activation reporters
FLIM – Fluorescence lifetime imaging microscopy

FRET – Förster resonance energy transfer
GAP – GTPase activating protein
GCPR – G-coupled protein receptor
GDI – GDP-dissociation inhibitor
GDNF – Glial cell-line derived neurotrophic factor
GDP – Guanosine diphosphate
GEF – Guanine nucleotide exchange factor
GEM – Genetically engineered mouse
GFP – Green fluorescent protein
GM-CSF - Granulocyte macrophage colony-stimulating factor
GTP – Guanosine triphosphate
GTPase - Guanosine triphosphate hydrolase
H&E – Hematoxylin and eosin
HBSS – Hank's Balanced Salt Solution
HDL – High density lipoprotein
HEPES – 4-(2-hydroxyethyl)-1-piperazineethanesulfonic acid
HET – Heterozygous
HIF-1α – Hypoxia inducible factor-1α
HMG-CoA – 3-hydroxy-3-methylglutaryl-conenymeA
HOM – Homozygous
HUVEC – Human umbilical vein endothelial cells
IBD – Inflammatory bowel disease
IF – Immunofluorescence
IGF – Insulin-like growth factor
IGFBP2 – Insulin-like growth factor binding protein 2
IGFR – Insulin-like growth factor receptor
IHC – Immunohistochemistry
IMP3 – Insulin-like growth factor 2 mRNA binding protein 3
IP4P – Inositol polyphosphate 4-phosphatase
IRSp53 – Insulin receptor substrate p53/p58
KD – Knock down
KO – Knock out
KPC – $KRas^{G12D/+}$; $p53^{R172H/+}$; Pdx1-Cre
KPFLC – $KRas^{G12D/+}$; $p53^{floxed/+}$; p48-Cre
KRas – Kirsten rat carcinoma viral oncogene homolog
LARG – Leukemia-associated RhoA guanine exchange factor
LIMK – LIM domain kinase
LMW-PTP – Low molecular weight phosphotyrosine phosphatase
LPA – Lysophosphatidic acid
LSL – Lox stop lox
LUT – Look up table
MAPK – Mitogen-acivated protein kinase
MIN – Mammary intra-epithelial neoplasia
miR – MicroRNAs
MMP – Matrix metalloprotease
MMTV – Mouse mammary tumour virus
mTOR – Mechanistic target of rapamycin
MWCO – Molecular weight cut-off
Nap – Nck-associated protein
Nck – Non-catalytic region of tyrosine kinase adaptor protein

Net1 – Neuroepithelial transforming gene 1
NF-κB – Nuclear factor kappa-light-chain-enhancer of activated B cells
NHERF1 – Na^+/H^+ exchanger regulatory factor 1
OPO – Optical parametric oscillator
P-Rex1 – Phosphatidylinositol 3,4,5-triphosphate Rac exchange factor 1
p130Cas – Breast cancer anti-estrogen resistance protein 1
PAK – p21 protein-activated kinase
PanIN – Pancreatic intraepithelial neoplasia
Par3 – Protease activated receptor 3
PBD – Pak1 binding domain
PBS – Phosphate buffered saline
PDAC – pancreatic ductal adenocarcinoma
PDGF – Platelet-derived growth factor
PDGFR – Platelet derived growth factor receptor
Pdx1 – Pancreatic and duodenal homeobox 1
PEAK1 – Pseudopodium-enriched atypical kinase 1
PH – Pleckstrin homology domain
PI3K – Phosphoinositide 3-kinase
PI3KCA - Phosphatidylinositol 3-Kinase, Catalytic Subunit Alpha
PIG – p53-induced genes
PIP2 – Phosphatidylinositol-4,5-biphosphate
PIP3 – Phosphatidylinositol-3,4,5-triphosphate
PKN – Protein kinase N
PMT – Photomiultiplier tubes
PR – Progesterone receptor
PyMT – Polyoma virus middle T-antigen
Qdot – Quantum dot
Rac – Ras-related C3 botulinum toxin substrate
Ral – Ras-like GTPase
Rb – retinoblastoma protein
RBD – Rho binding domain
RCT – Reverse cholesterol transport
RFP – Red fluorescent protein
Rho – Ras homolog family member
RIPA buffer – Radioimmunoprecipitation assay buffer
RNA – Ribonucleic acid
ROCK – Rho-associated coiled-coil containing protein kinase
ROS – Reactive oxygen species
RPMI – Roswell Park Memorial Institute-1640
RTK – Receptor tyrosine kinase
SD – Standard deviation
SDS-PAGE - Sodium dodecyl sulfate polyacrylamide gel electrophoresis
SEM – Standard error of the mean
SFK – Src family kinases
SH2 – Src homology 2
SH3 – Src homology 3
SHG – Second harmonic gerneration
Shh – Sonic hedgehog
shRNA – Short hairpin RNA
Sra – Specifically Rac-1-assciated protein

Src – Sarcoma
sREACh – Super-Resonance-Energy-Accepting Chromoprotein
TBST – Tris-buffered Saline and Tween 20
TCSPC – Time correlated single photon counting
TFP – Teal fluorescent protein
TGF – Transforming growth factor
THG – Third harmonic generation
Tiam1 – T-Cell Lymphoma Invasion And Metastasis 1
TIFF – Telomerase immortalized foetal fibroblast
TNF – Tumour Necrosis Factor
TrkB1 – Tropomyosin-related kinase B splice variant 1
v-Src – Viral Src
VEGF – Vascular endothelial growth factor
WAVE – Wasp family verprolin homologs
WT – Wild type
YFP – Yellow fluorescent protein
YPet – YFP for energy transfer

1 Introduction

1.1 Tumour progression and invasion

1.1.1 Tumour progression models in mammary and pancreatic cancer

There are many mutations in tumour suppressor genes and oncogenes associated with pancreatic cancer (Sohn and Yeo, 2000). Over 90 % of pancreatic ductal adenocarcinomas (PDAC) present with point mutations in the *KRas* gene (Almoguera *et al*., 1988). This in turn results in constitutively active signal transduction in pancreatic cancer cells through MAPK/Erk, PI3K/Akt and Ral GTPase pathways (Lim *et al*., 2005; Feldmann *et al*., 2010; Collisson *et al*., 2012; Eser *et al*., 2013, 2014). Furthermore, the tumour-suppressor gene *p16* is inactivated in over 95 % of pancreatic cancer as well (Caldas *et al*., 1994; Schutte *et al*., 1997). This leads to uncontrolled growth, through phosphorylation of the Rb protein by cyclinD-Cdk4/6. These are usually inhibited by the action of *p16* (Liggett and Sidransky, 1998). The third most frequent mutation encountered in PDAC is the tumour-suppressor gene *p53,* which is found in > 50 % of PDACs. p53 controls the transcription of a large number of genes including *p21, 14-3-3 sigma* and *p53-induced genes* (*PIG*) which are important in maintaining G2 cell cycle arrest. Mutation of *p53* abrogates these functions leading to unchecked cell cycle progression amongst other things in cancer cells (Macleod *et al*., 1995; Hermeking *et al*., 1997; Yu *et al*., 1999). *p53* inactivation in pancreatic cancer, however, constitutes a late event in tumourigenesis (Wilentz *et al*., 2000).

Notably, a cooperation of the *KRas* and *p53* mutation has been demonstrated previously (Hinds *et al*., 1989; Kalthoff *et al*., 1993). *KRas* mutation was associated with early initiating events and *p53* was needed for the progression from lower to higher grades of PDAC (Pellegata *et al*., 1994). The specific mutations for both KRas and p53 most common in human PDAC were further identified as being $KRas^{G12D}$ (Hingorani *et al*., 2003) and $p53^{R175H}$ with the murine ortholog $p53^{R172H}$ (Olivier *et al*., 2002). These mutant drivers were then expressed in a mouse model of pancreatic cancer under the pancreas lineage specific Pdx1-Cre. This model recapitulated human disease in progressive stages of pancreatic intraepithelial neoplasias *in situ* (PanINs) to invasive PDAC and liver metastasis

(Hingorani *et al*., 2005; Hruban *et al*., 2006). Further analysis of this model concluded that the invasive behaviour was dependent on $p53^{R172H}$ expression and not loss of p53. This represents a gain of function by mutant p53, as it promotes metastasis. It was also established that a key driver of metastasis was the kinase Src (Morton *et al*., 2010a, 2010b).

Mammary cancer presents a more heterogeneous disease with many driver mutations (Vargo-Gogola and Rosen, 2007). One particular subtype is represented by the overexpression of the ErbB2 receptor tyrosine-protein kinase (also called Her2/neu), which is a family member of ErbB receptors that includes EGFR (Schechter *et al*., 1984). Amongst others, two main signalling pathways are activated by ErbB dimerization, the MAPK and PI3K-Akt pathways (Olayioye *et al*., 2000; Yarden and Sliwkowski, 2001; Baselga and Swain, 2009). Expression of ErbB2 under the MMTV-Cre promoter, targeting expression to the mammary ducts in transgenic mice, resulted in metastatic disease in these animals (Guy *et al*., 1992). Another mouse model of metastatic mammary carcinoma was described with overexpression of the viral polyoma virus middle-T-antigen under the control of MMTV promoter (PyMT model) (Guy *et al*., 1992b). It has been demonstrated that upon progression toward invasive carcinoma in this model, ErbB2 expression was strongly upregulated, and expression of estrogen receptor (ER) and progesterone receptor (PR) strongly downregulated. It was thus concluded that the PyMT model represents another late stage ErbB2 overexpression model, indirectly resulting in ErbB2 overexpresssion (Lin *et al*., 2003).

1.1.2 Cytoskeletal regulation of invasion

The cytoskeleton is comprised of three different filament networks. Intermediate filaments such as vimentin and keratin provide structural support and resilience. Microtubules form a dynamic network, which mediates chromosomal rearrangement during mitosis, but also mediates the transportation of vesicular cargo. Finally, the actin cytoskeleton presents a dynamic structural network which mediates protrusion, adhesion and retraction of the cell body (Fletcher and Mullins, 2010; Alberts *et al*., 2015). In recent years the cross-talk between the actin and microtubule networks, especially regulation of the actin cytoskeleton by microtubules has been an area of intense research.

Rho family GTPases have been shown to regulate the actin cytoskeleton (Hall, 1998). This occurs in a variety of ways and has therefore been associated with migration and metastatic progression in cancer (Karlsson *et al*., 2009; Sahai and Marshall, 2002). Epithelial to mesynchymal transition (EMT) is a developmental process in which cancer cells undergo genetic and morphologic changes allowing them to break free from their primary loci to colonize distant sites. This has been described in great detail for both pancreatic and mammary carcinoma previously. Briefly, for pancreatic cancer several stages of PanINs are passed (1-3) until fully developed PDAC can be observed. These are in turn a result of intense cytological and architectural atypia following the accumulation of genetic aberrations such as *KRas* mutation, ErbB2 overexpression and *p53* mutation to name a few (Hruban *et al*., 2000). In ErbB2 driven mammary carcinoma EMT can be observed by the formation of ductal carcinoma in situ (DCIS) which are presented in the ErbB2 mouse model by orthologous mammary intraepithelial neoplasms (MIN). These then further progress into invasive carcinomas (Ursini-Siegel *et al*., 2007; Tomaskovic-Crook *et al*., 2009).

Cells that have undergone EMT exhibit reorganization of their cortical actin cytoskeleton, with structures like lamellipodia and filopodia, to facilitate their movement and sensing of their extra-cellular milieu (Ridley, 2011). Invasive structures in turn, which are termed invadopodia degrade components of the ECM in order for cancer cells to move (McNiven, 2013). These are mainly associated with the action of Rac-1 and Cdc42. Furthermore, activation of either of the two GTPases has been shown to activate the family of p21 activated kinases (PAKs) resulting in

cell migration (Ha *et al*., 2015). Increased stress fiber formation and contractility is further associated with cancer progression via the action of RhoA. Actomyosin contractility is enhanced by the activation of Rho-associated kinase (ROCK) and the formin diaphanous 1 (DIA1), through RhoA signalling. Furthermore, LIM kinase (LIMK) acts to inactivate cofilin-mediated actin severing, stabilizing actin at the plasma membrane (Narumiya *et al*., 2009). Finally Rho family GTPases regulate adherens junctions and mediate cell-cell contacts. During EMT p120 catenin is expressed, which inhibits the function of Rho and allows for the breaking down of cell junctions. This in turn can activate Rac-1 and Cdc42 resulting in cell migration and the formation of protrusions (Anastasiadis and Reynolds, 2001; Lamouille *et al*., 2014).

The kinase Src has further been associated with many aspects of cancer cell migration and metastasis (Guarino, 2010). To name a few, it functions as a negative regulator of Rho-associated cell-ECM adhesion structures in cellular adhesion (Yeatman, 2004). Src activity is further associated via integrin signalling (Klinghoffer *et al*., 1999) and adhesion disassembly (Webb *et al*., 2004), allowing for cell migration to occur. Crosstalk therefore exists between Src and Rho signalling (Huveneers and Danen, 2009). Invasion is further aided by ECM breakdown by matrix-metalloproteases the expression of which is upregulated by Src (Hsia *et al*., 2003; Rivat *et al*., 2003).

As these proteins constitute key regulators of cancer cell migration and invasion processes, they were examined in more detail in the context of mammary and pancreatic cancer.

1.2 Src

1.2.1 Morphology and functions of Src

The non-receptor tyrosine kinase Src is the first proto-oncogene to be described. In 1911 a virally transmissible tumour growth was shown in chickens (Rous, 1911) (later named: Rous Sarcoma virus (Rubin, 1955)) leading to virally induced tumour cells. In the 1970s the viral Src-gene (v-Src) was identified in the viral genome (Czernilofsky *et al*. 1980; Takeya *et al*. 1982; Takeya & Hanafusa 1982). v-Src is evolutionarily conserved in vertebrates differing in sequence from the human cellular Src (c-Src) only in C-terminal deletions, with v-Src lacking the negative regulatory domain of c-Src (Figure 1.1 A). This in turn leaves v-Src with stronger transforming capabilities than c-Src. c-Src further plays a significant role in the development of several human cancers (Hjelle *et al*., 1988).

The structure of Src contains (like all Src family kinases, SFKs) four Src homology domains (SHs), a unique domain and a regulatory domain (Brown and Cooper, 1996; Frame, 2002; Hilbig, 2008). While the SH4/unique domain constitutes the membrane localization signal via myristoylation (Sefton *et al*., 1982), interaction through SH3, SH2 and the kinase domain SH1 have been shown to regulate activity of Src. Autophosphorylation of the tyrosine 416 has been found to activate Src (Patschinsky *et al*., 1982) and leads, through the loss of interaction of the SH3 (Erpel *et al*., 1995), SH2 (Gonfloni *et al*., 1997) and the kinase domain to an open confirmation of the kinase upon activation (Gonfloni *et al*. 1999; Xu *et al*. 1999). Finally the autoinihibitory/regulatory domain at the N-terminal end of Src, is regulated via another tyrosine phosphorylation site: Y527, that upon phosphorylation by CSK (c-Src tyrosine kinase) leads to binding of the SH2 domain to the N-terminal domain and inactivation of Src (Figure 1.1 B) (Okada & Nakagawa 1989; Cooper *et al*., 1986). This domain further binds platelet-derived growth factor β-receptor (PDGFβR) (Mori *et al*., 1993).

Targeting of active Src to the membrane has further been demonstrated previously to depend on coordination of RhoB and actin polymerization. Moreover, Src controls the actin dependence of RhoB endosome movement toward the plasma membrane (Sandilands *et al*., 2004). This membrane-associated activation of Src was further linked to palmitoylation (Sandilands *et al*., 2007).

Down-stream effectors of Src include, amongst others, focal adhesion kinase (FAK) and CRK-associated substrate (Cas), the binding of which results in an activation of Src as well (Thomas *et al*., 1998). p130Cas in particular has been shown to associate with Src (Kanner *et al*. 1990*;* Honda *et al*. 1998) and regulate FAK dependent cell motility (Cary *et al*., 1998). E-cadherin levels in cells have further been linked to the activity of Src and other tyrosine kinases, leading to ubiquitination and the endosomal degradation of E-cadherin (Fujita *et al*., 2003). E-cadherin is further regulated via its associated p120-catenin, which in turn is phosphorylated by Src (Roura *et al*., 1999).

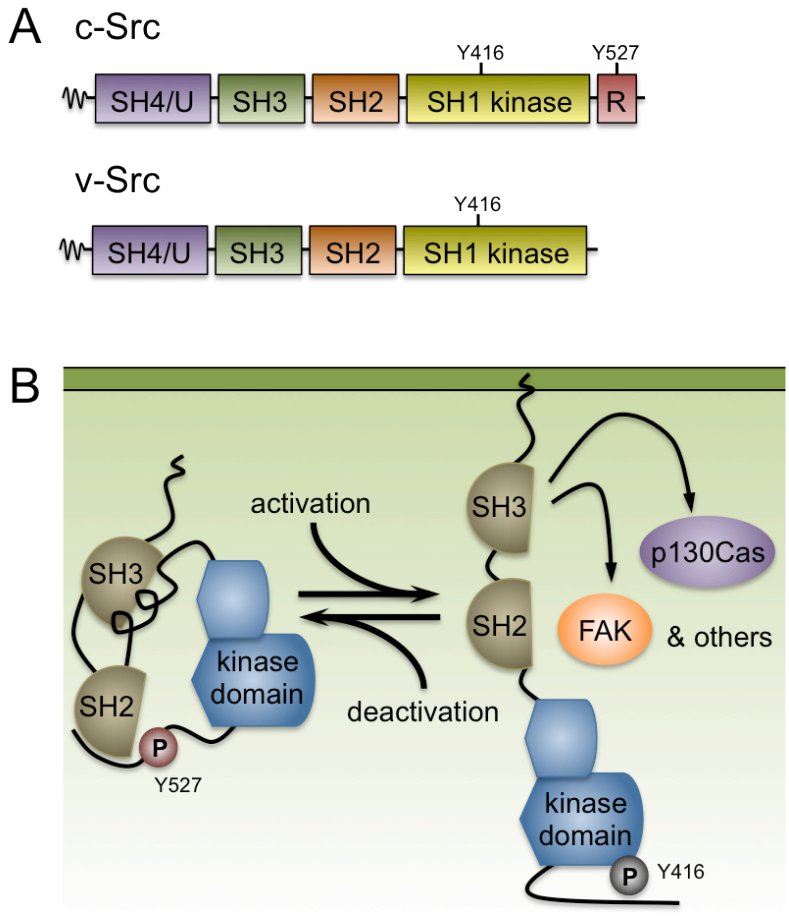

Figure 1.1: Schematic of the tyrosine kinase Src and its membrane-associated activation
A Schematic of the domain structure of cellular Src (c-Src) and viral Src (v-Src), with an amino-terminal myristoylated and key tyrosine phosphorylation sites at Y416 and Y527. The C-terminal regulatory domain (R) is missing in v-Src. **B** Schematic of Src activation and unfolding upon dephosphorylation of the Y527, displacement of SH2 and SH3 or autophosphorylation of Y416. Selected associated proteins in the active state include FAK and p130Cas (adapted from Frame, 2002).

1.2.2 Src and pancreatic cancer

Overexpression of Src was shown in immunohistochemical stains of human pancreatic carcinoma tissue, as well as by Western blot analysis, when compared to normal pancreatic tissue. Kinase activity was further upregulated in the carcinoma cells, linking cell proliferation with Src activity in pancreatic cancer cells (Lutz *et al*., 1998). Furthermore, expression of Src in pancreatic cancer cell lines was linked to metastatic dissemination. Culturing of pancreatic cancer cell lines on collagen type I and collagen type III substrate led to a reduction E-cadherin expression and increase in proliferation and migration. This was further linked to elevated c-Src activity within these cells (Menke *et al*., 2001).

Src overexpression was shown to increase insulin-like growth factor I (IGF-1) expression in human pancreatic cancer cells. This in turn stimulated IGF-1 dependent proliferation in these cells (Flossmann-Kast *et al*., 1998). Activation of Akt was further linked to this feedback, controlling IGF-1R expression and increasing invasion in pancreatic cancer cells (Tanno *et al*., 2001). Co-expression of IGF-1R and c-Src was moreover shown in biopsies of human pancreatic ductal adenocarcinoma (PDAC) (Hakam *et al*., 2003a). Caveolin-1 (Cav-1) is furthermore overexpressed in human pancreatic cancer cell lines, mouse models of PDAC and in biopsies of human pancreatic tumours. It was associated with worse clinical outcome and advanced tumour grades. Depletion of Cav-1 *in vitro* and *in vivo* led to a change in Src activation (Tyr416 dephosphorylation and Tyr527 auto-inhibitory phosphorylation) and decreased invasive potential (Chatterjee *et al*., 2015).

The secreted calcium binding protein S100A4 has also been found to be markedly overexpressed in pancreatic cancer, linking its expression with poorer clinical outcome in patients (Ai *et al*., 2008). In a patient derived orthotopic tumour model suppression of S100A4 expression led to a reduction in growth, invasion and metastasis *in vivo*. Furthermore, S100A4 was shown to activate Src/FAK within the pancreatic cancer cells promoting tumour progression (Che *et al*., 2015).

Finally, crosstalk between KRas and Src was observed in PDAC after the deletion of C-terminal Src kinase (CSK) *in vivo*. In KRas driven PDAC cooperative action of KRas and Src could further contribute to genomic instability (Shields *et al*., 2011). Moreover, mutant KRas was shown to induce an activation loop between Src, PEAK1 (pseudopodium-enriched atypical kinase 1) and ErbB2 in PDAC,

driving tumour growth and metastasis *in vivo*. Inhibition of ErbB2 further led to an increased Src-dependent expression of PEAK1, indicating an observed resistance in patients with PDAC to be dependent on the feedback loop of these kinases (Kelber *et al*., 2012).

1.2.3 Src inhibition in pancreatic cancer

Targeting Src in pancreatic cancer has been explored in great detail previously. In a study employing patient derived xenografts of pancreatic cancer tissue in nude mice, Src was inhibited *in vivo* using the anilinoquinazoline AZM475271. This decreased primary cancer growth by 40 % and in conjunction with gemcitabine was able yield a reduction of growth up to 90 %. Also, in the combination treatment metastasis and lymph node invasion was significantly inhibited in the xenografts (Yezhelyev *et al*., 2004). In another study, xenografts of a pancreatic cancer cell line treated with AZM475271 lead to an abrogation of liver metastasis and a reduction in angiogenesis. Phosphorylation of FAK and activity of Src was reduced in the treated mice, as well as in the pancreatic cancer cell lines. The same held true in human umbilical vein endothelial cells (HUVECs) *in vitro,* indicating a potential role of Src and FAK in angiogenic processes (Ischenko *et al*., 2007).

Another inhibitor used in inhibiting Src activity in pancreatic cancer was dasatinib (previously called: BMS-354825), with the commercial name Sprycel®. Dasatinib is a tyrosine kinase inhibitor, targeting Bcr-Abl kinases, c-Src, c-KIT and amongst others also the platelet derived growth factor receptor (PDGFR) (Lombardo *et al*., 2004). Cell lines were isolated from a previously described model of PDAC the KPC model (*Pdx1-Cre, KRas*$^{G12D/+}$*, p53*$^{R172H/+}$), which has been shown to accurately recapitulate human disease progression and metastasis sites of the liver *in vivo* (Hingorani *et al*. 2005; Morton *et al*. 2010; Olive & Tuveson 2006). Treatment of these PDAC cell lines with dasatinib displayed reductions in phosphorylation levels of Src, FAK and p130Cas. Progressive stages of PDAC in the KPC model were shown to display increased levels in Src phosphorylation. While *in vivo* treatment with dasatinib did not confer a survival advantage, a marked decrease in the incidence of metastasis was reported (Morton *et al*. 2010).

Dasatinib, however, failed in phase II clinical trails, not conferring a survival advantage when administered as a single agent (Chee *et al*., 2013) or in conjunction with gemcitabine treatment (Carlson 2014). This could be due to poor distribution of dasatinib in the treated PDACs and thus ineffective inhibition of Src activity. These results highlight the need for more precise pre-clinical *in vivo* modelling of drug pharmacodynamics and the possible optimization of treatment delivery and efficacy before moving to clinical trials. One such approach could be the *in vivo* imaging of genetically engineered mouse (GEM) models and their visualized response to therapy on a single cell level in the context of the tumour microenvironment. Evaluating treatment response at this level could help determine limitations of drug treatments occurring in the native tumour microenvironment. Strategies of improved delivery, dosing or scheduling could therefore be tested in more detail, than with other methods before moving to clinical trials.

1.3 Rac-1

1.3.1 Rac-1 and its effectors

Rac-1 is a member of the family of small Rho GTPases, three of which have been the main focus of investigation: Rac1, RhoA and Cdc42.

Rac-1 has been associated with the leading edge of cells, together with another small GTPase Cdc42 (Kurokawa *et al*. 2004; Nobes & Hall 1995). There, lamellipodia formation is driven by Rac-1 activation. It further associates with downstream effectors of the WAVE complex, which are localized at the leading edge (Kawamura *et al*. 2004; Innocenti *et al*. 2005). The WAVE complex components linking to Rac, have been shown to be IRSp53 (Suetsugu *et al*., 2006), Sra-1 and Nap1 (Steffen *et al*., 2004). WAVE in turn activates Arp2/3, which induces actin branching morphogenesis (Machesky & Gould 1999; Mullins & Pollard 1999; Ridley 2006).

Next to the cytoskeletal regulatory action of Rac-1, it has been shown that Rac-1 is required for cell proliferation and cell cycle progression. It has been demonstrated that expression of a dominant negative form of Rac-1 in fibroblasts resulted in cell cycle arrest and an accumulation of cells in G2/M phase (Olson *et al*., 1995; Moore *et al*., 1997). Rac-1 has further been found to be a major regulator of cell cycle

and proliferation via mTOR (Saci *et al*., 2011), formation of cell-cell adhesions (Ehrlich *et al*., 2002) as well as contact inhibition regulated by merlin (Bosco *et al*., 2010). Finally, Rac-1 was found to be essential in Ras transformation in fibroblasts (Khosravi-Far *et al*. 1995; Qiu *et al*. 1995). Elevated levels of Rac-1 and its activation were moreover associated with and found to be required for KRas transformation in the lung (Kissil *et al*. 2007), skin (Samuel *et al*. 2011; Wang *et al*. 2010), ulcerative colitis (Muise *et al*., 2011) and pancreatic cancer (Heid *et al*., 2011). Finally, activating mutations in the Rac1 gene have been identified in sun-exposed melanomas (Krauthammer *et al*., 2012).

1.3.2 Rac-1 in pancreatic and mammary carcinoma

Rac-1 overexpression and hyperactivation has been reported in pancreatic cancer (Crnogorac-Jurcevic *et al*., 2001) and play a vital role in progression and survival (Murga *et al*. 2002; Westwick *et al*. 1997; Guo *et al*. 2013a). E-cadherin mediated adherens junctions were inhibited in pancreatic cancer cells, where expression of dominant negative Rac-1 led to an increase in E-cadherin levels and expression of a constitutively active form of Rac-1 led to a decrease (Hage *et al*., 2009). Rac-1 expression was increased in human and murine pancreatic carcinoma, especially in the stroma. Deleting Rac-1 expression in PDAC progenitor cells, Heid and colleagues showed that upon $KRas^{G12D}$ induction, the formation of acinar-ductal metaplasia (ADM), PanINs and tumours was reduced. Further the survival of the mice was significantly increased (Heid *et al*., 2011). Rac-1 dependent superoxide production further led to an increase in proliferation in pancreatic cancer cells (Du *et al*., 2011).

Rac-1 has further been found to be upregulated in breast cancer tumours (G. Fritz *et al*. 1999; G. Fritz *et al*. 2002) and in triple-negative breast cancer cell lines (Feng *et al*., 2014). Overexpression and identification of a common splice isoform Rac-1b was moreover shown. Schnelzer and colleagues further demonstrated in their study by IHC that Rac-1 expression was particularly prominent in ductal carcinoma in situ (DCIS), primary breast cancer and lymph node metastasis. In line with this, in benign mammary carcinoma, Rac-1 expression was low (Schnelzer *et al*., 2000).

In a subtype of mammary carcinoma, Rac-1 activity has previously been strongly linked to the expression of the receptor tyrosine kinase ErbB2 and its activation (Arias-Romero *et al*. 2010; Sosa *et al*. 2010). Activation of Erk and Akt pathways was observed in ErbB2 expressing ER positive cells in 3D culture. This in turn was dependent on activation of the p21-activated kinase-1 (PAK1) – Rac-1 pathway, with inhibition of either leading to a downregulation in Akt and Erk signalling cascades (Arias-Romero *et al*., 2010). Furthermore, mutation of the ErbB2 receptor, leading to a resistance to tratuzumab, was associated with Rac-1 activated TGF beta overexpression as well as VEGF secretion (Wang *et al*. 2010). Exposure of mammary epithelial cells to MMP-3, upregulated in many breast tumours (Sternlicht and Werb, 2001), was further shown to result in an increase in the expression of Rac-1b, cellular reactive oxygen species (ROS) and epithelial-mesenchymal transition (EMT) via Snail (Radisky *et al*., 2005).

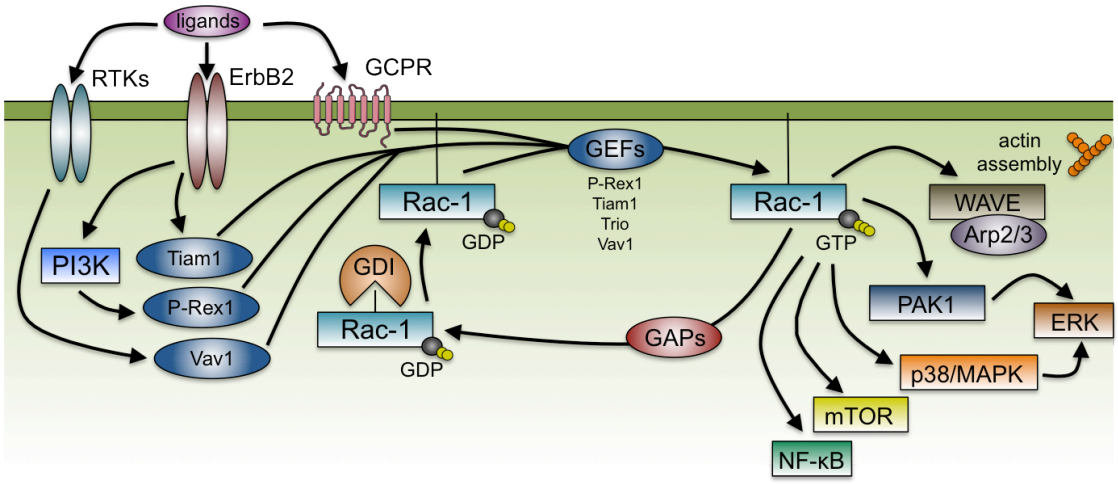

Figure 1.2: Overview of Rac-1 activation via selected GEFs and downstream effectors
Schematic depiction of Rac-1 activation via selected GEFs such as Tiam1, P-Rex1 and Vav1 and stimulation of these GEFs by receptor tyrosine kinases (RTKs), ErbB2 receptor dimerization and activation, as well as via G-coupled protein receptors (GCPRs). Effectors of GTP-bound Rac-1 include the WAVE and Arp2/3, PAK1, MAPK, mTOR and NF-κB to name a few (adapted from Bid *et al*. 2013).

1.3.3 Rac-1 GEFs

Small Rho family GTPases are controlled in cells by the action of GTPase activating proteins (GAPs) and guanine-nucleotide exchange factors (GEFs). The latter activate the GTPases by opening the binding sites of specifically GDP bound forms, allowing for an exchange of GDP to GTP (Worthylake *et al*., 2000). GEF activity was first found to be stimulated by the Dbl-homology (DH) domain of the GEFs, catalysing GDP to GTP exchange in the GTPase upon binding of the GEF to the GTPase (Hart *et al*. 1991). DH domains in turn have further been described in many GEFs (Kjoller and Hall, 1999). GTP hydrolysis on the GTPases is stimulated by GAPs, thereby inactivating GTPases (Garrett *et al*. 1991; Hart *et al*. 1991). GTPases are further regulated by the action of guanine nucleotide dissociation inhibitors (GDIs). GDIs in turn inhibit the localisation of the GTPases to the membrane and keep them as inactive complexes in the cytoplasm. They further prevent the activation of GTPases by inhibiting GDP dissociation (Olofsson, 1999; Hoffman *et al*., 2000; Grizot *et al*., 2001; Ridley, 2001). Here, a select few GEFs will be introduced, especially in the context of their action in pancreatic and mammary carcinomas.

Vav1 is part of a family of GEFs (Vav1-3), with Vav1 recently emerging as an important player in the pathogenesis of pancreatic cancer. Patients with Vav1 positive tumours had poorer survival rate compared to patients with Vav1 negative tumours. Furthermore Vav1 was found to be acting together with EGFR to promote pancreatic cancer cell proliferation (Fernandez-Zapico *et al*., 2005). This GEF has also been found to be ectopically expressed in invasive pancreatic tumour cells, promoting matrix degradation and invadopodia formation via its activation of Cdc42 (Razidlo *et al*., 2014). Further, treatment of KPFLC mice (*p48-Cre, KRas*$^{G12D/+}$, *p53*$^{floxed/+}$) mice with a Vav1 inhibitor, azathioprine, inhibited metastasis in these mice. This was in a Vav1 dependent manner, as Vav1-negative cell lines and tumours were largely resistant to azathiopurine treatment (Razidlo *et al*., 2015a).

Tiam1 (T-cell Lymphoma Invasion and Metastasis 1) is another GEF with emerging importance in both mammary and pancreatic carcinoma. It has been found to be partially upregulated in pancreatic cancer cells and to mediate the invasive behaviour through activation of Rac-1 in cells with high expression levels of α4β6 integrins (Cruz-Monserrate & O'Connor 2008). Tiam1 was further found to be upregulated in primary stages of pancreatic cancer, with increasing expression observed in cancers without lymph node involvement and distant metastasis (Guo *et al*. 2013a). Ablation of Par3 expression has previously been established to disrupt epithelial tight junction assembly. This was further linked to Rac-1 activity via Tiam1, showing that Par3 inhibits Tiam1-Rac-1 signalling (Chen & Macara 2005). Par3 was also shown to be downregulated and interacting with Tiam1 in pancreatic cancer. Furthermore knocking down Par3 resulted in a reduction of tight junctions and increased pancreatic cancer cell invasion and migration (Guo *et al*. 2015). In breast cancer, Tiam1 was found to overexpressed in higher grades of clinical stages (Adam *et al*., 2001) and in triple negative breast cancer cell lines (Chavez *et al*., 2010). Additionally, heregulin-β1 stimulation of cells led to redistribution of Tiam1 to membrane ruffles and loosening of cellular junctions (Adam *et al*., 2001). Moreover, binding of Tiam1 to the cytoskeletal protein ankyrin was shown to promote breast tumour cell invasion and migration (Bourguignon *et al*., 2000). Apicobasal polarity is controlled by Par3 at the apical and by β–syntrophin at the basal surface of polarised epithelia. Both control Rac-1 activation via Tiam1, with β–syntrophin promoting and Par3 inhibiting activation (Mack *et al*., 2012). *In vivo*, downregulated Tiam1 expression in stromal cells led to a decrease in invasion and metastatic potential of breast cancer cells (Xu *et al*. 2010). Tiam1 was also found to be essential for ErbB2-driven tumour formation and metastatic progression, but not in c-myc induced breast cancer mouse model mice (Strumane *et al*., 2009).

Trio overexpression has previously been linked to poor outcome in breast cancer patients (Lane *et al*., 2008). Furthermore, in breast cancer cells, Trio-Rac-1-PAK1 signalling axis has been linked to invadopodia disassembly, by phosphorylation of cortactin (Moshfegh *et al*., 2014).

P-Rex1 is part of the P-Rex (**P**hosphatidylinositol 3,4,5-triphosphate **R**ac **ex**change factors) family of Dbl-type GEFs (Welch 2015). It has been shown by Welch *et al*. to function downstream of phosphatidylinositol 3,4,5-triphosphate (PIP_3) and Gβγ, directly linking Rac-1 activation to PI3 kinase activity and G-protein coupled receptors (GPCR) (Welch *et al*. 2002). KO mice of P-Rex1 have been described to have mild neutrophilia, with neutrophils impaired in their capability to be recruited to sites of inflammation, displaying, however, only slightly impaired chemotactic abilities (Welch *et al*. 2005). In breast cancer, P-Rex1 was overexpressed in estrogen receptor positive (ER^+) and ErbB2 expressing human tumours. Activation of P-Rex1 was further linked to ErbB2 receptor activation, and the GCPR CXCR4 was described as a key mediator of Rac-1 activation via P-Rex1 (Sosa *et al*., 2010). The phosphorylation status of P-Rex1 was further linked to Rac-1 activation, after ErbB2 signalling. This further regulated both proliferation and invasiveness of breast cancer cells. A correlation between P-Rex1 expression and poor patient outcome was moreover shown (Montero *et al*., 2011). P-Rex1 expression was further found to be linked to sensitivity of PIK3CA mutated and ErbB2 overexpressing breast cancer cells, acting downstream of PIP_3 and PI3K. Inhibition of PI3K was particularly effective in these subsets of breast cancer and led to a downregulation of both Akt and Rac1/Erk pathways (Ebi *et al*., 2013). In line with this, P-Rex1 knockdown or Rac-1 inhibition caused a downregulation of PI3K/Akt and MEK/Erk pathways. Furthermore, P-Rex1 promoted insulin growth factor 1-receptor (IGFR1) activation, suggesting a feedback-loop between P-Rex1 and PI3K activators (Dillon *et al*., 2015).

Recently, the crystal structure of P-Rex1 revealed the auto-inhibitory confirmation of P-Rex1 prior to PIP_3 or Gβγ signalling. P-Rex1 binding of the latter, allowed it to assume on open conformation permitting access to its GEF-acting domains (DH and PH domain) in order to in turn activate Rac-1 (Lucato *et al*., 2015) (Figure 1.3 B).

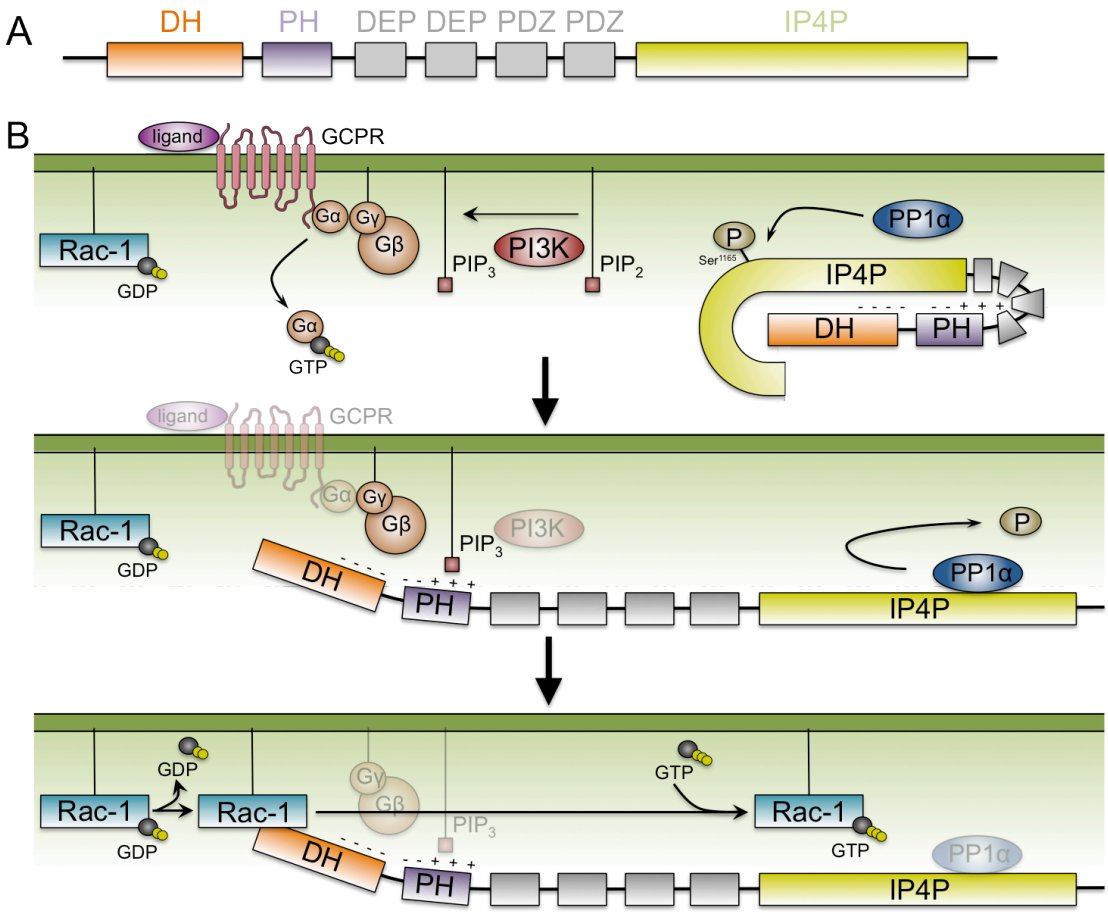

Figure 1.3: The Rac-1 GEF P-Rex1 and its activation
A The **P**hosphatidylinositol 3,4,5-triphosphate **R**ac **ex**change factor P-Rex1, contains 3 key domains, the inositol polyphosphate 4-phosphatase domain (IP4P) regulating its auto-inhibitory confirmation and the DH, PH domains responsible for its GEF activity. **B** Upon G-coupled protein receptor (GCPR) activation and Gα GTP binding, phosphatidylinositol(3,4,5)P_3 (PIP_3) synthesis by PI3K and de-phosphorylation of P-Rex1 by protein phosphatase 1α (PP1α), P-Rex1 can assume an open confirmation exposing the DH and PH domains. These in turn can then bind Gβγ and PIP_3 allowing for P-Rex1 GEF function on Rac-1 to take place (adapted from Lucato *et al*. 2015; Barber *et al*. 2012).

1.4 RhoA

1.4.1 RhoA in breast cancer

In normal murine mammary epithelial cells, RhoA activity is amongst other GAPs, downregulated via the action of p190RhoGAP. This GAP is in turn activated via β3 integrin binding to fibronectin and subsequent EGFR activation cross-talk (Balanis *et al*., 2011).

RhoA overexpression in turn has been shown to be able to transform preneoplastic human mammary epithelial cells showing alteration in several genes associated with malignant transformation and breast cancer progression, such as *ZNF217*, *ELF3* and *S100P* (Zhao *et al*. 2009).

In MCF-7 breast cancer cells conversely, p190RhoGAP phosphorylation is maintained by Brk (Breast tumour kinase), a kinase that is often found to be overexpressed in breast cancer cells. p190RhoGAP is further associated with p120RasGAP, which in turn downregulates Ras activity. When Brk is activated by EGFR signalling, it was shown to downregulate RhoA activity via p190RhoGAP, but upregulate Ras activity by attenuating p120RasGAP function (Shen *et al*. 2008). Contrary to this, RhoA activation in a different breast cancer cell line, MDA-MB-231, has been shown to be downstream of EGF stimulation via galectin-3 and phospho-caveolin-1, leading to cell migration and dorsal actin ruffling (Boscher and Nabi, 2013).

Ephrin receptor A2 (EphA2) was shown to be involved in RhoA activity in the breast cancer cell line 4T1 *in vitro* and *in vivo*. Upon loss of the cytoplasmic domain of the receptor or a mutation in the kinase domain, RhoA activity was lost and cells displayed reduced cell migration as well as a reduction in the number of lung metastasis in an injection mouse model (Fang *et al*. 2005). Furthermore, overexpression of EphA2 in MCF-10A breast cancer cells led to a weakening of E-cadherin mediated cell-cell adhesion and RhoA activation. This was in conjunction with the action of Src and the low molecular weight phosphotyrosine phosphatase (LMW-PTP) dephosphorylating p190RhoGAP (Fang *et al*. 2008). Gab2 docking protein overexpression in MCF-10A breast cancer cells delays cell spreading and enhanced cell migration. It further supressed RhoA activation in these cells via the action of p190A RhoGAP (Herrera Abreu *et al*., 2011).

In the MMTV-ErbB2 overexpressing breast cancer mouse model, loss of the EphA2 receptor was concurrent with downregulation of Ras and RhoA activity. This led to impairment in tumour initiation and metastatic progression. The same was not observed in the MMTV-PyMT model in which EphA2 was also eliminated by genetic editing (Brantley-Sieders *et al*., 2008). ErbB2 signalling was further shown to phosphorylate Plexin-B1, leading to an activation of RhoA via the RhoGEF11/12 in human breast cancer cell lines. In MMTV-ErbB2 mice, loss of Plexin-B1 led to a reduction in lung metastasis. Moreover, Plexin-B1 high expression was correlated with poorer patient disease free survival (Worzfeld *et al*., 2012). In a study looking at statin inhibition of ErbB2 overexpressing mouse tumours, it was demonstrated that the treatment resulted in a decrease in Ras/Erk1/2 signalling, but an upregulation of the RhoA/ROCK/NF-κB pathway. Combined treatment of statins with NF-κB inhibitors circumvented this problem (Riganti *et al*., 2011).

RhoA activation in breast cancer cells in the context of the tumour microenvironment was shown recently by interaction of the cancer cells with macrophages. There, the intravasation of breast cancer cells was demonstrated following contact with macrophages *in vitro* or *in vivo*, leading to invadopodia formation and penetration through the basement membrane (Roh-Johnson *et al*., 2014). The ability of macrophages to activate RhoA in cancer cells, had been established before in gastric and colon carcinoma that same year (Cardoso *et al*., 2014).

Loss of polarity in breast cancer cells before progression to invasive stages has been shown to be regulated by an increase in RhoA activity via several proteins. PDLIM2, a regulator of NF-κB and other transcription factors, has been associated with the maintenance of polarity in mammary acini structures. Loss or downregulation of PDLIM2 led to an upregulation of RhoA and ROCK activity in MCF10A breast cancer cells (Deevi *et al*., 2014). In progressive stages of breast cancer, WNT5A, a planar cell polarity ligand, is highly expressed in invasive mammary carcinoma cells. In atypical and ductal carcinoma *in situ* cells conversely its expression level is basal. The upregulated expression of WNT5A also resulted in higher RhoA activity in these cells (MacMillan *et al*., 2014). Overexpression of the protein 14-3-3τ is found in several types of breast cancer. It furthermore regulates progression via binding of RhoGDIα and thus increasing levels of active RhoA and ROCK.

Increased invasion and metastatic potential of breast cancer cells was demonstrated both *in vitro* and *in vivo* (Xiao *et al*. 2014).

NHERF1 (Na^+/H^+ exchanger regulatory factor) expression is enhanced in human breast cancer biopsies and associated with metastatic progression and HIF-1α (hypoxia inducible factor-1α) expression. NHERF1 overexpression was further associated with a more invasive phenotype in breast cancer cells, potentiated in a serum free milieu and 3D culture. This was linked to protein kinase A (PKA)-RhoA and p38 signalling (Cardone *et al*., 2007).

Several microRNAs (miRs) have been implicated in breast cancer progression and associated with RhoA activation. Upregulation of miR-182 has been shown in the malignant cell line variants for both human MCF10 and mouse 4T1 cell line groups. Overexpression led to an increase of invasion *in vitro* and *in vivo*. Furthermore, miR-182 was shown to directly target MIM (Missing in Metastasis), which normally supressed the activity of RhoA (Lei *et al*. 2014). Another microRNA directly targeting RhoA transcription has been shown to be miR-155 (Johansson *et al*., 2013). Knockdown of miR-155 in breast cancer cells resulted in a decrease of previously shown TGF-β induced EMT (Bhowmick *et al*., 2001), migration and invasion as well as RhoA activity (Kong *et al*., 2008).

1.4.2 RhoA GEFs and associated receptors in breast cancer

A wide variety of GEFs have been associated with regulating RhoA activity. The GEF SmsGDS has been shown to be a key regulator of RhoA and NF-κB in breast cancer cells. It was further demonstrated that elevated SmsGDS expression is correlated with poorer prognosis and survival outcome in breast cancer patients (Hauser *et al*., 2014).

The Neuroepithelial transforming gene 1 (Net1) is a GEF associated with branching morphogenesis in the ductal tree of the native mammary gland (Zuo *et al*., 2014). It is furthermore overexpressed in breast cancer cells and associated with controlling FAK activation and ameboid invasion (Carr *et al*., 2013). Moreover, Net1 expression together with α6β4-integrins was shown as a prognostic factor associated with reduced metastatic-free and overall survival in ERα positive breast cancer patients (Gilcrease *et al*., 2009).

The GEF termed Leukemia-associated RhoA guanine exchange factor (LARG) was shown previously to regulate the motility and invasion of breast cancer cells T47D by the iodide transporter NIS. Overexpression of NIS has been shown in breast cancer (Tazebay *et al*., 2000) and was associated with RhoA activation in T47D cells (Lacoste *et al*., 2012).

Expression of the adhesion G-protein-coupled receptor GPR116 was positively correlated with metastatic progression in breast cancer cells *in vitro* and *in vivo* via the p63RhoGEF and RhoA and Rac-1 activation. Knock-down of the receptor led to a decrease in RhoA and Rac-1 activity. This furthermore reduced the invasive capabilities of the breast cancer cells. Elevated expression of GPR116 was also demonstrated in progressive stages of human breast cancer biopsies, as well as correlated with decreased recurrence-free and distant metastasis-free survival (Tang *et al*. 2013).

Estrogen-related receptor α (ERRα) controls RhoA protein turnover in MDA-MB-231 breast cancer cells via the activated expression of BACURD2 (BTB/POZ domain-containing adaptor for Cullin2-mediated RhoA degradation 2). This protein in turn is responsible for RhoA targeted degradation (Sailland *et al*., 2014).

Kiss1 receptor (GPR54) has been shown to drive metastasis in the PyMT mammary cancer model through activation of RhoA via p63RhoGEF. Kiss1 receptor knock out mice crossed to the PyMT model showed that the loss of one copy of Kiss1 receptor led to haploinsufficiency. This in turn resulted in slowed tumour initiation, progression and decreased lung metastasis (Cho *et al*. 2011).

1.4.3 Pancreatic Cancer and RhoA signalling

Activation of RhoA signalling can lead to cancer cell migration and invasion in pancreatic cancer. Listed here are a variety of factors that can contribute to this process.

PDAC cells derived from a KPC model (*Pdx1-Cre* + $KRas^{G12D/+}$ + $p53^{R172H/+}$) showed spatially defined RhoA activation at the leading edge and the rear of the cells in a 3D context both *in vitro* and *in vivo*. This activity of RhoA was absent in PDAC cells derived from a KPFLC model (*Pdx1-Cre* + $KRas^{G12D/+}$ + $p53floxed^{+/+}$), showing an involvement of mutant p53 in driving pancreatic cancer cell invasion (Timpson *et al*., 2011a).

In pancreatic cancer cells p190RhoGAP expression led to a downregulation of RhoA activity and metastatic capability of these cells. Inhibited RhoA activity in pancreatic cancer cells injected intrasplenically into nude mice resulted in a reduction in number and size of metastasis in the liver as compared to mice injected with control cells (Kusama *et al*., 2006).

The tropomyosin-related kinase B splice variant 1 (TrkB1) has been associated with RhoA signalling in pancreatic cancer cells, by sequestering RhoGDI and thus activating RhoA. Further downstream activation of ROCK led to an increased invasive phenotype of pancreatic cancer cells. An increase in liver metastasis by TrKB1 overexpression was further observed (Li *et al*. 2009). It has been reported that there is a balance between RhoA activity and Tiam1/Rac1 activation in pancreatic cancer cells. While Tiam1/Rac1 signalling promoted PDAC proliferation and tumour growth via Wnt signalling *in vitro* and *in vivo*, RhoA activation resulted in increased invasion and migration (Guo *et al*. 2013b).

Lysophosphatidic acid (LPA) receptors are common chemotactic regulators and were shown to be expressed in pancreatic cancer cell lines. LPA stimulation resulted

in Ras activity and the marked activation of first RhoA and then Rac-1 (Stähle *et al*., 2003).

Insulin-like growth factor 2 mRNA binding protein 3 (IMP3) has been found to be overexpressed in pancreatic cancer cells and associated with poor prognosis in PDAC. Knock down of IMP3 showed decreased motility, invasion and adhesion of PDAC cells *in vitro*, via RhoA signalling reduction (Pasiliao *et al*. 2015).

Stimulation of PANC-1 pancreatic cancer cells with the glial cell-line derived neurotrophic factor (GDNF) led to a transient activation of RhoA signalling as well as Rac-1 and their respective down stream pathways, including the PI3K/Akt and the Ras-Raf-MAP/Erk pathway. Inhibition of the two pathways stopped GDNF stimulated cancer cell invasion both *in vitro* and *in vivo* (Veit *et al*., 2004). RhoA activity was further shown to be activated by EGFR signalling. Moreover, EGF stimulated ROCK activity as well as that of Erk1/2 and Akt (Nakashima *et al*., 2011).

Elevated RhoA activity and invasion in pancreatic cancer has therefore become a key target with several approaches aimed toward inhibition of these processes. In *p48-Cre* + $KRas^{G12D/+}$ mice treated for 35 weeks with a first generation EGFR inhibitor, a marked reduction in tumour progression and initiation events in the pancreas was recorded. Moreover, reduced levels of protein expression for a number of proteins, including RhoA was observed (Mohammed *et al*., 2010a). Treatment of *p48-Cre* + $KRas^{G12D/+}$ mice with a statin drug, Atorvastatin, showed dose dependent reduction in PDAC, PanIN3 formation and development of primary lesions. Moreover, a variety of genes showed reduced expression, including amongst others RhoA and the PI3K/Akt signalling axis, after prolonged treatment of 35 weeks (Mohammed *et al*., 2012).

Treating PDAC cell lines with cAMP elevating agents resulted in a reduced invasion and migration of these cells. cAMP elevating drugs also hindered TGF-β directed PDAC cell migration and levels of active RhoA amongst other proteins was reduced (Zimmerman *et al*., 2015).

Inhibition of HMG-CoA (3-hydroxy-3-methylglutaryl-conenymeA) with HMG-CoA reductase inhibitors resulted in a reduction in pancreatic cancer cell invasion *in vitro* and liver metastasis *in vivo* following intrasplenic injection. EGF stimulated cancer cell invasion was also blocked *in vitro* by a reduction in RhoA membrane translocation following reductase treatment (Kusama *et al*., 2002).

1.5 FRET biosensors and FLIM

1.5.1 Fluorescence Lifetime Imaging (FLIM)

Fluorescence lifetime imaging microscopy (FLIM) (Lakowicz *et al*., 1992) measures the fluorescent lifetime of a fluorophore, i.e. how fast an electron decays after excitation to be emitted as fluorescence. FLIM is independent of the fluorophore's intensity and concentration as well as the local excitation intensity and detection efficiency. Furthermore it has been demonstrated that FLIM is largely insensitive to moderate levels of photobleaching (Van Munster & Gadella 2004; Chen & Periasamy 2004). The fluorescent lifetime is a unique property of every fluorophore, however, the surrounding environment of a fluorophore can influence this value via e.g.: the pH (Sanders *et al*., 1995) and the temperature (Foguel *et al*., 1992).

Measuring FLIM can be done by either of two approaches: The time domain method using time correlated single photon counting (TCSPC) (O'Connor & Phillips 1984) or the frequency domain method (Jameson *et al*. 1984, Chang *et al*. 2007). TSCPC is performed by the use of a pulsed laser excitation source being split into two beams. One beam excites the sample, while the other triggers a "timer" (Figure 1.4 A). After the detector collects the emission i.e. single photons from the sample, with the detector signal stopping the timer and the recorded event allocated to a time bin. The time-binned signal, quantifying the number of photons in each time interval, is then plotted in a histogram and an exponential decay reconstructed (Figure 1.4 B). The half-life of the decay is called the fluorescence lifetime in nanoseconds measured.

In the frequency method conversely a sinusoidally modulated light source is used. The exaction light is modulated at a frequency of multiple of 10 mHz (Figure 1.4 C). The resulting emission signal will mirror this modulation with a delay in time in the form of a phase shift, and a decrease in the modulation depth. In order to detect this, the intensified camera detection is modulated with the same frequency as the excitation light source. Furthermore, the detector sensitivity is shifted in and out of phase with the emission fluorescence in a pseudorandom order, resulting in the frequency domain FLIM signal. This signal in turn is a function of the phase difference between the excitation light and detected emission for each pixel in the image. In order to accurately determine the correct lifetime, the system needs to be

calibrated at the pixel level with a reference fluorophore, of which the lifetime is known. The lifetime is then calculated by comparing the phase and modulation shift of the sample with the phase and modulation shift of the reference (Figure 1.4 D).

Förster Resonance Energy Transfer (FRET) is another factor that can influence fluorescence lifetime of a fluorophore. When FRET occurs, the lifetime of the donor fluorophore decreases for a population of fluorophores, because the longer lifetimes are removed from the detection signal by FRET. Advantages of measuring FRET via FLIM include the fact that only the lifetime of the donor fluorophore needs to be measured in order to detect FRET (Elangovan *et al*., 2002). In other detection methods of FRET such as ratiometric FRET, both the intensities of the donor and the acceptor fluorophore have to be reported to obtain a read-out. Application of FLIM to measure FRET therefore removes the necessity of recording two fluorophores simultaneously.

Furthermore, FLIM measurements are not intensity dependent, allowing for application of FLIM-FRET in high scattering surroundings such as an *in vivo* imaging setting (Wallrabe and Periasamy, 2005). Again a ratiometric approach is very much dependent on the intensity of the fluorophores used, making it difficult to measure FRET in high scattering surroundings, without the application of rigorous corrections and control read-outs. Eliminating these extra measurements and being intensity independent, FLIM allows for the reliable measurement of FRET in an *in vivo* setting.

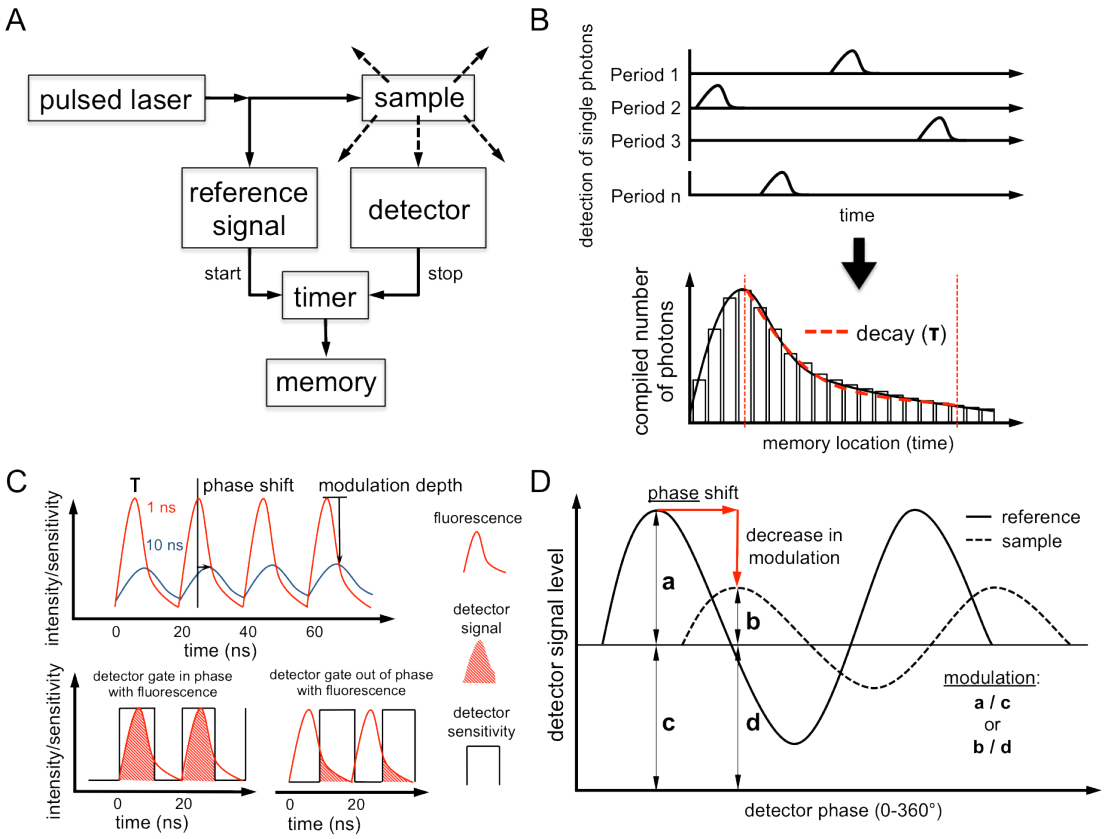

Figure 1.4: Time correlated single photon counting (TCSPC) and frequency domain methods for the determination of fluorescent lifetimes

A Set-up of a TCSPC system and **B** collection and quantification of single photons after excitation of the sample. **C** Frequency domain approach, with phase shifting detection of the modulated emission from the sample (adapted from Borst and Visser, 2010). **D** Frequency domain signals of the reference and sample fluorophores, with the respective shifts in phase and modulation (adapted from Lambert Instruments: http:// www. lambertinstruments. com/ technologies -1/ 2014/ 12/ 4/ frequency- domain- flim- for- beginners).

1.5.2 Förster Resonance Energy Transfer (FRET)

Förster Resonance Energy Transfer is a non-radiative process, that was first described in 1946 (Förster 1946; 1948). The process occurs when molecules are in close proximity to each other, in the order of several nanometres. This in turn is to scale with the size of proteins, their interactions with each other and the thickness of biological membranes. It has therefore been proposed that FRET can be used as a spectroscopic ruler in cells, occurring between a range of 1-8 nm (Stryer & Haugland 1967; Bücher *et al*. 1967). Measuring the distance of either fluorophores or dye-tagged proteins and thus their interaction within cells was further explored (Sun *et al*. 2013; Stryer 1978). FRET can occur when the emission of the donor overlaps with the excitation spectrum of the acceptor (Figure 1.5 A). Upon excitation of the donor fluorophore non-radiative energy transfer occurs when the two molecules are in close proximity of each other. Commonly used FRET pairs in terms of the fluorophores, are represented by cyan fluorescent protein (CFP) paired with yellow fluorescent protein (YFP) and green fluorescent protein (GFP) with red fluorescent protein (RFP). There has further been a great effort invested in optimizing fluorophores in order to increase their photostability, quantum yield as well as their fluorescent lifetimes, making them longer (in ns) and presenting with mono-exponential decays. Useful variants of CFP include: mTFP (Day *et al*. 2008), mCerulean (Rizzo *et al*., 2004) or mTurqouise (Goedhart *et al*., 2010). Similar efforts were undertaken in order to improve the properties of acceptor fluorophores as well, such as for YFP with YPet (YFP for energy transfer). There an increase in FRET was observed compared to normal YFP variants (Nguyen and Daugherty, 2005). Use of dark acceptors lacking an emission signal, such as YFP based super-Resonance-Energy-Accepting Chromoprotein (sREACh) represent further optimization of the FRET pairing of fluorophores (Ganesan *et al*., 2006; Murakoshi *et al*., 2008).

Next to optimal overlapping spectral properties of the donor and the acceptor, FRET can indeed also be influenced by the dipole orientation of the fluorophores to each other within the reporters (Dale *et al*., 1979). FRET is optimal when fluorophores are aligned perfectly parallel to each other and can decrease when this is not the case.

To circumvent this problem one approach has been to use circular permutated fluorescent proteins, changing the order of amino acid sequence in the protein while conserving its overall 3D structure as closely as possible (Klarenbeek *et al*. 2015; Fritz *et al*. 2013).

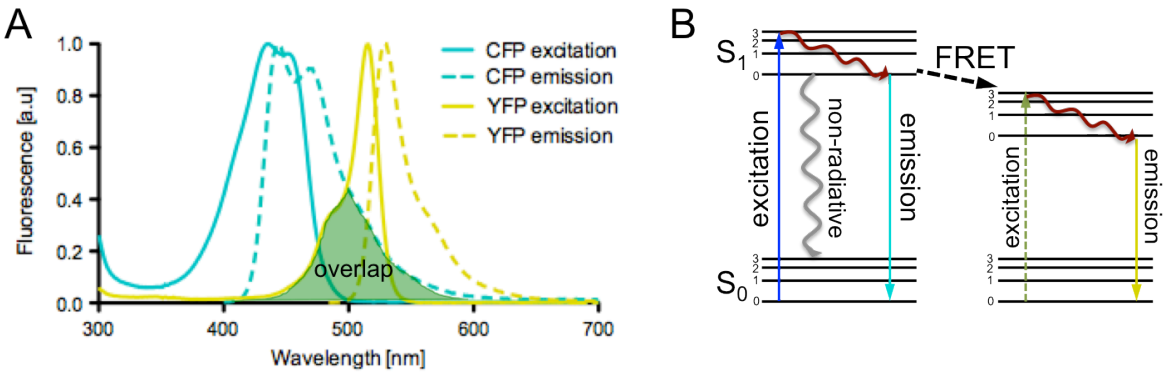

Figure 1.5: Förster Resonance Energy Transfer between CFP and YFP
A Spectral overlap as demonstrated on the frequently used fluorophore pair CFP and YFP, with the emission of CFP overlapping with the excitation of YFP (spectral data taken from http://www.tsienlab.ucsd.edu/Documents.htm). **B** Jabłoński diagram illustrating FRET, with transmission of energy of the excited electrons in the donor over to the acceptor and subsequent fluorescence emission (adapted from Ishikawa-Ankerhold *et al*. 2012).

1.5.3 FRET biosensors

There are a variety of FRET based biosensors that have been described to date. Among these, different kinds of architectures exist, with probes either containing full-length proteins of interest and/or response regions subject to conformational changes upon activation, static membrane association or free cycling on and off the plasma membrane. In this section, the FRET-biosensor probes used to analyse the functionality of the proteins of interest in the subsequent chapters will be introduced.

A FRET reporter able to track spatially defined Src activity within cells was first described by Wang and colleagues in 2005. The biosensor is made up of a donor fluorophore, ECFP, an SH2 domain, a substrate peptide sequence for c-Src derived from p130Cas (WMEDYDYVHLQG) and the acceptor fluorophore YPet. In an unphosphorylated state the probe would assume a FRET conformation with the two fluorphores in close proximity to each other. However, when Src was active

within cells, it would phosphorylate the substrate peptide, resulting in a binding of the substrate peptide region to the SH2 domain and a conformational change in the reporter (Figure 1.6A). This would abrogate FRET and could be antagonized by the action of cellular phosphatases.

It was further shown that there was some activity of Fyn kinase toward the reporter in SYF cells (deficient for Src, Yes and Fyn kinases), when c-Fyn was reconstituted in these cells. Other SFKs displayed negligible responses in terms of FRET on the reporter. The probe responded both to stimulation via EGF, PDGF as well as to inhibition by the Src inhibitor PP1 (Wang *et al*. 2005).

The GTPase Raichu probes were developed previously in order to track the activation of cellular GTPases such as Rac-1, Cdc42 and RhoA at the plasma membrane. To this end, the reporters were tethered to the membrane via a CAAX box of K_t-Ras. The reporters therefore contained the CAAX conjugated donor fluorophore fused to the full-length GTPase, followed by a PAK1 responsive fragment for Rac-1 (Itoh *et al*., 2002) and a protein kinase N (PKN) fragment for RhoA (Yoshizaki *et al*., 2003a) via a flexible linker region. Finally this sequence was followed by the acceptor fluorophore. In the original reporters the FRET fluorophore pair was made up of ECFP and YPet. However, in a second generation reporter for the RhoA probe they were swapped for EGFP and mRFP (Timpson *et al*., 2011a).

In a GDP bound state of the GTPase, the probes would assume an open, non-FRET conformation. Upon the activity of GEFs within the cell, GDP would be exchanged for GTP on the GTPases and they would bind their respective responsive regions within the probe. This would result in a closed and thus FRET conformation of the probes. When the activity of GAPs within the cells would however be prominent, the GTPase part of the reporter would become GDP-bound and the probe once again assume an open conformation (Figure 1.6 B+C).

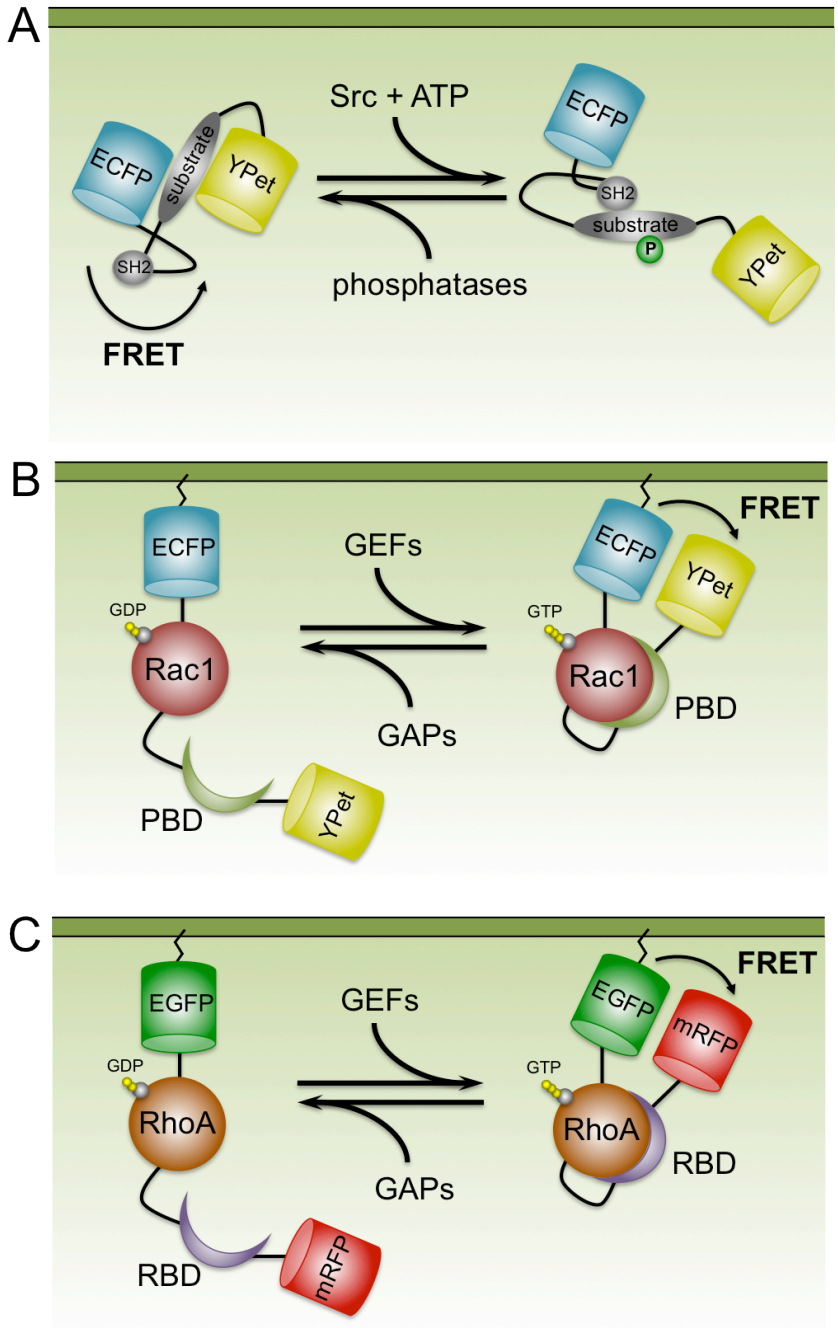

Figure 1.6: Schematics of the FRET biosensors used reporting on Src, Rac-1 and RhoA activity in cells (adapted from Wang *et al.* 2005, Itoh *et al.* 2002 and Yoshizaki *et al.* 2003)

A The Src FRET reporter reacts to phosphorylation by Src, of its p130Cas fragment substrate, resulting in a conformational change of the reporter, hindering FRET. Upon the action of cellular phosphatases the probe assumes a conformational change resulting in FRET (Wang *et al.* 2005). **B** + **C** The Rac-1 and RhoA-Raichu probes are membrane tethered by their donor fluorophore to the membrane by a CAAX motif. Upon the action of GEFs the GTPase bind their responsive regions resulting in FRET. This process is turn is antagonized by the action of cellular GAPs (Itoh *et al.* 2002; Yoshizaki *et al.* 2003).

1.5.4 Multiphoton Imaging

The theory of multiphoton excitation was first introduced in 1931 (Göppert-Mayer, 1931), however, the first functional instrumentation for the application of multiphoton imaging in a biological setting was first described in 1990 by Denk and colleagues (Denk *et al*. 1990). The focal plane is where photon density is the highest. A pulsed laser is needed to achieve such required photon density. Excitation is further limited to the optical section in focus, as excitation by two photons simultaneously outside the focal plane is extremely unlikely. Using a near-infrared excitation source is required as each photon has double the wavelength and therefore half the energy required for excitation of the fluorphore compared to excitation with a conventional visible light source. Near-infrared thus allows for deeper imaging in tissues and avoids scattering to a greater extent than with conventional confocal microscopy. Because multiphoton excitation is confined to the focal volume of the objective, photobleaching outside the focal plane is minimal compared to confocal microscopy and allows for longitudinal imaging without extensive photodamage to the tissue (Centonze & White 1998; Squirrell *et al*. 1999; Helmchen & Denk 2005). Thermal damage due to the near-infrared excitation laser may, however, occur if the sample contains chromophores such as melanin (Liu *et al*. 1994; Pustovalov 1995). Using a femtosecond pulsed excitation source, with a repetition rate of up to 80 mHz, an enhancement of the signal can be achieved (Cox & Sheppard 2004). This is due to the non-linearity of the emission intensity, which works out as being the laser power squared. Furthermore, the excitation source can be modulated to wavelengths ranging from 770 to 880 nm with a Titanium-Sapphire laser, further extendable to reach up to 1600 nm with an optical parametric oscillator (OPO) (Figure 1.7 A). The emission is collected by photomultiplier tubes (PMTs) via a non-descanned detection light path. There is no signal loss due to scattering as observed with confocal microscopy, resulting in deeper imaging depths achievable. Following excitation of the sample, the emitted light is the same wavelength of the corresponding single photon excitation, i.e. in two photon excitation the resultant emission signal is approximately half that of the near-infrared wavelength laser used (Figure 1.7 B). Another advantage of multiphoton imaging is the production of so called second and third harmonic generation signals (SHG/THG) (Freund & Deutsch 1986; Barad *et al*. 1997; Zipfel, Williams & Webb 2003).

These signals allow for the visualization of non-centrosymmetric ordered biological structures such as collagen (SHG) (Zipfel *et al*. 2003) or lipids (THG) (Débarre *et al*., 2006). This results in a non-linear polarization when two photons simultaneously interact with e.g. collagen. SHG and THG do not represent fluorescence but rather the merging of 2 photons of a certain wavelength to a new photon of half that wavelength (Figure 1.7 C). For THG this is in turn 3 photons merging to a photon with a third of the wavelength as the original excitation photons. This again constitutes a non-linear process, like 2-photon excitation, only working at high laser intensities and thus requiring a pulsed laser excitation source.

This endogenous signal has been used extensively in the imaging of collagen I in tissues (Zipfel *et al*. 2003; Mohler *et al*. 2003; Campagnola *et al*. 2002), also in the context of cancer research revealing differential arrangement and amount of collagen I structures in e.g. breast cancer models *in vivo* (Wang *et al*. 2002; Provenzano *et al*. 2009).

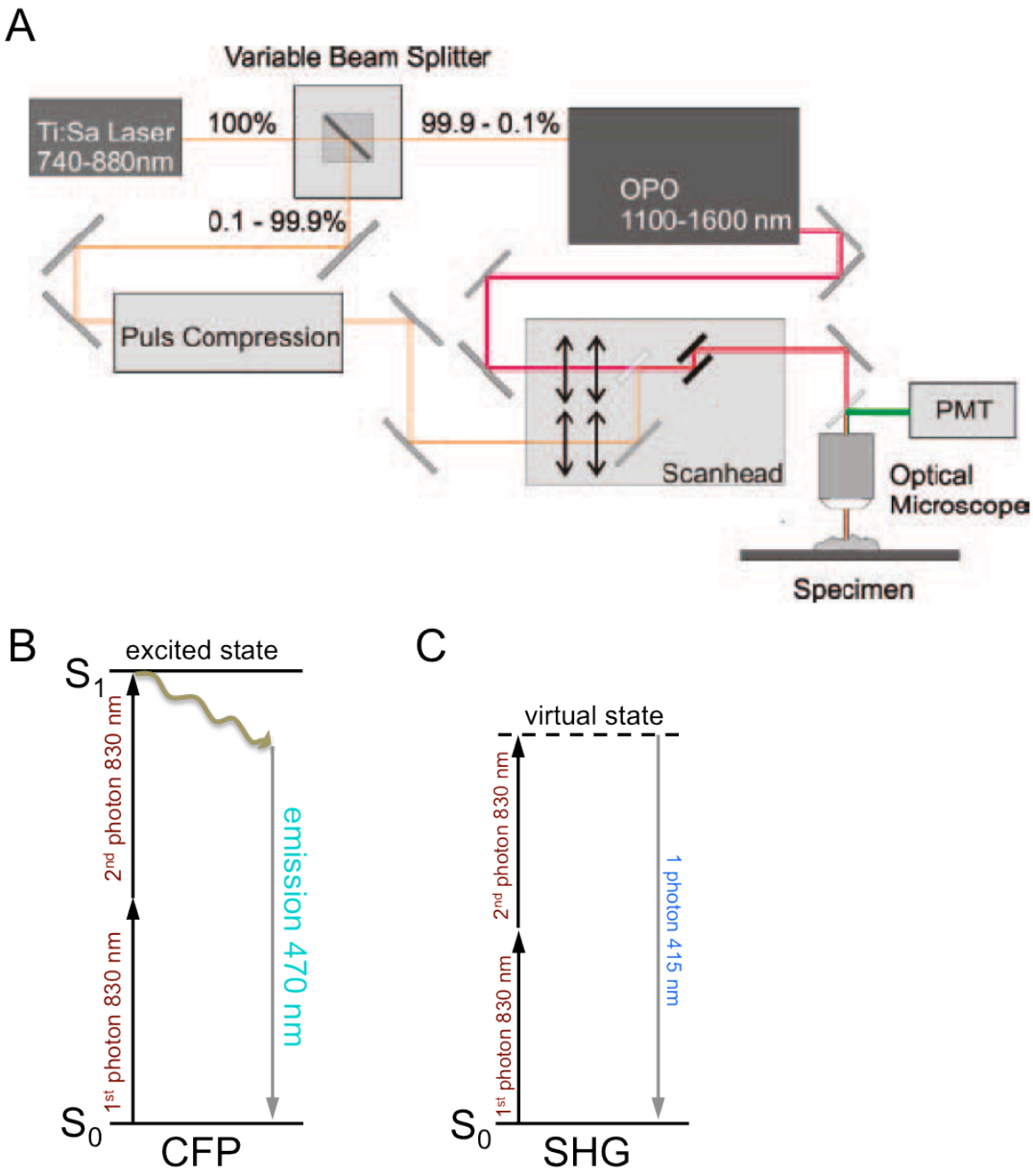

Figure 1.7: Set up of the multiphoton LaVision TrimScope, two photon near-infrared excitation imaging and SHG
A Schematic of the mutliphoton imaging set up, with a Titanium Sapphire (Ti:Sa) laser, variable beam splitter, allowing for imaging with a two tuneable wavelengths simultaneously, 740-880 nm and through the optical parametric oscillator (OPO) 1100-1600 nm. The emission from the sample is collected by photomultiplier tubes (PMTs) (taken from: http://www. lavisionbiotec. com/ files/TriM-Scope-II.pdf). **B** Two-photon excitation of a fluorophore with photons in the near-infrared range of 830 nm, leading to an emission from CFP at 470 nm. **C** Second harmonic generation signal (SHG) leading upon excitation of a non-centrosymmetric structures such as collagen I to a combining of 2 photons of 830 nm in wavelength to one emitted photon of 415 nm (adapted from Provenzano *et al*. 2009).

2 Materials and Methods

2.1 Antibodies, reagents and buffers

2.1.1 Antibodies and reagents

Antibody target	Species	Source	Dilution (Western/IHC)
Src	rabbit	NEB Cell Signaling	1:1000
phospho-Src^{Tyr416}	rabbit	NEB Cell Signaling	1:1000 / 1:200
GFP	rabbit	Abcam	1:1000 / 1:100
Rac-1	mouse	Cytoskeleton	1:1000
Rac-1-GTP	mouse	New East Bioscience	1:1000 / 1:100
RhoA	mouse	Cytoskeleton	1:1000
PAK1	rabbit	NEB Cell Signalling	1:1000 / 1:50
phospho-PAK1^{Thr423}	mouse	Santa Cruz	1:1000 / 1:50
GAPDH	rabbit	NEB Cell Signaling	1:5000
actin	rabbit	Sigma	1:1000
α-tubulin	mouse	Sigma	1:1000
anti-mouse-IgG-HRP	horse	NEB Cell Signaling	1:10000
anti-rabbit-IgG-HRP	goat	NEB Cell Signaling	1:10000
anti-mouse-IgG IRDye®800/680	goat	Lorne	1:10000
anti-mouse-IgG IRDye®800/680	goat	Lorne	1:10000

Reagent	Source	Stock	Final (*in vitro*/*in vivo*)
hEGF	Stem Cell Technologies	20 µg/mL	10 ng/mL
insulin	Roche	20 mg/mL	5 µg/mL
Cholera Toxin	Sigma	100 µg/mL	10 ng/mL
GM-CSF	PeproTech	10 µg/mL	10 ng/mL
EHT 1864	Tocris	50 mM	20 µM/4 mg/kg
NSC 23766	Tocris	100 mM	50 µM/ 4 mg/kg
IPA-3	Tocris	10 mM	10 µM/ 4 mg/kg
Dasatinib	Bristol Meyer Squibb	10 mM	100 nM/ 10mg/kg
Erlotinib	LC Laboratories	10 mg/mL	100 mg/kg
Qtracker®655	Life Techonolgies	2 µM	200 nM

2.1.2 Ripa buffer

Reagent	Source	Final
Tris pH 7.5	Fisher Scientific	50 mM
NaCl	Fisher Scientific	150 mM
SDS	Fisher Scientific	0.1 %
Na-deoxycholate	Sigma	1 %
Inhibitor Cocktail	Calbiochem MERCK	1x
NP 40	Sigma	1 %

2.1.3 Modified Ripa buffer

Reagent	Source	Final
Tris pH 7.5	Fisher Scientific	50 mM
NaCl	Fisher Scientific	150 mM
SDS	Fisher Scientific	0.1 %
Na-deoxycholate	Sigma	0.5 %
Inhibitor Cocktail	Calbiochem MERCK	1x
Triton X-100	Sigma	1 %
NaOrthoP	Aldrich	1 mM
NaF	Sigma	1 mM
PMSF	Sigma	2.85 mM

2.1.4 Inhibitor cocktail composition (Calbiochem MERCK)

Product	MW	1x Concentration	Target Protease
AEBSF, Hydrochloride	239.5	500 μM	Serine Proteases
Aprotinin, Bovine, Lung, Crystalline	6512	150 nM	Serine Proteases and Esterases
E-64 Protease Inhibitor	357.4	1 μM	Cysteine Proteases
EDTA, Disodium	372.2	0.5 mM	Metalloproteases
Leupeptin, Hemisulfate	475.6	1 μM	Cysteine Proteases and Trypsin-like Proteases

2.1.5 Anaesthesia and analgesia

Reagent	Source/Commercial Name	Concentration	Administered
Midazolam	Roche/Hypnovel	1 mg/mL	12 mg/kg
Fentanyl	VetaPharma Limited/Hypnorm	0.3 mg/mL	3.6 mg/kg
Fluanisone	VetaPharma Limited/Hypnorm	10 mg/mL	120 mg/kg
Carprofen	Pfizer/Rimadyl	1 mg/mL	5 mg/kg

2.2 Cell culture and cell line generation

2.2.1 PDAC cells expressing the Src-biosensor

Primary murine PDAC cells were derived from KPC mice and a stable cell line established (Morton *et al*., 2010a). PDAC cells were maintained in complete medium composed of Dulbecco's Modified Eagle Medium (DMEM) supplemented with 10 % FBS, 2 mM L-glutmaine, 100 U/mL penicillin and 100 ug/mL streptomycin (1%) (Gibco). These cells were transfected with ECFP-YPet version of the Src-biosensor (Wang *et al*., 2005b) using polyfectamine as per the manufacturers protocol (Qiagen). Stable pools were generated using standard procedures including the application of 0.6 mg/mL G418.

2.2.2 Isolation of primary mammary carcinoma cell lines

Primary murine mammary carcinoma cell lines from either *MMTV-PyMT* (Guy *et al*., 1992b) or *MMTV-ErbB2/neu* (Her2) (Guy *et al*., 1992b) expressing mice crossed with the Rac-1-FRET mouse (Johnsson *et al*., 2014) were isolated by dissection of primary tumours and washing once in PBS. Tumours were finely minced using 2 scalpels in tandem and placed in a T75 flask with 10 mL of growth factor supplemented medium made up of DMEM with 10 % FBS, 2 mM L-glutmaine, 1 % penicillin/streptomycin (Gibco), 5 µg/mL insulin (Roche), 10 ng/mL EGF (Stem Cell Technologies) and 10 ng/mL Cholera Toxin (Sigma). Cells were allowed to adhere and grow out of bits of tumour for up to 2 weeks. After that, cells were washed rigorously with PBS and passaged up to 10 times in order to obtain immortalized mammary carcinoma cell lines. Stock cells were maintained in the growth factor supplemented medium, while during experimental conditions cells were cultured in normal complete medium.

2.2.3 Isolation of primary neutrophils from bone marrow

Primary neutrophils were isolated from wildtype mice as described previously (Condliffe *et al*., 2005; Damoulakis *et al*., 2014). Tibia and femurs were dissected from mice and washed in Hank's Balanced Salt Solution without $-Ca^{2+}$ and $-Mg^{2+}$

supplemented with 15 mM HEPES and 0.25 % (w/v) endotoxin-free BSA (Sigma) ($HBSS^{--/++}$) and kept on ice. Bone marrow was extracted by flushing the bones with pre-chilled $HBSS^{--/++}$ through a 25 gauge needle. The marrow was then put through a 40 μm cell strainer. 10 mL of pre-chilled 58% of Percoll Plus (with phenol red in HBSS $–Ca^{2+}$ and $–Mg^{2+}$) were aliquoted into a 50 mL falcon tube and the cell suspension carefully layered on top. The gradient was spun at 160 x g for 30 min at 4°C at the slowest acceleration and deceleration settings (Beckman Coulter). The top layer above the Percoll and excess HBSS were discarded and the Percoll fraction containing the neutrophils, just above the pelleted red blood cells, was resuspended in $HBSS^{--/++}$. The suspension was centrifuged again at 330 x g for 10 minutes at 4°C and the Percoll subsequently discarded. Remaining erythrocytes were removed by the addition of Gey's solution (Sigma) for 5 minutes. Subsequently, $HBSS^{--/++}$ was added again to resuspend the pellet and spun again at 330 x g for 10 min at 4°C. The neutrophil pellet was resuspended in 10 μL of $HBSS^{--/++}$ and added atop the respective organotypic matrices.

2.2.4 Isolation of primary dendritic cells from bone marrow

Primary dendritic cells were cultured from the bone marrow of Rac-1-FRET mice (Johnsson *et al*., 2014), as described previously (Lutz *et al*., 1999). Tibia and femurs were dissected from mice and bone marrow isolated by flushing the bones with Roswell Park Memorial Institute-1640 (RPMI) medium, supplemented with 10% FBS, 1% penicillin/streptomycin, 2 mM L-glutamine and 50 μM β-mercaptoethanol (Sigma). The suspension was passed through a 40 μm cell strainer and centrifuged of 1200 rpm for 5 minutes. The pellet was then resuspended in RPMI supplemented as above plus 20 ng/mL of GM-CSF (Peprotech) and seeded at a density of 1 x 10^6 cells per glass bottom dish (MatTek). The cells were allowed to differentiate into primary dendritic cells for up to 9 days with the medium being changed every 3 days.

2.2.5 Generation of lentiviral vectors

Lentiviral vectors were produced using the pLKO.1 TRC cloning vector (Addgene) backbone system in HEK-293T cells as described previously

(Moffat *et al*., 2006). HEK-293T cells were seeded at a density of 2 x 10^6 cells per 10 cm^2 dish. The following day the cells were transfected using the calcium phosphate system with helper plasmids encoding for viral envelope glycoprotein VSV-G in pMD2.G and packaging proteins gag, pol, rev and tat in psPAX2 and the pLKO.1 with the specific hairpin sequences targeting murine TRAIL-R2 sh23 5'-CCGG-GCTCT TCAGTATTATGAGAAT- CTCGAG- ATTCTCATAATACTGAAGAGC-TTTTT-3' (TRCN0000012323) (Sigma) and sh25 5'-CCGG- GCTCTTCAGTATTATGA GAAT-CTCGAG-ATTCTCATAATACTGAAGAGC-TTTTT-3' (TRCN0000012325) (Sigma). On the third day, the medium was replaced on the transfected cells with 6 mL of DMEM, 20 % FBS, 2 mM L-glutamine and 1 % penicillin/streptomycin. On the same day recipient PDAC cells were seeded at a density of 1 x 10^5 cells per well in a 6 well dish. After overnight incubation viral particles were harvested, passed through a 0.45 μm filter and added to the PDAC cells supplemented with 10ng/mL polybrene. 6 mL of fresh medium was added to the transfected HEK-293T cells and the infection process repeated a second round. After this the medium containing viral particles was removed and PDAC cells were selected to generate stable pools using 10 μg/mL of puromycin.

2.2.6 Collagen extraction from rat tail tendons

Collagen I was extracted from rat tail tendons as described previously (Chandrakasan *et al*., 1976; Rhodes and Miller, 1978; Timpson *et al*., 2011b). 12 to 14 adolescent rat tails were used either fresh or frozen (at -70°C) and washed in 70 % ethanol. Using a scalpel the skin was removed by slicing down the middle of the tail from top to bottom. The tendons were then detached from the proximal region of the tail (about 1 cm from where the tail was cut) by the use of teethed forceps and further removed down the length of the tail. The extracted tendons were then placed in 1.5 L of pre-chilled 0.5 M acetic acid for the duration of 48 h at 4°C in order to solubilize the collagen. The extract was then centrifuged at 7500 x g for 30 min and any pellet discarded. The supernatant was collected in a pre-chilled beaker and precipitated by the addition of 10 % (w/v) NaCl, under stirring for 60 min at 4°C. The precipitate was centrifuged again at 10,000 x g for 30 minutes and the supernatant discarded. The pellets were again collected in a pre-chilled beaker and resolubilised at 4°C using cold 0.25 M acetic acid for 24 h under stirring. Dialysis of the extract was

performed using BioDesignDialysis Tubing™ (14,000 MWCO, Fisher Scientific). 30 cm of tubing was soaked in heated H_2O and heated prior to being filled with the extract. Avoiding bubbles, the tubing was closed by knots. The collagen solution was dialysed for 3 - 4 days in 5 L of 17.5 mM acetic acid, changed twice daily. On the final day the solution was removed from the tubing and centrifuged for 1.5 h at 30,000 x g at 4°C to remove any residual debris. The viscous supernatant was put into a sterile glass tissue culture bottle and adjusted to a final concentration of about 0.5 mg/mL using 0.5 mM acetic acid. The collagen I solution was then kept at 4°C until use for organotypic assay analysis.

2.2.7 Organotypic Culture

Organotypic invasion assays were preformed as described previously (Timpson *et al*., 2011b). Either primary human fibroblasts or mCherry expressing telomerase immortalized foetal fibroblast cell lines (TIFF) (Munro *et al*., 2001) were embedded at a density of approximately 1 x 10^5 cells/mL in a matrix of rat tail collagen I. The matrix with the embedded fibroblasts was allowed to polymerize overnight, then detached from the edges of 35 mm petri dishes and supplemented with 2 ml of DMEM containing 10 % FBS, 2 mM L-glutamine and 1 % penicillin/ streptomycin. The matrices were allowed to further contract for about 7-14 days to a final size of around 1.5 cm in diameter. They were then transferred using sterile forceps to 24-well plates and seeded with cells of interest at a density of 5 x 10^4 or 1 x 10^5 cells per well. The cells were then allowed to grow to confluence for up to 3 days. Subsequently, the matrices were mounted on a metal grid resulting in an air/media interface, in which the matrices are fed from below with complete medium. This was changed every 2 days. Cells were allowed to invade for up to 12 days and drug treated matrices were treated up to 2 days prior to imaging with 100 nM dasatinib or every 2 days with the respective Rac-1 inhibitors. After the invasion period, the individual matrices were either imaged or fixed in 4 % paraformalehyde and processed using standard techniques for haematoxylin and eosin (H&E) staining by internal Histology Services.

2.2.8 Immunoblotting

Cells of interest were seeded at a density of 2 x 10^5 cells per well in a 6 well dish, drug treated the following day and harvested at the appropriate time points after treatment. The cells were put on ice, washed once with PBS and then lysed in RIPA buffer (2.1.2). Tissue samples we dissected from mice and snap frozen on dry ice. Following thawing, the samples were suspended in modified RIPA buffer (2.1.3). The tissue samples were lysed using a tissue homogenizer (Precellys®24) and ceramic beads (Precellys® Lysing Kit). Cell lysates and tissue protein extracts were spun down at 13,400 rpm for 15 min at 4°C and subsequently run on a 4 % to 12 % Bis-Tris acrylamide SDS-PAGE gel (NuPAGE®). The proteins were then transferred on to a nitrocellulose membrane, blocked with 5% BSA in TBST and incubated for one hour or overnight at 4°C on a shaker with 1:1000 anti-phospho-Src^{Tyr416}, (NEB Cell Signalling), 1:2000 anti-GFP ab290 (Abcam), 1:1000 anti-Src (NEB Cell Signalling), or 1:1000 anti-actin (Sigma), respectively. The next day the membrane was incubated with either anti-mouse or anti-rabbit horseradish peroxidase-conjugated (NEB Cell Signalling) or IRDye® 680LT and IRDye® 800CW (Licor) secondary antibody at 1:10000 and visualized using enhanced chemiluminescence (ECL) (Amersham) and the Odyssey® CLx Imager (Licor).

2.3 Mice

2.3.1 Genetically engineered mouse model breeding

Animals were kept in conventional animal facilities and all experiments were carried out in compliance with UK Home Office guidelines. Mice were kept on a 12 hour day-night cycle and fed ad libitum. Rac-1-FRET mice (Johnsson *et al*., 2014), where the lox-stop-lox (LSL) site was removed previously by a deletor-CRE, were crossed with PyMT (Guy *et al*., 1992b) or ErbB2 (Guy *et al*., 1992a) expressing mice on a mixed background to obtain homozygous expression of the FRET reporter in the F2 generation. Rac-1-FRET mice still retaining the LSL were crossed with KPC mice, rendering expression of the FRET reporter in Pdx-1 linage cells, mainly in the pancreas, but also liver, duodenum and the haematopoietic system.

In order to examine the effect of P-Rex1 knock out on Rac-1 signalling in these model systems, the previously generated P-Rex1 KO (Welch *et al*., 2005) mice were crossed with the PyMT, ErbB2 and KPC described above. The newly generated RhoA mouse was crossed with a deletor-CRE, which was later crossed out again, in order to remove the LSL site and analyse RhoA activity in a variety of tissues. This mouse was further crossed to the Her2 model. The LSL retaining RhoA-FRET mouse in turn was crossed with *MMTV-Cre* (Andrechek *et al*., 2000) and PyMT and put through 1-2 rounds of gestation in order to induce expression of the FRET reporter. In order to look at RhoA signalling in different stages of PDAC progression the RhoA mouse was crossed to *Pdx1-CRE* mice and the KPC model.

2.3.2 Generation of the RhoA FRET mouse

The conditional RhoA reporter mouse was generated by David Stevenson at the CRUK Beatson Institute. Briefly, a modified RhoA-Raichu probe (Yoshizaki *et al*., 2003b) was used, expressing the fluorophore pair EGFP and mRFP (Timpson *et al*., 2011a). The final targeting vector was generated as described previously by targeting a lox-stop-lox transgene under the control of a CAGSA promoter to the HPRT locus (Bronson *et al*., 1996; Samuel *et al*., 2009; Schachtner *et al*., 2012). The conditional strain was then crossed with a strain expressing a X-chromosomal *Cre* recombinase (Schwenk *et al*., 1995) to allow for ubiquitous expression of the reporter and the *Cre* later crossed out again. Homozygous offspring were healthy, fertile, exhibited no abnormal behavioural defects and followed the expected Mendelian ratio of hereditary transmission.

2.3.3 Immunohistochemistry

Immunohistochemistry was preformed as described previously (Morton *et al*., 2010b). Briefly, formalin-fixed (10 %) and paraffin-embedded tissue or organotypic sections were deparaffinised in xylene and subsequently rehydrated in a graded alcohol series. Antigen retrieval was preformed using microwave heated 1 mM EDTA buffer for 20 minutes. Quenching of endogenous peroxidases was carried out using 3 % hydrogen peroxide. The sections were blocked in 5 % goat serum in PBS + 0.05 % Tween20 for 30 min and afterwards incubated overnight at 4°C with a dilution

of 1:200 of the primary antibody anti-pSrc^{Tyr416} (Cell Signaling Technologies). The next day, the sections were incubated with the secondary biotinylated anti-rabbit IgG antibody for 30 min and amplified using avidin/biotin conjugated with HRP mix (Vectastain ABC System). Visualization by 3,3'-diaminobenzidine chromogen (DAB) was carried out as well as counterstaining with hematoxylin.

2.4 Intravital and *In vivo* Imaging

2.4.1 Intravital imaging using skinflaps

Intravital imaging was preformed as described previously (Nobis *et al*., 2013; Timpson *et al*., 2011a). Following trypsinization, 1 x 10^6 cells were resuspended in 100 µl HBSS (Gibco) and subcutaneously injected into the rear flank of a CD1$^{-/-}$ nude mouse. Tumours were then allowed to develop for 7 days. Mice were subsequently treated 3 days with daily gavages of 10 mg/kg dasatinib. To permit imaging, mice were non-recovery anaesthetized using an intraperitoneal (i.p.) injection of 300 µL of an anaesthetic combination of 1:1:3 hypnorm - hypnovel - H_2O. Following induction of anaesthesia the subcutaneous tumour was surgically exposed and the mouse restrained on a 37ºC heated stage for imaging on the multiphoton microscope.

2.4.2 Cutaneous and Abdominal Imaging Windows Surgeries

The application of optical imaging windows in *in vivo* imaging and their implantation into either the skin (Kedrin *et al.*, 2008; Gligorijevic *et al*., 2009; Zomer *et al*., 2013) or in the peritoneal wall (Ritsma *et al*., 2012, 2013) were described in detail previously. Prior to the surgeries and 1 – 2 days afterwards the mice were kept on 5 mg/kg of the analgesic Carprofen (Rimadyl) (Ingrao *et al*., 2013) in the drinking water. To the titanium window ring to be used, a glass coverslip with a diameter of 12 mm was glued with cyanoacrylate on top a day prior to the surgery. For both surgeries the incision site was cleared of hair by shaving and depilation and disinfected with 70 % ethanol. For the cutaneous imaging windows, an incision was made in the skin overlying the palpable primary developed tumour. For the abdominal imaging windows the incision was placed down the midline of the peritoneum for imaging of the small intestine or to the left of the midline of the mouse for the imaging

of the pancreas or KPC tumours. After blunt dissectioning of the skin surrounding the incision, a purse string suture (Mersilk, non-absorbable silk based) was placed either through the skin alone (for the cutaneous imaging window) or though the skin and muscle of the abdominal wall (for the abdominal imaging window). This creates a continuous suture around the incision site, with four loops exposed to the outside for later tightening. In order to avoid peristaltic and respiration-associated movement of the organs to be imaged in the peritoneum, a drop of cyanoacrylate was place at the inner ring of the abdominal imaging windows and the organ of interest immobilized at the edge. Positioning was done using sterile cotton gauzes. The respective windows were then inserted into the incisions with the skin alone or in conjunction with the muscle layer placed in the groove of the windows. Finally the suture was tightened and firmly tied of at the ends. The mice were allowed to recover from the surgery up to 2 days, actively foraging, grooming and feeding within minutes after being removed from the anaesthesia respirator.

2.4.3 *In vivo* Imaging

After transfection of PDAC shCtr and shTRAIL-R2 (sh23 and sh25) cell lines with a GFP and RFP version of the Rac-1-FRET reporter (Mack *et al*., 2012) and selection for stable expression with neomycin, 2 x 10^6 cells were subcutaneously injected into the flanks of nude mice. The same was done for PDAC cells expressing the Src-biosensor. Following primary tumour development of 7-8 days a cutaneous imaging window described previously (Zomer *et al*., 2013) was surgically implanted on top of the tumours as described above. The same was done once PyMT and ErbB2 mice expressing either the Rac-1 or RhoA FRET reporter had developed primary tumours. For KPC mice and WT mice expressing the RhoA reporter under the *Pdx1-CRE* the abdominal windows were surgically implanted into the peritoneal wall of the mice. Imaging was performed through the optical window at regions away from the fixed part of the tissue. For drug treatments, mice were gavaged with either 10 mg/kg dasatinib, 100 mg/kg erlotinib, or injected i.p. with 4 mg/kg of either EHT 1864 or NSC 23766. Mice were subsequently imaged for up to 2 h at a time or at several timepoints after treatment was administered on a 37°C heated stage under isoflurane, using the system described below (2.5.2, Figure 1.7 A).

For treatment of mTRAIL KO PDAC subcutanoues tumours, mice were imaged prior to, and 1 h post i.p. injection of either PBS or 0.5 mg/mouse of mTrail-Fc-R2. In order to visualize the local vasculature mice were intravenously injected with 200 µL of Quantum Dots Qtracker®655 (2 nM) prior to intravital or *in vivo* imaging.

2.5 Microscopy

2.5.1 Frequency Domain FLIM-FRET

Widefield fluorescence lifetime microscopy (FLIM) measurements were conducted on a Nikon Eclipse TE 2000-U microscope equipped with a ×60 objective and a filter block consisting of a 436/20 excitation filter, a T455LP dichroic mirror, and a 480/40 emission filter, using a Lambert Instruments LIFA system. Frequency domain FLIM-FRET was performed as described previously (Nobis *et al*., 2013) (Figure 1.4 B + C). Briefly, a modulated 445 nm LED was used as light source and fluorescein (10 µM in 0.1 M Tris-Cl, pH >10) as reference standard with a known lifetime of 4.0 ns. The donor lifetime (ECFP), τ, was analyzed using the LI-FLIM software (version 1.2.12; Lambert Instruments, Netherlands) recording the phase lifetime of ROIs comprising individual cells.

Spinning disk FLIM was performed using a Nikon Eclipse TE 2000-U microscope with a Lambert Instruments LIFA attachment equipped with a Yokogawa CSU 22 confocal scanner unit and a ×100 1.4 NA oil objective. FLIM-FRET for the GFP donor was measured as described previously (Mack *et al*., 2012). A 488 nm laser modulated at 40 mHz (60 mW, Deepstar, Omicron) was used together with a GFP-filterblock (470/40X, T495LP, 525/50M) to detect GFP emission. Erythrosin B (1 mg/mL) was used as a reference standard with a known lifetime of 0.086 ns. Donor lifetime was analysed by manually drawing ROIs around whole cell membranes using the LI-FLIM software.

2.5.2 Multiphoton TCSPC FLIM-FRET

Intravital and *in vivo* imaging was performed as described previously (Timpson *et al*., 2011b; Nobis *et al*., 2013), on a Nikon Eclipse TE2000-U inverted microscope with an Olympus long working distance 20× 0.95 NA water immersion

lens. A Titanium:Sapphire femtosecond pulsed laser (Chameleon) was used as an excitation source tuned to optimal EGFP and ECFP excitation wavelengths of 890 nm and 840 nm, respectively. A dichroic filter (Chroma 475 nm or 455 nm) was used to separate the second harmonic signal from the donor EGFP or ECFP. SHG, EGFP and ECFP signals were passed through band pass filters (Semrock 435/60, 525/50 and 460/60 respectively) and detected by non-descanned detectors (Hamamatsu). For FLIM a 16-anode PMT (FLIMx16, LaVision Biotec) was used for time correlated single photon counting (TSCPC). Fluorescent lifetimes were analysed using ImSpectorPro (Version 292, LaVision Biotech) by drawing ROIs around single cells and recording the half-life (τ) of the single exponential function fit to the fluorescence decay data. Lifetime values for multiple cells were then entered into Excel and the mean as well as the standard deviation calculated. Lifetime maps were further generated with intensity thresholds set to the average background pixel value for each recording. The raw data was smoothed 3 x 3 and a standard rainbow colour look up table (LUT) applied with a 1.5 to 3.5 ns limit for ECFP measurements and 1.0 to 3.0 ns for EGFP. Src activity was displayed by yellow to red colours, while green to blue represented Src inactivity. However, due to the different nature of the Raichu probes (see Chapter 1.4.3 FRET biosensors), Rac-1 and RhoA activity are displayed by green to blue regions and their respective inactivity by yellow to red colours in the lifetime maps. Areas where no lifetime measurement above the background noise could be achieved were displayed in black. Finally, for smoothing purposes, a 5 x 5 median or 3 x 3 mean filter was further applied.

2.6 Statistics

Statistical analysis of the data was performed using Graph Pad Prism v 5.0. Either unpaired, two-tailed student's *t*-test or one-way ANOVA analysis were applied, as indicated in the respective figure legends. Unless otherwise stated a minimum of 3 independent experiments were performed for each experiment. Statistical significance was defined as groups with a confidence interval of above 95 %, i.e. $p < 0.05$.

3 Drug targeting efficiency of the Src inhibitor Dasatinib monitored live by *in vivo* imaging

3.1 Summary

The aim of this chapter was to establish FLIM-FRET as an *in vivo* imaging tool for the analysis of drug pharmacodynamics over time and in the context of the local tumour microenvironment. To that end, a previously established Src inhibitor, dasatinib (Lombardo *et al*., 2004; Morton *et al*., 2010b), was used in cells isolated from an invasive PDAC model, which in turn has previously been shown to have upregulated Src activity. Further stable expression of a Src-FRET biosensor (Wang *et al*., 2005a) in these cells, then allowed for the live monitoring of Src activity. This was done on 3D invasion matrices as well as in primary allograft tumours. Using intravital imaging, treatment with dasatinib, the ECM remodeller cyclopamine, as well as combination treatment of the two was followed. This revealed the spatial distribution of Src activity with respect to the local vasculature in the control situation, as well as a spatially confined effective inhibition after treatment. Employing cutaneous imaging windows further allowed for *in vivo* imaging of a CXCR2 inhibitor, showing Src inhibition in spatially distinct regions away from the vasculature.

3.2 Introduction

Inefficient drug targeting *in vivo* still remains a large challenge in the treatment of many types of cancer (Kola and Landis, 2004), with 16 % of Phase I clinical trial drugs still failing due to their poor pharmacokinetics and bioavailability (Waring *et al*., 2015). Therefore, in order to increase effective drug delivery, more innovative approaches to monitor drug targeting in live tissue at a molecular level are needed. The role of the tumour microenvironment is important in drug targeting and thus analysing treatment regimens for cancer in this context is vital. Intravital imaging can be used as a tool to address this need. The technical read-outs of protein activity on a cellular level provides a context dependent signal in both 2D and 3D

environments *in vitro* as well as *in vivo*. Furthermore, a temporal aspect of drug delivery can be examined in the readily treatable *in vitro* situation as well as the more complex *in vivo* setting that is subject to different environmental cues influencing protein activity. FLIM-FRET in this context can provide a strong tool to link the *in vitro* to the *in vivo* drug response data, as the same biosensor read-out is used and assay differences can be avoided. The PDAC tumour microenvironment in particular is characterized with low vascularity as well as dense accumulation of ECM components in the large stromal compartment, leading to especially poor drug targeting efficacy (Vincent *et al*., 2011; Jacobetz *et al*., 2013).

Therefore here, cells were used from a primary tumour developed from the KPC ($KRas^{G12D}$, $p53^{R172H}$, *Pdx1-Cre*) mouse model (Morton *et al*., 2010a), which has been shown previously to accurately recapitulate the observed histophathlogy of human disease (Hingorani *et al*., 2005; Hruban *et al*., 2006). In human pancreatic cancer, point mutations in the *KRas2* proto-oncogene are present in over 90 % of the cases. Furthermore, point mutations in the *TP53* tumour suppressor gene were identified in over 75 % of pancreatic cancers, along with other deletions and mutations of different genes to a lower extent (Almoguera *et al*., 1988; Pellegata *et al*., 1994; Sohn and Yeo, 2000). Expression of these two specific mutations in a mouse model driven by the pancreas lineage specific Pdx1-Cre promoter, has been shown to result in invasive progressive PDAC by chromosomal instability and metastasis of the liver, as observed in human PDAC (Hingorani *et al*., 2005). Furthermore, this model has been used previously in the assessment of treatment response (Olive and Tuveson, 2006) in PDAC. The KPC model has additionally been shown to have up-regulated Src activity, that could be effectively inhibited with a Src inhibitor, dasatinib, *in vitro* and *in vivo* (Morton *et al*., 2010b). Alteration in Src activity in turn has been shown to be associated with invasive tumour cell behaviour by deregulating cellular adhesions (Lutz *et al*., 1998; Frame, 2002), seen in a variety of pancreatic cancers (Hakam *et al*., 2003b). Src and phospho-Src levels have further been shown to be important indicators of prognosis in human PDAC, lymph node and vascular invasion (Morton *et al*., 2010b).

The anti-metastatic activity of dasatinib could potentially be improved by a combination treatment with tumour stroma targeting agents, thereby modulating the microenvironment to be more permissive to specific drug targeting (Yu and Tannock, 2012).

A key defining feature of the pancreatic cancer microenvironment is the dense deposition of extra-cellular matrix (ECM) components, such as e.g. collagen or hyaluronan by cancer associated fibroblasts and stellate cells (Toole, 2004; Toole and Slomiany, 2008). High desmoplasia of pancreatic tumours in turn leads to a high interstitial pressure in these tumours, inducing vascular collapse. This results in a barrier to perfusion and diffusion and can greatly hinder drug targeting response. Breaking down these physical barriers by enzymatic targeting of e.g. hyaluronan, led to an increased drug perfusion in these tumours and increased drug response to common chemotherapeutics (Provenzano *et al*., 2012).

A G-protein-coupled cell surface chemokine receptor, CXCR2, has also been found to be overexpressed in pancreatic cancer (Wang *et al*., 2013) and further identified to be crucial for neutrophil movement. CXCR2 has therefore been considered as another important target in the crosstalk between PDAC and its microenvironment (Hertzer *et al*., 2013).

In order to more accurately monitor treatment response *in vitro* and *in vivo* we wanted to explore, whether a FRET biosensor for Src could be utilized in the introduced context of pancreatic cancer and Src signalling. Furthermore we wanted to test whether temporal and spatial evaluation of drug targeting efficacy was feasible using FLIM-FRET *in vitro* and in allograft tumours *in vivo*. Finally the possibility of monitoring combination treatments targeting Src and the ECM of allograft tumours in the context of the tumour microenvironment was explored.

To address these questions, the Src-FRET biosensor, previously described (Wang *et al*., 2005b) (see Chapter 1.4.3 Figure 1.6 A) to report on activation states of Src, was used as a pre-clinical imaging tool to monitor Src activity of PDAC cells in native 3D environments over time and in response to different treatment regimens *in vitro* and *in vivo*.

3.3 Results

3.3.1 Characterization of the Src-biosensor in PDAC cell lines

PDAC cells isolated previously from KPC mice (Morton *et al*., 2010a) were stably transfected with a ECFP-YPet version of the Src-FRET biosensor (Wang *et al*., 2005b) (Figure 3.1 A). Expression was controlled for by immunoblotting for GFP, with an expected molecular weight of the reporter at ~ 70 kDa (Figure 3.1 B). The probe consists of the two fluorophores ECFP and YPet, between which a peptide sequence of the Src substrate p130cas and the SH2 domain is located. The mode of action of the Src-biosensor depends on fluorescence resonance energy transfer (FRET). FRET involves energy transfer from a donor to an acceptor fluorophore, providing the two are within a ~ 5 nm distance of each other. When the Src substrate p130cas is phosphorylated within the cell, the probe undergoes a conformational change, which pushes the two fluorophores apart to a distance greater than 5 nm and thus impeding FRET. The conformational change of the probe is therefore based on the differential affinity of the SH2 domain to the phosphorylated and non-phosphorylated forms of the p130cas peptide. The probe is further targeted by cellular phosphatases antagonizing Src phosphorylation. Thus, when kinase activity is dominant over that of phosphatases the probe will be phosphorylated and there will be no FRET. However, under conditions where the phosphatase activity dominates the probe will be non-phosphorylated and react by juxtaposition of the two fluorophores to one another resulting in FRET. Using FLIM, the lifetime of the donor fluorophore ECFP was measured, which decreases upon FRET. The fluorescence lifetimes in turn are presented as lifetime heat maps, with a scale ranging from 1 ns to 3.5 ns. Low lifetimes and consequently Src inactivity are displayed in cold colours, such as blue and green, while higher lifetimes, and therefore Src activity, are mapped in warm colours ranging from yellow to red. Areas with low signal to noise ratio, where lifetimes could not be recorded, are coloured in black (Figure 3.1 C).

First, the dynamic range of the biosensor and its behaviour in the cells of interest had to be established. The PDAC cells were therefore subjected to dasatinib treatment *in vitro* at the previously established inhibitory concentration of 100 nM (Morton *et al*., 2010b), in order to establish the FLIM lifetimes acquired as an accurate read-out of Src activity in these cells. Indeed, once a histogram of the lifetimes

recorded from individual cells was made, it became apparent that there was a normal distribution of lifetimes. In control cells the distribution of lifetimes ranged from 2.2 ns up to 2.8 ns and a peak was observed in the frequency of occurrence between 2.4 and 2.5 ns. In dasatinib treated cells this distribution shifted toward shorter lifetimes, ranging from 1.9 ns up to 2.7 ns with a peak between 2.2 and 2.3 ns (Figure 3.2 A). This shift enabled us to define a cut-off value at 2.35 ns in order to classify cells as either "active" for Src at lifetimes above 2.35 ns or "inactive" at respective lifetimes below 2.35 ns. This classification scheme, then allowed for quantification of the percentage of individual active and inactive within a population in each treatment condition. A shift from 88.2 ± 3.4 % to 16.7 ± 7.1 % in the active cell population was thus observed after treatment of the cells with dasatinib for 2 hours (Figure 3.2 B). Finally, this classification allowed us to accurately evaluate Src activity in the following experiments *in vitro* and *in vivo*.

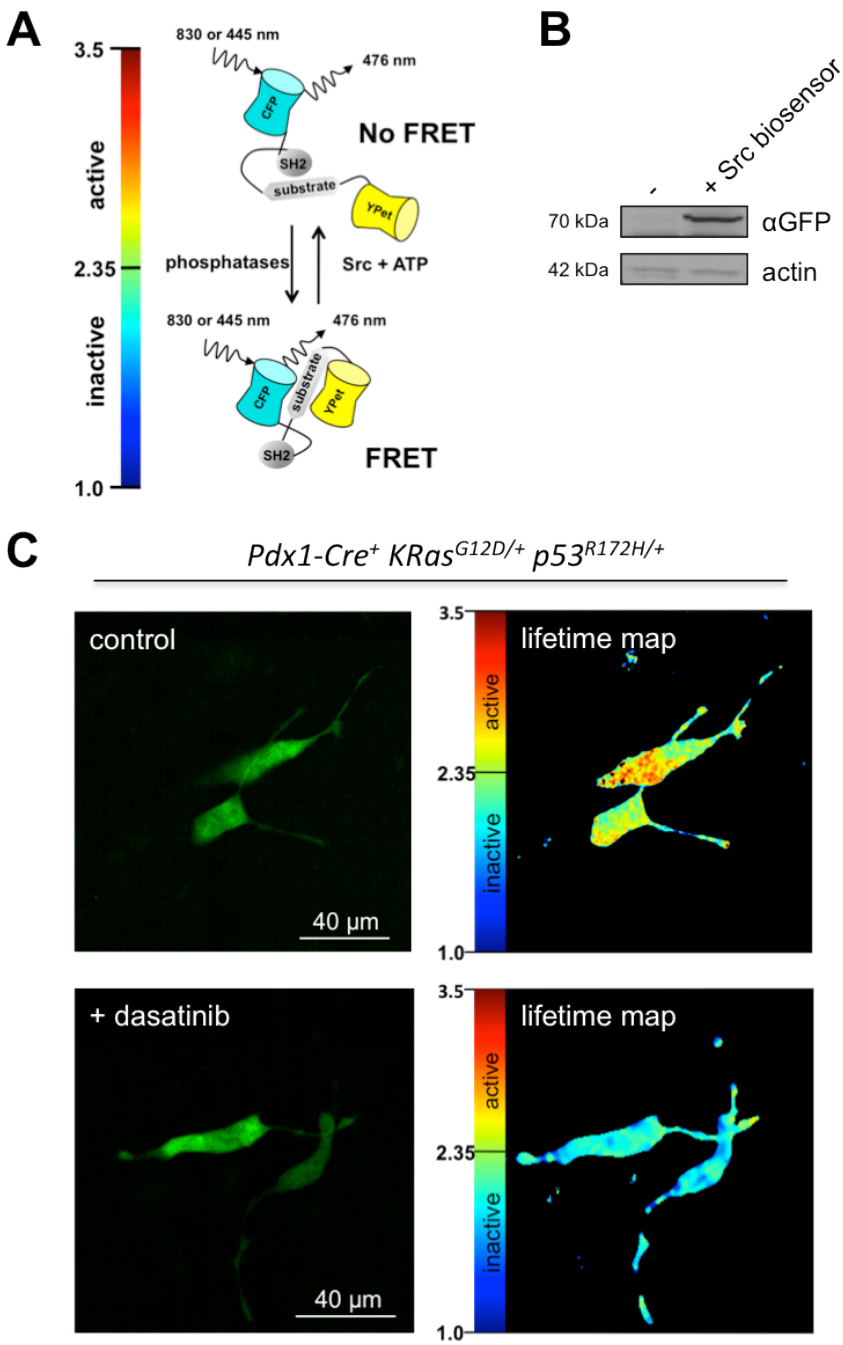

Figure 3.1: Establishment of a stable cell line expressing the Src-FRET-biosensor in PDAC cells

A Schematic representation of the Src-biosensor (as adapted from Wang *et al*. 2005), with the FRET probe in the confirmations resulting in active/inactive lifetimes, respectively, following Src acitivty. The lifetime colour map scale is associated with either active (yellow to red) or inactive (blue to green) lifetimes after the action of Src phosphorylation or cellular phosphatases on the p130Cas substrate region. **B** Immunoblot of PDAC cells stably expressing the Src-biosensor, detected by a positive GFP band at ~ 70 kDa, the expected molecular weight of the expressed biosensor. **C** Representative intensity (left panel) and lifetime map images (right hand) of the PDAC + Src-biosensor cell lines challenged with 100 nM of dasatinib for 2 hours *in vitro*

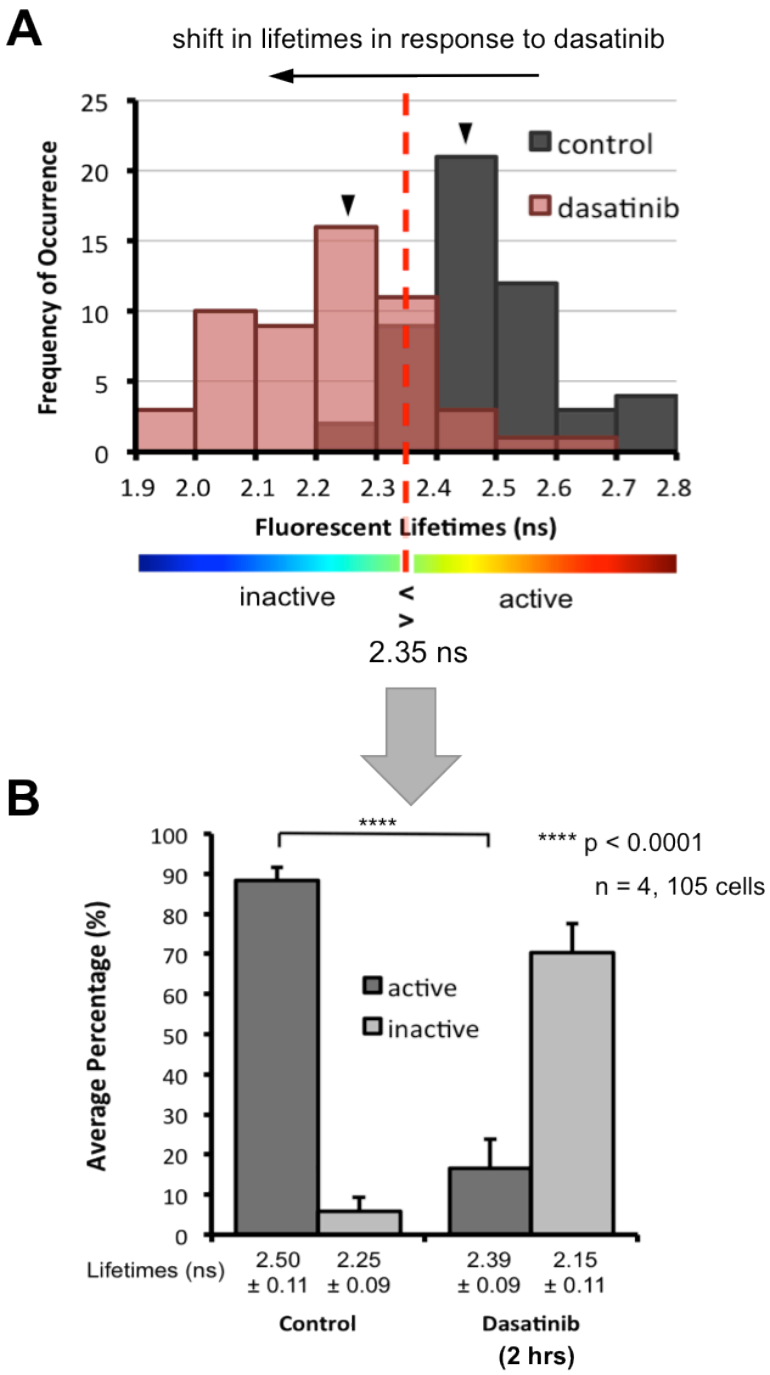

Figure 3.2: FLIM of dasatinib treated PDAC cells reveals a distinct distribution and cut off value of Src-FRET lifetimes *in vitro*

A Quantification of a distinct shift in lifetime distribution of Src activity *in vitro* after treatment of PDAC cells for 2 hours with 100 nM of dasatinib. With a bin size of 0.1 ns, a cut-off value at 2.35 ns was chosen for grouping cells displaying either Src "activity" or "inactivity" based on the distribution peaks for both groups. **B** Representation of the data from A, with lifetimes classified as "active" or "inactive" in terms of Src activity, with the average lifetimes per group displayed below each column ± the SD; n = 4 independent experiments with 105 cells in total; columns: mean; error bars: SEM; **** $p < 0.0001$ by unpaired standard student's *t* test

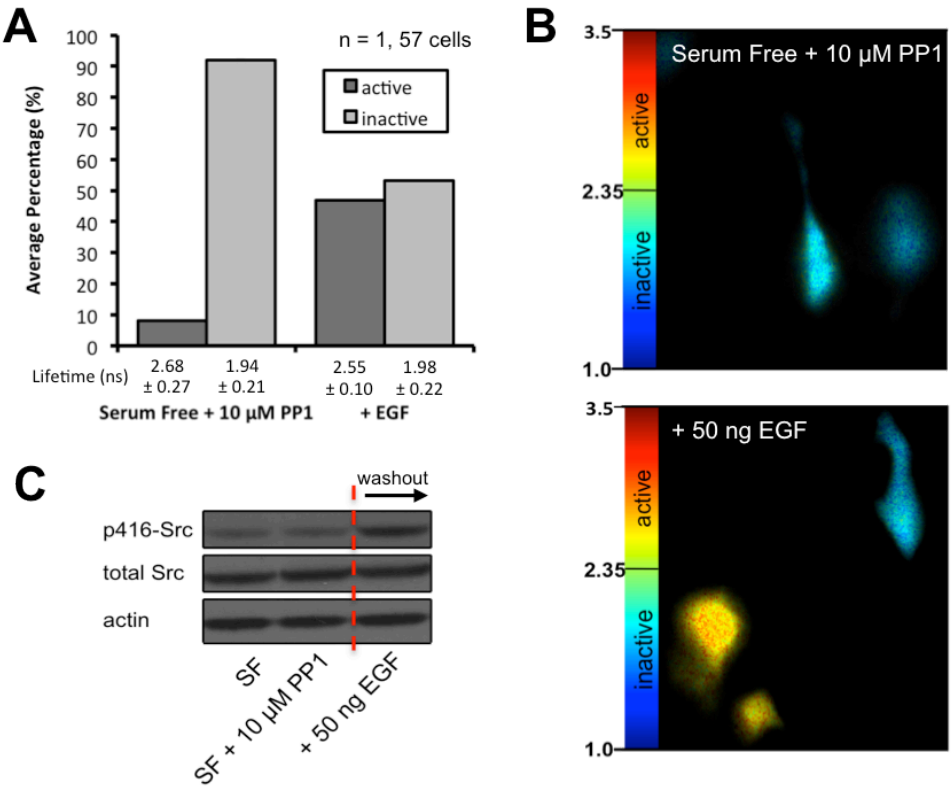

Figure 3.3: Stimulation with EGF increases number of Src active cells after serum starvation and pre-treatment with Src inhibitor PP1 *in vitro*
A Quantification of Src active and inactive cells *in vitro* after serum starvation in conjunction with pre-treatment with 10 µM of Src-inhibitor PP1, as well as after 5 minutes of stimulation with 50 ng/mL of EGF; columns: mean. **B** Representative lifetime images of Src-FRET before and after EGF stimulation showing the differential responses of individual cells. **C** Immunoblot analysis of Src auto-phosphorylation in PDAC cells at serum starvation, pre-treatment with the PP1 Src inhibitor and EGF stimulation after PP1 removal, with anti-phospho-Src Y416, anti-total Src and anti-actin.

As a proof of principle and in order to establish that the FRET-sensor, and thus Src activity, was also able to respond to stimulus and not only inhibition, PDAC cells were serum starved overnight and pre-treated with 10 µM of the Src family kinase inhibitor PP1. This resulted in a predominantly inactive cell population in the sample and following washout of the inhibitor and stimulation with 50 ng/mL of EGF resulted in an increase in the percentage of Src-active cells imaged (Figure 3.3 A+B). This was further confirmed by immunoblotting the PDAC cells for phosphorylated Src using an anti-phospho-Src^{Y416} (p416-Src) antibody, detecting the autophosphorylation of the kinase (Figure 3.3 C).

Immunoblotting of phosphorylated proteins with phospho-specific antibodies is the established standard approach to assessing protein kinase activity. I therefore wanted to compare assessment of Src activity using the Src FRET reporter with Src activity detected with immunoblotting of p416-Src.

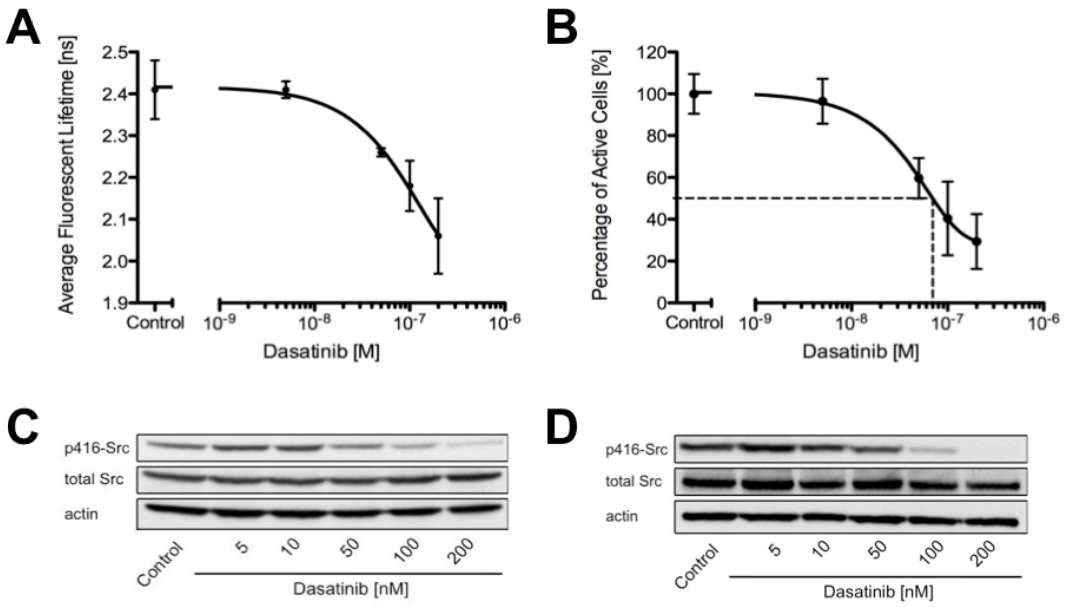

Figure 3.4: FLIM-FRET of single cells reveals IC_{50} of dasatinib on Src active PDAC cells *in vitro*
A Quantification of the average fluorescent lifetimes of Src activity in PDAC cells at specific concentrations of dasatinib *in vitro* as well as quantification of percentage of Src active cells (**B**) after exposure to 5 – 200 nM of dasatinib for 2 hours *in vitro*. **C** Immunoblot analysis of Src auto-phosphorylation in PDAC cells, with anti-phospho-Src^{Y416}, anti-total Src and anti-actin, after inhibition with 5 – 200 nM of dasatinib for 2 hours and (**D**) 24 hours; data point: mean; error bars: SEM; line: non-linear fit

In order to establish a drug response curve, PDAC cells stably expressing the Src-biosensor were further exposed to increasing concentrations of dasatinib (5 to 200 nM) and FLIM measured. A drug response curve to dasatinib on a single cell basis was created with the average fluorescent lifetime in each sample (Figure 3.4 A). The percentage of active cells was further plotted, normalized to 100 % in the control. From this, an IC_{50} of Src-active cells at around 70 nM of dasatinib could be determined (Figure 3.4 B). Src inhibition was further controlled for by immunoblotting for $pSrc^{Y416}$ levels and control total Src levels, showing a steady decrease is Src autophosphorylation after 2 and 24 hours of exposure to increasing concentrations of dasatinib (Figure 3.4 C+D).

3.3.2 Application of FLIM-FRET for the rapid monitoring of dynamic drug targeting *in vitro*

In order to see how Src-FRET compares to p416-Src blots in the temporal monitoring of Src response to dasatinib treatment *in vitro*, PDAC cells were treated with 100 nM of dasatinib. Immunoblots for p416-Src were conducted and controlled to total Src levels, to see at what time point after dasatinib treatment the Src autophosphorylation was maximal. It became apparent that the n-fold reduction in phospho-Src levels was already maximal after 1 hour of treatment and remained constant for up to 24 hours of observation (Figure 3.5 A+B).

Wash-out experiments of dasatinib-inhibited PDAC cells were further conducted, in order to show temporal drug targeting monitoring. First, immunoblots for phospho-Src levels were performed at 30 minutes after dasatinib inhibition and between 30 minutes and 24 hours after removal of the medium containing the inhibitor (Figure 3.5 C). Three independent experiments were then quantified for the n fold change in p416-Src levels (Figure 3.5 D). The data showed a 5.5 fold increase in the level of Src autophosphorylation after only 30 minutes following dasatinib removal. This further decreased steadily to 2 fold after 24 hours of drug removal. A compensatory mechanism of the “re-bound” up-regulated cellular p416-Src levels following drug removal can be observed, with the overactivation of Src following dasatinib wash-out. The original equilibrium was moreover steadily approached again in the time period monitored up to 24 hours.

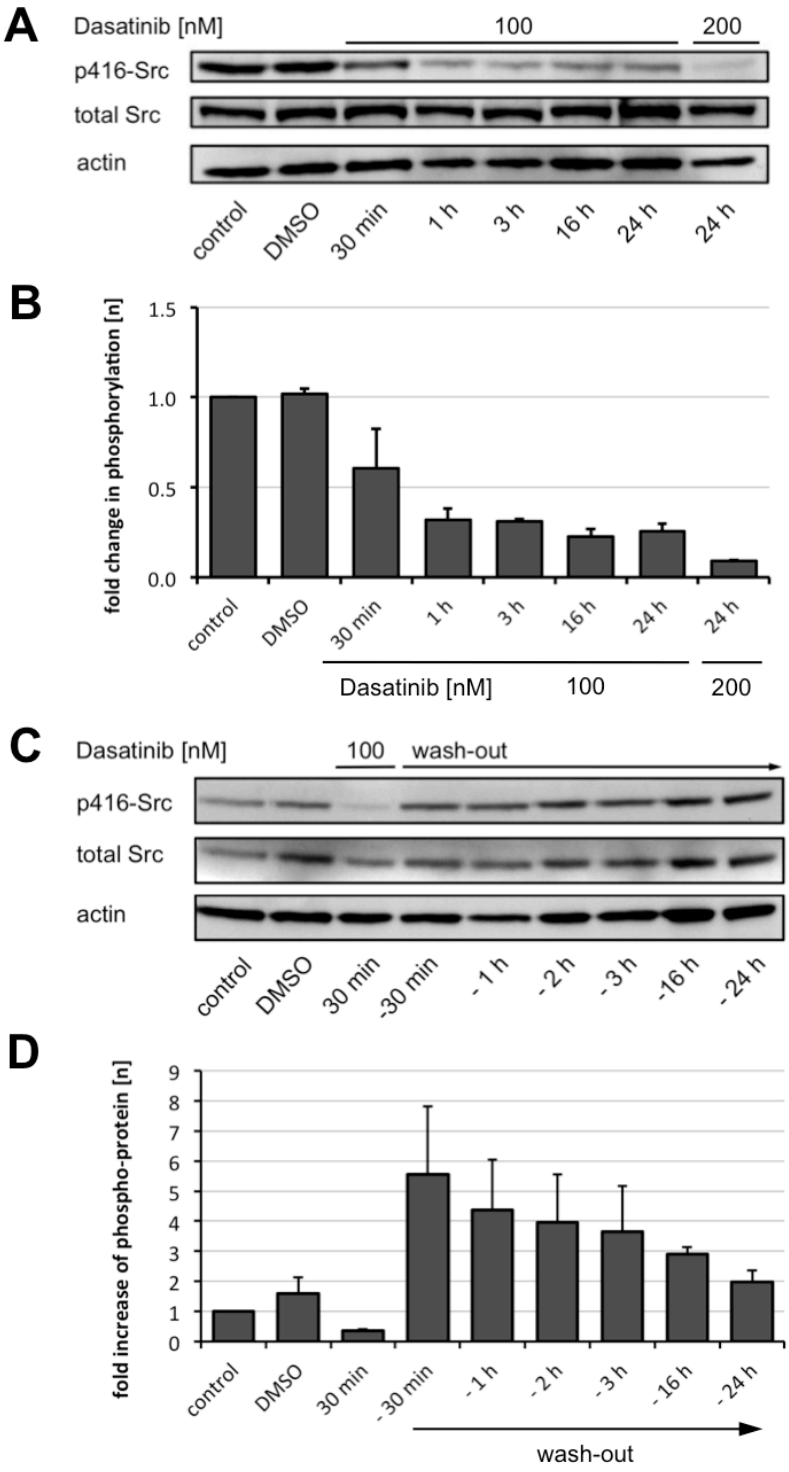

Figure 3.5: Recovery of phospho-Src *in vitro* quantified by immunoblot after dasatinib treatment and wash-out

A Immunoblot analysis of Src auto-phosphorylation in PDAC cells with anti-phospho-Src^{Y416}, anti-total Src and anti-actin before and after defined time-points of treatment with dasatinib (100 nM or 200 nM) *in vitro* and **B** quantification of the n-fold change in Src phosphorylation of 3 independent experiments. **C** Representative experiment showing washout of 100 nM of dasatinib and monitored by Src phosphorylation over a period of 24 hours. **D** Quantification of the n-fold change in Src phosphorylation for 3 independent repeats of the washout experiment; columns: mean; error bars: SEM

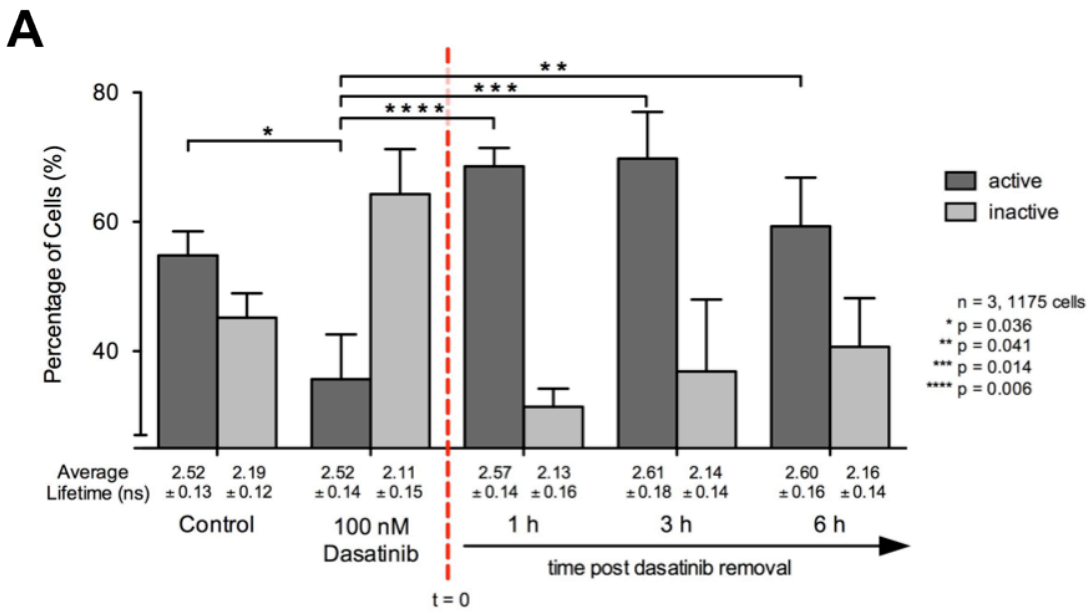

Figure 3.6: FLIM-FRET can be used to monitor Src activity on the single cell level after dasatinib washout *in vitro*
A Quantification of Src activity based on single cell lifetimes measured *in vitro*, before and after treatment with 100 nM of dasatinib as well as up to 6 hours after washout of dasatinib. Src "activity" was assigned above 2.35 ns of lifetimes measured, cells grouped accordingly and the average lifetimes ± SD recorded below each column; n = 3 independent repeats, 1175 cells in total; column: mean; error bars: SEM; * p = 0.036, ** p = 0.041, *** p = 0.014, **** p = 0.0006 by unpaired standard students *t* test

In order to see how the FRET biosensor would compare to the immunoblot read-out, the same washout experiment was conducted, with the Src activity assessed using FLIM-FRET. This revealed a slightly different temporal dynamic. As with the immunoblot, a significant decrease in the percentage of active cells was observable following dasatinib treatment (from 54.8 ± 3.7 % to 35.7 ± 6.9 %). Also in line with the immunoblot results the percentage of active cells was increased (68.6 ± 2.8 %) relative to the control at 1 hour following drug washout. Further, however, monitoring at 6 hours showed a return in the percentage of Src active cells to the levels observed in the control (Figure 3.6). Thus, following drug washout, cells assessed by Src-FRET returned to baseline sooner (at 6 hours) than cells assessed by p416-Src (past 24 hours).

3.3.3 Src activity is spatially regulated in 3D environments *in vitro*

In order to monitor the spatial distribution of Src activity, PDAC cells were seeded on top of organotypic matrices (Timpson *et al*., 2011b), preconditioned and contracted by either primary or immortalized human fibroblasts (Figure 3.7 A).

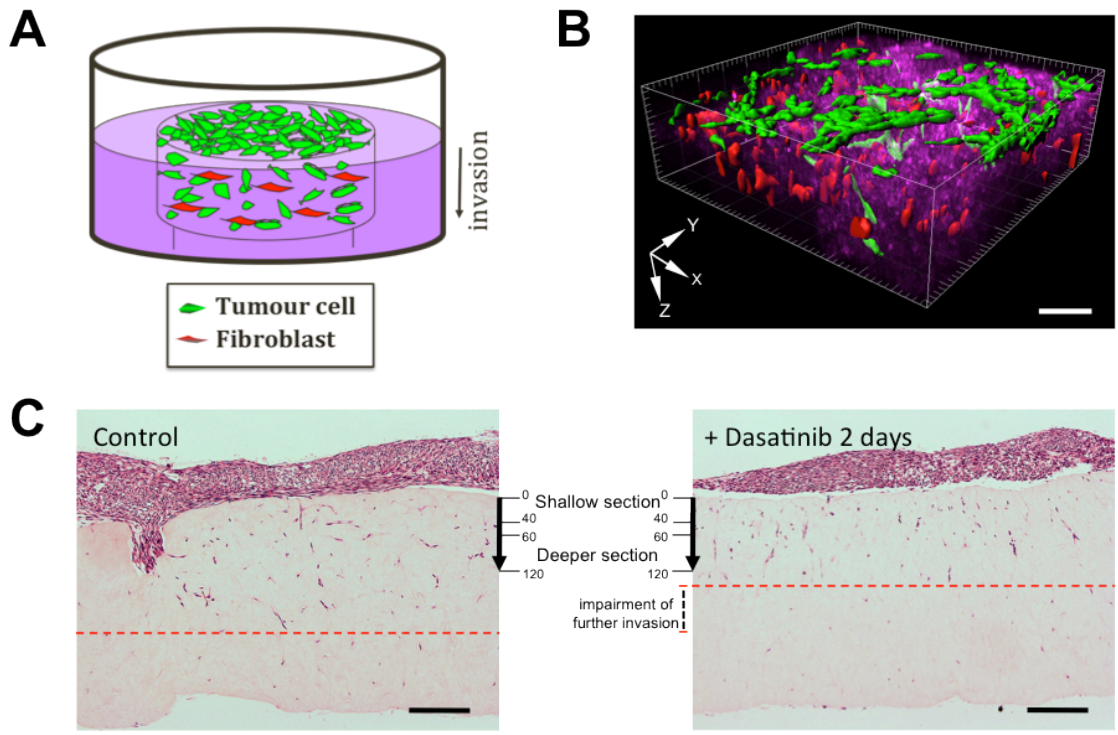

Figure 3.7: Dasatinib treatment impairs invasion of PDAC cells on organotypic matrices
A Schematic representation of an organotypic invasion assay set-up (adapted from Timpson *et al*. 2011). Invading tumour cells are presented in green and fibroblasts within the organotypic matrix comprised of rat tail collagen I are depicted in red. The organotypic matrix rests on a metal mesh grid and the invading cells are exposed to air, creating an air-liquid interface with the medium (in purple) as well as a serum gradient across the matrix from bottom to top. **B** 3D rendering of a region of an organotypic matrix, with invading GFP-labeled PDAC cells (green) and mCherry expressing TIF fibroblasts (red) embedded in the collagen I matrix (SHG in magenta). **C** H&E cross-sections of organotypics with PDAC cells expressing the Src-biosensor invading into the matrices for a total of 8 days, with maximum invasion denoted by red dotted line. During the last 2 days, treatment of 100 nM of dasatinib was applied, impairing further invasion during that time in the respective matrices; scale bars: 100 µm

The invasive properties of the PDAC cells could therefore be assessed in the context of a collagen I matrix and in the presence of fibroblasts. Following contraction of the matrices and subsequent seeding of PDAC cells at confluent density on top, the matrices were transferred on to a metal grid, allowing for an air-liquid interface to form. Complete medium containing 10% FBS was added to the bottom, thus creating a serum gradient across the matrix. The PDAC cells were then allowed to invade and then visualized. This was done either by multiphoton imaging, with the PDAC cells expressing GFP (green), the immortalized TIF fibroblasts (Munro *et al*., 2001) expressing mCherry (red) and the collagen I being visualized by SHG signalling (magenta) (Figure 3.7 B) or by fixation in paraformaldehyde and conventional H&E staining (Figure 3.7 C). PDAC cells were allowed to invade into the matrices for a total of 8 days and during the last two days the cells were challenged with 100 nM of dasatinib. Drug treated matrices showed a reduction in PDAC penetration depth compared with untreated controls (Figure 3.7 C). The relative depth of cells inside the matrix was classified into "shallow sections" (0, 20 and 40 μm) and "deeper sections" (60 – 120 μm, at 20 μm intervals).

The Src activity of invading PDAC cells within the organotypic matrix was assessed by FLIM-FRET and revealed that the fraction of Src active cells increased with increasing penetration depth into the matrix (Figure 3.8 A+B). Matrices were further analysed by immunohistochemistry with the p416-Src antibody, showing positive staining especially in cells that had penetrated into the collagen I matrix and negative staining PDAC cells which remained on the top (Figure 3.8 C). With this method, however, there was no gradient of any kind detectable in terms of Src activity in a spatial manner. Dasatinib treated organotypics in turn showed a complete loss of Src active cells in deeper sections as assessed by FRET, while the more shallow sections displayed the same basal percentage in Src active cells as observed in the control matrices (Figure 3.8 D).

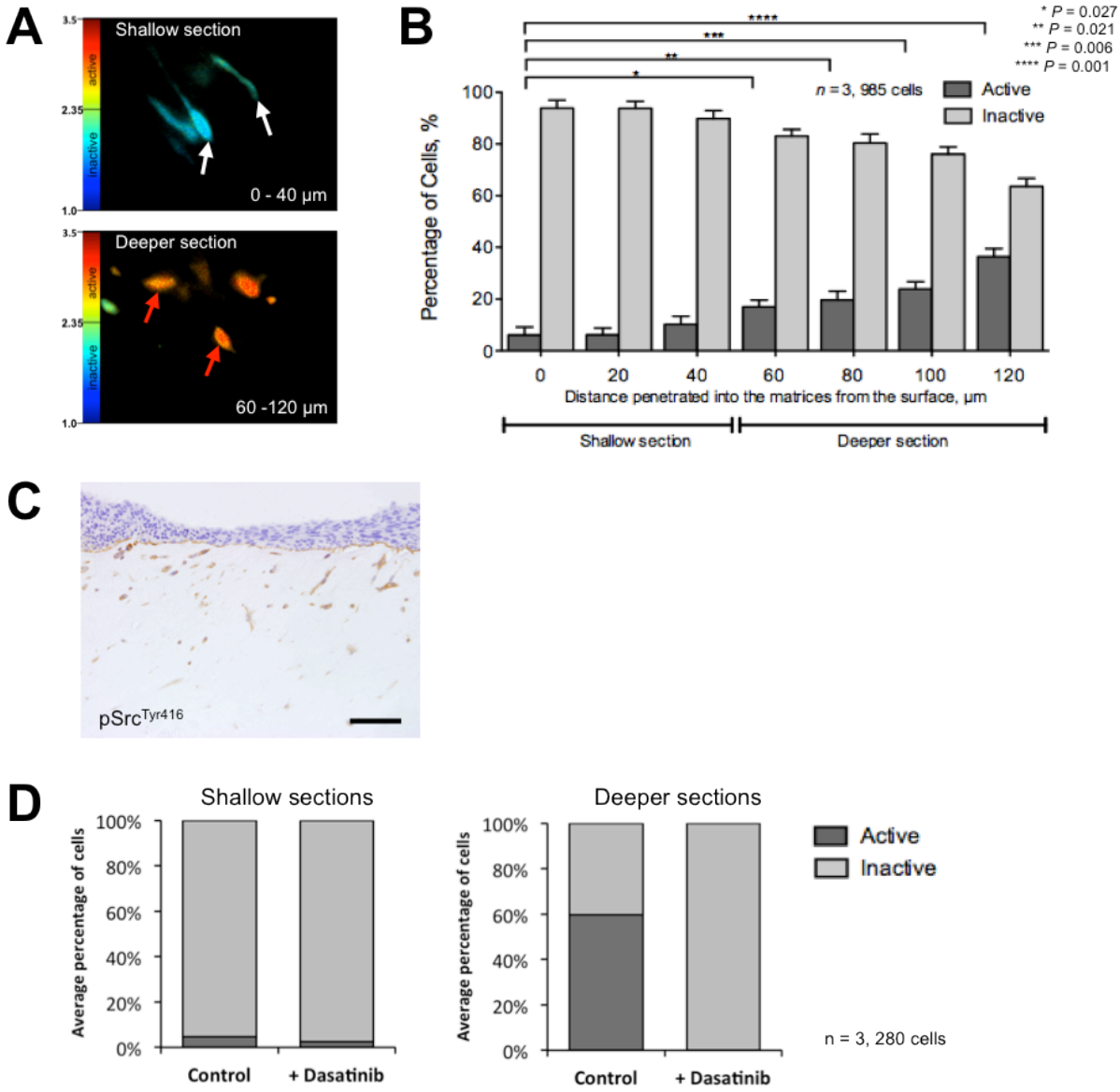

Figure 3.8: FLIM-FRET reveals spatially distinct Src activation of PDAC cells invading on organotypic matrices

A Representative lifetimes maps of Src-activity of PDAC cells invading into organotypic matrices, in shallow (0 – 40 µm) and deeper (60 – 120 µm) sections, with white arrows denoting Src inactive cells and red arrows showing cells displaying Src activity. **B** single cell quantification of Src-activity after FLIM-FRET imaging of invading PDAC cells on and into organotypic matrices; n = 3 independent repeats, with 965 cells measured in total. **C** IHC of Src phosphorylation in invading PDAC cells using anti-phospho-Src Y416. **D** Quantification of Src activity in shallow and deeper sections of organotypic matrices untreated or treated with 100 nM of dasatinib for the last 2 days of invasion; n = 3 independent repeats and 280 cells measured in total; columns: mean; error bars: SEM; * p = 0.027, ** p = 0.021, *** p = 0.006 and **** p = 0.001 by unpaired students *t* test; scale bar: 100 µm

3.3.4 FLIM-FRET imaging can be used to monitor live drug targeting in the tumour microenvironment *in vivo*

The tumour microenvironment can have a significant impact on drug delivery *in vivo*. It can lead to impaired drug delivery especially in PDAC by the dense disposition of ECM and poor vascularization (Provenzano *et al*., 2012). We therefore wanted to assess whether FLIM-FRET imaging represents a robust tool in the monitoring of temporal drug targeting in the context of the tumour microenvironment *in vivo*. First, the temporal drug targeting of dasatinib treatment in allograft tumours was examined. Therefore, PDAC cells stably expressing the Src-FRET biosensor were subcutaneously injected in to CD1$^{-/-}$ nude mice and primary tumours allowed to develop for up to 7 days. Mice were further treated daily for 3 consecutive days with oral gavages at a previously established inhibitory dose of 10 mg/kg dasatinib (Morton *et al*., 2010b) and then imaged at defined time points after the final gavage was administered (Figure 3.9 A).

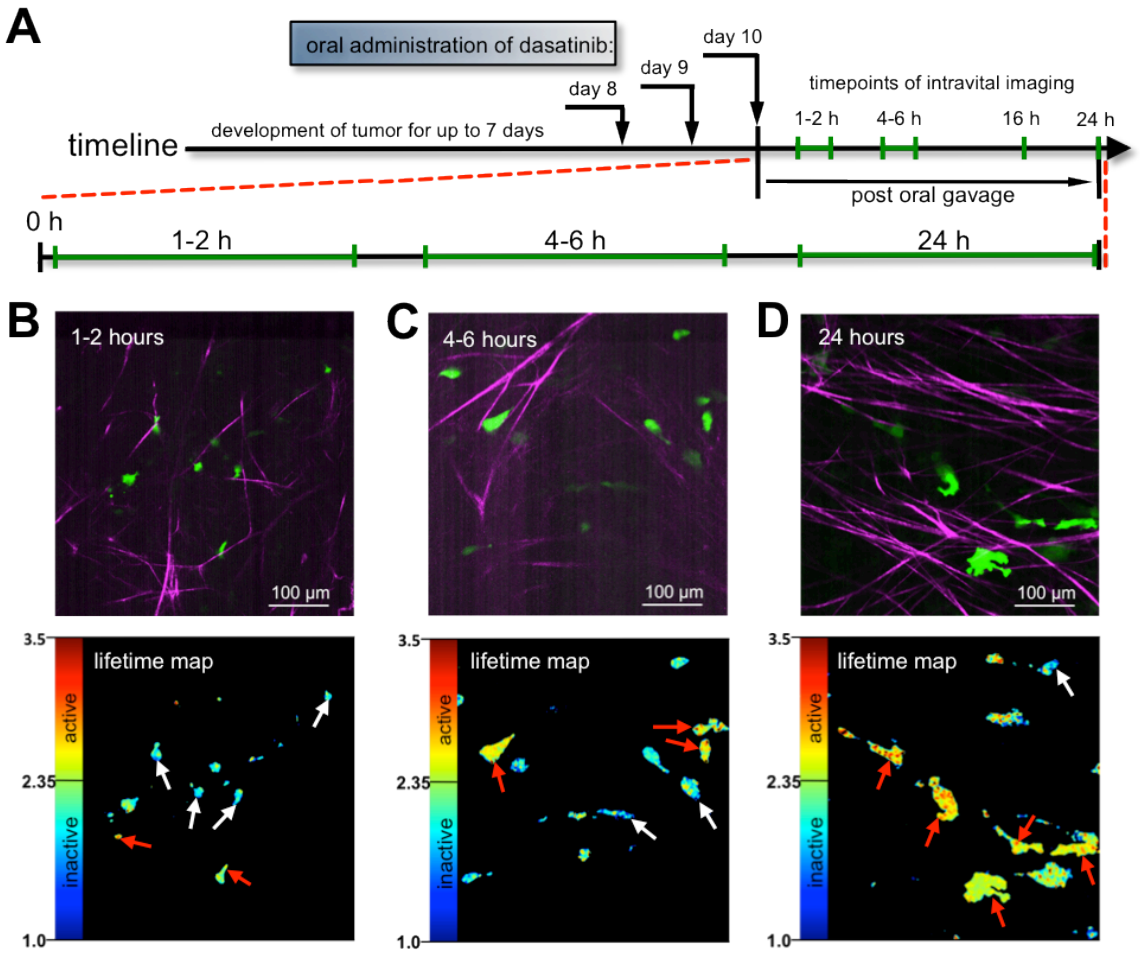

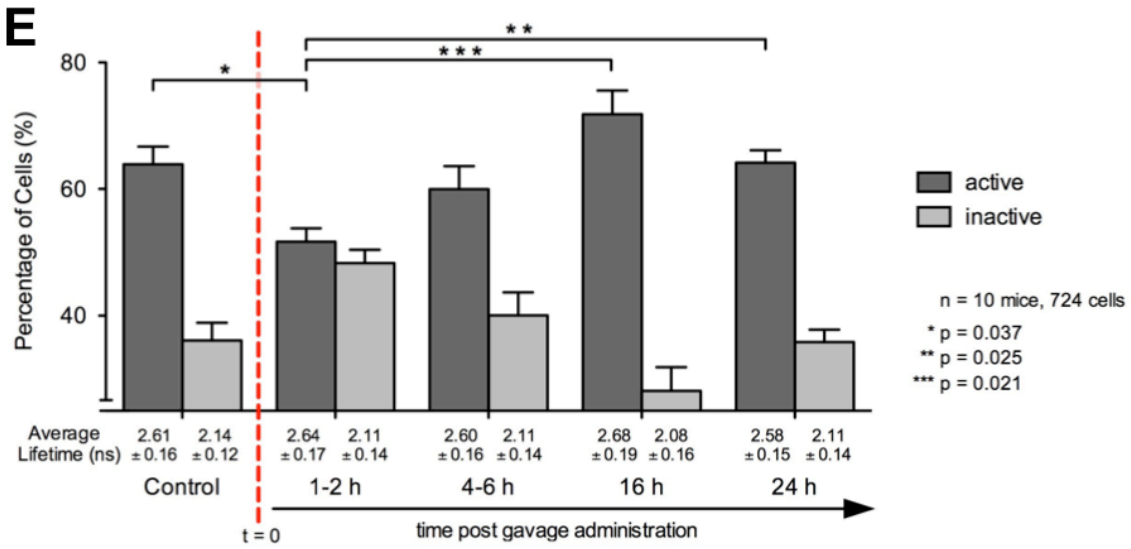

Figure 3.9: Intravital FLIM-FRET can be used to measure the response of single cells to Src inhibition in living tumours
A Schematic of the timeline of the intravital imaging to monitor drug-targeting efficacy of dasatinib. Primary tumours were allowed to form for up to 7 days. Mice were then treated with daily oral gavages of 10 mg/kg of dasatinib (day 8, 9 and 10) and imaged at specific timepoints after the final gavage was administered. **B** Representative images of PDAC allograft tumours (Src-biosensor: green, collagen I visualized by SHG: magenta) and corresponding Src activity (lifetime maps) with white arrows denoting Src inactive cells and red arrows cells displaying Src activity at 1-2 hours, 4-6 hours (**C**) and 24 hours (**D**) after the final gavage was administered. **E** Quantification of Src activity as measured by FLIM-FRET on a single cell basis at 1-2 hours, 4-6 hours, 16 hours and 24 hours after the final gavage was administered, with the average lifetimes ± SD in each group displayed below each column; n = 10 mice and 724 cells measured in total; columns: means; error bars: SEM; * p = 0.037, ** p = 0.025 and *** p = 0.021 by unpaired standard students *t* test

The percentage of Src active cells was significantly reduced after 1-2 hours of the final gavage being administered from (63.9 ± 2.8 % to 51.7 ± 2.1 %). A re-bound effect was observed again as in the *in vitro* wash-out experiments, but on a different time scale (after 16 hours), with the percentage of active cells being increasing to 71.9 ± 3.8 %. After 24 hours post-treatment, Src activity finally returned to control values (Figure 3.9 E).

3.3.5 Spatial regulation of Src activity can be observed *in vivo* within tumour subpopulations

It is known that a subset of tumour cells respond better to therapy than others, but it is not entirely understood why. One possible cause of differential response to therapy could be the position within the tumour, i.e. the tumour microenvironment and its constituents such as tumour fibroblasts. These in turn can influence therapeutic efficiency by regulating collagen I disposition as described previously (Loeffler *et al*., 2006; Minchinton and Tannock, 2006). It is currently still quite difficult to assess response of individual cells in different tumour regions. Therefore, in order to understand how different tumour regions respond to treatment we compared Src activity quantified in both the core of primary tumours and their border. These regions in turn were defined by their distinct collagen I signal. The SHG revealed that tumour centre regions had an anisotropic distribution of collagen fibres, while the border regions displayed isotropic, frizzled collagen fibres of the tissue surrounding the allograft tumour mass (Figure 3.10 A+B). Primary PDAC tumours of both control and dasatinib treated mice were compared and an increased percentage of Src active cells observed in the border regions. This was effectively reverted by dasatinib treatment from a predominantly active cell percentage to a majority of Src inactive cells. The distribution of Src active and inactive cells was, however, not altered at the tumour core of treatment animals (Figure 3.10 C).

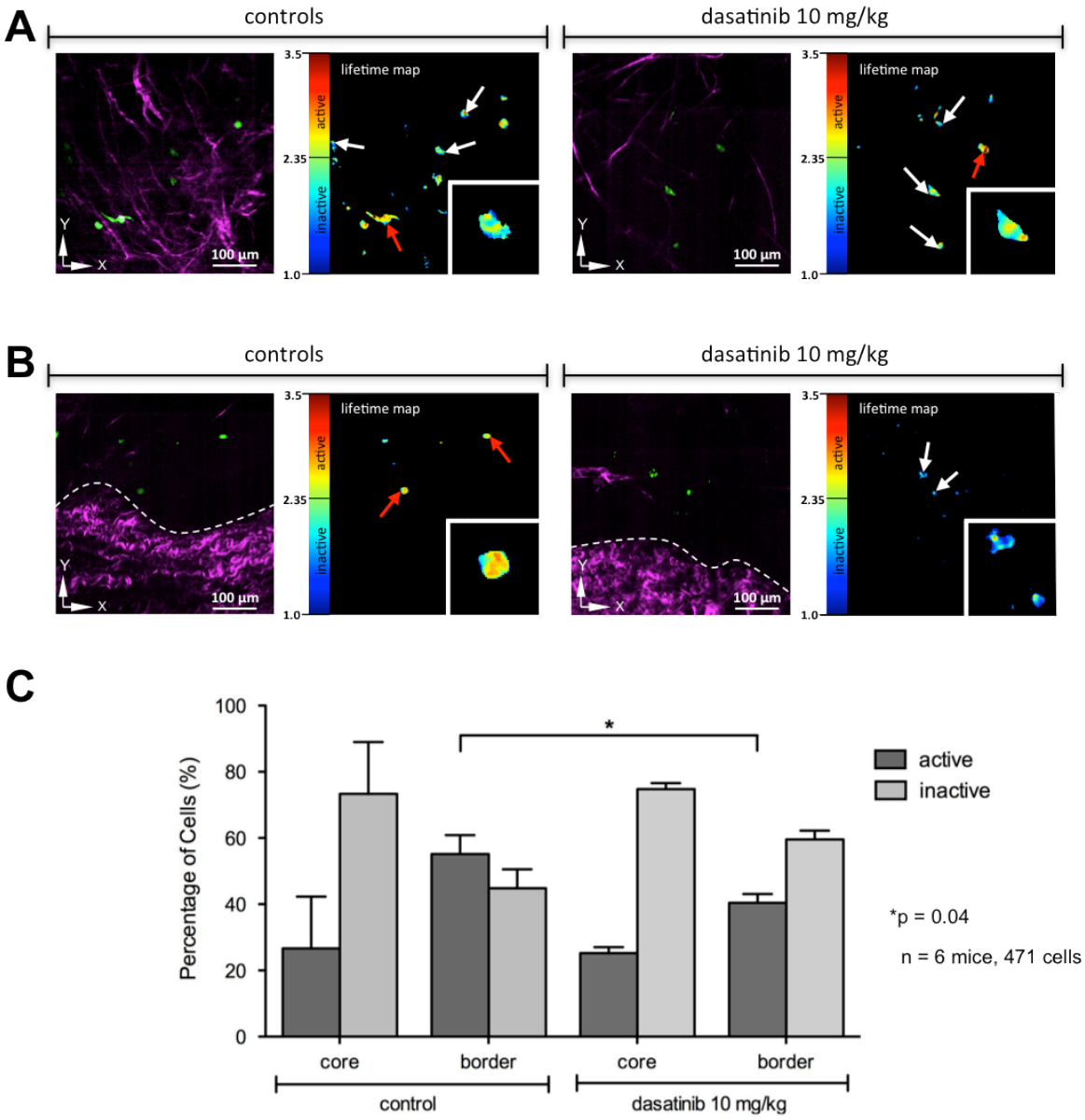

Figure 3.10: FLIM-FRET reveals that Src activity is increased and effectively inhibited by dasatinib at the tumour border in PDAC allografts

A Representative intensity images of PDAC cells stably expressing the Src-biosensor (green) *in vivo* in the tumour core (collagen I/SHG signal in magenta), before and after dasatinib treatment with the respective lifetime maps of Src activity. **B** The border of the allograft tumours was visualized by the frizzled collagen I detected by SHG and the Src activity of the PDAC cells in the vicinity measured. **C** Quantification of Src activity of PDAC cells in the tumour core and borders of control and dasatinib treated mice; n = 6 mice and 471 cells measured in total; columns: mean; error bars: SEM; * p = 0.04 by unpaired standard students *t* test

3.3.6 Drug delivery with respect to tumour vasculature can be monitored by *in vivo* imaging

The targeting efficacy of dasatinib was further assessed in relation to the local tumour vasculature using Src FLIM-FRET intravital imaging. Tumour bearing mice were i.v. injected with quantum dots (Qdot tracker^{655}) in order to label the vasculature prior to imaging, and Src activity was imaged and correlated to the distance of the cells away from the closest vessel (Figure 3.11 A). This revealed distinct zones of Src activity from proximal to distal regions, which were defined as 0-25 µm, 25-50 µm, 50-100 µm and above 100 µm from the nearest vessel. In control mice Src activity steadily increased with progressive distance from a vessel. The Src activity was effectively inhibited by gavaging the mice with dasatinib, switching the PDAC cells to being predominantly Src inactive up to about 100 µm away from the vasculature. Cells were no longer effectively targeted by dasatinib treatment in terms of Src activity, displaying a similar predominantly active cell population as observed in the control at a distance beyond 100 µm away from the vasculature This could be due to a perfusion limit at this point (Figure 3.11 B).

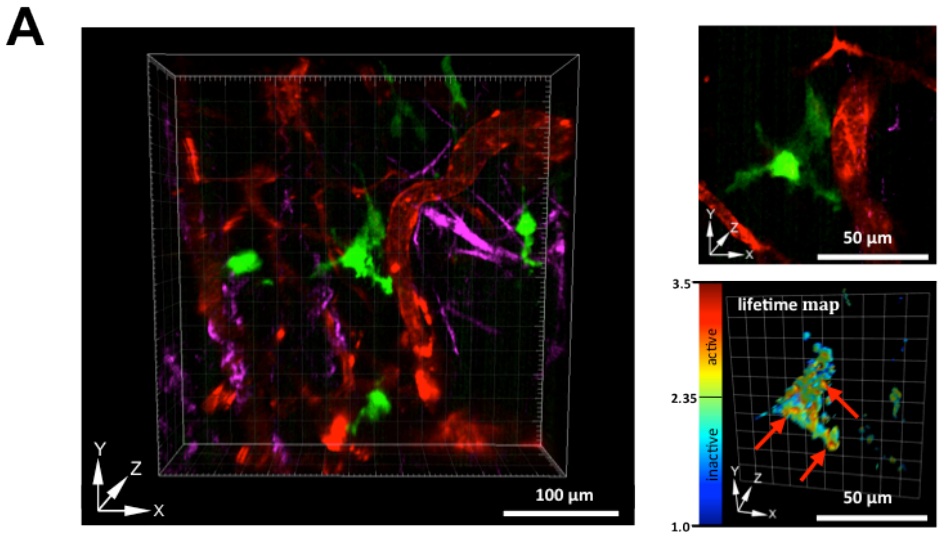

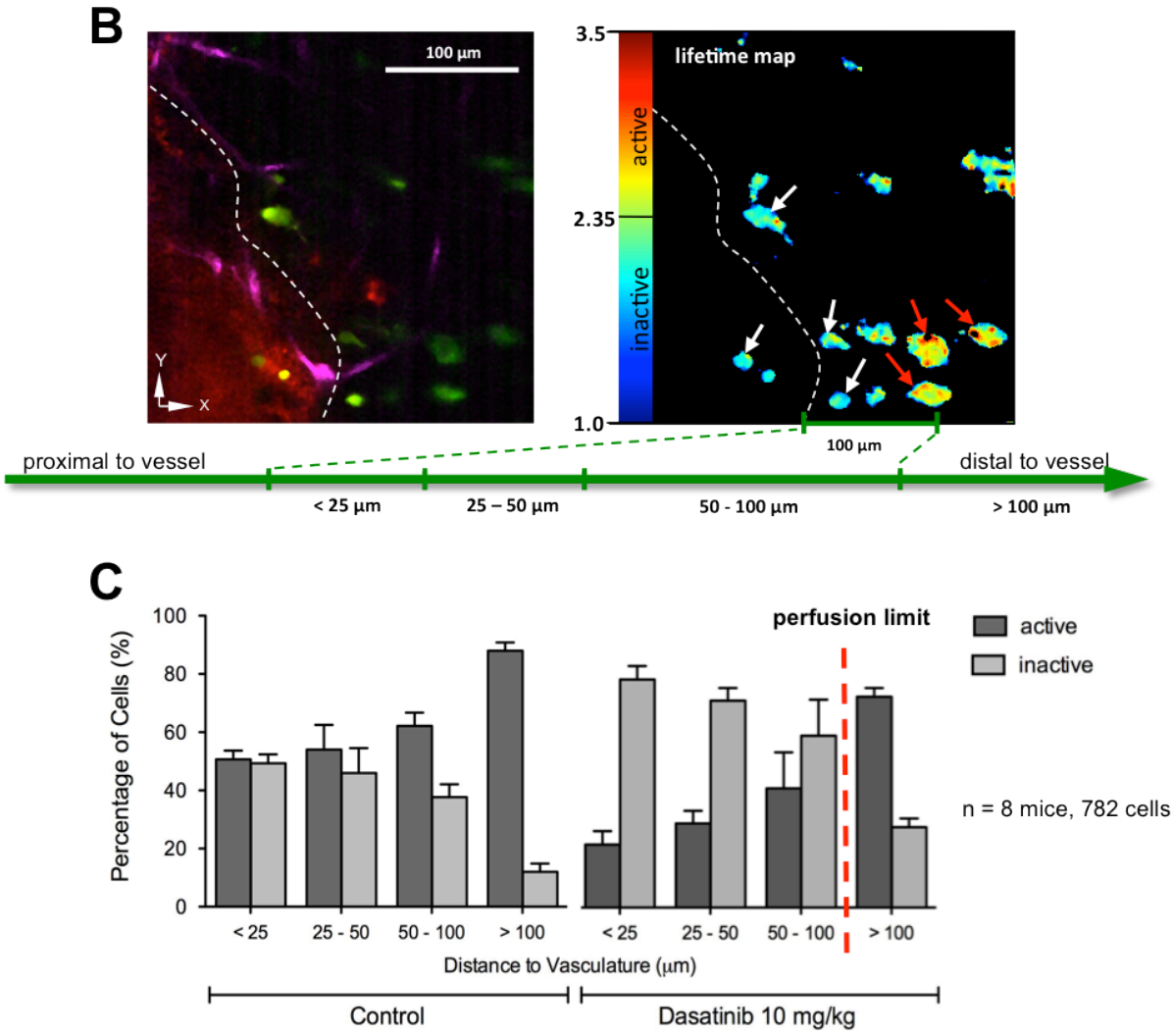

Figure 3.11: Intravital FLIM-FRET allows for measuring of Src activity and quantification of drug delivery *in vivo* in relation to local vasculature
A Representative 3D rendering of PDAC cells expressing the Src-biosensor (green) *in vivo*, in relation to the local vasculature labeled by i.v. injection of quantum dots (Qdot-tracker^{655}: red) prior to imaging and visualization of the local ECM by SHG of the collagen I (magenta). **B** Visualization and (**C**) quantification of Src activity inside PDAC cells by FLIM imaging on a single cell basis of Src activity at certain distances away from the local vasculature, within regions ranging from < 25 µm, 25-50 µm, 50 -100 µm and > 100 µm. Control mice or mice treated with 10 mg/kg dasatinib were imaged and a limit in the shift to Src inactivity after dasatinib treatment observed at regions above 100 µm away from the local vasculature; n = 8 mice with 782 cells analyzed in total; columns: mean; error bars: SEM; red arrows denoting Src activity inside cells and white arrows Src inactivity

3.3.7 Dasatinib penetration efficiency is improved by the use of a combination therapy targeting the tumour stroma

In order to potentially improve the rather poor distribution of dasatinib inside the primary tumour away from the local vasculature, the tumour stroma was considered as a potential target (Yu and Tannock, 2012). The dense desmoplasia observed in pancreatic cancer is a key barrier to drug perfusion in this cancer type, that can be optimized by targeting ECM deposition (Provenzano *et al*., 2012). To that end, a previously described inhibitor of sonic hedgehog signalling, cyclopamine (Thayer *et al*., 2003), was employed to modulate the tumour microenvironment. Cyclopamine inhibits sonic hedgehog (Shh) signalling in cells, which has been shown previously to lead to a reduction in ECM deposition in KPC mice (Olive *et al*., 2009). Organotypic matrices were therefore treated with 10 μM of cyclopamine during contraction of the collagen I by the embedded fibroblasts. It was observed that the diameter of treated matrices was greater than that of untreated and that they contracted to a smaller extent (Figure 3.12 A). The organotypics were treated with increasing concentrations of cyclopamine, ranging from 2.5 to 10 μM and the area calculated (Figure 3.12 B). The matrices were further imaged on a multiphoton system and the amount of fibrillar collagen I visualized by SHG signalling, with less fibrillar collagen I observed in the cyclopamine treated samples (Figure 3.12 C). This was subsequently quantified by an Image J plug-in, calculating the total area covered by fibrillar collagen in any given Z-stack of SHG signal collected. The total peak coverage was significantly decreased from 85.6 ± 6.4 % to 41.4 ± 10.7 % in the cyclopamine treated organotypics (Figure 3.12 D).

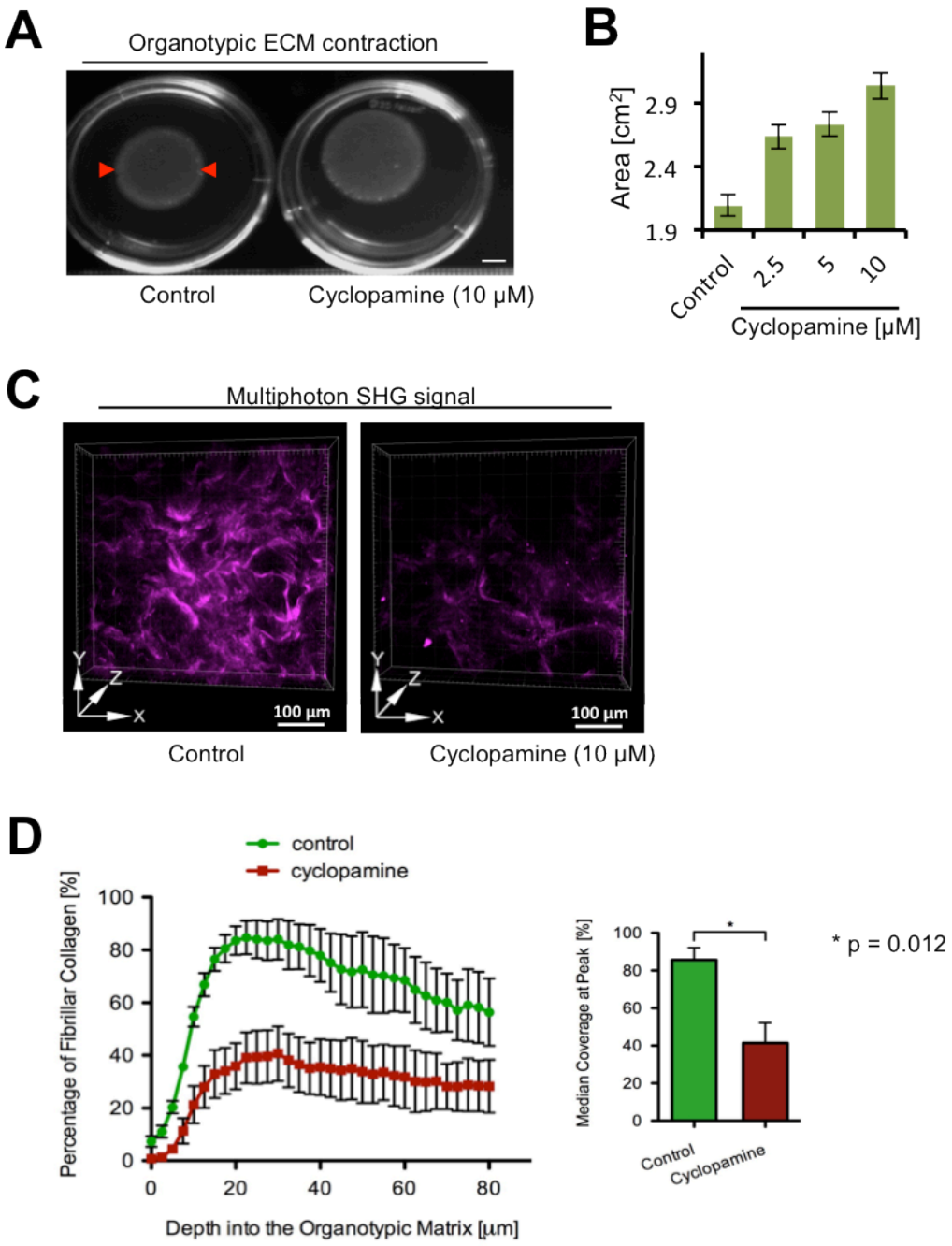

Figure 3.12: Cyclopamine decreases contraction and deposition of fibrillar collagen I in organotypic matrices

A Representative images of organotypic matrices after 10 days of contraction in control medium or medium supplemented with 10 µM of cyclopamine. **B** Quantification of the area in cm^2 of matrices treated with different concentrations of cyclopamine. **C** 3D rendering of collagen I as visualized by SHG signal in control organotypics and matrices treated with cyclopamine. **D** Quantification of SHG signal by representation of fibrillar collagen percentage at depths into the matrices, as well as the peak median percentage for both control and cyclopamine treated matrices; column/data points: mean; error bars: SEM; * p = 0.012 by unpaired standard students *t* test (experiments performed and analysed by Dr. Paul Timpson and Dr. Ewan McGhee)

Src activity was further found to be unaffected by cyclopamine treatment at concentrations ranging from 2.5 µM to 20 µM *in vitro* as observed by FLIM-FRET imaging or immunoblotting for p416-Src (Figure 3.13 A+B).

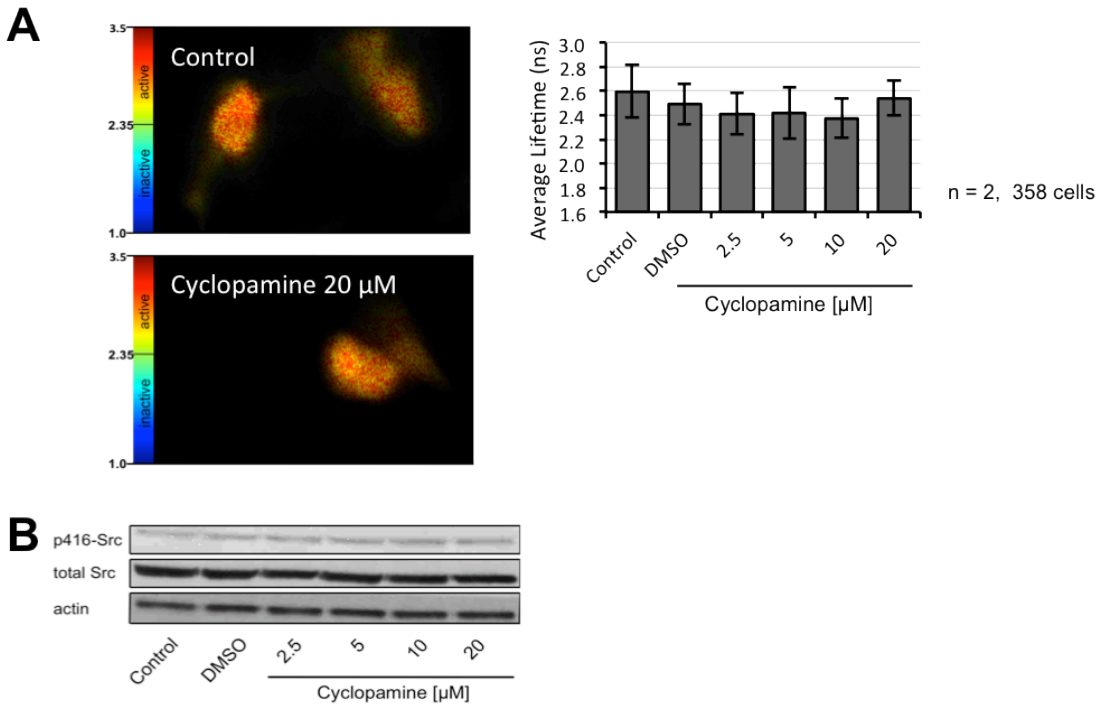

Figure 3.13: Src activity in PDAC cells is not decreased by cyclopamine treatment *in vitro*
A Representative lifetime images of Src activity in control and cyclopamine-treated PDAC cells *in vitro* and quantification of 2 independent experiments comprising 358 cells; columns: mean; error bars: SEM. **B** Immunoblot of phospho-Src levels in PDAC cells treated with increasing concentrations of cyclopamine.

Nude mice were injected again with PDAC cells stably expressing the Src-biosensor and treated for 6 consecutive days with daily gavages of 25 mg/kg (Thayer *et al*., 2003) of cylopamine, in order to assess the effect of cyclopamine treatment on primary tumours *in vivo*. While the cyclopamine treatment did not affect Src activity *in vitro*, there was an ablation of the previously observed Src activity away from the vasculature. This could be due to the mice having a more normalized tumour ECM, and thus have an indirect effect on the Src activity distribution away from the local vasculature (Figure 3.14 A). Further combination treatment of the mice with both cyclopamine and dasatinib increased the targeting efficacy of the latter, particularly in regions proximal to the local vasculature.

Compared to dasatinib treatment alone, the percentage of Src inactive cell increased from 71.1 ± 4.4 % to 95.8 ± 4.2 % at 25-50 μm, in the mice that received the combination treatment regimens (Figure 3.11 C vs Figure 3.14 B). However, the effect of the combination treatment at distances greater than 100 μm away from the vasculature was the same in the cyclopamine only treated animals, indicating that a shift in the limit was not achieved by this treatment (Figure 3.14 A vs B).

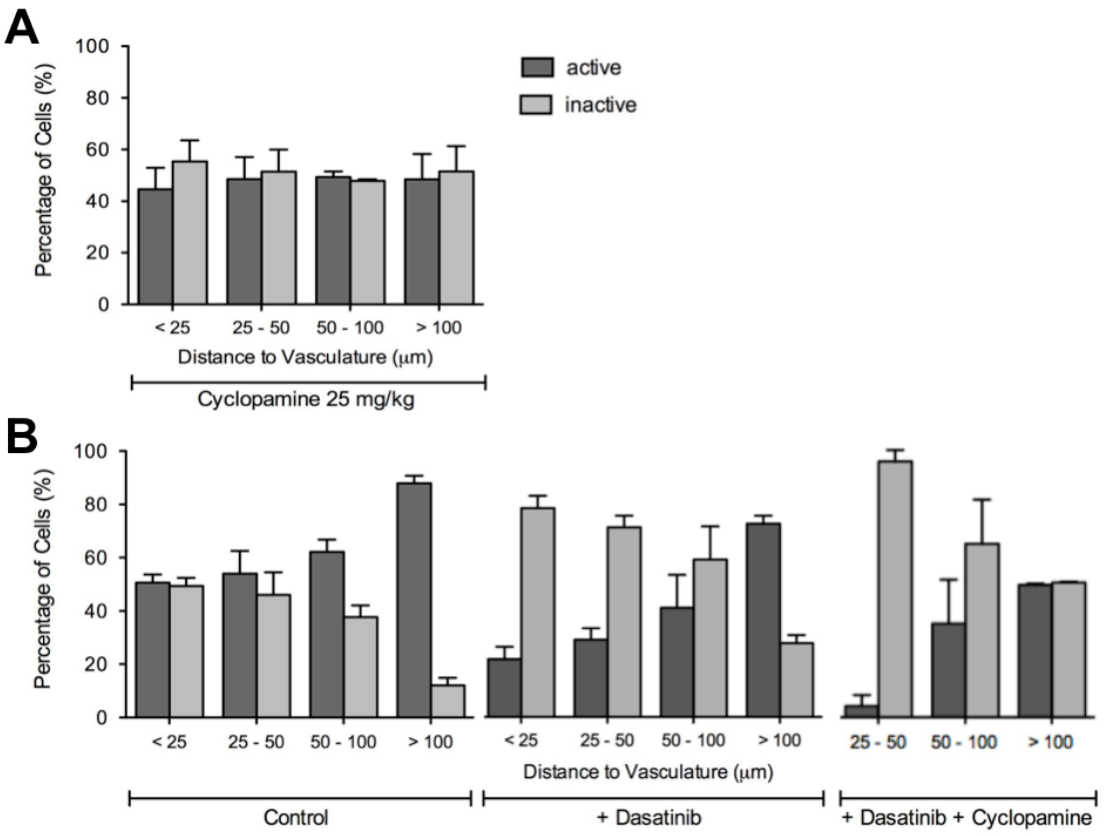

Figure 3.14: Cyclopamine treatment *in vivo* ablates Src activity distribution of PDAC cells away from local vasculature and increases in drug penetrance of dasatinib in vessel proximal regions
Quantification of the distribution of Src activity in PDAC cells in relation to the local tumour vasculature of mice treated with 3 daily gavages of (**A**) 25 mg/kg cyclopamine; n = 3 and 236 cells quantified. Data from Figure 3.11 C was plotted in (**B**) to compare to combination treatments consisting of 25 mg/kg cyclopamine and 10 mg/kg dasatinib; n = 3 mice and 131 cells quantified; columns mean; error bars: SEM

3.3.8 CXCR2 inhibition reduces Src activity *in vitro* and *in vivo*

Neutrophils have previously been associated with the tumour stroma in pancreatic cancer and have been shown to actively influence tumourigenesis and pancreatitis through CXCR2 signalling (Jamieson *et al*., 2012; Steele *et al*., 2015). We therefore sought to determine, whether inhibition of CXCR2 signalling by a small molecule inhibitor (CXCR2SM) would influence the invasive behaviour of PDAC cells on organotypic matrices and whether Src signalling would be perturbed in these assays and in primary allograft tumours *in vivo*. Co-incubation of PDAC cells with primary BM isolated neutrophils seeded on top of organotypic matrices showed an increase in invasion of the PDAC cells (Figure 3.15 A). There were no detectable differences in invasion of the invading PDAC cells in control and CXCR2SM treated matrices as visualized by H&E staining (Figure 3.15 B). Further quantification of Src activity by FLIM confirmed the distribution of increased Src activity in control cells that had invaded further into the matrices (see Figure 3.8 B). This was, however, abolished upon CXCR2SM treatment, decreasing Src activity especially in cells that had invaded into deeper sections of the organotypic matrices (Figure 3.15 C).

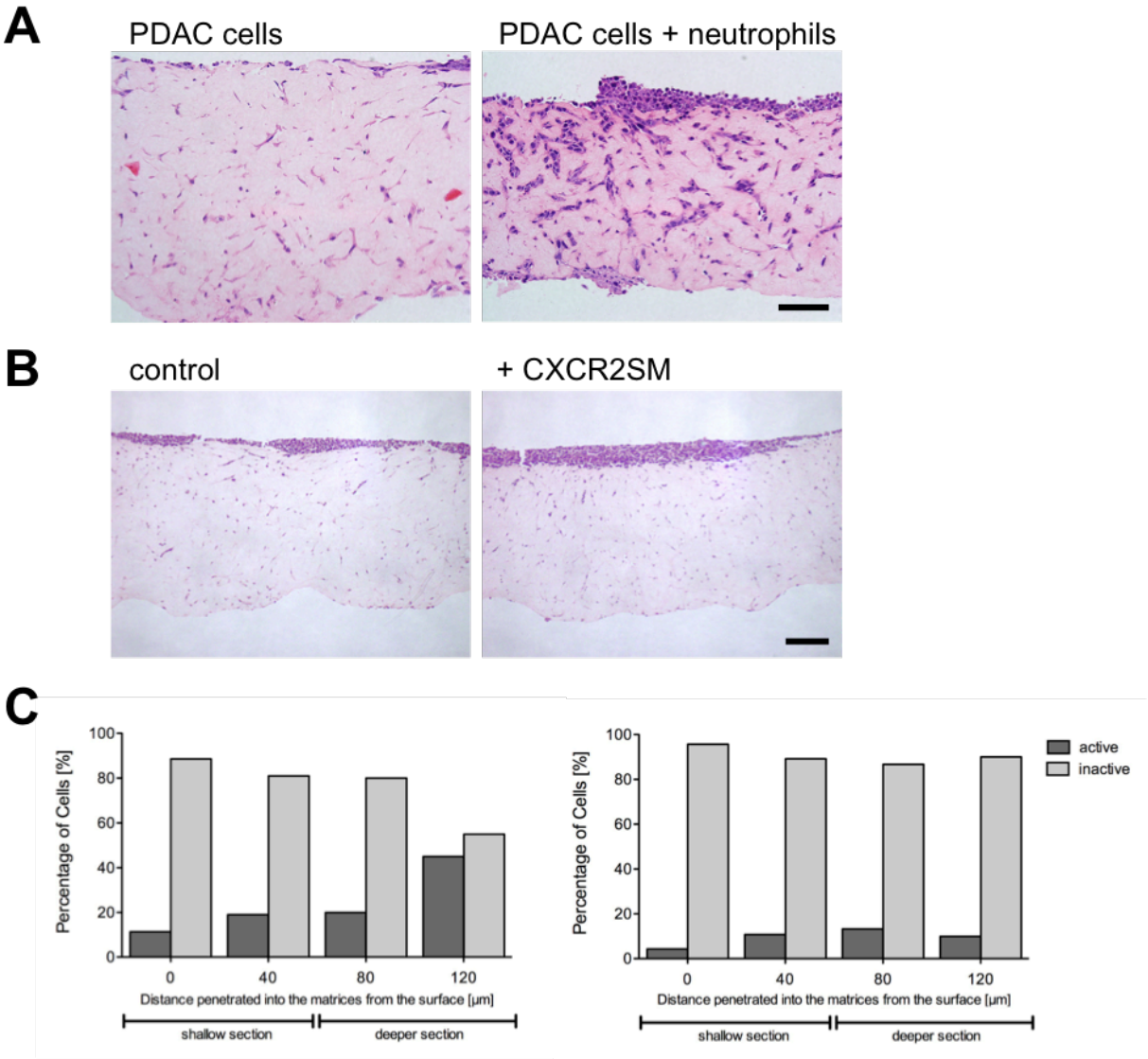

Figure 3.15: CXCR2 inhibition results in a decrease of invasion of PDAC cells on organotypic matrices and reduces Src activity

A Co-incubation of PDAC cells with primary neutrophils on top of organotypic matrices results in an increase in invasion of the PDAC cells. **B** Organotypic matrices with PDAC cells stably expressing the Src-biosensor invading for 6 days with or without treatment of 20 µM of CXCR2SM; scale bars: 100 µm. **C** Src activity was quantified on a single cell basis using FLIM-FRET in control and CXCR2SM treated organotypics at depths of 0 µm, 40 µm, 80 µm and 120 µm into the matrices. n = 1 and 306 cells quantified; columns: mean

In order to further gauge Src activity in response to CXCR2SM, optical imaging windows were implanted on top of developed primary PDAC subcutaneous tumours. The window consisting of a titanium ring and a glass coverslip was inserted into the skin on top of the previously developed tumours (see Materials and Methods 2.4.2) (Figure 3.16 A). Mice were then allowed to recover from surgery for a day. Prior to imaging mice were treated with gavages of either the vehicle or CXCR2SM at 100 mg/kg, two times a day for 3 days, and on the final day with an i.v. injection of Qdot tracker^{655} to visualize the local tumour vasculature. Representative intensity images display the PDAC cells expressing the Src-biosensor (green), SHG signal (magenta) and the local vasculature (red) (Figure 3.16 B, top) as well as the corresponding lifetime maps in the control and CXCR2SM treatment situation (Figure 3.16 B, bottom). Quantification of Src activity in relation to the vasculature revealed a similar gradient of Src activity with increasing distance to the vasculature as observed previously (see Figure 3.11 C). Additionally, in the CXCR2SM treated mice there was an increase in the percentage of Src inactive cells, especially below 25 μm from a local vessel (Figure 3.16 C).

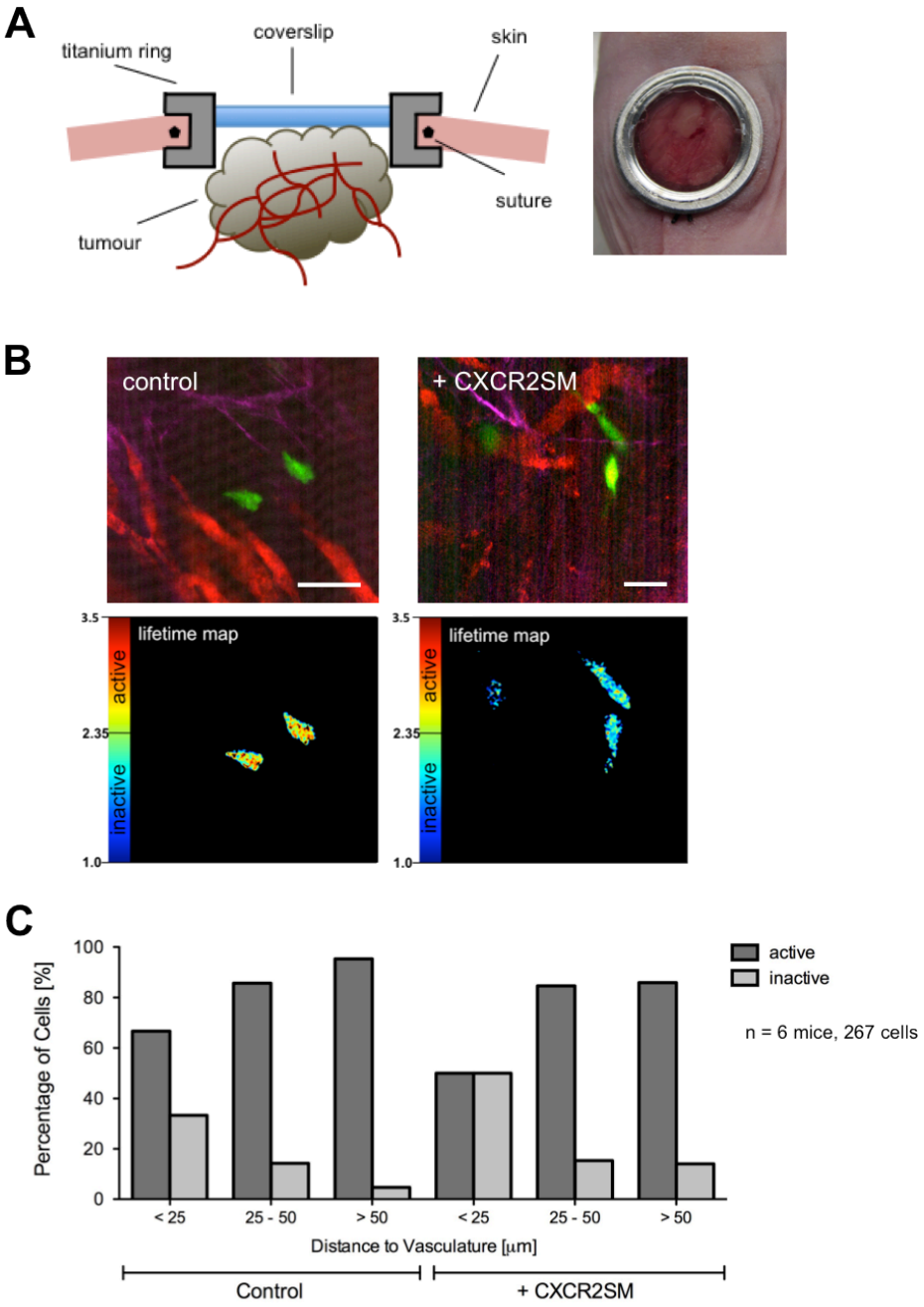

Figure 3.16: *In vivo* FLIM-FRET imaging using CIWs reveals decreased Src activity close to the local vasculature upon CXCR2SM inhibition

A Schematic representation of the titanium cutaneous imaging window (CIW) implanted in the skin on top of a developed primary tumour, allowing for imaging of the tumour in its native microenvironment. **B**, top: Representative intensity images of PDAC cells expressing the Src-biosensor (green) *in vivo*, in relation to the local vasculature labeled by i.v. injection of quantum dots (Qdot-tracker^{655}: red) prior to imaging and visualization of the local ECM by SHG of collagen I (magenta). **B**, bottom: Visualization of Src activity by FLIM-FRET imaging inside PDAC cells in control and 100 mg/kg CXCR2SM treated tumours, in relation to the local vasculature. **C** Quantification on a single cell basis of Src activity at < 25 µm, 25-50 µm, and > 50 µm away from the local vasculature in control and CXCR2SM treated mice; n = 6 mice with 267 cells analyzed in total; columns: mean; scale bar: 50 µm

3.4 Discussion

High drug attrition rate in drug development is still a major concern and continuing reason for substandard treatment regimens in, amongst others, cancer therapies (Kola and Landis, 2004; Hay *et al*., 2014; Waring *et al*., 2015). Intravital and *in vivo* imaging on a single cell basis of key signalling molecules in cancer can help in that respect. A more reliable testing of specific drug targeting in pre-clinical models, not achieved currently by conventional drug screening tools can help to reduce the high attrition rates of drugs encountered in the clinical setting (Kamb 2005; Isherwood *et al*., 2011). The results in this chapter illustrate how FLIM-FRET can be used to assess dynamic biomarkers in the pre-clinical evaluation of specific therapeutic targets. The longitudinal and spatially defined nature of the cellular read-out acquired can help in the optimization of treatment regimens. By providing a temporal readout treatment scheduling could be improved. Furthermore, the spatial readout can help identify barriers that the treatment needs to overcome to be effective throughout the tumour mass. Both in turn can moreover help in evaluating the application of combination treatments with complementary therapeutic agents.

Using cells from a mouse model that accurately recapitulates the histopathology of human pancreatic cancer (Hingorani *et al*., 2005; Hruban *et al*., 2006) in conjunction with FLIM-FRET imaging, I first showed that the temporal dynamics of dasatinib treatment of PDAC cells could be reliably monitored *in vitro*. There was, however, a notable difference in the "re-bound" effect observed after the removal of the primary dasatinib inhibition, when monitoring Src activity by immunoblotting for p416-Src compared to FLIM-FRET. While the immunoblot showed a 4.5 times increase in phospho-Src levels 1 hour after drug removal the Src-FRET reporter only showed an increase in about ~ 14 % of Src active cells compared to the initial controls. There are several possible reasons for this discrepancy in readouts, which can be attributed to the specific methodologies used for the read-outs and thus the different cellular cues observed. While the immunoblot reports on the state of autophosphorylation of Src itself, the Src-FRET reporter actually reports, due to its architecture, on the ability of Src to phosphorylate a substrate, more specifically the responsive region of p130Cas (Wang *et al*., 2005b). The reporter may well also be phosphorylated in part by Fyn kinase, but seeing as dasatinib also inhibits all Src family kinases (SFK), this should not play a role. Next to SFKs, dasatinib also inhibits

phosphorylation of p130Cas directly, which could further account for the lower shift observed after drug removal in the FLIM-FRET read-out compared to that of the immunoblot (Buettner *et al*., 2008). Another explanation for differences in read-outs could be that the reporter is subject to the whole range of cellular phosphatases. It thus reports on the dynamic system of antagonistic phosphatases competing with the phosphorylation of the reporter by Src, rather than just on Src phosphorylation itself. The "re-bound" was, however, also observed *in vivo*, at an expected delayed time point. This indicates that over-activation of Src after drug removal occurs both physically *in vitro* or by metabolic processes *in vivo*. This side-effect, when treatment subsides, could be overcome by more stringent treatment time points, assuring optimal inhibition of Src over time.

On the spatial site, the observed gradient in Src activity across the section of organotypic matrices in the control situation, showed the power of FLIM-FRET imaging in more accurately differentiating in activity of Src on a single cell basis in a 3D context. As seen in Figure 3.8 C mere positivity of phospho-Src could be detected by IHC staining, failing to detect the gradient of acitivty as revealed by FLIM imaging (see Figure 3.8 B). Two things could possibly explain the observed increase in Src activity with penetration depth in the PDAC cells. The serum gradient created across the matrix, with higher concentrations of FBS and associated growth factors near the bottom could account for an increase in Src activity observed at deeper penetration depths. The exposure to an air interface could further negatively regulate Src signalling inside the cells, which may in turn be increased by a more hypoxic setting. This becomes especially apparent when looking at the *in vivo* results of Src activity away form the local vasculature. Src activity appears to increase with increasing distances from a labelled blood vessel. This could be due to the decreasing concentration of oxygen away from the vessels and therefore the increase in hypoxia. The observation is in line with a previous study showing exactly that, namely that Src activity, and more precisely phospho-Src levels increase in hypoxic settings inside xenograft tumours (Pham *et al*., 2009).

It has been established in the KPC model that the inhibition of Shh by cyclopamine leads to a reduction in ECM (Olive *et al*., 2009). A normalization of this distribution of Src activity away from vessels after cyclopamine treatment could therefore be attributed to a decrease in ECM disposition in these tumours.

This in turn could further decrease interstitial pressure and allowing for a more free diffusion of oxygen and other soluble factors, away from local vasculature. Further, the decrease in ECM components could account for the decrease in Src signalling, as there may be fewer interactions via the integrin-FAK-Src axis to the local microenvironment (Chen *et al*., 2013). Finally, the fact that the effect of cyclopamine plus dasatinib on Src signalling was the same as cyclopamine treatment alone above 100 μm away from the local tumour vasculature, shows the inability of this combination treatment to improve drug efficacy above this threshold.

The results illustrating a decrease in Src activity after CXCR2SM inhibition both on organotypics and during *in vivo* imaging shows the usefulness of FLIM-FRET imaging in predicting treatment response for different treatment methods. Further refining intravital imaging, with the use of cutaneous imaging windows, helped to preserve the native tumour environment in this setting in especially, where neutrophil response was particularly important. Surgical exposure of the primary tumour for imaging can result in an influx of neutrophils, as it has been described previously that cutaneous wounds lead to an influx of inflammatory cells such as neutrophils (Singer and Clark, 1999). This in turn could perturb the therapeutic read-out of the CXCR2SM treatment. Using imaging windows therefore can allow for proper *in vivo* imaging to be conducted, without the immediate infiltrate of neutrophils following incision wounding.

4 Rac-1 activity dynamics revealed by the Rac-1 FRET mouse in a variety of mouse cancer models *in vivo*

4.1 Summary

Rac-1 is a small GTPase and an essential regulator of cell motility. To assess its role in variety of tissues and disease models, the Rac-1 FRET mouse was made. Rac-1 activity was found to be governed by autophagy in dendritic cells and upregulated in PyMT, ErbB2-driven breast cancer models as well as in the KPC pancreatic cancer model. Rac-1 activity was further spatially regulated both in 3D model *in vitro* and in tumour model *in vivo*. The GEF P-Rex1 constitutes an important regulator of Rac-1 activity in these models, with its loss leading to reduction or ablation of Rac-1 activity in primary tumours. Application of optical imaging windows showed differential spatial regulation of Rac-1 activity in PyMT and ErbB2-driven tumours, subject to cues from the local tumour microenvironment. Furthermore, longitudinal imaging in PyMT tumours revealed different response levels to Rac-1 inhibitors EHT 1864 and NSC 23766. Finally, elevated Rac-1 activity in KPC cells was linked to mTRAIL-receptor expression, the stable knock down and inhibition of which lead to a reduction in Rac-1 activity *in vitro* and *in vivo*.

4.2 Introduction

The Rho-GTPase Rac-1 is a key regulator of actin cytoskeletal organization, reactive oxygen species (ROS) production and cell migration. Its activity is upregulated in breast cancer (Schnelzer *et al*., 2000; Vega and Ridley, 2008; Feng *et al*., 2014). To assess the activity of Rac-1 *in vivo* in different tissues and in the context of different breast cancer models, the Rac-1 FRET mouse was made (Johnsson *et a*l., 2014). To this end the Rac-1 Raichu FRET sensor was used (Itoh *et al*., 2002), targeted to the *ROSA 26* locus and ubiquitously expressed.

Inhibition of autophagy in dendritic cells (DCs) has been shown to lead to increased activation of the adaptive immune response in inflammatory bowel disease (IBD) (Wildenberg *et al*., 2012). Furthermore, an increase in ruffling and reduction in filopodia formation was observed in autophagy deficient human DCs (Wildenberg M. A. personal communication). Rac-1 activity has been shown to regulate membrane ruffling (Ridley *et al*., 1992). In order to examine Rac-1 activity in DCs, bone marrow was isolated from Rac-1 FRET mice and differentiated to DCs using GM-CSF (Inaba *et al*., 1992). These were then treated with 3-methyladenine (3-MA), a common inhibitor of autophagy.

The activity of Rac-1 is governed by guanine nucleotide exchange factors (GEFs) and GTPase activating proteins (GAPs) (Rossman *et al*., 2005; Wertheimer *et al*., 2012). A particular GEF, phosphatidylinositol-3,4,5-trisphosphate-dependent Rac exchange factor 1 (P-Rex1) has been shown to be overexpressed in breast cancer. Furthermore, it has been demonstrated that P-Rex1 is associated with ErbB2 overexpression and can regulate PI3K signalling in breast cancer cells (Sosa *et al*., 2010; Montero *et al*., 2011; Hynes and Gattelli, 2011; Ebi *et al*., 2013). Rac-1 activity was shown to be unregulated in several mouse model of cancer such as the PyMT, KPC (Johnsson *et al*., 2014) and Erbb2-driven models (Johnson *et al*., 2010). As it is not entirely clear which of many possible GEFs control Rac-1 activity in these mouse models, the influence of P-Rex1 has been investigated in more detail here, by crossing the Rac-1 FRET cancer mouse models to P-Rex1 KO mice (Welch *et al*., 2005). Moreover, inhibition of Rac-1 has been shown (Rosenblatt *et al*., 2011; Katz *et al*., 2012;), by the inhibitor EHT 1864, effecting binding of GTP to Rac-1 and thus association of it with its effector proteins such as Pak1 and others (Désiré *et al*., 2005; Onesto *et al*., 2008; Shutes *et al*., 2007).

Another inhibitor of Rac-1 activity is NSC23766. It acts by inhibiting Rac-1 GEF exchange activity, notably that of Tiam1 and Trio (Gao *et al*., 2004). Understanding how these inhibitors fare *in vitro* would be the next step in models that display overactivation of Rac-1 such as the PyMT model. Further evaluation *in vivo* would give an idea of how the inhibitors would fare in primary PyMT tumours expressing the Rac-1 FRET reporter. The application of surgically engrafted with optical imaging windows (Kedrin *et al*., 2008; Gligorijevic *et al*., 2009) and longitudinal imaging could help to answer these questions. If Rac-1 activation in the context of the tumour microenvironment would be spatially regulated in both PyMT and ErbB2 primary tumours in the *in vivo* situation could further be investigated. Another aspect in which Rac-1 activity may be differentially regulated is mammary tumour progression to invasive carcinoma, described previously (Lin *et al*., 2003; Cowell *et al*., 2013). This in turn could have strong implications as to when Rac-1 is most potent and at which stage treatment of mammary cancers with Rac-1 inhibitors would yield the greatest benefit.

In a $KRas^{G12D}$ driven mouse model of pancreatic cancer, Rac-1 loss lead to a reduction in PanIN and adenoma formation with significantly prolonged survival rates (Heid *et al*., 2011). It has been shown that there are high levels of TRAIL apoptosis receptors expressed in pancreatic cancer cell lines (Ozawa *et al*., 2001). This seems counterintuitive when considering that tumours generally insensitive to TRAIL induced apoptosis and have even shown to upon inhibition lead to increased metastasis of pancreatic cancer cells (Trauzold *et al*., 2006). However, tumour cells still retain TRAIL expression, with murine cells in turn only expressing mTRAIL-R (Wu *et al*., 1999). When knocking down mTRAIL-R in cells, they displayed a more rounded morphology and a reduction in lamellopodia formation (Von Karstedt *et al*., 2015). This morphology was described before for cells lacking Rac-1 expression (Steffen *et al*., 2013). It would there fore be prudent to investigate what could contribute to this dependency on Rac-1 activity by expressing the Rac-1 Raichu reporter in KPC cells, knocking down mTRAIL-R and thus being able to measure Rac-1 activity *in vitro* and *in vivo*.

4.3 Results

4.3.1 Generation of the Rac-1 FRET mouse and reduction of Rac-1 in primary DCs after autophagy inhibition

A constitutively expressing Rac-1 FRET mouse was generated as described by Johnsson *et al*., 2014. The Rac-1 FRET reporter used was the Rac-1 Raichu probe (Itoh *et al*., 2002). It consists of full length Rac-1 and an active Rac-1 binding domain of PAK1 (a known effector of active Rac-1, see Chapter 1.2.2), flanked by the YFP and CFP (Figure 4.1 A). The donor CFP in turn is tethered to the membrane by a CAAX motif. When guanine nucleotide exchange factors (GEFs) are active in the cell, the GDP bound to Rac-1 in the probe is exchanged with GTP, leading to a conformational change in the reporter and the binding of Rac-1 to Pak1-domain. This in turn results in CFP and YFP being in close proximity to each other, resulting in FRET, when CFP is excited. This process is reversed upon the action of GTPase-activating proteins (GAPs) within the cell, rendering the probe in a non-FRET confirmation (Figure 4.1 A). This process in turn can be detected by FLIM of the donor fluorophore CFP. A short lifetime (FRET) indicates an active state of Rac-1, whereas a long lifetime (no FRET) indicates low Rac-1 activity. Therefore, through the action of GEFs and GAPs, Rac-1 activity at the membrane of the cells can be assessed live in a variety of tissues in these mice.

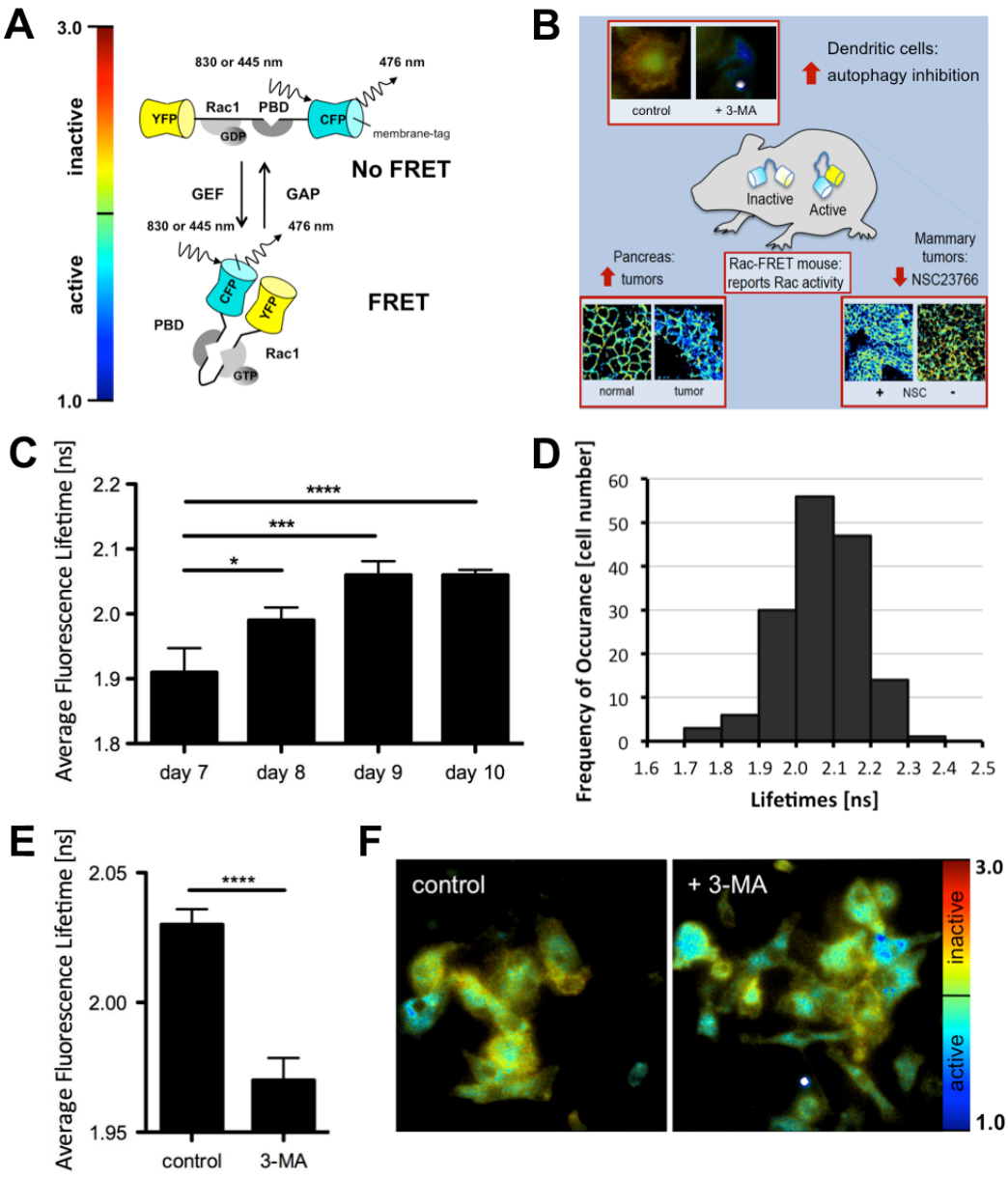

Figure 4.1: Rac-1 activity is down-regulated during DC maturation and increased upon autophagy inhibition

A Schematic of the Rac-1 FRET reporter with the fluorophore pair CFP and YFP, full length Rac-1 and an active Rac-1 binding domain of PAK1 (adapted from Itoh *et al*. 2002). **B** Tissues analysed with the Rac-1 FRET reporter mouse (adapted from Johnsson *et al*. 2014). **C** Primary dendritic cells differentiated from the bone marrow of the Rac-FRET reporter mice, quantified for Rac-1 activity *in vitro* during successive days of differentiation ranging from day 7 to day 10, n = 2-3 mice per condition, 302 cells in total; Mann Whitney U test, * $p < 0.05$, *** $p < 0.001$, **** $p < 0.0001$. **D** Distribution of Rac-1 FRET lifetimes at a bin size of 0.1 ns at day 10 of differentiation; n = 3 mice, 157 cells. **E** Quantification of average lifetimes of DCs at day 9 to 10 of differentiation, untreated and treated with 20 µM of 3-MA; n = 3 mice per condition, 646 cells in total; columns: mean; bars: SEM; Mann Whitney U test, **** $p < 0.0001$. **F** Representative lifetime map images of control DCs between day 9 and 10 of differentiation and DCs treated with 3-MA.

Treatment of isolated bone marrow cells with GM-CSF has been demonstrated to be an effective way of obtaining a large number of dendritic cells (DCs) (Inaba *et al*., 1992). Therefore, primary DCs were first differentiated from isolated bone marrow of Rac-1 FRET mice in culture. During the days 6 to 10 of the differentiation under GM-CSF *in vitro*, a decrease in Rac-1 activity was observed (Figure 4.1 C). A distribution of the single cell lifetimes and thus Rac-1 activity in the DC population at day 10 was also recorded (Figure 4.1 D). This in turn indicates that a range of Rac-1 activity can be found in a control situation *in vitro*. We further found, that Rac-1 could be activated to an extent in DCs by stimulation with an autophagy inhibiting agent, 3-MA, resulting in lower average lifetimes and thus more Rac-1 activity (Figure 4.1 E+F).

4.3.2 Rac-1 activity is upregulated in PyMT tumours and reduced upon heterozygous loss of P-Rex1

In order to determine whether Rac-1 activity was increased in an *in vivo* setting of a genetic mouse breast cancer model, the Rac-1 FRET mouse was crossed with the polyoma-middle-T antigen model (Guy *et al*., 1992b). Indeed, when compared to the native mammary epithelial tissue, Rac-1 was observed to be upregulated in PyMT driven lesions (Figure 4.2 A). The Rac-1 FRET reporter is subject to GEF activity inside the cells, which act upstream of Rac-1. We therefore further sought to determine whether the presence of a specific GEF, which has been recently implicated in breast cancer (Sosa *et al*., 2010; Hynes and Gattelli, 2011; Montero *et al*., 2011; Lucato *et al*., 2015), namely P-Rex1, would have an effect on Rac-1 activity in this model. The Rac-1 FRET expressing PyMT mice were consequently crossed with P-Rex1 KO mice (Welch *et al*., 2005) and allowed to form primary tumours. Heterozygous loss of P-Rex1 already revealed significantly reduced Rac-1 activity, when imaged *ex vivo* (Figure 4.2 B, mean ± SEM: MMTV-PyMT + P-Rex1$^{+/+}$: 1.82 ± 0.02 ns vs MMTV-PyMT + P-Rex1$^{+/-}$: 1.93 ± 0.02 ns).

Furthermore, the survival of PyMT mice crossed with the P-Rex1 KO mice revealed significantly increased survival in both heterozygous and homozygous KO mice compared to the WT PyMT cohort (Figure 4.2 C, from an average of 98 days survival in the WT control to 112 days in the homozygous KO).

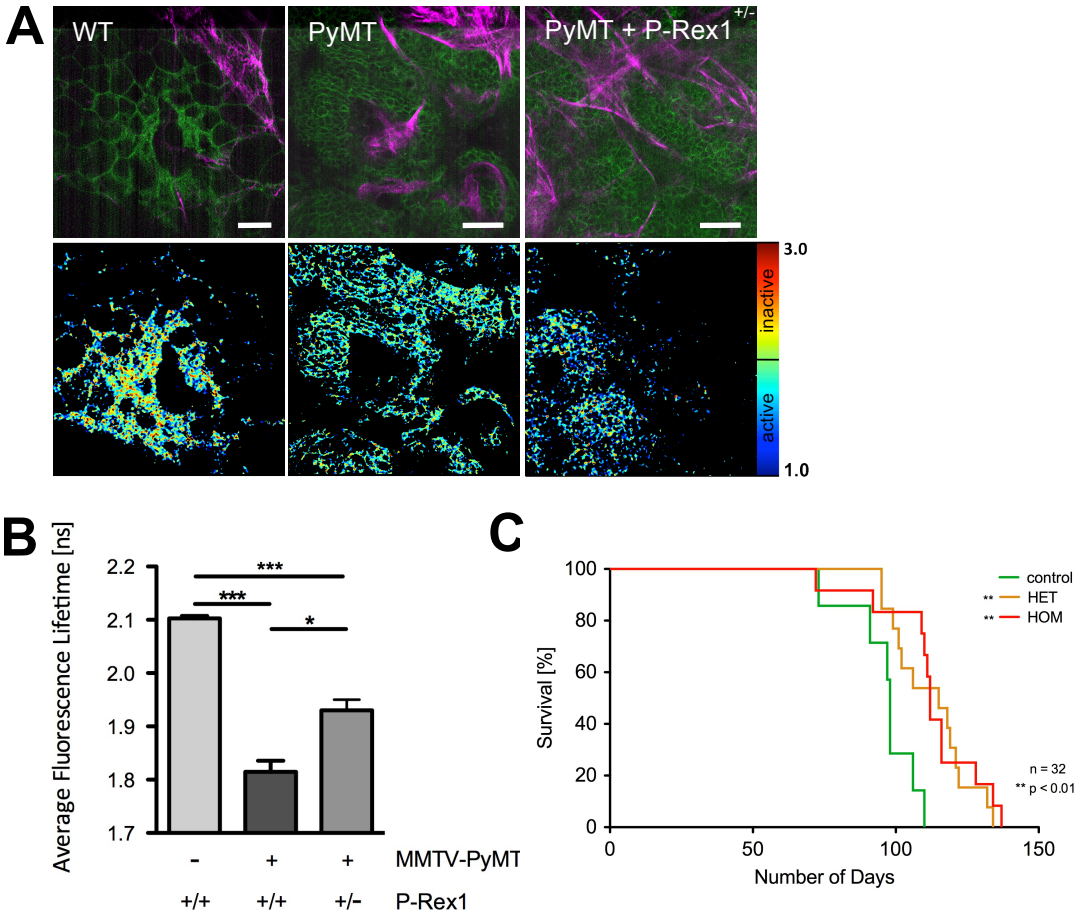

Figure 4.2: Rac-1 activity is upregulated in PyMT tumours and reduced upon heterozygous KO of P-Rex1. PyMT mice show increased survival upon KO of P-Rex1

A Rac-FRET mice crossed with MMTV-PyMT and P-Rex1 KO, taken at clinical endpoint of < 1.5 cm primary tumour size and imaged *ex vivo*, with intensity image in green for the Rac-FRET reporter and magenta for the SHG of collagen I, as well as the corresponding lifetime maps for each condition; scale bars: 50 µm. **B** Quantification of average lifetimes of individual cells inside the tumour mass, n = 3 mice per condition, 147 cells in total; columns: mean; bars: SEM; one way ANOVA, *** $p < 0.001$, * $p < 0.05$. **C** Survival curve of P-Rex1 KO mice; n = 32, Log-rank (Mantel-Cox) Test, ** $p< 0.01$

4.3.3 Rac-1 FRET expression in PyMT breast cancer models reveals differential Rac-1 activity in 2D versus 3D environments

To assess whether the inhibition of elevated Rac-1 activity observed in primary PyMT tumours expressing the Rac-1 FRET reporter could be effectively monitored by FLIM imaging using commercially available small molecule Rac-1 inhibitors, cell lines were isolated from primary PyMT tumours. Rac-1 has also been implicated next to migration in cell cycle progression (Olson *et al*., 1995; Moore *et al*., 1997; Saci *et al*., 2011). The cells were therefore first subjected to an MTT assay, in order to determine whether the Rac-1 inhibitors EHT 1864 and NSC 23766 had any effect on cell proliferation *in vitro*. 6 days of incubation at increasing concentrations of the respective inhibitors revealed that proliferation was not negatively altered for NSC 23766. For EHT 1864, however, there was a pronounced effect at concentrations above 1 μM (Figure 4.3 A).

Measuring the average fluorescent lifetime of the Rac-1 FRET reporter in these cells showed a significant reduction in Rac-1 activity *in vitro*, when they were subjected to previously established inhibitory concentrations of 20 μM EHT 1864 and 50 μM for NSC 23766 (Katz *et al*., 2012) for 1 hour prior to imaging (Figure 4.3 B+C).

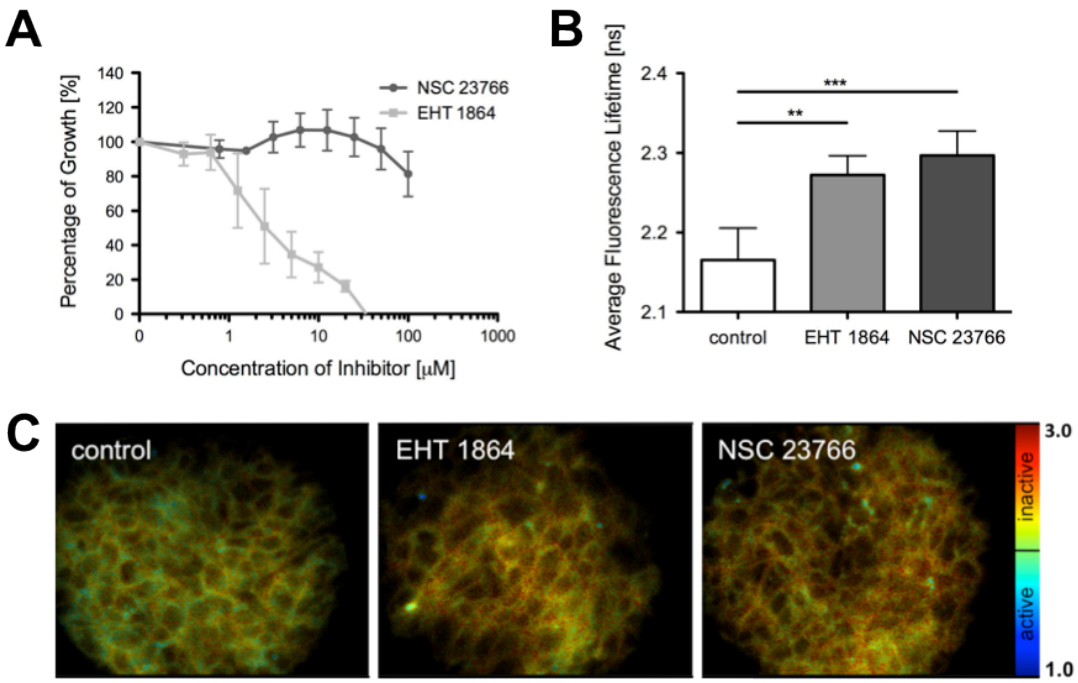

Figure 4.3: Rac-1 activity is effectively inhibited *in vitro* using EHT 1864 and NSC 23766
A PyMT cell line isolated from a primary PyMT tumour expressing the Rac-1 FRET reporter was subjected to increasing concentrations of EHT 1864 and NSC 23766 for 6 days and proliferation assessed by MTT assay; 3 independent experiments, data points: mean, bars: SEM. **B** Quantification of the average fluorescent lifetime of the Rac-1 FRET reporter expressed in the PyMT derived cell line, subjected to previously established inhibitory concentrations of EHT 1864 with 20 μM and NSC 23766 with 50 μM *in vitro* (Katz *et al*., 2012), with representative lifetimes heat map images in **C**; n = 2, columns: mean; bars: SEM; Mann Whitney U test, ** $p < 0.01$, *** $p < 0.001$

Rac-1 has been shown to be induced in cells via integrin engagement on ECM substrates previously (Berrier *et al*., 2002). Furthermore, plating of invasive breast cancer cells on a dense fibrillar collagen matrix resulted in increased invadopodia formation and Rac-1 activation (Artym *et al*., 2015). Having established that Rac-1 can be effectively inhibited in 2D culture, I wanted to examine whether Rac-1 inhibition could influence invasion in the PyMT cell line, as indicated previously (Katz *et al*., 2012). Rac-1 FRET expressing PyMT cells were therefore seeded on top of 3D organotypic matrices and allowed to invade for up to 12 days. During this time, cells completely traversed the matrices in the control situation, while in the presence of both EHT 1864 and NSC 23766 a reduction in invasion could be observed (Figure 4.4 A).

Further quantifying Rac-1 FRET signal of the invading PyMT cells, on a single cell basis, revealed increased Rac-1 activity with correlation to the depth penetrated in to the matrices (Figure 4.4 B+C).

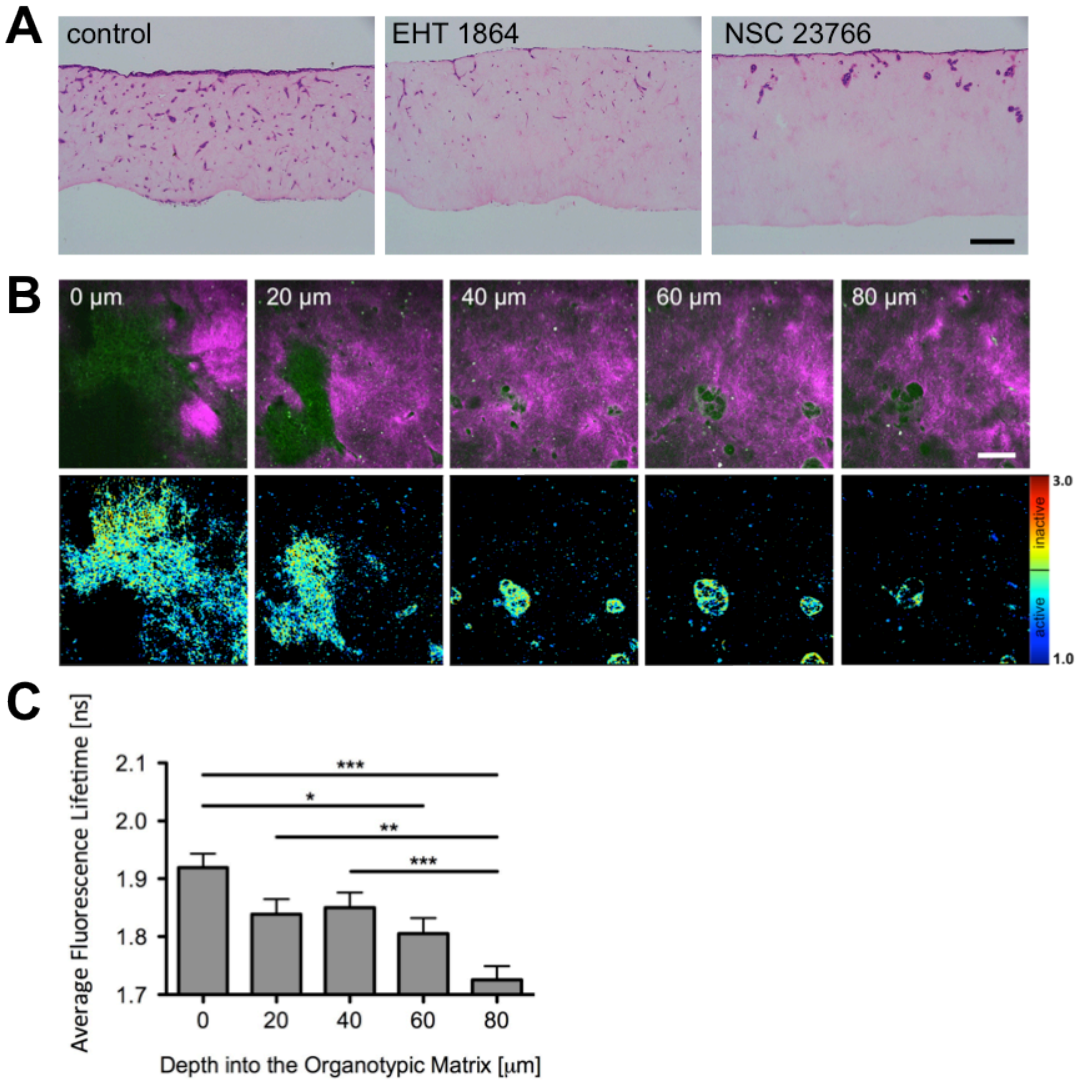

Figure 4.4: Rac-1 activity in PyMT cells is spatially regulated in organotypic matrices, the invasion into which is moderately inhibited by both EHT 1864 and NSC 23766

A PyMT cells isolated from a primary PyMT tumour expressing the Rac-1 FRET reporter were allowed to invade in to organotypic matrices for up to 12 days in a control setting and display a reduction in invasion in the presence of EHT 1864 (20 µM) and NSC 23766 (50 µM); 3 independent experiments. **B** Representative images of PyMT cells expressing the Rac-1 FRET reporter (green) invading into an organotypic matrix (collagen I from the SHG signal in magenta) with the respective lifetime heat map images at depths from 0 to 80 µm into the matrix. **C** Quantification of increased Rac-1 activity in invading PyMT cells, correlating to the penetration depth up to 80 µm into the matrices, on a single cell basis; n = 3 with 225 cells in total; columns: mean; bars: SEM; One-way ANOVA, ** $p < 0.05$, ** $p < 0.01$, *** $p < 0.001$

4.3.4 Rac-1 is differentially active during progressive stages of PyMT tumourigenesis and in different compartments of the tumour microenvironment as imaged *in vivo*

Having established that Rac-1 activity is differentially regulated in cell lines derived from primary Rac-1 FRET expressing tumours, I wanted to determine whether there was an influence of tumour progression on Rac-1 activity. Progressive stages of PyMT-driven tumours have been described previously, with hyperplasias progressing via adenomas to invasive carcinomas (Lin *et al*., 2003). PyMT mice expressing the Rac-1 FRET reporter were therefore allowed to develop primary tumours, which in turn were then imaged *ex vivo* during their progressive stages, from hyperplastic lesions to metastasis of the lung (Figure 4.5 A). Quantification of the single cell FLIM-FRET signal revealed that Rac-1 activity steadily deceased in progressive stage of cancerous lesions in the PyMT beast cancer model (Figure 4.5 B, mean ± SEM: hyperplasia: 1.66 ± 0.02 ns vs carcinoma: 1.86 ± 0.02 ns). It should be noted, that even at the carcinoma and metastasis stage, Rac-1 activity is still high, when compared to the native mammary tissue, which exhibited basal to no activity (Figure 4.5 vs Figure 4.2, mean ± SEM: carcinoma/metastasis: 1.86 ± 0.02 ns vs mammary: 2.10 ± 0.01 ns;).

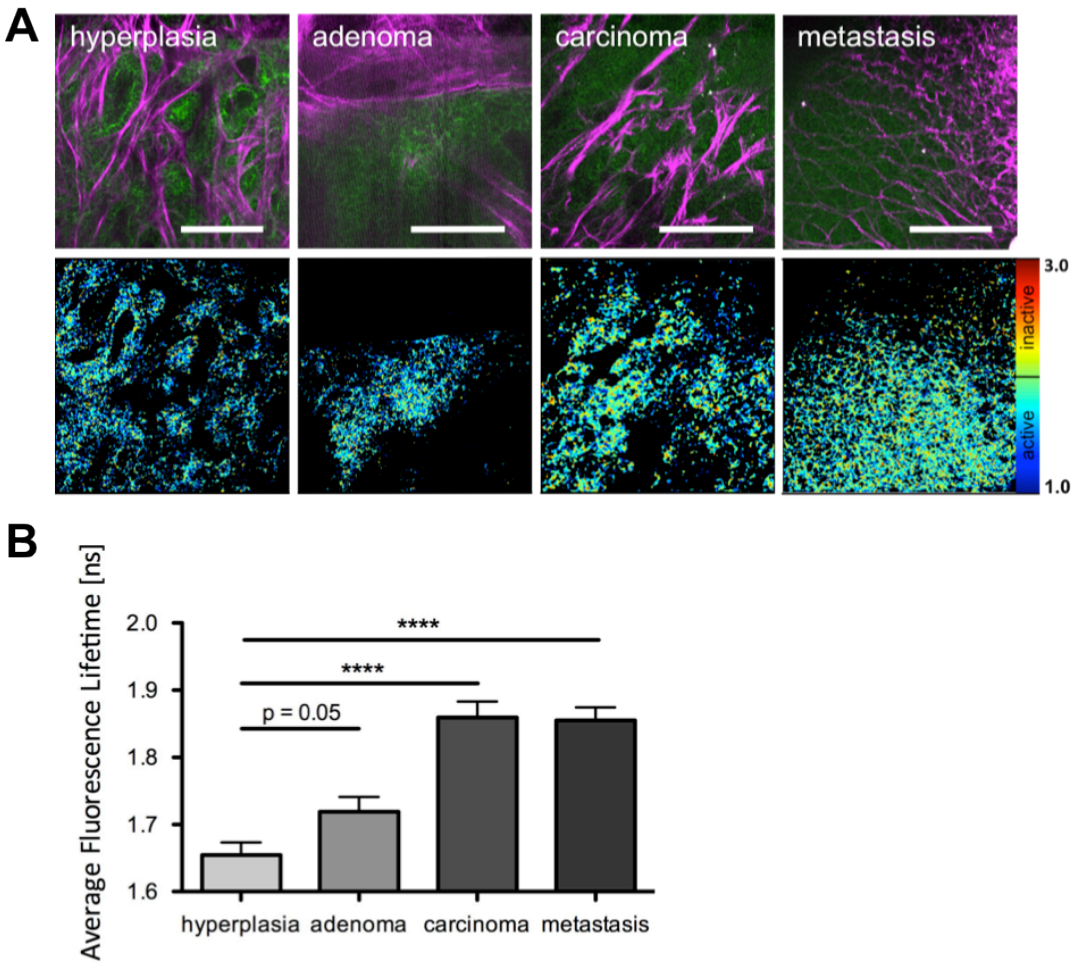

Figure 4.5: Rac-1 activity decreases in progressing stages of PyMT driven breast cancer

A Representative images of PyMT model expressing the Rac-1 FRET imaged *ex vivo* during progressing stages of breast cancer including hyperplasia, adenoma, carcinoma and metastasis of the lung, with intensity image in green for the Rac-1 FRET reporter and magenta for second harmonic generation (SHG) of collagen I as well as the corresponding lifetime maps. **B** Quantification of average lifetimes of individual cells inside the PyMT tumour mass at different stages of progression, n = 3 mice, 133 cells in total; columns: mean; bars: SEM; Mann Whitney U test, **** $p < 0.0001$; scale bars: 100 µm

The analysis of the PyMT cell lines expressing the Rac-1 FRET reporter revealed that Rac-1 was spatially regulated and indeed more active in a 3D environment compared to 2D (Figure 4.3 B vs Figure 4.4 C, mean ± SEM: on glass: 2.17 ± 0.04 ns vs on organotypic matrix: 1.92 ± 0.04 ns). An analysis of Rac-1 activity in the native tumour microenvironment was the logical next step in order to investigate whether Rac-1 was differentially regulated *in vivo*. PyMT mice expressing the Rac-1 FRET reporter were therefore allowed to develop primary tumours and optical windows surgically engrafted on top of them. Following 1-2 days of recovery mice were imaged. PyMT tumours and isolated cells have been shown to be locally invasive (Waldmeier *et al*., 2012) and form invasive border regions (Lin *et al*., 2003). Therefore, first the tumour border regions versus the center were analysed. The border and center regions were distinguished from one another by their probe expression, absent from beyond the border regions and their distinct collagen I (SHG) signature, observed previously from PyMT and human breast cancer cells xenograft tumours imaged on a multiphoton system (Wang *et al*., 2002; Provenzano *et al*., 2009). This revealed slightly elevated activity of Rac-1 at the primary tumour borders (Figure 4.6 A+B).

Another feature of the tumour microenvironment of interest is the local vasculature. In order to assess Rac-1 activity away from vessels, tumour and optical windows bearing mice were intravenously injected with a tracer dye prior to imaging (quantum dots, Qdot-tracker^{655}) (Figure 4.6 C). This allowed for the visualization of the vessels, measuring the proximity of single cells to the vasculature and correlating this with their respective Rac-1 activity signals. A general decrease of Rac-1 activity away from local vessels was recorded (Figure 4.6 D), with a distinct sharp increase between 10 μm and 20 μm.

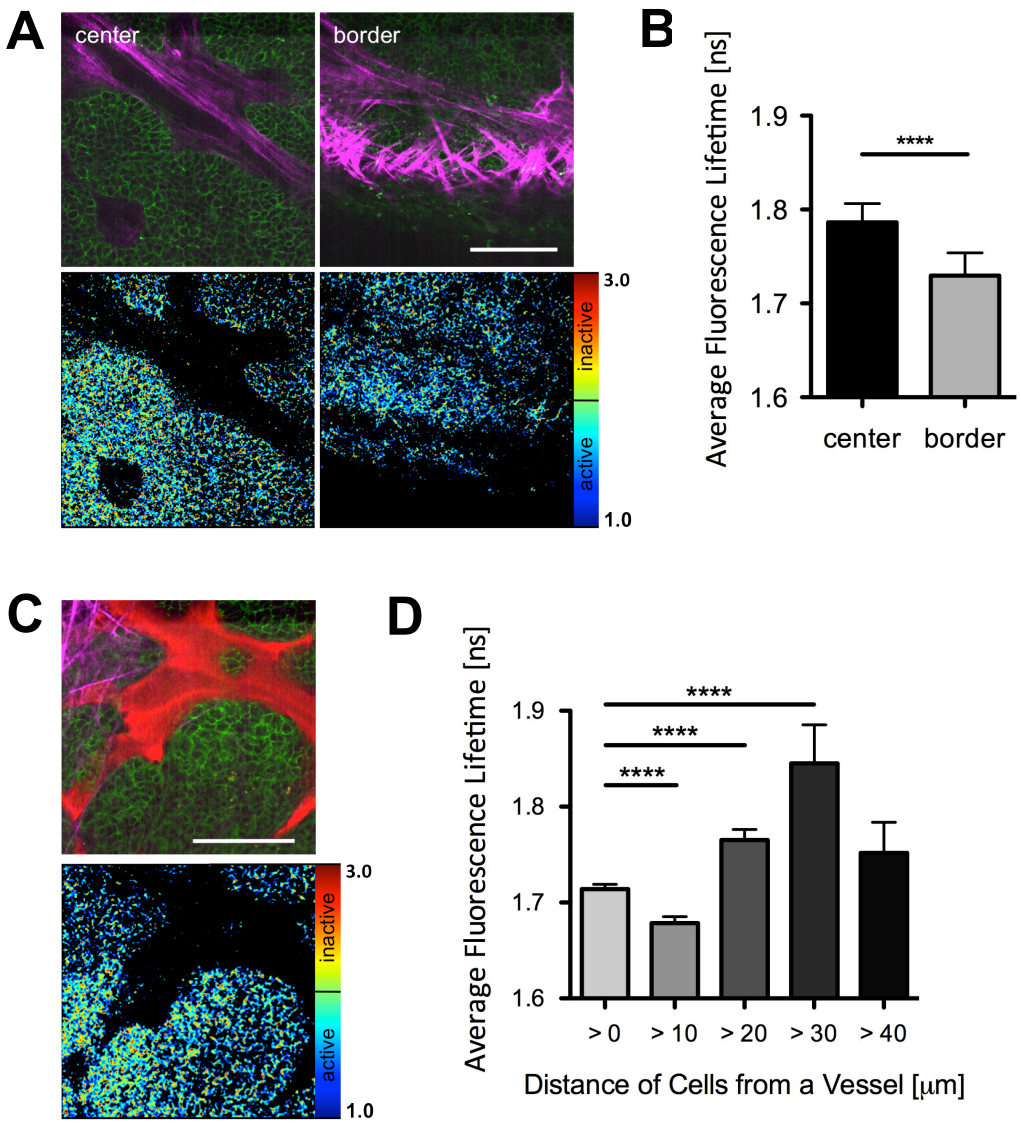

Figure 4.6: Rac-1 activity is upregulated at the border of PyMT tumours and decreases away from the local tumour vasculature

A Representative images of primary PyMT models expressing the Rac-1 FRET reporter imaged, implanted with AIWs, imaged *in vivo*, with intensity image in green for the Rac-1 FRET reporter and magenta for second harmonic generation (SHG) of collagen as well as the corresponding lifetime maps for both center and border regions. **B** Quantification of average lifetimes of individual cells inside the PyMT tumour mass at either center and borders regions, n = 3 mice per condition, 180 cells in total; Mann Whitney U test, **** $p < 0.0001$. **C** Representative image of the local tumour vasculature in red (Qdot-tracker^{655}) and corresponding lifetime map. **D** Quantification of the average fluorescent lifetime in 10 μm steps away form the local vasculature; n = 3 mice, 160 cells in total; columns: mean; bars: SEM; Student *t* test, **** $p < 0.0001$; scale bars: 100 μm

4.3.5 Longitudinal imaging of Rac-1 activity in the PyMT model *in vivo* reveals different pharmacodynamics of two Rac-1 inhibitors

Many factors can influence the ability of a drug to reach its target in an *in vivo* setting, including metabolic clearing, unspecific binding, uptake by non-target cells and their chemical composition (Benet and Zia-Amirhosseini, 1995; Lipinski, 2001). As Rac-1 activity is elevated in PyMT tumours and commercially available Rac-1 inhibitors effectively inhibited Rac-1 *in vitro* both in a 2D and 3D environment to different extents (Figure 4.3 vs Figure 4.4), an *in vivo* evaluation of these inhibitors was the next step. PyMT tumour bearing mice with a cutaneous optical imaging window (CIW) engrafted on top of their primary tumour were therefore imaged longitudinally to examine drug efficacy *in vivo*. First, in a control situation, mice were imaged up to 2 hours and an image acquired every 10 minutes. This revealed little to no fluctuation in Rac-1 activity *in vivo*, when Rac-1 FLIM lifetimes were quantified (Figure 4.7).

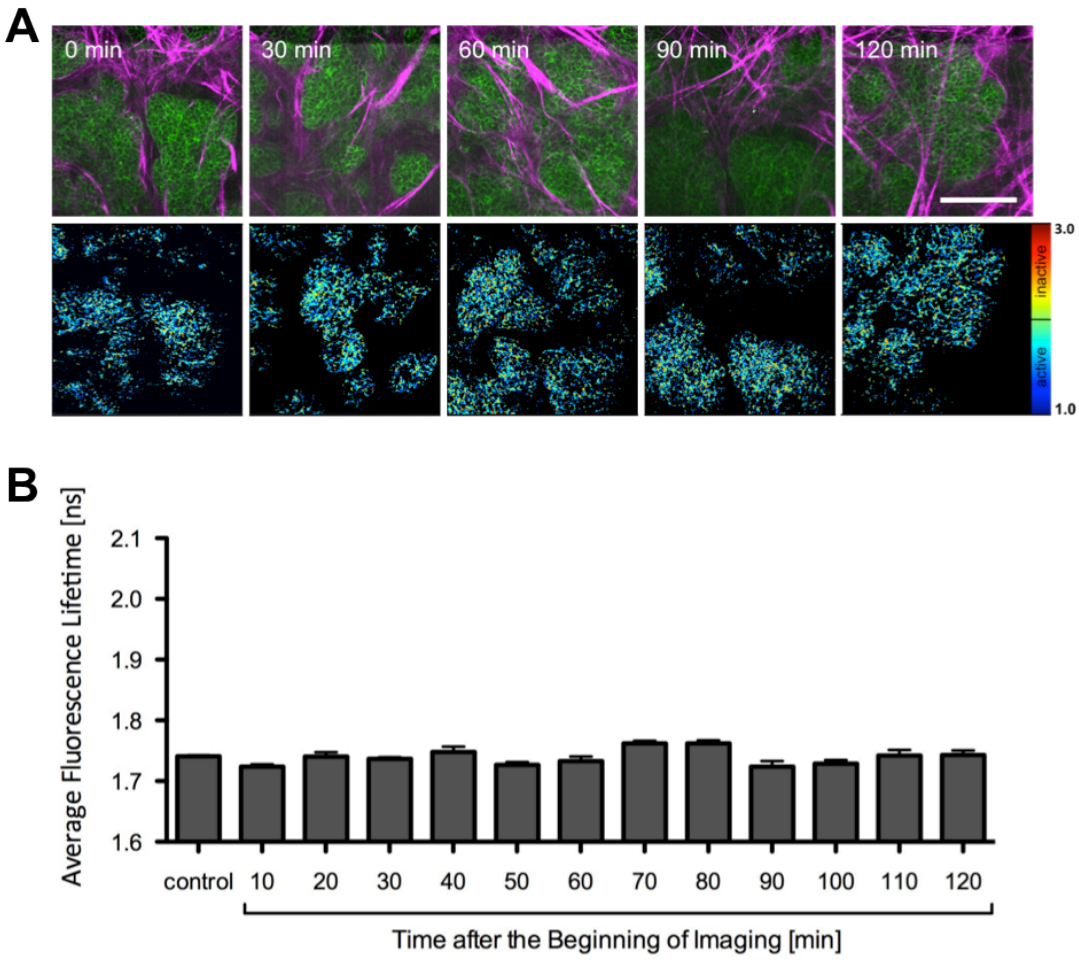

Figure 4.7: Rac-1 activity in primary PyMT tumours is unaltered during prolonged imaging *in vivo*
A Representative images of primary PyMT models expressing the Rac-1 FRET reporter, implanted with CIWs, imaged *in vivo*, with intensity image in green for the Rac-1 FRET reporter and magenta for second harmonic generation (SHG) of collagen as well as the corresponding lifetime maps during 2 hour time courses; scale bars: 100 µm. **B** Quantification of average lifetimes of individual cells inside the PyMT tumour mass after 10 minute intervals up to 2 hours; n = 3 mice per condition, 380 cells in total; columns: mean; bars: SEM

Next, mice were treated with a single intraperitoneal (i.p.) injection of 4 mg/kg of the Rac-1 inhibitor NSC 23766. This revealed a distinct targeting efficacy of this Rac-1 inhibitor by showing an effective inhibition after 50-60 minutes of the injection being administered to the mice (Figure 4.8 A+B). Further follow-up revealed that Rac-1 remained inactive up to 6 hours after the i.p. injection, increasing again further at 18 hours and finally returning to control values after 24 hours (Figure 4.8 C).

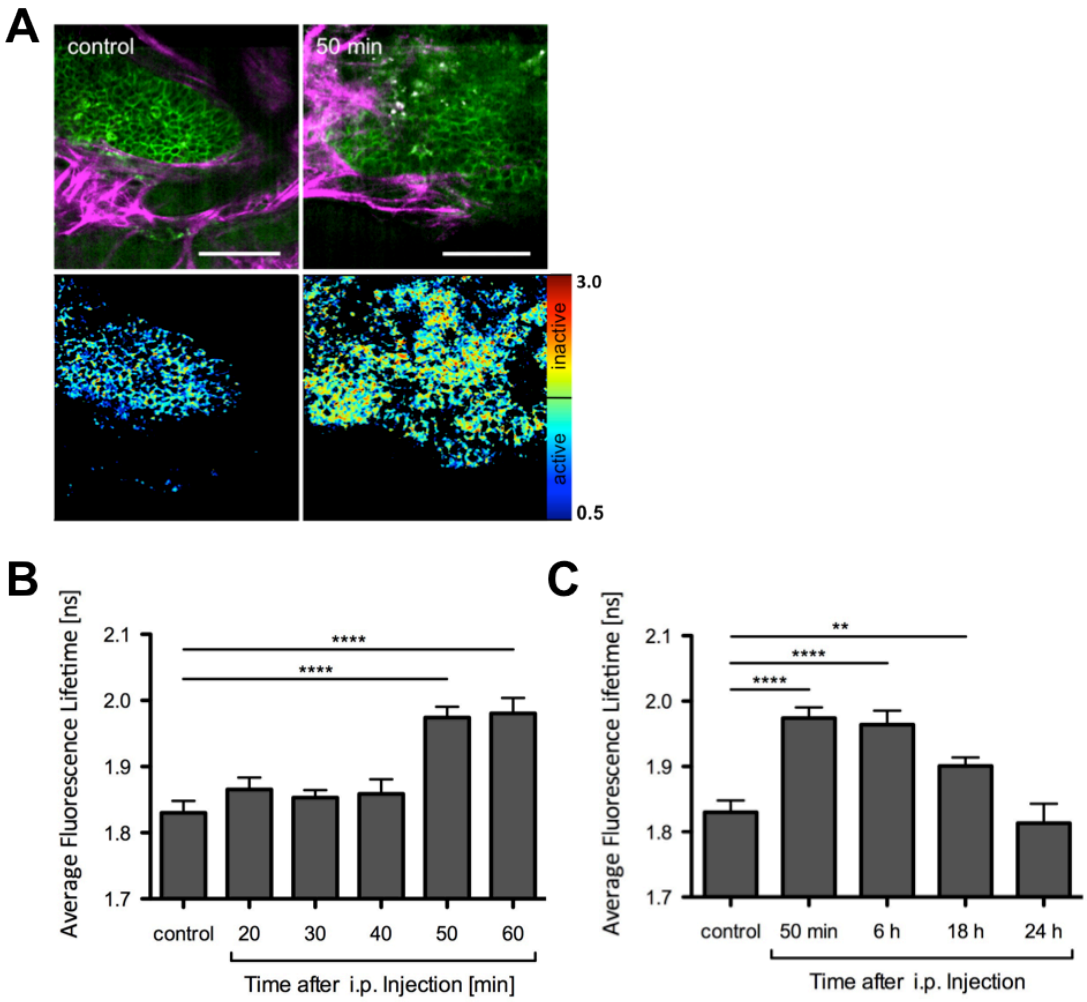

Figure 4.8: Rac-1 activity decreases upon treatment with NSC 23766 *in vivo* over time in PyMT driven breast carcinomas

A Representative images of primary PyMT carcinomas expressing the Rac-1 FRET reporter as imaged through CIWs *in vivo*, before and 50 minutes after i.p. administered treatment of 4 mg/kg of NSC 23766, with intensity image in green for the Rac-1 FRET reporter and magenta for second harmonic generation (SHG) of collagen I as well as the corresponding lifetime maps. **B** Quantification of average lifetimes of individual cells inside the PyMT carcinoma mass at different time points during NSC 23766 treatment up to 1 hour. **C** Quantitative monitoring *in vivo* of NSC 23766 treatment in PyMT carcinomas up to 24 hours post i.p. injection, n = 2 mice, 402 cells in total; columns: mean; bars: SEM; Mann Whitney U test, ** $p < 0.01$, **** $p < 0.0001$; scale bars: 100 µm

Evaluation of a different Rac-1 inhibitor, EHT 1864, affecting binding of active Rac-1 to down-stream targets, by imaging GTP-binding (Désiré *et al*., 2005), revealed poorer targeting *in vivo* by comparison. Here, Rac-1 activity was only effectively inhibited 120 minutes post i.p. (Figure 4.9 A+B) and already returned to control values after 6 hours of the injection being administered, demonstrating poor inhibition (Figure 4.9 C).

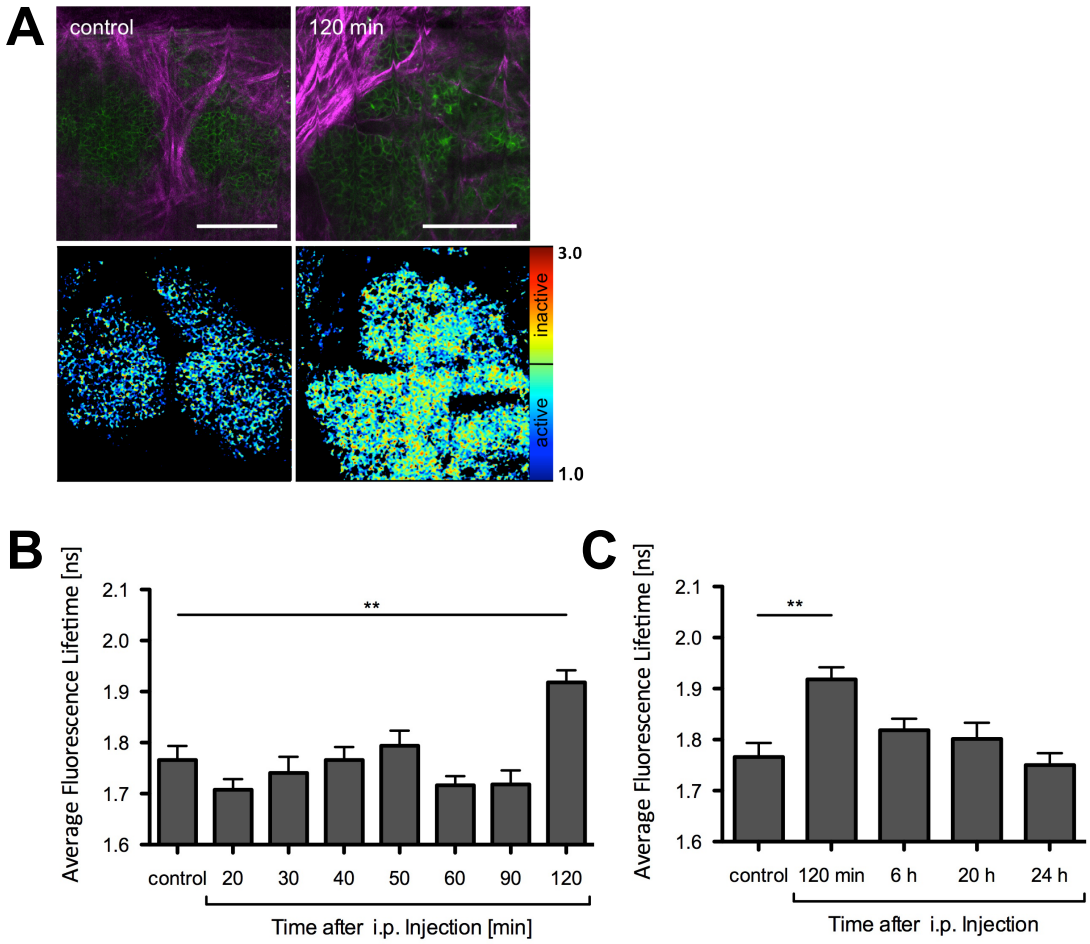

Figure 4.9: Rac-1 activity decreases upon treatment with EHT 1864 *in vivo* over time in PyMT driven breast carcinomas
A Representative images of primary early PyMT carcinomas expressing the Rac-1 FRET reporter as imaged through CIWs *in vivo*, before and 120 minutes after i.p. administered treatment of 4 mg/kg of EHT 1864, with intensity image in green for the Rac-1 FRET reporter and magenta for second harmonic generation (SHG) of collagen I as well as the corresponding lifetime maps. **B** Quantification of average lifetimes of individual cells inside the PyMT carcinoma mass at different time points during EHT 1864 treatment up to 2 hours. **C** Quantitative monitoring *in vivo* of EHT 1864 treatment in early PyMT carcinomas up to 24 hours post i.p. injection, n = 2 mice, 270 cells in total; columns: mean; bars: SEM; Mann Whitney U test, ** $p < 0.01$; scale bars: 100 µm

4.3.6 Rac-1 activity is upregulated in Her2 driven carcinomas and absent upon loss of P-Rex1

P-Rex1 has previously been strongly linked to regulating Rac-1 activity in ErbB2 receptor (Her2/neu) overexpressing breast cancer (Montero *et al*., 2011; Sosa *et al*., 2010). To examine this in the context of a transgenic mouse model, the Rac-1 FRET reporter mouse was first crossed to the MMTV-ErbB2 expressing breast cancer model (Guy *et al*., 1992a). These mice in turn were further crossed to the P-Rex1 KO mice (Welch *et al*., 2005). This revealed that Rac-1 activity is indeed upregulated in ErbB2 overexpressing tumours compared to the native mammary tissue. Further, the loss of P-Rex1 decreased Rac-1 activity in a gradual, dose dependent manner. Heterozygous loss led to a reduction in Rac-1 activity and a homozygous KO of P-Rex1 lead to basal Rac-1 activity, comparable to that found in the native mammary tissue (Figure 4.10 A+B).

Looking at the overall survival of the MMTV-ErbB2 tumour bearing mice, in terms of their clinical endpoint, revealed that despite the measurable reduction in Rac-1 activity observed in P-Rex1 heterozygous mice, only complete loss of P-Rex1 in the homozygous KO conferred a significant survival advantage (Figure 4.10 C).

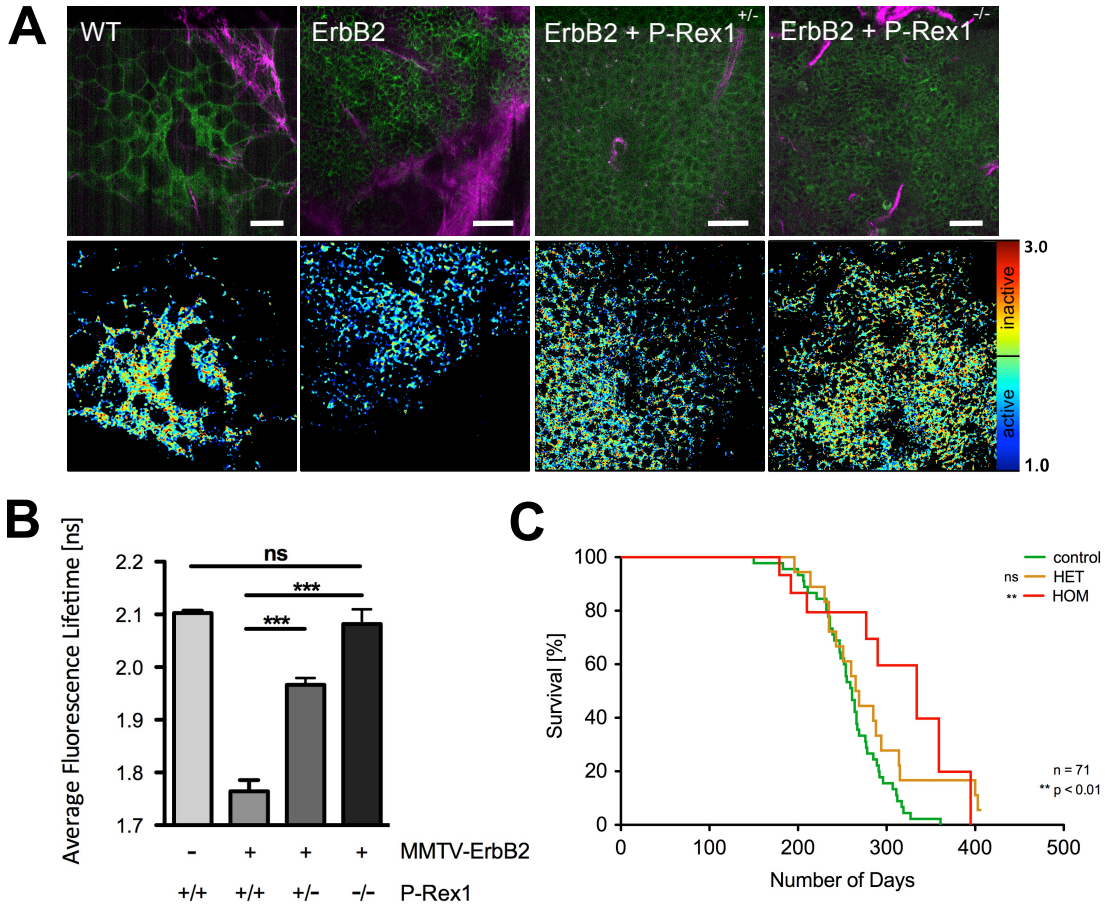

Figure 4.10: Loss of P-Rex1 abrogates upregulated Rac-1 activity in ErbB2 tumours and increases survival

A Rac-1 FRET mice crossed with MMTV-ErbB2 and P-Rex1 KO, taken at clinical endpoint of < 1.5 cm primary tumour size and imaged *ex vivo*, with intensity image in green for the Rac-1 FRET reporter and magenta for second harmonic generation (SHG) of collagen as well as the corresponding lifetime maps for each condition; scale bars: 50 µm. **B** Quantification of average lifetimes of individual cells inside the tumour mass, n = 3 mice per condition, 277 cells in total; columns: mean; bars: SEM; one way ANOVA, *** $p < 0.001$. **C** Survival curve of P-Rex1 KO mice, n = 71, Log-rank (Mantel-Cox) Test, ** $p < 0.01$

4.3.7 *In vivo* imaging reveals the ErbB2 breast cancer model displaying differential Rac-1 activation during disease progression and in specific compartments of the tumour microenvironment

In order to look at progressing stages of ErbB2 breast cancer mice, primary tumour bearing mice were implanted with optical imaging windows. This revealed high Rac-1 activity in imaged hyperplasias, which was significantly reduced in solid mammary intra-epithelial neoplasia (MIN) stage of ErbB2 tumour progression (Figure 4.11 A+B). It is worth noting again, that the Rac-1 activity is still very high at the MIN stage, when compared to the native mammary epithelial tissue (Figure 4.11 vs Figure 4.10 mean ± SEM: carcinoma/metastasis: 1.75 ± 0.03 ns vs mammary: 2.10 ± 0.01 ns).

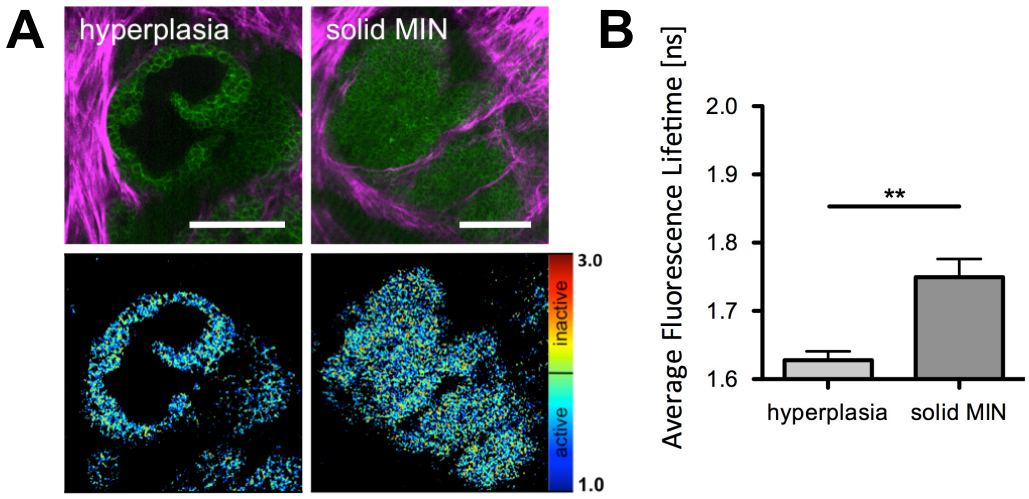

Figure 4.11: Rac-1 activity decreases in progressing stages of ErbB2 driven breast cancer
A Representative images of ErbB2 model expressing the Rac-1 FRET reporter during progressing stages including hyperplasia and solid mammary intra-epithelial neoplasia (MIN), with intensity image in green for the Rac-1 FRET reporter and magenta for second harmonic generation (SHG) of collagen I as well as the corresponding lifetime maps. **B** Quantification of average lifetimes of individual cells inside the ErbB2 tumour mass at different stages of progression, n = 1 mouse, 60 cells in total; columns: mean; bars: SEM; Mann Whitney U test, ** $p < 0.01$; scale bars: 100 µm

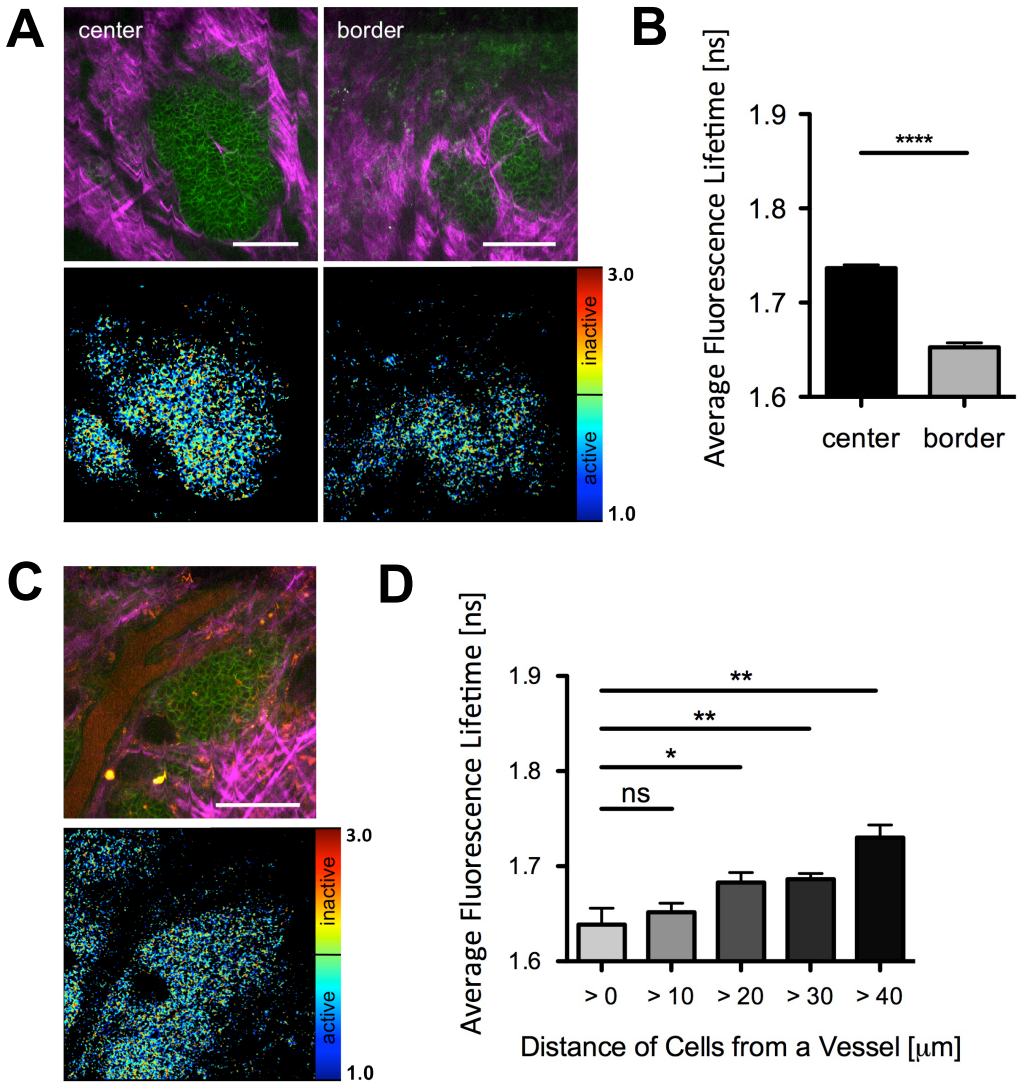

Figure 4.12: Rac-1 activity is upregulated at the border of ErbB2 tumours and decreases away from the local tumour vasculature

A Representative images of primary ErbB2 models expressing the Rac-1 FRET probe and implanted with CIWs were imaged *in vivo*, with intensity image in green for the Rac-1 FRET reporter and magenta for second harmonic generation (SHG) of collagen as well as the corresponding lifetime maps for both center and border regions. **B** Quantification of average lifetimes of individual cells inside the ErbB2 tumour mass at either center and borders regions, n = 4 mice per condition, 160 cells in total; Mann Whitney U test, **** $p < 0.0001$. **C** Representative image of the local tumour vasculature in red and corresponding lifetime map. **D** Quantification of the average fluorescent lifetime in 10 µm steps away from the local vasculature; n = 3 mice, 168 cells in total; columns: mean; bars: SEM; Student *t* test, * $p < 0.05$, ** $p < 0.01$; scale bars: 100 µm

Further, evaluating Rac-1 activity in the MMTV-ErbB2 overexpressing tumour mice in the context of the local tumour microenvironment revealed significant upregulation of Rac-1 activity in the border regions as imaged *in vivo* (Figure 4.12 A+B). In the context of the local vasculature Rac-1 decreased again steadily the further the cells were situated away from the closest vessel (Figure 4.12 C+D).

4.3.8 Rac-1 activity is upregulated in KPC tumours with haploinsufficiency of P-Rex1 leading to reduced native tissue levels of activity

Loss of Rac-1 has been shown to reduce the occurrence of tumours and early PanIN lesions in a $KRas^{G12D}$ driven PDAC model (Heid *et al*., 2011). We therefore wanted to determine whether Rac-1 signalling was upregulated in KPC tumours compared to the native pancreas tissue and whether the GEF, P-Rex1 had an influence on this activity. Rac-1 FRET mice were therefore crossed to the KPC model of PDAC and further with P-Rex1 KO mice. First and foremost this revealed that Rac-1 activity is indeed upregulated in primary PDAC compared to the native pancreas. Furthermore, heterozygous loss of P-Rex1 resulted in haploinsufficiency by showing a close to complete loss in Rac-1 activity in PDAC lesions. This activity was at basal levels, comparable to that of control pancreata (Figure 4.13 A+B, mean ± SEM: WT: 2.03 ± 0.01 ns vs KPC + P-Rex1+/-: 2.00 ± 0.03 ns).

No significant advantage or disadvantage in terms of survival became apparent, when comparing the KPC mice to the P-Rex1 heterozygous knock-out cohort (Figure 4.13 C).

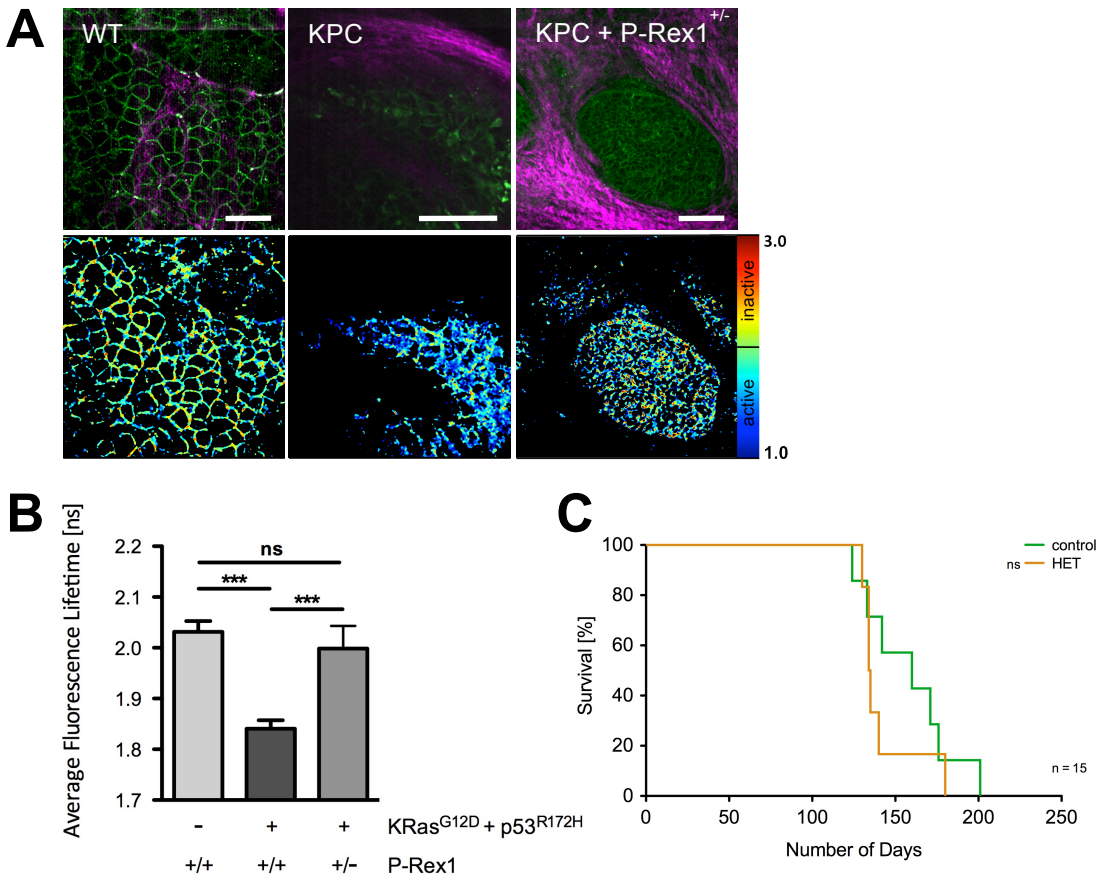

Figure 4.13: Rac-1 activity is upregulated in KPC tumours and reduced upon haploinsufficiency of P-Rex1

A Rac-1 FRET mice crossed with the KPC model and P-Rex1 KO mice, taken at clinical endpoint and imaged *ex vivo*, with intensity image in green for the Rac-1 FRET reporter and magenta for second harmonic generation (SHG) of collagen as well as the corresponding lifetime maps for each condition; scale bars: 50 µm. **B** Quantification of average lifetimes of individual cells inside the tumour mass, n = 3 mice per condition, 744 cells in total; column: mean; bars: SEM; one way ANOVA, *** $p < 0.001$, **C** Survival curve of KPC mice vs P-Rex1$^{+/-}$ mice, n = 15, Log-rank (Mantel-Cox) Test

4.3.9 Rac-1 upregulation in KPC tumours is dependent on mTRAIL-R expression *in vitro* and *in vivo*

Overexpression of TRAIL and its receptor have been shown previously in human pancreatic cancer cell lines (Ozawa *et al*., 2001). Mice in turn only express a single TRAIL like receptor, mTRAIL-R (Wu *et al*., 1999). Here, we sought to determine, whether knock down (KD) of mTRAIL-R decreases the previously observed high activity of Rac-1 in KPC cells.

To examine this, an EGFP/mRFP version of the Rac-1 Raichu FRET reporter was used (Figure 4.14 A). Stable KD PDAC cell lines, transduced with either a control vector (shCtr) or short-haiprin RNAs targeted toward mTRAIL-R (sh23, sh25) were generated (Figure 4.14 B). These were subsequently transfected with the EGFP/mRFP Rac-1 FRET reporter and Rac-1 measured *in vitro* (Figure 4.14 C). This revealed that, particularly for sh25, stable knock down cells showed a reduction of Rac-1 activity (Figure 4.14 D). Furthermore, treatment of the shCtr PDAC cell line with recombinant receptor blocking protein mTRAIL-R-Fc, lead to a significant reduction in Rac-1 activity, which was not observed in turn, when cells were treated with the vehicle (Figure 4.14 E).

In order to see if the *in vitro* results would hold true in an *in vivo* setting, $CD1^{-/-}$ nude mice were subcutaneously injected with the stable KD cell lines and primary tumours allowed to develop. Optical imaging windows were subsequently implanted on top of the primary tumours and Rac-1 activity imaged *in vivo* (Figure 4.15 A). This revealed that both sh23 and sh25 had indeed an effect on reducing Rac-1 activity in the stable PDAC cell lines (Figure 4.15 B). Furthermore, to see if the blocking protein mTRAIL-R-Fc in mice bearing shCtr PDAC allograft tumours would result in inhibition of Rac-1 activity *in vivo*, tumour-bearing mice were treated by i.p. injections. This showed effective inhibition of Rac-1 activity *in vivo* after 1 hour of the injection being administered (Figure 4.15 D). This in turn was not observed when mice were treated with the PBS vehicle control (Figure 4.15 C).

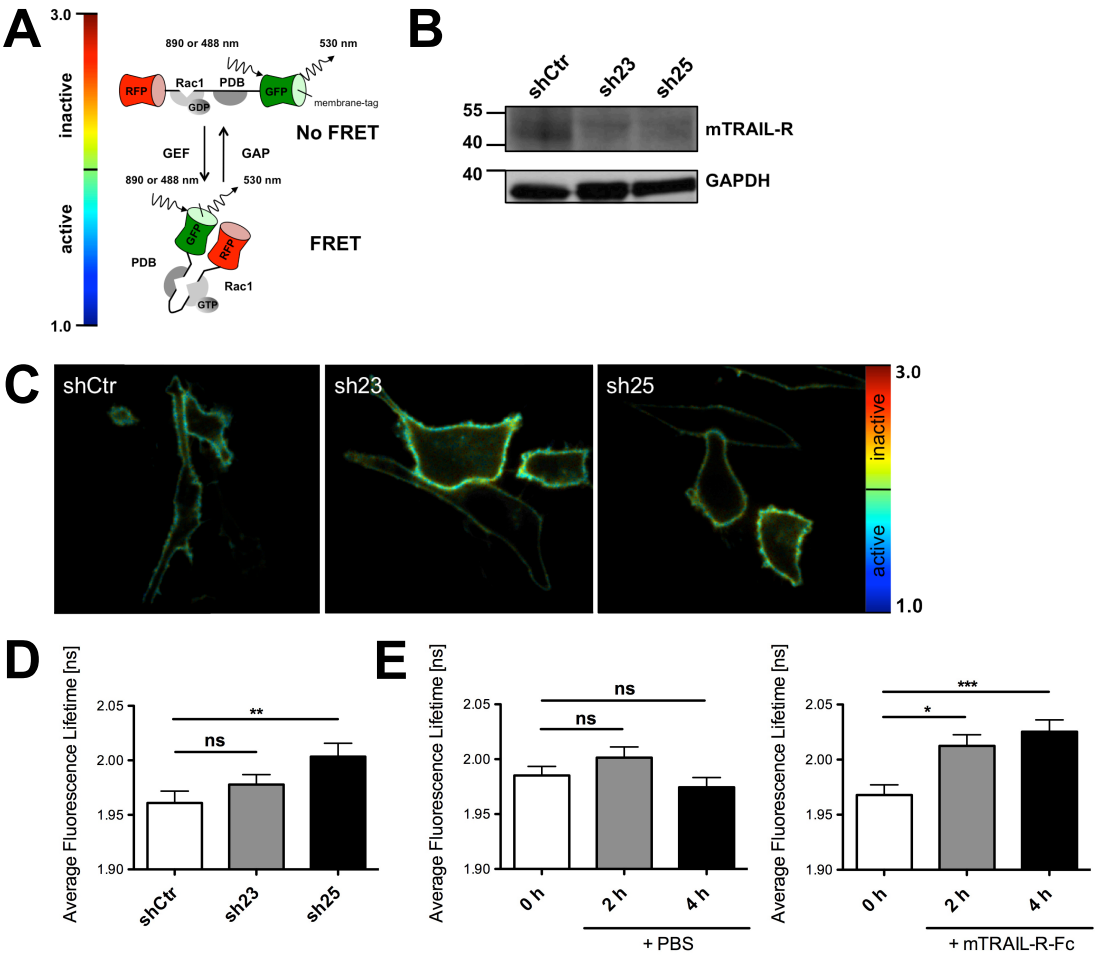

Figure 4.14: Knock down of mTRAIL-R in PDAC cells as well as treatment with mTRAIL-R-Fc results in a reduction in Rac-1 activity *in vitro*

A Schematic of the Rac-1 Raichu FRET reporter, expressing the fluorophore pair EGFP and mRFP. (adapted from Itoh *et al*. 2002). **B** Immunoblot for mTRAIL-R expression, with GAPDH as a control, in PDAC cells stably expressing a control shRNA (shCtr) or shRNAs for mTRAIL-R (sh23 and sh25). **C** Representative FLIM images of control and stable KD (sh23 and sh25) PDAC cells *in vitro*. **D** Quantification of single cell Rac-1 activity before and after KD of mTRAIL-R *in vitro*, n = 3, 93 cells; Mann Whitney U test, ** $p < 0.01$, **E** PDAC shCtr expressing the Rac-1 FRET reporter treated with either PBS or the recombinant mTRAIL-R-Fc protein, with single cell Rac-1 activity quantified before, 2 and 4 hours after addition *in vitro*, n = 3, 182 cells; columns: mean; bars: SEM; Mann Whitney U test, * $p < 0.05$, *** $p < 0.001$

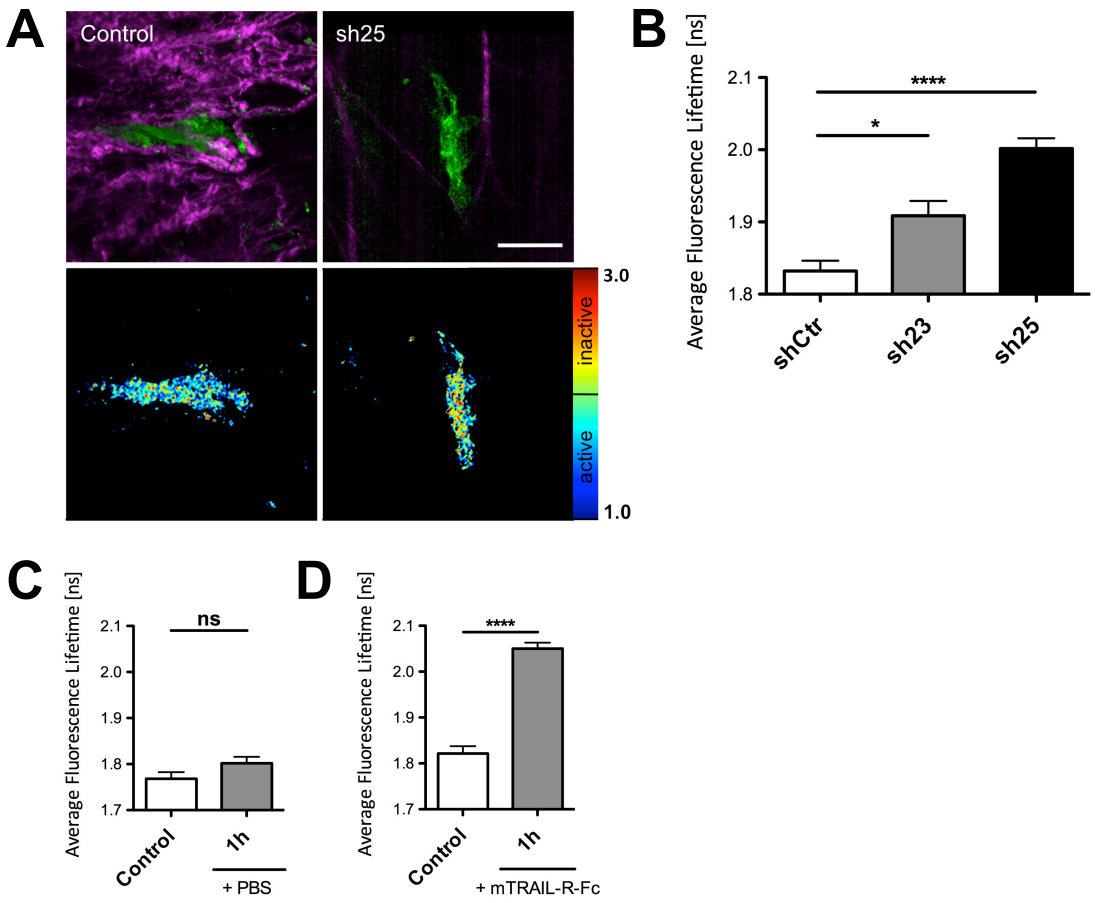

Figure 4.15: Knock down of mTRAIL-R and treatment with mTRAIL-R-Fc leads to reduced Rac-1 activity in PDAC cells imaged through optical imaging windows *in vivo*

A Representative images of PDAC cells expressing the Rac-FRET reporter and a control shRNA (shCtr) or a shRNA targeted toward mTRAIL-R (sh25) in an allograft tumour, implanted with optical skin imaging windows, with intensity image in green for the Rac-1 FRET reporter and magenta for second harmonic generation (SHG) of collagen I as well as the corresponding lifetime maps. **B** Quantification of single cell Rac-1 activity of PDAC cells stably expressing shCtr, sh23 or sh25 *in vivo*, respectively, n = 3 mice per condition, 389 cells. **C** Quantified single cell Rac-1 activity in primary PDAC allograft tumours treated with an i.p. injection of PBS (vehicle), n = 3 mice per condition, 364 cells. **D** or the recombinant mTRAIL-R-Fc protein and imaged 1 hour post i.p., n = 3 mice per condition, 349 cells; column: mean; bars: SEM; Mann Whitney U test, * $p < 0.05$, **** $p < 0.0001$; scale bar: 50 µm

4.4 Discussion

In this chapter the activity of Rac-1 in a variety of tissues and cancer mouse models was described, using the Rac-1 FRET mouse (Johnsson *et al*., 2014) on the basis of the Rac-1 Raichu FRET sensor (Itoh *et al*., 2002).

In primary murine DCs Rac-1 was increasingly down-regulated in progressing days of differentiation (Figure 4.1 C). In a different immune cell population present in IBD, namely macrophages, Rac-1 and Rac-2 are dispensable for directional movement (Wheeler *et al*., 2006). Moreover, increased Rac-1 activity results in arrest of macrophage locomotion (Pagler *et al*., 2011), potentially trapping the cells at sites of chronic inflammation. A similar mechanism may occur in DCs deficient for autophagy, which have been shown to increase the adaptive immune response (Wildenberg *et al*., 2012). Here we have shown that inhibition of autophagy in these cells increased Rac-1 activity (Figure 4.1 E). Migration in primary DCs was further greatly reduced when autophagy was inhibited (Wildenberg M., personal communication, data not shown). Thiopurines, which are commonly used in the treatment of IBD, inhibit Rac-1 activity. They have previously been shown in macrophages to restore migration in trapped Rac-1 hyper-activated cells, by inhibiting that Rac-1 activity (Park *et al*., 2012). Thiopurines were therefore applied to autophagy reduced DCs and showed a reduction in Rac-1 activation levels as well (Wildenberg M., personal communication, data not shown). Rather than migration, it becomes clear that Rac-1 functions in these cell types in a different capacity. This could be for example as a regulator of the actin cytoskeleton track along which autophagosome trafficking inside the cells could occur. This has been described before, again in macrophages, where Rac-1 mediated actin remodelling is required the for recycling of endosome-mediated secretion of tumour necrosis factor (TNF) (Stanley *et al*., 2014).

Upregulation of Rac-1 activity in breast cancer cells, conversely, has been established to drive invasion in an integrin dependent manner on collagen substrate (Keely *et al*., 1997). This is in line with our observation that Rac-1 activity was upregulated in PyMT cells on top of collagen I organotypic matrices compared to 2D culture on glass (Figure 4.3 B). Further, increasing depths penetrated by the PyMT cells was correlated to increased Rac-1 activity in these cells (Figure 4.4 C). This can be further attributed to the activation of Rac-1 in cells by serum (Ridley *et al*., 1992).

A gradient of serum has been proposed to exist across the organotypic matrices by diffusion of the serum from the bottom upward into the matrix (Muinonen-Martin *et al*., 2014). Specifically growth factors contained in foetal bovine serum, such as transforming growth factor β (TGF-β), insulin-like growth factor (IGF) and insulin-like growth factor binding protein 2 (IGFBP2) (Zheng *et al*., 2006), amongst others, act on Rac-1 activation, cell motility and invasion (Wang *et al*., 2006a, 2006b; Zhao *et al*., 2011).

A similar argument can be made for the observation of the reduction in Rac-1 activity away from the local tumour vasculature (Figure 4.6 D and Figure 4.12 D). This would suggest that Rac-1 activity in both PyMT and ErbB2-driven primary carcinomas is dependent on growth factor diffusion away from local vessels. For PyMT mice a proteomic screen of the plasma identified, IFGBP2 and IGF, amongst others, to be upregulated (Pitteri *et al*., 2008). A further screen was conducted for the plasma of a doxycycline induced ErbB2 driven cancer model, which showed, amongst many others, IFGBP2 upregulated in the tumour bearing situation compared to wildtype controls (Schoenherr *et al*., 2011). Which growth factors play the dominant role in the tumour microenvironment, in terms of the tumour vasculature remains to be determined.

Inhibition of Rac-1 activity *in vitro* showed that both EHT 1864 (Shutes *et al*., 2007) and NSC 23766 (Gao *et al*., 2004) were able to actively reduce invasion on organotypic matrices (Figure 4.4 A). For EHT 1864, however, this activity may be linked to its negative effect on proliferation, rather than invasion, as shown by MTT assay. Rac-1/PAK1 signalling in turn has been shown to be disrupted by EHT 1864 treatment and further found to be essential in beast cancer cell proliferation and survival (Arias-Romero *et al*., 2010).

The Rac-1 GEF P-Rex1 has previously been described to be overexpressed in human breast cancers (Hynes and Gattelli, 2011) and closely associated with the action of the ErbB2 receptor (Sosa *et al*., 2010). Furthermore, it has been related to PI3K regulating ERK signalling (Ebi *et al*., 2013). Moreover, in breast cancer cells loss of expression of P-Rex1 results in a reduction of invasiveness (Montero *et al*., 2011). It comes as no surprise then, that upon loss of P-Rex1 in the PyMT and ErbB2 overexpressing mouse breast cancer models, Rac-1 activity was reduced. There are a variety of GEF associated with Rac-1 activity.

Here, loss of P-Rex1 indicates that this particular GEF plays the major role in regulating Rac-1 activity in the ErbB2 driven breast cancer model. This becomes apparent when looking at the fact that homozygous KO of P-Rex1 completely ablated Rac-1 activity in tumours.

Furthermore, the fact that heterozygous KO lead to an almost dose-dependent reduction in Rac-1 signalling, halfway between the WT and complete KO situation, points toward P-Rex1 being the major regulator of Rac-1 activity in this tumour type. Further to the reduction of Rac-1 activity, a survival advantage in both PyMT and ErbB2 overexpressing mice was observed upon P-Rex1 KO. This is in line with a previous report, stating that loss of either P-Rex1 or Rac-1 signalling leads to a decrease in viability in breast cancer cells *in vitro* and *in vivo* (Dillon *et al*., 2015).

Heightened Rac-1 activity was also observed in the KPC model, in line with previous reports that show a requirement of Rac-1 and its activity in the tumourigenesis and progression of PDAC tumours (Heid *et al*., 2011; Razidlo *et al*., 2015). The Rac-1 GEF Vav1 has recently been further associated with pancreatic cancer metastasis. Here, we find that, in turn, the heterozygous loss of the Rac-1 GEF P-Rex1 reduces Rac-1 signalling in primary KPC tumours down to levels comparable to that of the native pancreas (Figure 4.13 B). This indicates a key role of this GEF in the control of Rac-1 activity in pancreatic cancer. An impact on survival in the KPC mice with heterozygous loss of P-Rex1 was not observed (Figure 4.13 C). As demonstrated previously, however, reduction in for example metastatic formation, which was not yet examined in detail here, does not confer a survival advantage in the KPC model (Morton *et al*., 2010b). Further examination of the invasive capability of PDAC cells lacking P-Rex1, however, still needs to be evaluated, to establish its role in pancreatic cancer cell migration and invasion.

Taken together the data suggest that P-Rex1 plays a key role in regulating Rac-1 in these models of breast and pancreatic cancer. A small molecule inhibitor that hinders the GEF action of specifically P-Rex1, and none of the other GEFs, on Rac-1 has been described previously. It would therefore be prudent in the future to examine, whether this inhibtior, 1A-116 (Cardama *et al*., 2014), would have an effect on reducing this elevated activity *in vitro* and *in vivo* in the PyMT, ErbB2 and KPC tumour models.

It appears counterintuitive that many cancers overexpress apoptosis inducing TRAIL-R receptors (Daniels *et al*., 2005; Ganten *et al*., 2009; Macher-Goeppinger *et al*., 2009; Ozawa *et al*., 2001). In the case of pancreatic cancer, TRAIL-Rs have been shown to be overexpressed (Ozawa *et al*., 2001) and more specifically TRAIL-R2 expression has been found to promote tumour progression via non-apoptosis pathways (Haselmann *et al*., 2014). Furthermore, constitutive signalling from TRAIL-R2 increases invasion and promotes activation of the PI3K and Rac-1 signalling axis (Von Karstedt *et al*., 2015). PI3K regulation of Rac-1 in turn has been found to be required for mutant *KRas*-induced PanIN formation (Wu *et al*., 2014). We have shown here, that Rac-1 activity is indeed dependent on mTRAIL-R expression in murine PDAC cells, the loss of which in a knockdown led to the reduction of Rac-1 activity both *in vitro* and in a allograft *in vivo*.

Rac-1 in turn has been described as an important mediator of migration and invasion in several cell types (Sanz-Moreno *et al*., 2008; Yamazaki *et al*., 2009). In a model of pancreatic cancer, specific inhibition of the GEF Vav1 reduced Rac-1 signalling and thus invasion and metastasis (Razidlo *et al*., 2015b). Finally, the absence of human TRAIL-R2 or systemic treatment with TRAIL-R2-Fc inhibited lung tumour growth and KPC liver metastasis (Egberts *et al*., 2008), pointing toward an active role of Rac-1 signalling in the migration and invasion of PDAC cells. Here, we have shown that systemic treatment of PDAC cells *in vitro* and by i.p. injection *in vivo* with the TRAIL receptor inhibitory protein, mTRAIL-R-Fc, effectively inhibited Rac-1 activity and thus potentially cell migration and invasion.

5 A RhoA-FRET mouse reveals tissue and disease specific RhoA activity *in vivo*

5.1 Summary

RhoA constitutes another GTPase with key roles in several types of cancer in terms of proliferation and migration. In this chapter, the generation of a RhoA-FRET biosensor mouse, which expresses the Raichu-RhoA reporter in either all tissues or under the regulation of tissue specific Cre-recombinases was described. RhoA activity was assessed in healthy and disease states of skin, intestinal, pancreatic and mammary tissues. The basal RhoA activity observed both in normal mammary tissue and ErbB2 driven breast cancer was increased in the PyMT driven cancer model and effectively inhibited using dasatinib as observed using longitudinal imaging through cutaneous imaging windows. *In vivo* imaging using the abdominal imaging windows in turn allowed for the observation of RhoA activity in both the gut and the pancreas. There, RhoA activity was found to be decreased in progressing states of pancreatic cancer (PanINs) driven by mutant $KRas^{G12D}$ alone or in conjunction with mutant $p53^{R172H}$. However, in the end stages of PDAC, RhoA activity was increased again, especially at the invasive edge of the tumour and in metastasis of the liver. Targeting Src with dasatinib and EGFR with erlotinib treatment was effective at indirectly RhoA activity. Both were monitored *in vivo* employing abdominal imaging windows.

5.2 Introduction

It has been demonstrated that RhoA plays key roles in several aspects of cellular homeostasis, ranging from cell cycle progression, apoptosis, angiogenic factor secretion and cell motility (Karlsson *et al*., 2009). RhoA further plays a key role in regulating actomyosin contractility (Wheeler and Ridley, 2004). RhoA and Rac-1 have been shown to be reciprocally active at the edge of moving cells (Machacek *et al*., 2009), as well as function during different modes of migration, with Rac-1 activity associated with mesenchymal migration and RhoA with amoeboid migration (Friedl and Alexander, 2011). RhoA acts on stimulating actin polymerization through the activation of diaphanous-related formins (DRFs), which in turn act in conjunction with ROCKs to mediate stress fiber formation (Ridley *et al*., 2003). RhoA activity was also shown to be present at both protrusions and retractions of cells (O'Connor and Chen, 2013) and to be a key transforming factor in initial cancer formation as well as in metastatic processes (Ridley, 2004). RhoA activity has further been linked to metastasis in an invasive PDAC model in the presence of mutant $p53^{R172H}$ and shown to be active in both poles of invading cells *in vivo* (Timpson *et al*., 2011a).

Because of these observed pleiotropic functions of RhoA, a RhoA-FRET mouse was generated and RhoA activity monitored in a variety of tissues in health and cancerous disease models. To validate *in vitro* findings in an *in vivo* setting is crucial, especially for GTPase signalling events. As shown previously, RhoA signalling in particular can be impacted by several factors of the microenvironment not encountered in *in vitro* culture. These can include in the tumour setting in particular, signalling from the tumour specific ECM (Provenzano and Keely, 2011), tumour-associated immune infiltrates such as macrophages (Roh-Johnson *et al*., 2014) or soluble factors such as hypoxia inducible factors and TGF-β (Gilkes *et al*., 2014; Papageorgis and Stylianopoulos, 2015). All in turn have been shown to activate RhoA signalling in cancer cells. This in turn could further impact therapeutic interventions targeting RhoA. To achieve this, abdominal imaging windows (AIWs) were used to examine RhoA activity in native pancreatic and intestinal tissue as well as primary tumours of the pancreas.

5.3 Results

5.3.1 Generation of the RhoA-FRET mouse

A conditional RhoA-FRET reporter mouse was made, in order to examine RhoA activity in a variety of native tissues and during stages of different cancerous lesions. To that end, a modified RhoA-Raichu probe (Yoshizaki *et al*., 2003b), was used, expressing the fluorophore pair EGFP and mRFP (Timpson *et al*., 2011a) (Figure 5.1 A). The reporter is modulated by the action of cellular GEFs and GAPs in a similar manner as the Rac-1 Raichu probe. Upon the binding of GTP of the reporter encoded RhoA facilitated by cellular GEFs, the Rho-binding domain (RDB) is bound and a FRET conformation assumed by the membrane tethered reporter. When GAPs act on the sensor, GTP is hydrolysed and the probe assumes an open confirmation, in which FRET is hampered. FRET was measured as before by employing FLIM and recording the lifetime of the EGFP donor. Visual representation of the data was achieved by using lifetime colour maps, with blue to green colours showing RhoA activity and yellow to red inactivity.

The reporter headed by a lox-stop-lox (LSL) was targeted to the HPRT locus, as described previously, under the control of a CAGSA promoter (Bronson *et al*., 1996; Samuel *et al*., 2009; Schachtner *et al*., 2012). In order to allow for ubiquitous expression of the reporter in all tissues, the conditional mouse was crossed with an X-chromosomal *Cre* recombinase expressing mouse (Schwenk *et al*., 1995). This *Cre* was then later crossed out again. Indeed, the RhoA-FRET probe was detectable in a variety of tissues of interest such as the skin, intestine, pancreas and the liver, as detected by anti-GFP immunoblot, with an expected band at around 100 kDa (Figure 5.1 B).

A concern that arises with Raichu-reporter FRET mice is possible side-effects on the levels of endogenous signalling when overexpressing the full-length GTPases contained in the probe. In a recent example, the Rac-1 FRET mouse generated showed that endogenous levels of Rac-1 were not altered to a great extent in mice ubiquitously expressing the Rac-1-Raichu FRET reporter (Johnsson *et al*., 2014). Tissues from the RhoA-FRET mouse were therefore isolated and subjected to immunoblot analysis probing for levels of endogenous and reporter-associated RhoA by staining with a monoclonal RhoA antibody.

There, endogenous RhoA levels, detected at around 23 kDa, were not significantly altered in the RhoA-FRET mice, when compared to littermate wild types. Transgenic RhoA contained in the Raichu FRET reporter, at an expected band of around 100 kDa, was detected in the tissues of interest as well (Figure 5.1 C). FLIM of the respective tissues was further acquired and example images displaying RhoA activity at the membranes in lifetime maps recorded (Figure 5.1 D).

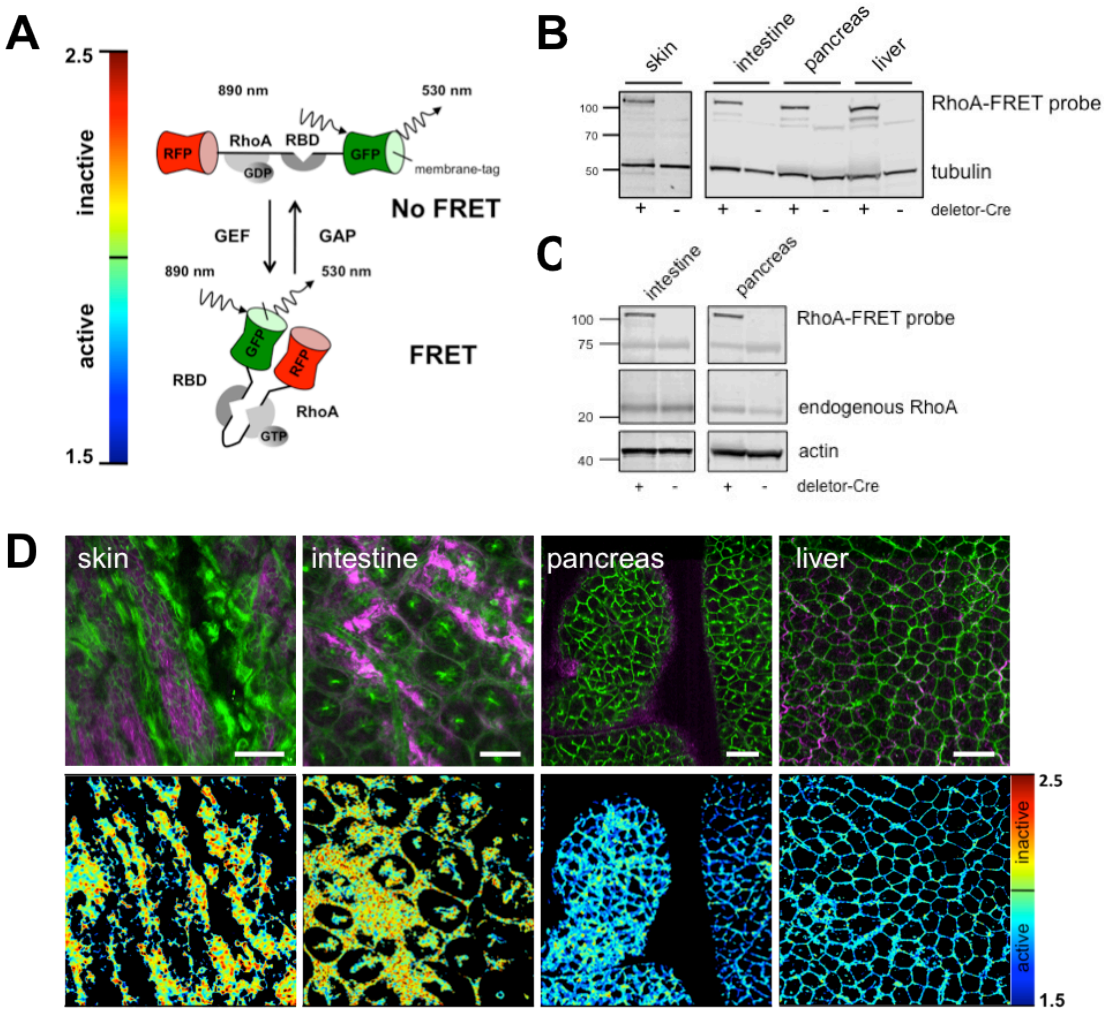

Figure 5.1: Generation of the RhoA-FRET biosensor mouse
A Schematic of the mode of action of Raichu-RhoA probe used in the generation of the transgenic mouse subject to the activation/inactivation of cellular GEFs/GAPs. **B** Expression levels of the RhoA-FRET probe as detected by α-GFP immunoblot after removal of the Lox-stop-Lox by deletor-Cre in different tissues of interest, the skin, intestine, pancreas and the liver. **C** Endogenous RhoA expression levels (~ 23 kDa) and that of the reporter at ~ 100 kDa). **D** Expression of the RhoA-FRET probe in skin, intestine, pancreas and liver shown in green, with second harmonic generation (SHG) of tissue collagen I in magenta and the corresponding lifetime maps of RhoA activity in these organs; scale bars: 50 µm

5.3.2 Rac-1 inhibition in melanocytes of embryonic skin explants can stimulate RhoA activity

It has recently been demonstrated that RhoA is localized both to protrusions and retractions of cells (Pertz *et al*., 2006). Further, RhoA has been identified to have a role in the initial formation of such protrusions, followed by the more widely studied activation of Rac-1 and Cdc42 (Machacek *et al*., 2009). It has been shown that loss of Rac-1 in the melanocyte lineage leads to a reduction in the formation of active protrusions in melanocytes in embryonic skin explants (Li *et al*., 2011) (Figure 5.2 A) and that strong Rac-1 activity can further antagonize RhoA activation (Sander *et al*., 1999; Nimnual *et al*., 2003).

First, the activity of RhoA in melanocytes was analysed by expressing the RhoA-FRET reporter with Tyr-CreB (Delmas *et al*., 2003) and isolating the embryonic skin at E14.5 - E15.5 (Figure 5.2 B). To see whether Rac-1 inhibition indeed leads to an increase in RhoA activity, embryonic skin explants were treated with the Rac-1 inhibitors EHT 1864 and NSC 23766. A significant activation of RhoA in the melanocytes was recorded following the treatment of the embryonic skin explants (mean ± SEM = 2.02 ± 0.01 ns) with Rac-1 inhibitors 75 μM of EHT 1864 (mean ± SEM = 1.90± 0.01 ns) and 100 μM of NSC 23766 (mean ± SEM = 1.86 ± 0.01 ns), with NSC 23766 being slightly more potent than EHT 1864 (Figure 5.2 C).

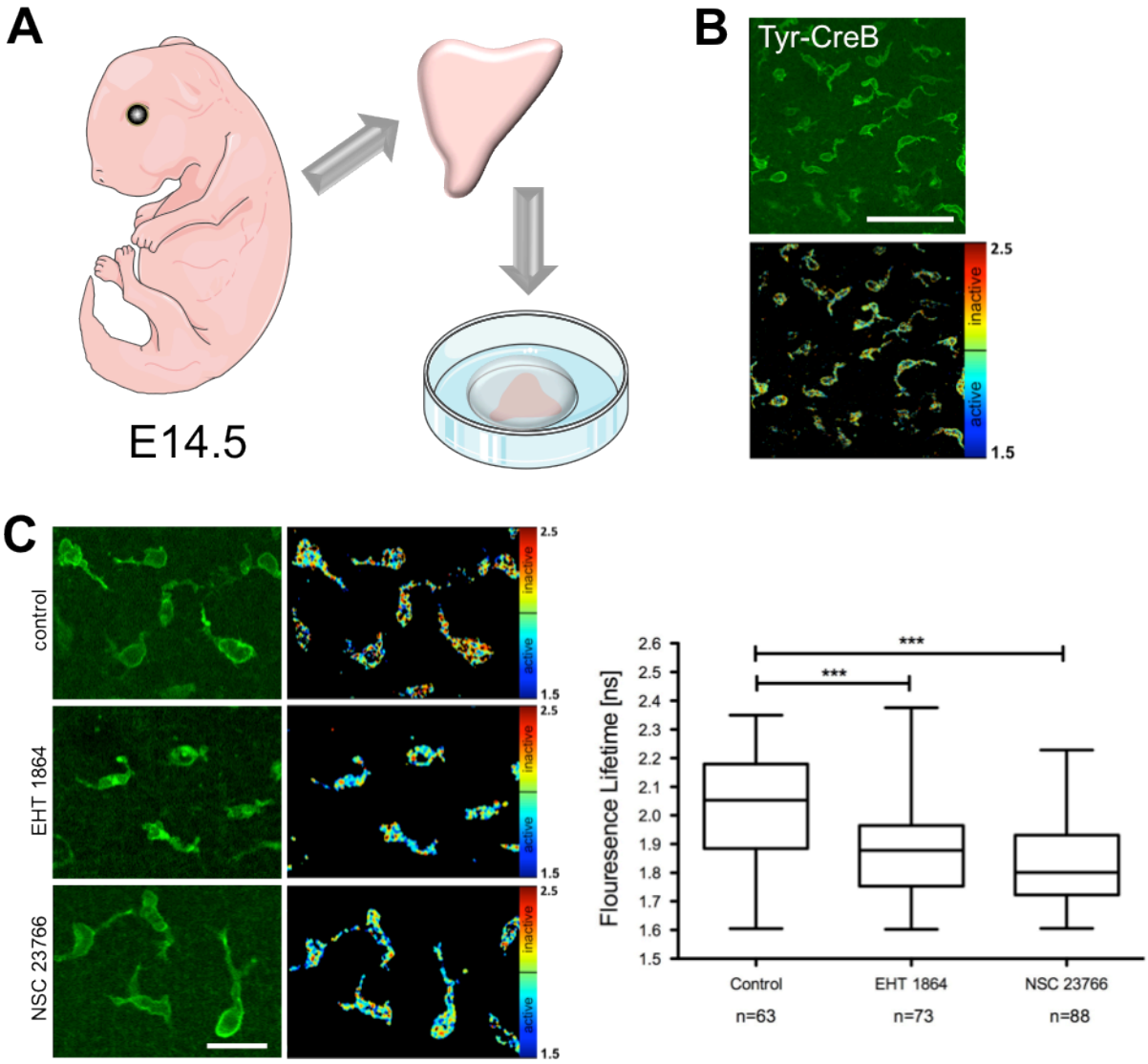

Figure 5.2: RhoA activity in E14.5 – E15.5 embryonic skin explants
A Schematic representation of the isolation of dorsal skin of E14.5 – E15.5 day old embryos (adapted from Servier Medical Art) and preparation of the *ex vivo* imaging set up, with the skin placed in a Lumox culture dish® with the epidermal side in contact with the gas permeable membrane and immobilized by matrigel. **B** Tyr-Cre-B expression of the RhoA-FRET sensor in melanocytes, revealing activated RhoA in the FLIM images; scale bar: 100 µm. **C** Treatment of the embryonic skin explants with the Rac-1 inhibitors EHT 1864 and NSC 23766, resulting in significantly increased RhoA activity in melanocytes; box: mean; bars: min-max values; n = 3 embryos of 2 independent matings for each condition; cell number below each condition; *** $p<0.001$ by one-way ANOVA; scale bars: 20 µm

5.3.3 PyMT but not ErbB2 driven breast cancer increases basal RhoA activity

In order to explore a possible role of RhoA activation in different types of mammary cancer, the RhoA FRET mouse was crossed with the ErbB2/Her2 receptor overexpressor (Guy *et al*., 1992a) as well as the PyMT driven breast cancer model (Guy *et al*., 1992b) (Figure 5.3 A). Previous reports show that there is only basal RhoA activity in Her2 overexpressing cancer cell lines (Novitskaya *et al*., 2014). In agreement with this we found that RhoA activity remained basal in normal mammary glands (mean ± SEM = 2.08 ± 0.02 ns) and in the presence of Her2 overexpression (mean ± SEM = 2.09 ± 0.01 ns). However, expression of the PyMT led to significant up-regulation of RhoA activity in PyMT breast cancer mice (Figure 5.3 B, mean ± SEM = 1.83 ± 0.01 ns).

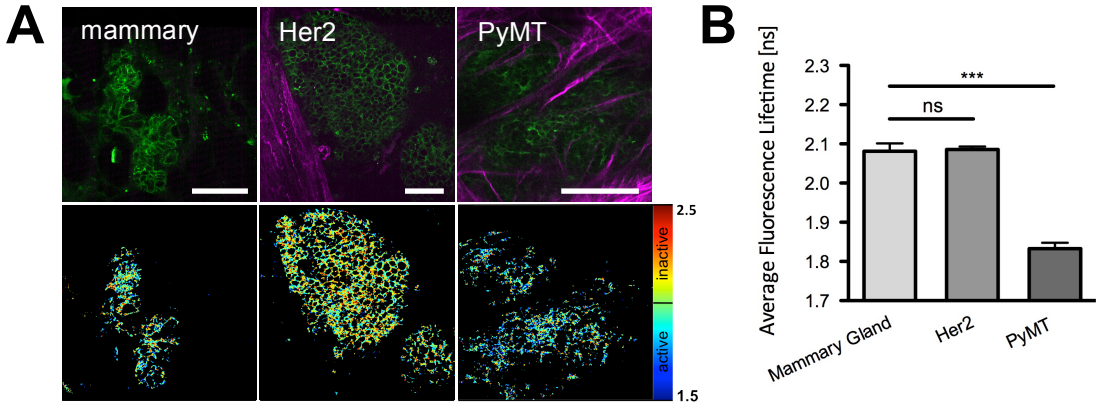

Figure 5.3: Mammary tissue displays differential RhoA activity in different disease states
A There was basal RhoA activity observed in virgin mammary tissue as well as Her2-driven tumours, however, observed elevated RhoA activity in PyMT-driven mammary tumours and quantified in **B**, n = 3 mice, 270 cells; columns: mean; bars: SEM; *** $p<0.001$ by one-way ANOVA; scale bars: 50 µm

5.3.4 RhoA activation in PyMT breast cancer displays effective inhibition over time by dasatinib in live imaged lesions

In order to see whether the RhoA activity observed in PyMT expressing mice could be effectively inhibited *in vivo* over time, the RhoA FRET reporter was expressed in the mammary ductal cells by MMTV-Cre (Guy *et al*., 1992a) and crossed to the PyMT model. To induce the MMTV-Cre, mice were put through 1-2 rounds of pregnancy and a primary PyMT tumour was allowed to develop. On top of such a tumour, the optical imaging window (Ritsma *et al*., 2013) was implanted into the skin and mice allowed to recover after surgery for 1 day. Mice were then gavaged with a previously established inhibitory concentration of 10 mg/kg of the Src inhibitor dasatinib (Morton *et al*., 2010b), which in turn has been shown previously to indirectly inhibit the activity of RhoA (Timpson *et al*., 2011a). RhoA activity was effectively inhibited after 2 hours of the gavage being administered and remained in an inactive state at 6 hours. After 24 hours of the mouse being gavaged for the first time, RhoA activity returned back to initial values (Figure 5.4 B).

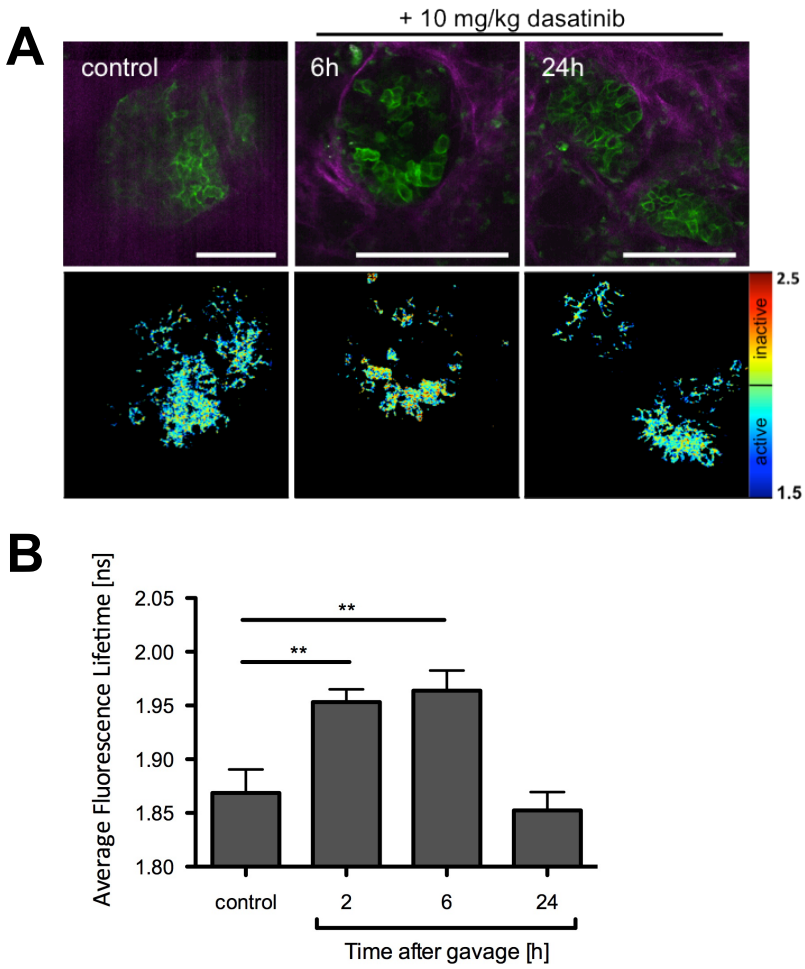

Figure 5.4: Elevated RhoA activity in PyMT can be effectively inhibited over time period of 6 hours by dasatinib treatment

A Live timecourse after the last of 3 daily oral gavages of 10 mg/kg dasatinib *in vivo* in a primary PyMT tumour imaged through skin imaging window, showing effective inhibition of RhoA after 2 h and 6 h, leveling off to initially detected RhoA activity after 24h after last treatment, quantified in **B**; n = 1 mouse, 100 cells; columns: mean; bars: SEM; ** $p<0.01$ by one-way ANOVA; scale bars: 100 µm

5.3.5 Live imaging of RhoA in the intestinal crypt reveals activity is governed by the 3D environment

Higher RhoA activity has previously been shown in undifferentiated intestinal crypt cells in conjunction with expression of $\alpha_8\beta_1$ integrins. In turn, when α_8 was knocked down, more differentiated villus cells as well as lower RhoA activity were observed (Benoit *et al*., 2009). Furthermore, the *LGR5*$^+$ stem cell compartment marker has previously been shown to extend between 10 and 40 μm up from the base of intestinal crypts. This bottom in turn was marked by a pronounced SHG signal of the underlying dense irregular layer of connective tissue (Roth *et al*., 2012).

To examine whether this reported RhoA activity could indeed be visualized *in vivo* using the RhoA reporter mouse, abdominal imaging windows were surgically implanted in the abdominal wall as described previously (Ritsma *et al*., 2012, 2013) (Figure 5.5 A). The activity of RhoA along the crypt-villus axis was imaged *in vivo* starting at the first cells observed (0 μm), which were about 10 μm above the dense irregular connective tissues' SHG signal, up to 30 μm into the crypt (Figure 5.5 B). Quantification of the RhoA-FRET signal revealed a gradient of RhoA activity, which was at its maximum at the crypt base and decreased to basal levels at about 30 μm in (Figure 5.5 C).

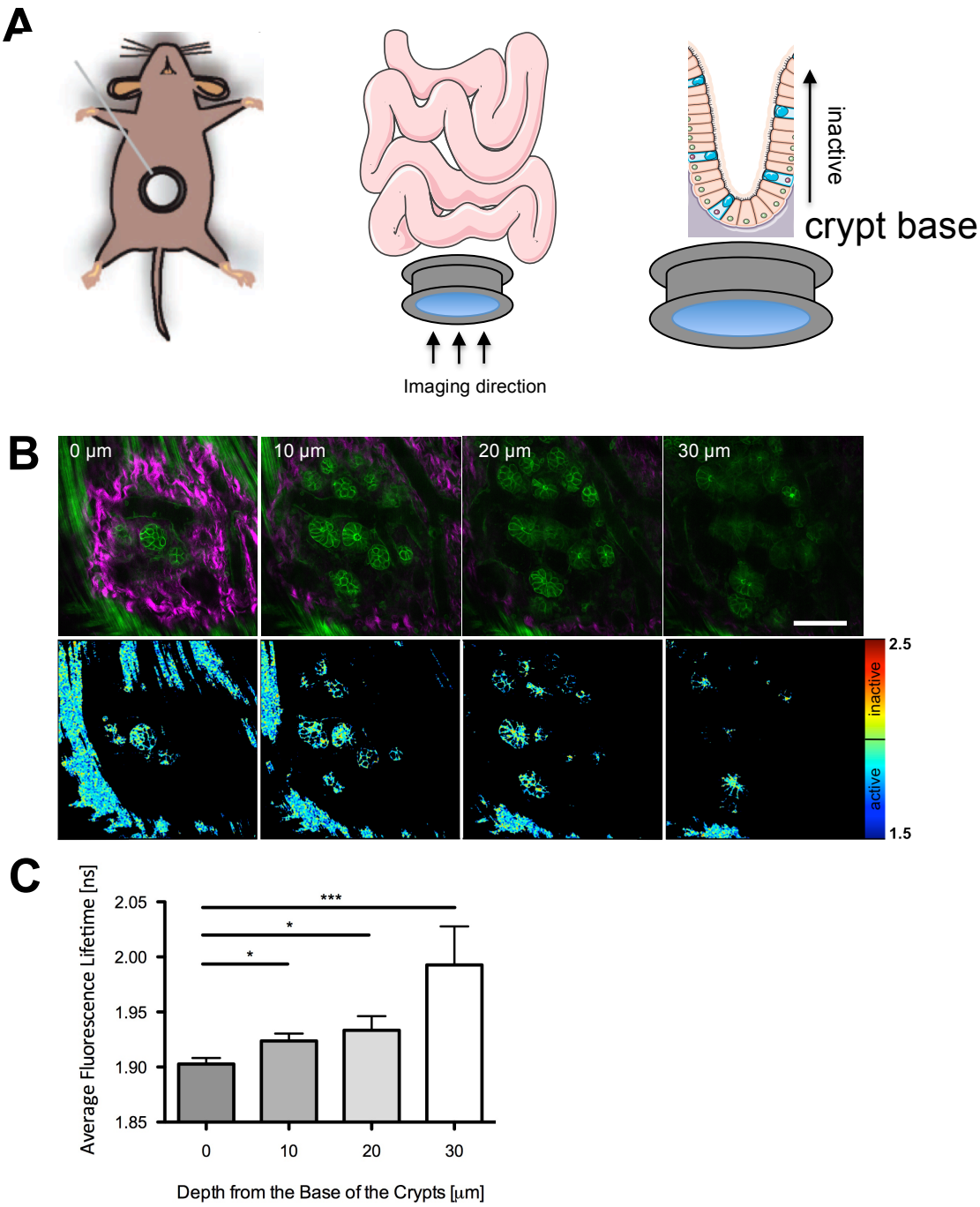

Figure 5.5: RhoA activity in the intestine is spatially confined to the base of the crypts

A Schematic of the surgical implantation of abdominal imaging windows (AIWs) for the live *in vivo* imaging of RhoA activity in organs of the peritoneal cavity and a schematic of *in vivo* imaging of intestinal crypts through abdominal imaging windows (adapted from Ristma *et al*. 2012 and Servier Medical Art). **B** Live *in vivo* imaging of RhoA activity in crypts of the duodenum, revealing spatial distinct RhoA activity reduction with the progression toward the villi away from the base of the crypts and the quantification thereof in **C**; columns: mean; bars: SEM; * $p < 0.05$, *** $p < 0.001$ by unpaired Student *t* test; scale bars: 100 µm

5.3.6 RhoA activity can be effectively inhibited *ex vivo* in the pancreas and is decreased in pre-cancerous lesions

RhoA activity has further been associated with a variety of tissues, such as the pancreas. There, RhoA has previously been associated with active insulin secretion in islet-like aggregate culture *in vitro* (Liu *et al*., 2014). To look at RhoA activity in the pancreas the RhoA-FRET reporter was expressed under the Pdx1-Cre (Hingorani *et al*., 2003), as confirmed by anti-GFP and anti-RFP IHC (Figure 5.6 A). FLIM-FRET imaging of the *ex vivo* excised pancreata revealed high levels of RhoA activity, which was effectively inhibited by gavaging the mice beforehand with 10 mg/kg of dasatinib (Figure 5.6 B).

To look at progressive stages of PDAC, the RhoA-FRET mouse was crossed to the KC (*Pdx1-Cre* + $KRas^{G12D}$) and the KPC (*Pdx1-Cre* + $KRas^{G12D}$ + $p53^{R172H}$) models. RhoA activity was decreased in consecutive PanIN stages in both KC and KPC tumours (Figure 5.6 C+D). Normal ducts displayed an activity of 1.85 ± 0.02 ns (mean ± SEM). In both KC and KPC similar values in PanIN-1 (mean ± SEM: KC = 1.94 ± 0.003 ns vs KPC = 1.93 ± 0.02 ns) and PanIN-2 (mean ± SEM: KC = 2.00 ± 0.004 ns vs KPC = 2.08 ± 0.01 ns) were observed. Complete RhoA inactivity was observed in PDAC, solely driven by $KRas^{G12D}$ (mean ± SEM = 2.11 ± 0.005) ns.

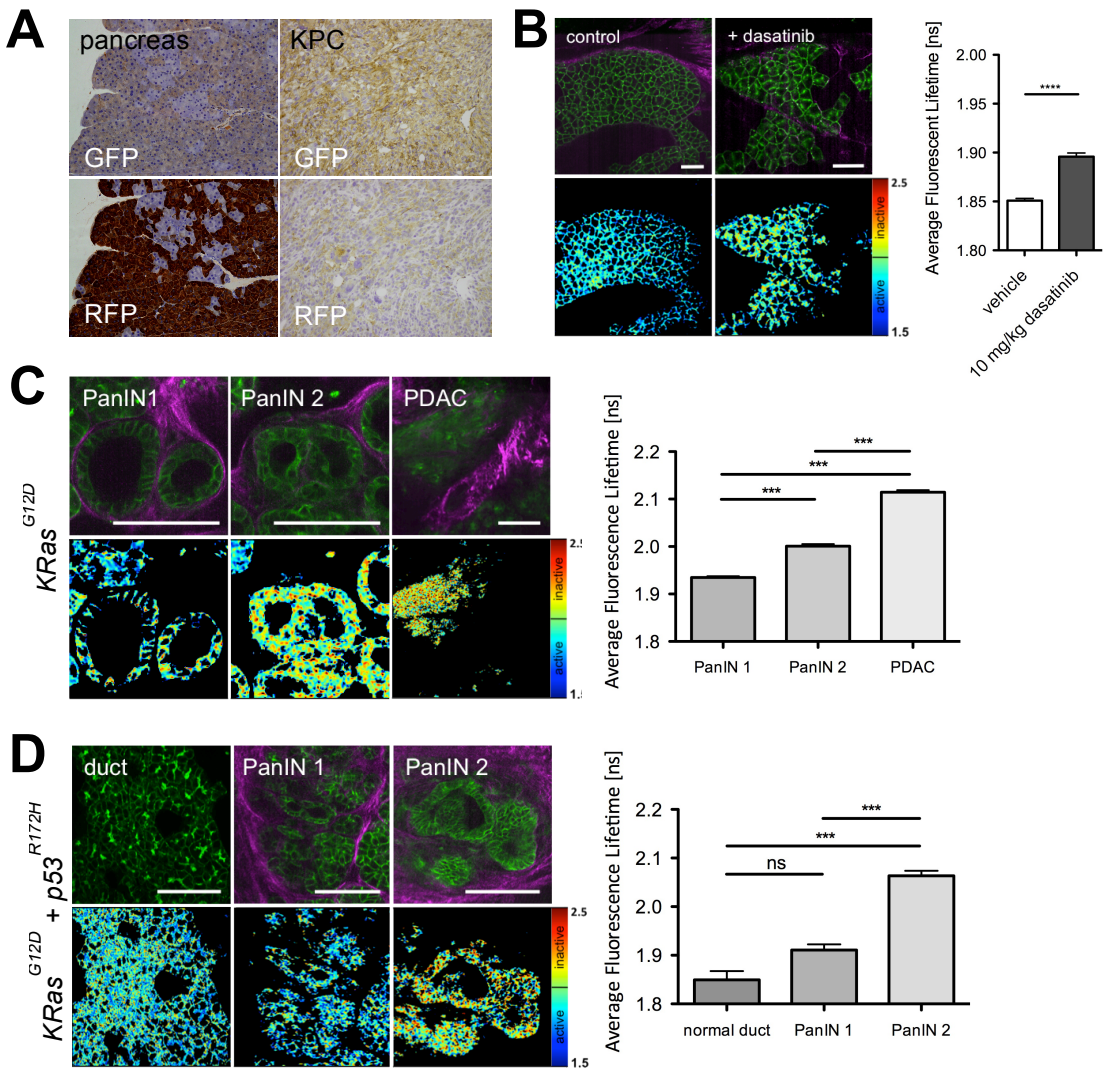

Figure 5.6: RhoA activity in the pancreas is decreased upon dasatinib treatment as well as in progressive stages of of KC and KPC

A IHC of the pancreas and KPC tumours stained with GFP and RFP antibodies respectively. **B** Pancreata of mice treated with 3 daily oral gavages of 10 mg/kg of dasatinib, displaying decreased RhoA activity after treatment; n = 3 mice per treatment group, and a total of 540 analysed. **C** RhoA activity in KC ($KRas^{G12D}$) PanIN stages and PDAC; n = 4 mice per stage, 200 cells, scale bars: 100 µm. **D** RhoA activity during the progression of KPC ($KRas^{G12D}$ + $p53^{R172H}$) tumours arising from the pancreatic ductal cells forming PanIN 1 and PanIN 2 stages; n = 3 mice per tumour stage, 274 cells; columns: mean; bars: SEM; *** $p < 0.001$, **** $p < 0.0001$ by unpaired Student *t* test and one-way ANOVA respectively; scale bars: 50 µm

5.3.7 KPC tumours exhibit distinct RhoA activation at the invasive edge and in metastatic sites of the liver

It was recently shown that KPC derived PDAC cells stably transfected with the RhoA-FRET reporter display a spatial activation in terms of RhoA in a subcutaneous allograft environment (Timpson *et al*., 2011a). This activity was further established to be dependent on the presence of mutant p53 ($p53^{R172H}$). The offspring of KPC crossed with the RhoA-FRET reporter mice, were therefore left to develop primary tumours and these imaged *ex vivo* for RhoA activity. This revealed, when comparing the tumour centres with their cortices, significantly up-regulated RhoA activity at the invasive borders (Figure 5.7 A). Furthermore, the large metastatic lesions of the liver in end stage tumour bearing mice were examined, which could easily be seen by eye (Figure 5.7 B). These also showed significantly increased RhoA activity when compared to the overall primary tumour mass (Figure 5.7 C). Hepatocytes, however, also expressed the RhoA FRET reporter, due to the leakiness of the Pdx1-Cre. These were distinguished from the metastatic tissue by simple bright field microscopy of the liver tissue, as well as the shape and size of the cells, and the disorganized collagen I structure visualized by second harmonic generation (SHG) (Figure 5.7 C, frizzled collagen I fibres in the normal liver versus long straight collagen I fibres associated with cancerous tissue).

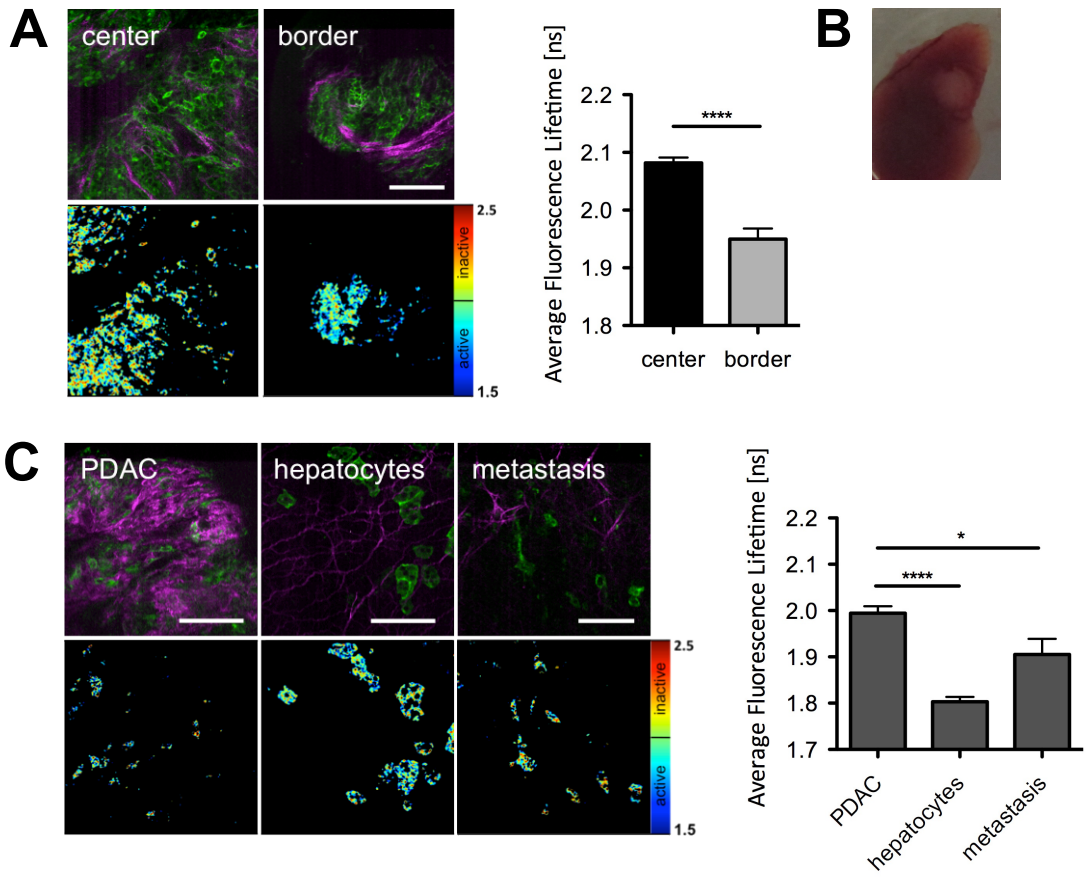

Figure 5.7: RhoA activity is increased at the border of KPC tumours and liver metastasis *ex vivo*

A Quantification of RhoA activity in late stage KPC tumours comparing the tumour center with border regions; n = 3 mice, 148 cells. **B** Picture of a liver metastasis. **C** Comparison of the RhoA activity in primary PDAC with that of liver metastasis and hepatocytes; n = 3 mice, 94 cells; columns: mean; bars: SEM; * $p < 0.05$, **** $p < 0.0001$ by unpaired Student *t* test; scale bars: 100 µm

5.3.8 RhoA activity can be imaged reliably in the pancreas and pancreatic cancer *in vivo*

There are several limitations encountered when imaging excised tissue *ex vivo*, including amongst others limited temporal viability of the sample. An additional problem is that only a single time point can be examined for individual samples. Construction of a time course thus requires use of multiple experimental animals, the comparison of which constitutes a source of unnecessary biological noise in the final read-out. Surgical engraftment of abdominal optical imaging windows is a way to circumvent this problem (Ritsma *et al*., 2012, 2013) (Figure 5.8 A). First, native pancreata were examined before and after treatment with 3 daily oral gavages of 10 mg/kg of dasatinib, which revealed the effective inhibition of RhoA activity *in vivo* (Figure 5.8 B, mean ± SEM: control = 1.75 ± 0.006 ns versus dasatinib = 1.82 ± 0.004 ns). RhoA activity was further found to be reduced, as observed *ex vivo*, in primary cancerous ductal cells. However, the surrounding untransformed acinar cells still displayed unaltered native RhoA signalling as observed before (Figure 5.8 B control: mean ± SEM = 1.75 ± 0.006 ns, versus Figure 5.8 C, acinar: mean ± SEM = 1.76 ± 0.01 ns).

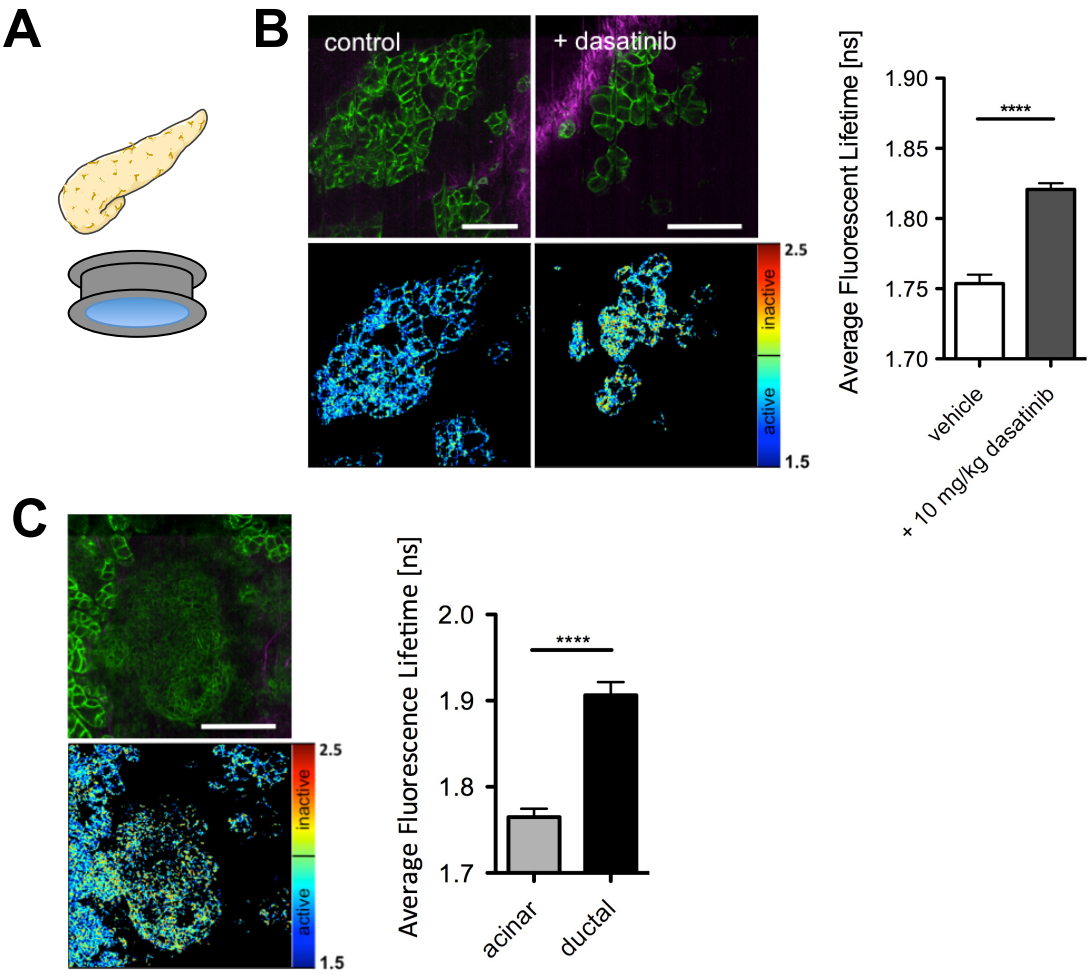

Figure 5.8: RhoA activity can be imaged *in vivo* in the pancreas and KPC tumours using AIWs

A Schematic of imaging performed on either native pancreas or primary KPC tumours through optical windows implanted in the abdominal wall (adapted from Servier Medical Art). **B** Quantification of RhoA activity in the pancreas before and after treatment with 3 daily oral gavages of 10 mg/kg dasatinib; n = 3 mice per treatment group, 1165 cells. **C** Comparison of the RhoA activity in ductal adenocarcinoma cells with remaining acinar cells; n = 3 mice, 293 cells; columns: mean; bars: SEM; **** $p < 0.0001$ by Mann-Whitney U test; scale bars: 100 µm

5.3.9 *In vivo* pharmacodynamics reveal different temporal dynamics of dasatinib and erlotinib in live imaged KPC tumours

Expanding on previous studies employing longitudinal imaging to monitor drug-targeting response in subcutaneous allograft tumours *in vivo*, primary KPC tumours, endogenously expressing the RhoA-FRET reporter, were allowed to develop and AIWs surgically implanted in the peritoneal wall. Mice were treated with 3 daily gavages of dasatinib and RhoA activity monitored before the last gavage was administered and at 3 h, 7 h and 24 hours afterwards (Figure 5.9 A). The baseline of RhoA activity was the same before the treatment regimen was started compared to the control time point on the day of the last gavage (Figure 5.9 B). Following the final treatment with dasatinib RhoA activity did not change at 3 hours, however, at 7 hours RhoA activity was effectively inhibited. By 24 hours, dasatinib appeared to be completely cleared from the primary tumour mass, with the RhoA-FRET FLIM read-out having returned to control values (Figure 5.9 B).

Another important therapeutic target in *KRas* driven pancreatic cancer has been as previously identified, the epidermal growth factor receptor (EGFR) (Navas *et al*., 2012). The EGFR has been previously targeted effectively *in vivo* by using the ATP competitive kinase inhibitor gefitinib (Mohammed *et al*., 2010b). Here, a second generation EGFR tyrosine kinase inhibitor, erlotinib, was administered by a single gavage of 100 mg/kg (Cufí *et al*., 2013) to mice with developed primary KPC tumours, bearing abdominal AIWs (Figure 5.9 C). RhoA activity was effectively inhibited after 3 hours and cleared to a similar extent as dasatinib after 24 hours of being administered (Figure 5.9 D).

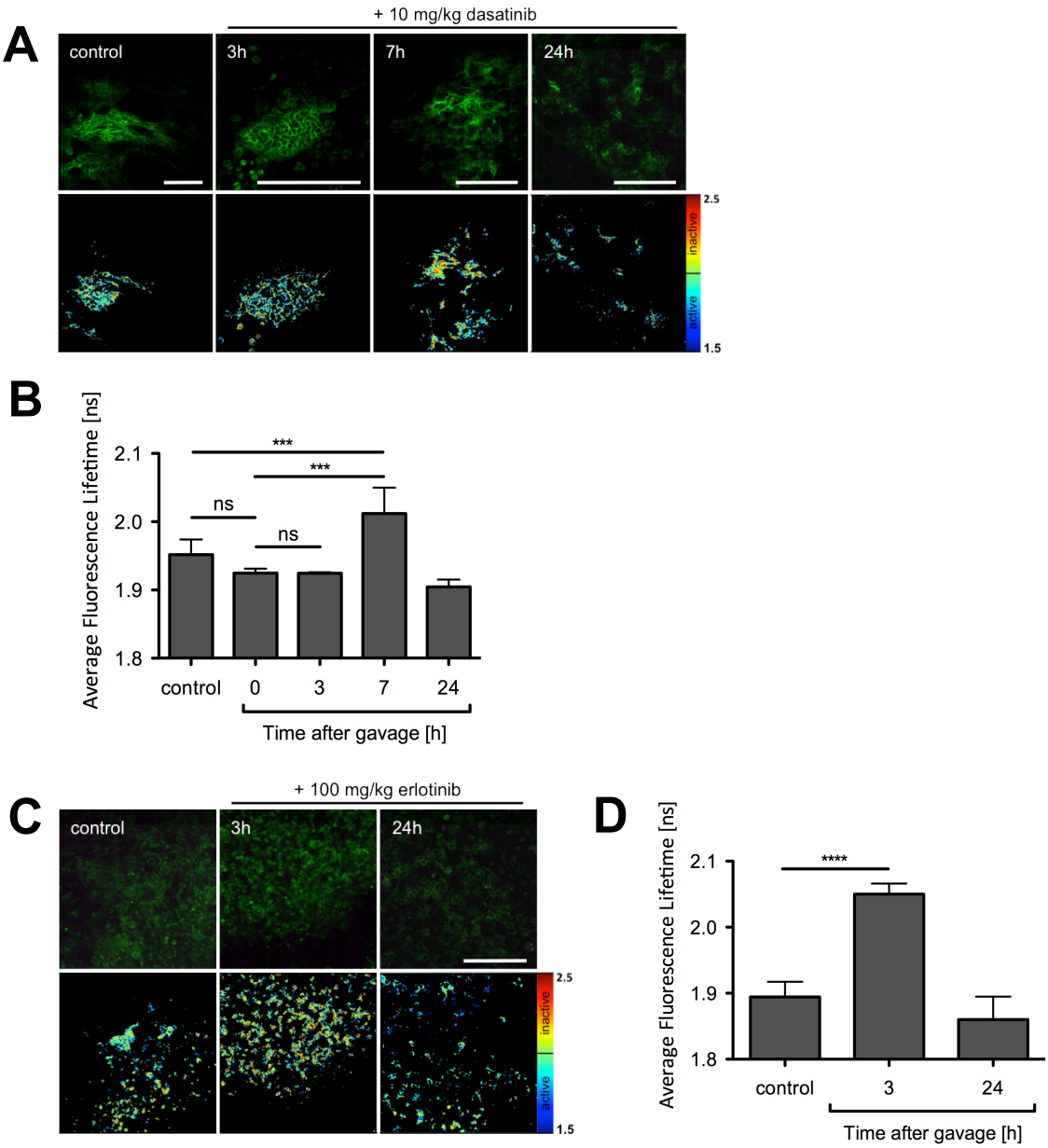

Figure 5.9: *In vivo* FLIM-FRET through AIWs reveals RhoA activity in KPC tumours is effectively inhibited by dasatinib and erlotinib in a temporal manner
A Live time course after the last of 3 daily oral gavages of 10 mg/kg dasatinib *in vivo* in a primary KPC tumour, showing effective inhibition of RhoA after 7 h, quantified in **B**, n = 3 mice, 351 cells, *** $p<0.001$ by one-way ANOVA. **C** Live time course after the last of 3 daily oral gavages of 100 mg/kg erlotinib *in vivo* in primary KPC tumours, showing effective inhibition of RhoA after 3 h, quantified in **D;** n = 3 mice, 90 cells; columns: mean; bars: SEM; **** $p < 0.0001$ by Mann-Whitney U test; scale bars: 100 µm

5.4 Discussion

Observing cellular signalling events on a time-resolved level and with high fidelity *in vivo*, is a major challenge in cancer biology. This holds true especially for GTPases, the activity of which are difficult to assess by conventional biochemical methods, due to the fast rates of GTP hydrolysis in samples extracted from cells and tissues. Here, we described a RhoA-FRET biosensor mouse based on a RhoA-FRET reporter described previously (Yoshizaki *et al*., 2003b). This mouse was then used to report on RhoA activity in a variety of tissues. Further crossing of the RhoA-FRET biosensor mouse to different models of cancer revealed the dynamics of RhoA signalling during different stages of cancerous lesions as well as its use as a tool to monitor drug-targeting efficiencies *in vivo*. Homozygous RhoA-FRET reporter mice, expressing the probe in all tissues, were healthy, fertile, exhibited no behavioural defects and followed the expected Mendelian ratio of hereditary transmission. Immunoblotting for GFP and RhoA, revealed effective expression in all examined tissues and no significant alteration of endogenous RhoA levels in the FRET-reporter mice, compared to littermate WT controls (Figure 5.1 B + C). A similar observation was made for the previous Rac-1 Raichu-FRET reporter expressing mouse, in terms of possible alterations of endogenous GTPase expression following the transgenic induction of a FRET reporter in tissues (Johnsson *et al*., 2014). We observed different basal levels of RhoA activity in the native skin and intestinal as well as higher RhoA activity in the pancreas and liver. This is not surprising and can most likely be attributed to differential expression of RhoA GEFs and GAPs in these respective native tissues.

Especially in the pancreas, the high level of RhoA acitivity observed seems contradictory with the high expression levels of GDP-dissociation inhibitor RhoGDIγ recorded previously in this organ (Adra *et al*., 1997). This in turn must then be outweighed by an, until now, unidentified GEF counteracting the activities of the RhoGDI via extracellular signalling through two possible routes, previously described in pancreatic acinar cells. The first is via the insulin-like growth factor receptor IGFR and the leukemia-associated Rho-GEF LARG (Taya *et al*., 2001). RhoA signalling has further been previously associated with cholecystokinin (CCK) stimulation of pancreatic acini and their subsequent secretion of amylases (Nozu *et al*., 1999) and cytoskeletal changes in morphology (Kiehne *et al*., 2002; Bi and Williams, 2005;

Bi *et al*., 2005). Therefore, the second possibility is signalling through CKK, which can activate RhoA via $G\alpha_{13}$ and the p115-Rho guanine nucleotide exchange factor (Sabbatini *et al*., 2010).

Down-regulation of these signalling cues, in turn, could account for the observed decrease in RhoA activity in progressive stages of PDAC either in the presence of $KRas^{G12D}$ mutation alone or in conjunction with mutant $p53^{R172H}$. We have previously observed that RhoA activity was indeed upregulated in invasive PDAC cells in a 3D environment in a subcutaneous allograft and in conjunction with $p53^{R172H}$ (Timpson *et al*., 2011a). These observations were further confirmed here, by showing elevated RhoA activity at the borders of primary KPC tumours and in liver metastasis.

The detected high RhoA activity in the liver seen by FLIM-FRET imaging was described previously in isolated primary cultures of rat hepatocytes (Dohda *et al*., 2004). Furthermore, the activity of RhoA and its downstream effector ROCK I has been associated with high density lipoprotein (HDL) endocytosis in hepatocytes via the $P2Y_{13}$ purinergic ADP-receptor (Malaval *et al*., 2009). This demonstrates a key metabolic function of RhoA activity in reverse cholesterol transport (RCT), in which HDLs act as carriers in transferring cholesterol form peripheral tissue to the liver for degradation. The RhoA-FRET mouse could therefore be used in the future to study RhoA signalling in the liver and its impact in metabolism or hepatocellular cancer.

In the skin in turn, it has been previously been shown that RhoA activity is dispensable for the development of the epidermis and maintenance of adherence junctions *in vivo* (Jackson *et al*., 2011), as mirrored by the basal activity detected in the adult RhoA-FRET mouse. However, RhoA activity was observed in protrusions of melanocytes in embryonic skin explants. Furthermore, the overall activity in melanocytes was increased by inhibiting Rac-1, which has previously been shown to be essential in the formation of protrusions in melanocytes (Li *et al*., 2011).

RhoA activity was found to be basal in both the native mammary tissue as well as in the ErbB2 amplified breast cancer mouse model, which is in line with the findings that show that ErbB2 overexpressing cell lines display low RhoA activity (Novitskaya *et al*., 2014). The elevated RhoA activity in *ex vivo* and *in vivo* in MMTV-PyMT driven tumours (see Figure 5.3B and Figure 5.4 B) could be attributed to several signalling cues described previously.

First and foremost it has been shown that KISS1 receptor (GPR54), through its ligands kisspeptins, regulates tumourigenesis in the PyMT model by activation of RhoA via the p63RhoGEF. Loss of this receptor in turn led to downregulation of RhoA activity and late onset of tumourigenesis in the PyMT model (Cho *et al*., 2011b). Another regulator of RhoA activity, that has been identified was the tetraspanin CD151, which acts through $\alpha_3\beta_1$ integrins as described previously (Johnson *et al*., 2009; Novitskaya *et al*., 2014). It was further shown that upon loss of CD151, PyMT tumourigenesis was reduced, by near significant reduction in tumour onset, as well as significant reduction in tumour sizes and numbers of lesions. RhoA activity was, however, not directly assessed in this context (Roselli *et al*., 2014). The PyMT mouse model most closely resembles luminal metastasising breast cancers. In conclusion, direct or indirect targeting of the RhoA signalling axis therefore could constitute a viable therapeutic approach in treating this breast cancer subtype (Vargo-Gogola and Rosen, 2007).

In the intestinal crypts, RhoA activity was found to be spatially regulated. While previous reports show that in this highly proliferative zone (Roth *et al*., 2012) RhoA is linked to expression of $\alpha_8\beta_1$ integrins (Benoit *et al*., 2009), the spatial distribution of RhoA activity visualized by *in vivo* imaging on a single cell level, could not have been achieved with such fidelity by conventional methods such as IHC or IF. This is in no small part due to the volatile nature of GTPase activity, which can be easily lost by fixing procedures leading to false readouts during the conventional biochemical processing of cells, and even more problematically, in whole tissues. By eliminating the need to excise and stain tissues, *in vivo* imaging can provide the necessary bridge when trying to observe and monitor these signals in a temporal and spatial manner in a live setting.

Another important advantage of *in vivo* imaging is demonstrated by the detected difference in RhoA signalling in *ex vivo* and *in vivo* imaged pancreatic tissue (Figure 5.8 B, control *in vivo*: mean ± SEM = 1.75 ± 0.01 ns, versus Figure 5.6 B, control *ex vivo*: mean ± SEM = 1.84 ± 0.02 ns). This observation further shows the need for *in vivo* imaging in maintaining the signalling events occurring in the native *in vivo* setting, especially in longitudinal monitoring of GTPase activity. This was finally achieved in full genetic primary KPC tumours and allowed for more accurate treatment response prediction than previously possible.

It showed, that unlike previously thought, oral gavages of dasatinib treatment did not achieve optimal inhibition in primary KPC tumours after 3 hours of the last gavage being administered, but rather after 7 hours. Further, an additive effect of dosing the mice with 3 daily gavages of dasatinib, rather than a singular treatment, was not observed. There, it was indeed possible to compare RhoA activity before the treatment regimen had commenced and before the final gavages had been administered (Figure 5.9 B). This detailed knowledge, on when drug inhibition is maximal and for how long, can be applied in the tailoring of more effective future treatment regimens. This in turn will allow for a more precise pre-clinical assessment of drug targeting efficacy in full genetically engineered mouse models and potentially optimize drug targeting in an *in vivo* setting, possibly reducing drug attrition rates in human clinical trials.

6 General Discussion

6.1 Summary

In this thesis I have described the use of FLIM-FRET imaging in the spatio-temporal monitoring of drug targeting in both allograft tumours and GEM models of mammary and pancreatic tumours. Different tumour microenvironmental cues, such as location within the tumour distance to the local vasculature, and their influence on signalling of Src, Rac-1 and RhoA were examined. Furthermore, the use of FRET-biosensor mice of the GTPases Rac-1 and RhoA were examined in the context of a variety of tissues as well as pancreatic and mammary tumour models. The successful utility of cutaneous and peritoneal imaging windows in monitoring tumour progression and treatment was additionally shown. In conclusion, these results demonstrate that FLIM-FRET imaging adds a new dimension to drug response readout *in vivo*, not achieved previously by other techniques. The FLIM readout further showed high fidelity, reproducibility and the potential applicability to a large range of models and proteins of interest.

6.2 *In vivo* imaging and FLIM-FRET biosensor

The application of *in vivo* imaging has recently provided unprecedented insight into several aspects of tumour progression and treatment. *In vivo* imaging has for example revealed clonal expansion dynamics of cancer stem cells using the confetti construct to be able to track single cell clones and their fates. The cutaneous imaging windows allowed for longitudinal monitoring of cancer stem cell fate upon differentiation in the PyMT model (Zomer *et al*., 2013). Furthermore, using abdominal imaging windows, a similar approach was used employing the confetti construct in the $LGR5^{+}$ stem cell compartment to track cell linages in intestinal crypt over time *in vivo* (Ritsma *et al*., 2014).

The application of FRET reporters has been explored previously as well to examine cancer dynamics and treatment responses. An example of a FRET-reporter mouse described previously constitutes the Erk-FRET mouse which has been used for the analysis of Erk activity in the MMTV-ErbB2 overexpressing breast cancer tumour model (Kumagai *et al*., 2015). Intravital FLIM-FRET has further been used to monitor chemotherapeutic response in xenograft tumours using *in vivo* imaging windows (Janssen *et al*., 2013).

Expression of FRET-reporter has been suggested to potentially lead to a perturbation of signalling pathways within the transfected cells. Overexpression of the e.g. full length and functional GTPases contained in FRET-reporters could lead to an alteration in their respective signalling. This in turn could lead to upregulation of their usual cellular functions and thus alter their innate responses, especially in cancer. It has been shown that overexpression of GTPases such as RhoA can for example lead malignant transformation of native mammary cells (Zhao *et al*., 2009).

As shown before in the Rac-1 biosensor mouse (Johnsson *et al*., 2014), ubiquitous expression of the FRET-reporter resulted in negligible expression alterations in the amount of cellular Rac-1 levels as detected by immunoblot. Here, we have shown a similar trend in the RhoA mouse. The ubiquitous expression of the RhoA reporter in tissues did not markedly alter the levels of endogenous RhoA in the tissues analysed (Figure 5.1 C).

The use of *in vivo* imaging techniques employing optical windows was further crucial in maintaining native GTPase signalling events, which were decreased over time when tissue was excised (Figure 5.8 B, control *in vivo*: mean ± SEM = 1.75 ±

0.01 ns, versus Figure 5.6 B, control *ex vivo*: mean ± SEM = 1.84 ± 0.02 ns). Assaying GTPase activity by conventional biochemical methods does not confer the same fidelity and often results in a rather poor read-out. Especially transient activation events may be lost during fixation steps due to the activity of cellular GAPs. Live tissue imaging furthermore prevents the possibility of preservation artefacts. Such staining artefacts observed in fixed tissue following e.g. IHC or IF can further be avoided, with genetically expressed biosensors representing a more specific readout of activity than can be achieved by secondary staining with e.g. antibodies.

The use of different FRET reporters could further improve the spatial read-out of protein activity in the future. The use of membrane cycling reporters could constitute a real alternative to the reporters described here, due to their ability to cycle on and off the membrane and thus allowing for more native spatially defined readouts on Src or GTPase activity in cells. The insertion of the fluorescent protein between the GTPase and the membrane tether (Figure 1.6 B+C) inhibits dissociation of the inactive form from the membrane. This insertion further blocks the association of the GTPase with GDIs, which would sequester inactive forms in the cytoplasm (Hoffman *et al*., 2000). However, they still require optimization in several aspects as described below.

The Src merobody biosensor comprises a fibronectin monobody able to bind to the SH3 domain of activated Src, a conjugated merocyanine dye, with reduced fluorescence upon hydrophobic pocket binding near the variable region of the monobody and fused cerulean on the opposite end (Figure 6.1 A). The probe directly reports on the action of Src on the membrane following stimuli, due to the membrane targeting of Src upon activation. Upon binding of the variable region of the monobody to the exposed SH3 domain of activated SFKs, the fluorescence of the merocynanine dye 53 increases, resulting in a change in ratiometric output of the dye and Cerulean fluoresence (Gulyani *et al*., 2011). Introducing a FRET pair of fluorophores could greatly enhance the utility of this biosensor in a live cell imaging system, as the sensor as is has to be injected into cells, after dye labelling. Using a permutated version of Venus has been done, but requires more characterization for FRET optimization.

To track GTPase activity in different subcellular contexts, the fluorescent activation reporters (FLAREs) were conceived and characterized previously (Kraynov *et al*., 2000; Machacek *et al*., 2009). They function in a similar manner as the Raichu reporters used here, with the difference that they constitute bi-molecular reporters that are not initially membrane tethered (Figure 6.1 B+C). A problem with the CAAX box motif is that, the Raichu reporters are unresponsive to RhoGDI inhibition (Itoh *et al*., 2002). In the FLARE reporter constructs, the membrane localization following GTP exchange on the donor fluorophore tagged GTPases is conserved. Once GTP bound and membrane localized, they again bind their respective responsive fragment tagged with the acceptor fluorophore, resulting in FRET. GAPs are once again able to revert this action, leading to GDI binding of the probes and disassociation from the membrane. A main problem with these probes, however, remains the expression of both parts of the reporter at equal levels within the cell, in order to avoid possible false positive/negative read outs of activity. This in turn can complicate the analysis and interpretation of data obtained.

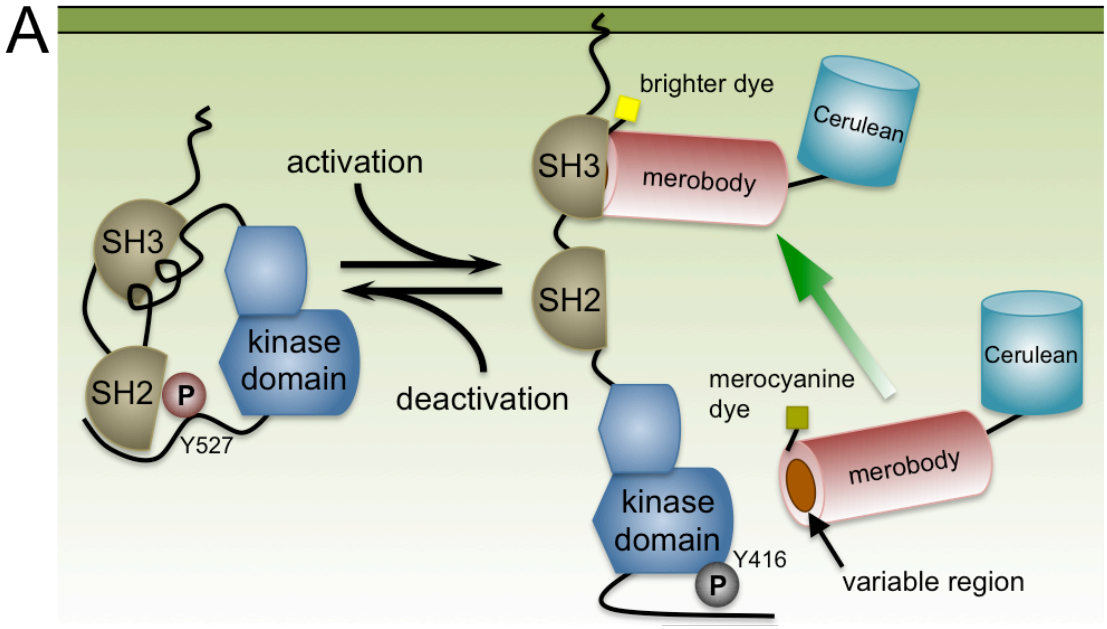

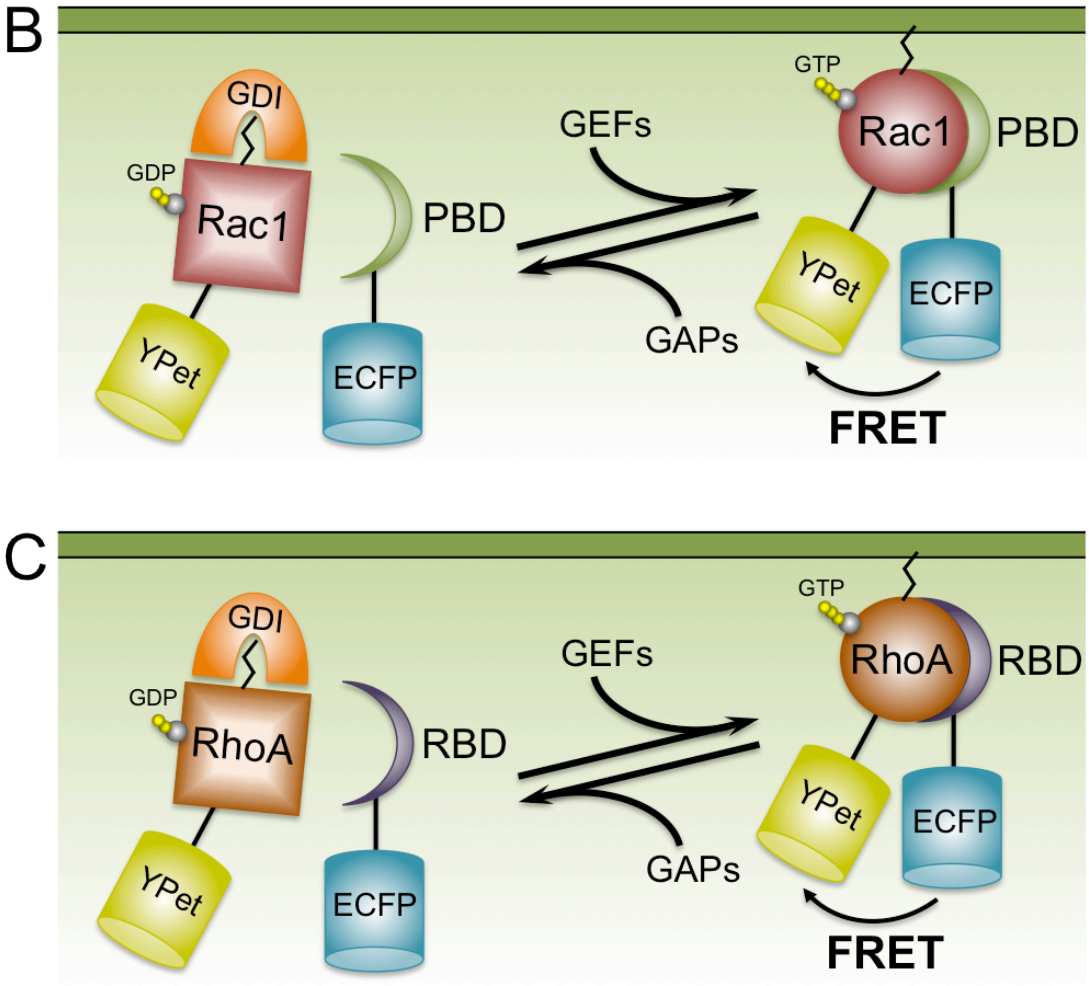

Figure 6.1: Schematic of Src and RhoGTPase biosensors as described by Hahn and colleagues

A A fibronectin monodoy binding to the SH3 domain of activated Src was conjugated to Cerulean and the merocyanine dye 53 on opposite ends. Fluorescence of the dye is decreased in association with the monobody and upon binding of the exposed SH3 domain of Src, fluorescence increases, changing the ratiometric readout between the mero53 and Cerulean (Gulyani *et al*., 2011). **B** + **C** Fluorescent activation reporter (FLARE) biosensors for Rac-1 and RhoA have been described by tethering YPet to full length Rac-1/RhoA and ECFP to a fragment the Pak1 binding domain (PDB) (Kraynov *et al*., 2000) and the RhoA binding domain of Rhotekin (RDB) (Pertz *et al*., 2006). The probes can cycle on and off the membrane in accordance to their activation status, with FRET occurring in the active state (adapted from Machacek *et al*. 2009).

6.3 *In vivo* pharmacodynamics

Using *in vivo* imaging in the native tumour setting can provide a powerful tool in order to more precisely monitor longitudinal and spatially drug treatment responses. This has been demonstrated previously by the use of intravital imaging to track the chemotherapeutic response of PyMT mice to doxorubicin. Doxorubicin itself displays fluorescence under 480 nm excitation, allowing for it to be tracked by imaging *in vivo* (Nakasone *et al*., 2012). Further, depletion of macrophages in this tumour model and its impact on therapeutic outcome was monitored by intravital imaging as well (Lohela *et al*., 2014). Expanding on previous studies, this has allowed for the monitoring of drug responses *in vivo* over time and in spatial contexts. This in turn is necessary when considering that several factors of the tumour microenvironment can contribute to reduced drug responses (Dittmer and Leyh, 2015). Among them are the ECM, stromal cells and immune infiltrating cells, which can contribute to drug resistance mechanisms. Using intravital imaging in monitoring the targeting of also stromal compartments as described before, could help to improve the efficacy of the primary drug treatments *in vivo*. This was done for example by treatment of tumour bearing mice with angiotensin, reducing collagen and hyaluronin deposition in the tumours and allowing for increased vascular perfusion und drug influx (Chauhan *et al*., 2013).

Here, we have shown that *in vivo* imaging can be achieved in conjunction with a mechanistic read-out of protein activity, combining FLIM-FRET and optical windows. This is especially useful, as it clearly mirrors a drug capability of reaching its target in the native tumour microenvironment. Inhibition in defined areas of a tumour, away from local vessels was shown (Figure 3.11 and Figure 3.16) and center versus border (Figure 3.10). This allowed for the gauging of the innate signalling in the native tumour microenvironment and how current treatment may target it. Further, the limitation of treatment was shown by the observed limits of treatment perfusion. Moreover, ways that these may be overcome by were explored with combination treatments modulating the ECM. Finally, longitudinal drug efficacy imaging was conducted (Figure 4.8; Figure 4.9 and Figure 5.9). Using this longitudinal readout can further aid in optimizing treatment regimens, by timed administration and exploring the possible additive effect of dose increase or combination with carrier molecules to facilitate drug delivery.

6.4 Future directions

In this thesis I have described the use of FLIM-FRET as a tool in assessing the pharmacodynamics of cancer treatments *in vivo*.

Having explored single time point treatments in the PyMT model with specific inhibitors of Rac-1, this could be expanded upon in the future by optimizing the inhibitor concentrations, timing and possible combination treatments. Assessing the same treatments used in the PyMT model could further be applied to the ErbB2 model as well, where an even higher level of Rac-1 activity was observed. Exploring other treatment options, such as those targeting down- or upstream effectors of Rac-1 signalling in these cells could also be done in the future. There, utilizing specific small inhibitors of e.g.: PAK1 with IPA-3 (Deacon *et al*., 2008) could be monitored for targeting efficacy *in vivo*.

The role of the GEF P-Rex1 in Rac-1 signalling in KPC tumours demonstrated here could also be further expanded upon. The loss of one copy of P-Rex1 resulted in haploinsufficiency in terms of Rac-1 signalling *in vivo* and decreased Rac-1 activity down to baseline wildtype pancreas levels. The possible resultant defect in migration and invasion of the KPC cells, could be examined in the future. Furthermore, since reduction of Rac-1 signalling upon loss of P-Rex1 was observed in all three tumour models examined (PyMT, ErbB2 and KPC), application of the inhibitor 1A-116, could also be explored. It has been shown that this inhibitor only targets P-Rex1 specific GTP exchange on Rac-1 and not that of other GEFs (Cardama *et al*., 2014).

Taking the application of FLIM-FRET further, multiplexing could be considered in observing multiple signalling pathways simultaneously. This could be done by the use of dark acceptors, opening the possibility of imaging another fluorophore without the need of spectral unmixing. Designing e.g. a reporter with a CFP-based donor and dark acceptor and co-expressing said reporter with another that contains fluorphores outside the CFP emission spectrum could be done. In this way there is no cross-talk between emission read-outs and 2 protein activities could be imaged simultaneously in the same cellular setting as demonstrated to an extent previously (Grant *et al*., 2008).

Finally, having demonstrated the using of *in vivo* FLIM-FRET imaging in the evaluation of drug treatment responses in several models using different targets shows that this technique could be further applied successfully to a board range of targets and treatment models in the future. A great variety of FRET reporters exist (Conway *et al*., 2014) that could be used in *in vivo* mouse models endogenously expressing them. As our understanding of different cancers and their drivers evolve, so does the possibility of targeted personalized therapies. Applying the techniques shown here can provide a powerful tool in the mechanistic read-out of pharmacodynamics of treatment regimes in the context of specific genetic drivers.

References

Adam, L., Vadlamudi, R.K., McCrea, P., and Kumar, R. (2001). Tiam1 overexpression potentiates heregulin-induced lymphoid enhancer factor-1/beta -catenin nuclear signaling in breast cancer cells by modulating the intercellular stability. The Journal of Biological Chemistry *276*, 28443–28450.

Adra, C.N., Manor, D., Ko, J.L., Zhu, S., Horiuchi, T., Van Aelst, L., Cerione, R.A., and Lim, B. (1997). RhoGDIgamma: a GDP-dissociation inhibitor for Rho proteins with preferential expression in brain and pancreas. Proceedings of the National Academy of Sciences of the United States of America *94*, 4279–4284.

Ai, K., Lu, L., Huang, X., Chen, W., and Zhang, H. (2008). Prognostic significance of S100A4 and vascular endothelial growth factor expression in pancreatic cancer. World Journal of Gastroenterology : WJG *14*, 1931–1935.

Alberts, B., Johnson, A., Lewis, J., Morgan, D., Raff, M., Roberts, K., and Walter, P. (2015). Molecular Biology of the Cell, Sixth Edition., pp. 1–1342.

Almoguera, C., Shibata, D., Forrester, K., Martin, J., Arnheim, N., and Perucho, M. (1988). Most human carcinomas of the exocrine pancreas contain mutant c-K-ras genes. Cell *53*, 549–554.

Anastasiadis, P.Z., and Reynolds, A.B. (2001). Regulation of Rho GTPases by p120-catenin. Current Opinion in Cell Biology *13*, 604–610.

Andrechek, E., Hardy, W., Siegel, P., Rudnicki, M., Cardiff, R., and Mueller, W. (2000). Amplification of the neu/erbB-2 oncogene in a mouse model of mammary tumorigenesis. Proceedings of the National Academy of Sciences of the United States of America *97*, 2–7.

Arias-Romero, L.E., Villamar-Cruz, O., Pacheco, a, Kosoff, R., Huang, M., Muthuswamy, S.K., and Chernoff, J. (2010). A Rac-Pak signaling pathway is essential for ErbB2-mediated transformation of human breast epithelial cancer cells. Oncogene *29*, 5839–5849.

Artym, V. V, Swatkoski, S., Matsumoto, K., Campbell, C.B., Petrie, R.J., Dimitriadis, E.K., Li, X., Mueller, S.C., Bugge, T.H., Gucek, M., et al. (2015). Dense fibrillar collagen is a potent inducer of invadopodia via a specific signaling network. The Journal of Cell Biology *208*, 331–350.

Balanis, N., Yoshigi, M., Wendt, M.K., Schiemann, W.P., and Carlin, C.R. (2011). β3 integrin-EGF receptor cross-talk activates p190RhoGAP in mouse mammary gland epithelial cells. Molecular Biology of the Cell *22*, 4288–4301.

Barad, Y., Eisenberg, H., Horowitz, M., and Silberberg, Y. (1997). Nonlinear scanning laser microscopy by third harmonic generation. Applied Physics Letters *70*, 922–924.

Barber, M. a, Hendrickx, A., Beullens, M., Ceulemans, H., Oxley, D., Thelen, S., Thelen, M., Bollen, M., and Welch, H.C.E. (2012). The guanine-nucleotide-exchange factor P-Rex1 is activated by protein phosphatase 1α. The Biochemical Journal *443*, 173–183.

Baselga, J., and Swain, S.M. (2009). Novel anticancer targets: revisiting ERBB2 and discovering ERBB3. Nature Reviews. Cancer *9*, 463–475.

Benet, L.Z., and Zia-Amirhosseini, P. (1995). Basic principles of pharmacokinetics. Toxicologic Pathology *23*, 115–123.

Benoit, Y.D., Lussier, C., Ducharme, P.-A., Sivret, S., Schnapp, L.M., Basora, N., and Beaulieu, J.-F. (2009). Integrin alpha8beta1 regulates adhesion, migration and proliferation of human intestinal crypt cells via a predominant RhoA/ROCK-dependent mechanism. Biology of the Cell / Under the Auspices of the European Cell Biology Organization *101*, 695–708.

Berrier, A.L., Martinez, R., Bokoch, G.M., and LaFlamme, S.E. (2002). The integrin beta tail is required and sufficient to regulate adhesion signaling to Rac1. Journal of Cell Science *115*, 4285–4291.

Bhowmick, N.A., Ghiassi, M., Bakin, A., Aakre, M., Lundquist, C.A., Engel, M.E., Arteaga, C.L., and Moses, H.L. (2001). Transforming growth factor-beta1 mediates epithelial to mesenchymal transdifferentiation through a RhoA-dependent mechanism. Molecular Biology of the Cell *12*, 27–36.

Bi, Y., and Williams, J.A. (2005). A role for Rho and Rac in secretagogue-induced amylase release by pancreatic acini. American Journal of Physiology. Cell Physiology *289*, C22–32.

Bi, Y., Page, S. Le, and Williams, J.A. (2005). Rho and Rac promote acinar morphological changes, actin reorganization, and amylase secretion. American Journal of Physiology. Gastrointestinal and Liver Physiology *289*, G561–70.

Bid, H.K., Roberts, R.D., Manchanda, P.K., and Houghton, P.J. (2013). RAC1: an emerging therapeutic option for targeting cancer angiogenesis and metastasis. Molecular Cancer Therapeutics *12*, 1925–1934.

Borst, J.W., and Visser, A.J.W.G. (2010). Fluorescence lifetime imaging microscopy in life sciences. Measurement Science and Technology *21*, 102002.

Boscher, C., and Nabi, I.R. (2013). Galectin-3- and phospho-caveolin-1-dependent outside-in integrin signaling mediates the EGF motogenic response in mammary cancer cells. Molecular Biology of the Cell *24*, 2134–2145.

Bosco, E.E., Nakai, Y., Hennigan, R.F., Ratner, N., and Zheng, Y. (2010). NF2-deficient cells depend on the Rac1-canonical Wnt signaling pathway to promote the loss of contact inhibition of proliferation. Oncogene *29*, 2540–2549.

Bourguignon, L.Y., Zhu, H., Shao, L., and Chen, Y.W. (2000). Ankyrin-Tiam1 interaction promotes Rac1 signaling and metastatic breast tumor cell invasion and migration. The Journal of Cell Biology *150*, 177–191.

Brantley-Sieders, D.M., Zhuang, G., Hicks, D., Fang, W. Bin, Hwang, Y., Cates, J.M.M., Coffman, K., Jackson, D., Bruckheimer, E., Muraoka-Cook, R.S., et al. (2008). The receptor tyrosine kinase EphA2 promotes mammary adenocarcinoma tumorigenesis and metastatic progression in mice by amplifying ErbB2 signaling. The Journal of Clinical Investigation *118*, 64–78.

Bronson, S.K., Plaehn, E.G., Kluckman, K.D., Hagaman, J.R., Maeda, N., and Smithies, O. (1996). Single-copy transgenic mice with chosen-site integration. Proceedings of the National Academy of Sciences of the United States of America *93*, 9067–9072.

Brown, M.T., and Cooper, J.A. (1996). Regulation, substrates and functions of src. Biochimica Et Biophysica Acta *1287*, 121–149.

Buettner, R., Mesa, T., Vultur, A., Lee, F., and Jove, R. (2008). Inhibition of Src family kinases with dasatinib blocks migration and invasion of human melanoma cells. Molecular Cancer Research : MCR *6*, 1766–1774.

Bücher, H., Drexhage, K.H., Fleck, M., Kuhn, H., Möbius, D., Schäfer, F.P., Sondermann, J., Sperling, W., Tillmann, P., and Wiegand, J. (1967). Controlled Transfer of Excitation Energy Through Thin Layers. Molecular Crystals *2*, 199–230.

Caldas, C., Hahn, S.A., Da Costa, L.T., Redston, M.S., Schutte, M., Seymour, A.B., Weinstein, C.L., Hruban, R.H., Yeo, C.J., and Kern, S.E. (1994). Frequent somatic mutations and homozygous deletions of the p16 (MTS1) gene in pancreatic adenocarcinoma. Nature Genetics *8*, 27–32.

Campagnola, P.J., Millard, A.C., Terasaki, M., Hoppe, P.E., Malone, C.J., and Mohler, W. a (2002). Three-dimensional high-resolution second-harmonic generation imaging of endogenous structural proteins in biological tissues. Biophysical Journal *82*, 493–508.

Cardama, G.A., Comin, M.J., Hornos, L., Gonzalez, N., Defelipe, L., Turjanski, A.G., Alonso, D.F., Gomez, D.E., and Menna, P.L. (2014). Preclinical development of novel Rac1-GEF signaling inhibitors using a rational design approach in highly aggressive breast cancer cell lines. Anti-cancer Agents in Medicinal Chemistry *14*, 840–851.

Cardone, R.A., Bellizzi, A., Busco, G., Weinman, E.J., Dell'Aquila, M.E., Casavola, V., Azzariti, A., Mangia, A., Paradiso, A., and Reshkin, S.J. (2007). The NHERF1 PDZ2 domain regulates PKA-RhoA-p38-mediated NHE1 activation and invasion in breast tumor cells. Molecular Biology of the Cell *18*, 1768–1780.

Cardoso, a P., Pinto, M.L., Pinto, a T., Oliveira, M.I., Pinto, M.T., Gonçalves, R., Relvas, J.B., Figueiredo, C., Seruca, R., Mantovani, a, et al. (2014). Macrophages stimulate gastric and colorectal cancer invasion through EGFR Y(1086), c-Src, Erk1/2 and Akt phosphorylation and smallGTPase activity. Oncogene *33*, 2123–2133.

Carlson R H (2014). Pancreatic Cancer: Dasatinib Trial Negative in Locally Advanced Pancreatic Cancer. Oncology Times *36*, 1–8.

Carr, H.S., Zuo, Y., Oh, W., and Frost, J. a (2013). Regulation of focal adhesion kinase activation, breast cancer cell motility, and amoeboid invasion by the RhoA guanine nucleotide exchange factor Net1. Molecular and Cellular Biology *33*, 2773–2786.

Cary, L.A., Han, D.C., Polte, T.R., Hanks, S.K., and Guan, J.L. (1998). Identification of p130Cas as a mediator of focal adhesion kinase-promoted cell migration. The Journal of Cell Biology *140*, 211–221.

Centonze, V.E., and White, J.G. (1998). Multiphoton excitation provides optical sections from deeper within scattering specimens than confocal imaging. Biophysical Journal *75*, 2015–2024.

Chandrakasan, G., Torchia, D.A., and Piez, K.A. (1976). Preparation of Intact Monomeric Collagen from Rat Tail Tendon and Skin and the Structure of the Nonhelical Ends in Solution. The Journal of Biological Chemistry *251*, 6062–6067.

Chang, C.-W., Sud, D., and Mycek, M.-A. (2007). Fluorescence lifetime imaging microscopy. Methods in Cell Biology *81*, 495–524.

Chatterjee, M., Ben-Josef, E., Thomas, D.G., Morgan, M. a, Zalupski, M.M., Khan, G., Andrew Robinson, C., Griffith, K. a, Chen, C.-S., Ludwig, T., et al. (2015). Caveolin-1 is Associated with Tumor Progression and Confers a Multi-Modality Resistance Phenotype in Pancreatic Cancer. Scientific Reports *5*, 10867.

Chauhan, V.P., Martin, J.D., Liu, H., Lacorre, D. a, Jain, S.R., Kozin, S. V, Stylianopoulos, T., Mousa, A.S., Han, X., Adstamongkonkul, P., et al. (2013). Angiotensin inhibition enhances drug delivery and potentiates chemotherapy by decompressing tumour blood vessels. Nature Communications *4*, 2516.

Chavez, K.J., Garimella, S. V, and Lipkowitz, S. (2010). Triple negative breast cancer cell lines: one tool in the search for better treatment of triple negative breast cancer. Breast Disease *32*, 35–48.

Che, P., Yang, Y., Han, X., Hu, M., Sellers, J.C., Londono-Joshi, A.I., Cai, G.-Q., Buchsbaum, D.J., Christein, J.D., Tang, Q., et al. (2015). S100A4 promotes pancreatic cancer progression through a dual signaling pathway mediated by Src and focal adhesion kinase. Scientific Reports *5*, 8453.

Chee, C.E., Krishnamurthi, S., Nock, C.J., Meropol, N.J., Gibbons, J., Fu, P., Bokar, J., Teston, L., O'Brien, T., Gudena, V., et al. (2013). Phase II study of dasatinib (BMS-354825) in patients with metastatic adenocarcinoma of the pancreas. The Oncologist *18*, 1091–1092.

Chen, X., and Macara, I.G. (2005). Par-3 controls tight junction assembly through the Rac exchange factor Tiam1. Nature Cell Biology *7*, 262–269.

Chen, Y., and Periasamy, A. (2004). Characterization of two-photon excitation fluorescence lifetime imaging microscopy for protein localization. Microscopy Research and Technique *63*, 72–80.

Chen, J.-S., Huang, X., Wang, Q., Huang, J.-Q., Zhang, L., Chen, X.-L., Lei, J., and Cheng, Z.-X. (2013). Sonic hedgehog signaling pathway induces cell migration and invasion through focal adhesion kinase/AKT signaling-mediated activation of matrix metalloproteinase (MMP)-2 and MMP-9 in liver cancer. Carcinogenesis *34*, 10–19.

Cho, S.-G., Wang, Y., Rodriguez, M., Tan, K., Zhang, W., Luo, J., Li, D., and Liu, M. (2011a). Haploinsufficiency in the prometastasis Kiss1 receptor Gpr54 delays breast tumor initiation, progression, and lung metastasis. Cancer Research *71*, 6535–6546.

Cho, S.-G., Wang, Y., Rodriguez, M., Tan, K., Zhang, W., Luo, J., Li, D., and Liu, M. (2011b). Haploinsufficiency in the prometastasis Kiss1 receptor Gpr54 delays breast tumor initiation, progression, and lung metastasis. Cancer Research *71*, 6535–6546.

Collisson, E.A., Trejo, C.L., Silva, J.M., Gu, S., Korkola, J.E., Heiser, L.M., Charles, R., Rabinovich, B.A., Hann, B., Dankort, D., et al. (2012). A central role for RAF→MEK→ERK signaling in the genesis of pancreatic ductal adenocarcinoma. Cancer Discovery *2*, 685–693.

Condliffe, A.M., Davidson, K., Anderson, K.E., Ellson, C.D., Crabbe, T., Okkenhaug, K., Vanhaesebroeck, B., Turner, M., Webb, L., Wymann, M.P., et al. (2005). Sequential activation of class IB and class IA PI3K is important for the primed respiratory burst of human but not murine neutrophils. Blood *106*, 1432–1441.

Conway, J.R.W., Carragher, N.O., and Timpson, P. (2014). Developments in preclinical cancer imaging: innovating the discovery of therapeutics. Nature Reviews. Cancer *14*, 314–328.

Cooper, J.A., Gould, K.L., Cartwright, C.A., and Hunter, T. (1986). Tyr527 is phosphorylated in pp60c-src: implications for regulation. Science (New York, N.Y.) *231*, 1431–1434.

Cowell, C.F., Weigelt, B., Sakr, R. a., Ng, C.K.Y., Hicks, J., King, T. a., and Reis-Filho, J.S. (2013). Progression from ductal carcinoma in situ to invasive breast cancer: revisited. Molecular Oncology *7*, 859–869.

Cox, G., and Sheppard, C.J.R. (2004). Practical limits of resolution in confocal and non-linear microscopy. Microscopy Research and Technique *63*, 18–22.

Crnogorac-Jurcevic, T., Efthimiou, E., Capelli, P., Blaveri, E., Baron, A., Terris, B., Jones, M., Tyson, K., Bassi, C., Scarpa, A., et al. (2001). Gene expression profiles of pancreatic cancer and stromal desmoplasia. Oncogene *20*, 7437–7446.

Cruz-Monserrate, Z., and O'Connor, K.L. (2008). Integrin alpha 6 beta 4 promotes migration, invasion through Tiam1 upregulation, and subsequent Rac activation. Neoplasia (New York, N.Y.) *10*, 408–417.

Cufí, S., Bonavia, R., Vazquez-Martin, A., Oliveras-Ferraros, C., Corominas-Faja, B., Cuyàs, E., Martin-Castillo, B., Barrajón-Catalán, E., Visa, J., Segura-Carretero, A., et al. (2013). Silibinin suppresses EMT-driven erlotinib resistance by reversing the high miR-21/low miR-200c signature in vivo. Scientific Reports *3*, 2459.

Czernilofsky, A.P., Levinson, A.D., Varmus, H.E., Bishop, J.M., Tischer, E., and Goodman, H.M. (1980). Nucleotide sequence of an avian sarcoma virus oncogene (src) and proposed amino acid sequence for gene product. Nature *287*, 198–203.

Dale, R.E., Eisinger, J., and Blumberg, W.E. (1979). The orientational freedom of molecular probes. The orientation factor in intramolecular energy transfer. Biophysical Journal *26*, 161–193.

Damoulakis, G., Gambardella, L., Rossman, K.L., Lawson, C.D., Anderson, K.E., Fukui, Y., Welch, H.C., Der, C.J., Stephens, L.R., and Hawkins, P.T. (2014). P-Rex1 directly activates RhoG to regulate GPCR-driven Rac signalling and actin polarity in neutrophils. Journal of Cell Science *127*, 2589–2600.

Daniels, R.A., Turley, H., Kimberley, F.C., Liu, X.S., Mongkolsapaya, J., Ch'En, P., Xu, X.N., Jin, B.Q., Pezzella, F., and Screaton, G.R. (2005). Expression of TRAIL and TRAIL receptors in normal and malignant tissues. Cell Research *15*, 430–438.

Day, R.N., Booker, C.F., and Periasamy, A. (2008). Characterization of an improved donor fluorescent protein for Forster resonance energy transfer microscopy. Journal of Biomedical Optics *13*, 031203.

Deacon, S.W., Beeser, A., Fukui, J.A., Rennefahrt, U.E.E., Myers, C., Chernoff, J., and Peterson, J.R. (2008). An isoform-selective, small-molecule inhibitor targets the autoregulatory mechanism of p21-activated kinase. Chemistry & Biology *15*, 322–331.

Deevi, R.K., Cox, O.T., and O'Connor, R. (2014). Essential function for PDLIM2 in cell polarization in three-dimensional cultures by feedback regulation of the β1-integrin-RhoA signaling axis. Neoplasia (New York, N.Y.) *16*, 422–431.

Delmas, V., Martinozzi, S., Bourgeois, Y., Holzenberger, M., and Larue, L. (2003). Cre-mediated recombination in the skin melanocyte lineage. Genesis (New York, N.Y. : 2000) *36*, 73–80.

Denk, W., Strickler, J.H., and Webb, W.W. (1990). Two-photon laser scanning fluorescence microscopy. Science (New York, N.Y.) *248*, 73–76.

Dillon, L.M., Bean, J.R., Yang, W., Shee, K., Symonds, L.K., Balko, J.M., McDonald, W.H., Liu, S., Gonzalez-Angulo, a M., Mills, G.B., et al. (2015). P-REX1 creates a positive feedback loop to activate growth factor receptor, PI3K/AKT and MEK/ERK signaling in breast cancer. Oncogene *34*, 3968–3976.

Dittmer, J., and Leyh, B. (2015). The impact of tumor stroma on drug response in breast cancer. Seminars in Cancer Biology *31*, 3–15.

Dohda, T., Nakamura, Y., Kamihira, M., and Iijima, S. (2004). Functional role of RhoA in growth regulation of primary hepatocytes. Journal of Biochemistry *135*, 631–637.

Du, J., Liu, J., Smith, B.J., Tsao, M.S., and Cullen, J.J. (2011). Role of Rac1-dependent NADPH oxidase in the growth of pancreatic cancer. Cancer Gene Therapy *18*, 135–143.

Débarre, D., Supatto, W., Pena, A., Fabre, A., Tordjmann, T., Combettes, L., Schanne-Klein, M.-C., and Beaurepaire, E. (2006). Imaging lipid bodies in cells and tissues using third-harmonic generation microscopy. Nature Methods *3*, 47–53.

Désiré, L., Bourdin, J., Loiseau, N., Peillon, H., Picard, V., De Oliveira, C., Bachelot, F., Leblond, B., Taverne, T., Beausoleil, E., et al. (2005). RAC1 inhibition targets amyloid precursor protein processing by gamma-secretase and decreases Abeta production in vitro and in vivo. The Journal of Biological Chemistry *280*, 37516–37525.

Ebi, H., Costa, C., Faber, A.C., Nishtala, M., Kotani, H., Juric, D., Della Pelle, P., Song, Y., Yano, S., Mino-Kenudson, M., et al. (2013). PI3K regulates MEK/ERK signaling in breast cancer via the Rac-GEF, P-Rex1. Proceedings of the National Academy of Sciences of the United States of America *110*, 21124–21129.

Egberts, J.-H., Cloosters, V., Noack, A., Schniewind, B., Thon, L., Klose, S., Kettler, B., Von Forstner, C., Kneitz, C., Tepel, J., et al. (2008). Anti-tumor necrosis factor therapy inhibits pancreatic tumor growth and metastasis. Cancer Research *68*, 1443–1450.

Ehrlich, J.S., Hansen, M.D.H., and Nelson, W.J. (2002). Spatio-temporal regulation of Rac1 localization and lamellipodia dynamics during epithelial cell-cell adhesion. Developmental Cell *3*, 259–270.

Elangovan, M., Day, R.N., and Periasamy, A. (2002). Nanosecond fluorescence resonance energy transfer-fluorescence lifetime imaging microscopy to localize the protein interactions in a single living cell. Journal of Microscopy *205*, 3–14.

Erpel, T., Superti-Furga, G., and Courtneidge, S.A. (1995). Mutational analysis of the Src SH3 domain: the same residues of the ligand binding surface are important for intra- and intermolecular interactions. The EMBO Journal *14*, 963–975.

Eser, S., Reiff, N., Messer, M., Seidler, B., Gottschalk, K., Dobler, M., Hieber, M., Arbeiter, A., Klein, S., Kong, B., et al. (2013). Selective requirement of PI3K/PDK1 signaling for Kras oncogene-driven pancreatic cell plasticity and cancer. Cancer Cell *23*, 406–420.

Eser, S., Schnieke, a, Schneider, G., and Saur, D. (2014). Oncogenic KRAS signalling in pancreatic cancer. British Journal of Cancer *111*, 817–822.

Fang, W. Bin, Brantley-Sieders, D.M., Parker, M. a, Reith, A.D., and Chen, J. (2005). A kinase-dependent role for EphA2 receptor in promoting tumor growth and metastasis. Oncogene *24*, 7859–7868.

Fang, W. Bin, Ireton, R.C., Zhuang, G., Takahashi, T., Reynolds, A., and Chen, J. (2008). Overexpression of EPHA2 receptor destabilizes adherens junctions via a RhoA-dependent mechanism. Journal of Cell Science *121*, 358–368.

Feldmann, G., Mishra, A., Hong, S.-M., Bisht, S., Strock, C.J., Ball, D.W., Goggins, M., Maitra, A., and Nelkin, B.D. (2010). Inhibiting the cyclin-dependent kinase CDK5 blocks pancreatic cancer formation and progression through the suppression of Ras-Ral signaling. Cancer Research *70*, 4460–4469.

Feng, M., Bao, Y., Li, Z., Li, J., Gong, M., Lam, S., Wang, J., Marzese, D.M., Donovan, N., Tan, E.Y., et al. (2014). RASAL2 activates RAC1 to promote triple-negative breast cancer progression. The Journal of Clinical Investigation *124*, 5291–5304.

Fernandez-Zapico, M.E., Gonzalez-Paz, N.C., Weiss, E., Savoy, D.N., Molina, J.R., Fonseca, R., Smyrk, T.C., Chari, S.T., Urrutia, R., and Billadeau, D.D. (2005). Ectopic expression of VAV1 reveals an unexpected role in pancreatic cancer tumorigenesis. Cancer Cell *7*, 39–49.

Flossmann-Kast, B.B., Jehle, P.M., Hoeflich, A., Adler, G., and Lutz, M.P. (1998). Src stimulates insulin-like growth factor I (IGF-I)-dependent cell proliferation by increasing IGF-I receptor number in human pancreatic carcinoma cells. Cancer Research *58*, 3551–3554.

Foguel, D., Chaloub, R.M., Silva, J.L., Crofts, A.R., and Weber, G. (1992). Pressure and low temperature effects on the fluorescence emission spectra and lifetimes of the photosynthetic components of cyanobacteria. Biophysical Journal *63*, 1613–1622.

Frame, M.C. (2002). Src in cancer: deregulation and consequences for cell behaviour. Biochimica Et Biophysica Acta (BBA) - Reviews on Cancer *1602*, 114–130.

Freund, I., and Deutsch, M. (1986). Second-harmonic microscopy of biological tissue. Optics Letters *11*, 94–96.

Friedl, P., and Alexander, S. (2011). Cancer invasion and the microenvironment: plasticity and reciprocity. Cell *147*, 992–1009.

Fritz, G., Just, I., and Kaina, B. (1999). Rho GTPases are over-expressed in human tumors. International Journal of Cancer. Journal International Du Cancer *81*, 682–687.

Fritz, G., Brachetti, C., Bahlmann, F., Schmidt, M., and Kaina, B. (2002). Rho GTPases in human breast tumours: expression and mutation analyses and correlation with clinical parameters. British Journal of Cancer *87*, 635–644.

Fritz, R.D., Letzelter, M., Reimann, A., Martin, K., Fusco, L., Ritsma, L., Ponsioen, B., Fluri, E., Schulte-Merker, S., Van Rheenen, J., et al. (2013). A versatile toolkit to

produce sensitive FRET biosensors to visualize signaling in time and space. Science Signaling *6*, rs12.

Fujita, Y., Krause, G., Scheffner, M., Zechner, D., Leddy, H.E.M., Sommer, T., and Birchmeier, W. (2003). Hakai, a c-Cbl-like protein, ubiquitinates and induces endocytosis of the E-cadherin complex. Nature Cell Biology *4*, 222–231.

Förster, T. (1946). Energiewanderung und Fluoreszenz. Naturwissenschaften *33*, 166–175.

Ganesan, S., Ameer-Beg, S.M., Ng, T.T.C., Vojnovic, B., and Wouters, F.S. (2006). A dark yellow fluorescent protein (YFP)-based Resonance Energy-Accepting Chromoprotein (REACh) for Förster resonance energy transfer with GFP. Proceedings of the National Academy of Sciences of the United States of America *103*, 4089–4094.

Ganten, T.M., Sykora, J., Koschny, R., Batke, E., Aulmann, S., Mansmann, U., Stremmel, W., Sinn, H.-P., and Walczak, H. (2009). Prognostic significance of tumour necrosis factor-related apoptosis-inducing ligand (TRAIL) receptor expression in patients with breast cancer. Journal of Molecular Medicine (Berlin, Germany) *87*, 995–1007.

Gao, Y., Dickerson, J.B., Guo, F., Zheng, J., and Zheng, Y. (2004). Rational design and characterization of a Rac GTPase-specific small molecule inhibitor. Proceedings of the National Academy of Sciences of the United States of America *101*, 7618–7623.

Garrett, M.D., Major, G.N., Totty, N., and Hall, A. (1991). Purification and N-terminal sequence of the p21rho GTPase-activating protein, rho GAP. The Biochemical Journal *276 (Pt 3*, 833–836.

Gilcrease, M.Z., Kilpatrick, S.K., Woodward, W.A., Zhou, X., Nicolas, M.M., Corley, L.J., Fuller, G.N., Tucker, S.L., Diaz, L.K., Buchholz, T.A., et al. (2009). Coexpression of alpha6beta4 integrin and guanine nucleotide exchange factor Net1 identifies node-positive breast cancer patients at high risk for distant metastasis. Cancer Epidemiology, Biomarkers & Prevention *18*, 80–86.

Gilkes, D.M., Xiang, L., Lee, S.J., Chaturvedi, P., Hubbi, M.E., Wirtz, D., and Semenza, G.L. (2014). Hypoxia-inducible factors mediate coordinated RhoA-ROCK1 expression and signaling in breast cancer cells. Proceedings of the National Academy of Sciences of the United States of America *111*, E384–93.

Gligorijevic, B., Kedrin, D., Segall, J.E., Condeelis, J., and Van Rheenen, J. (2009). Dendra2 photoswitching through the Mammary Imaging Window. Journal of Visualized Experiments : JoVE 3–5.

Goedhart, J., Van Weeren, L., Hink, M. a, Vischer, N.O.E., Jalink, K., and Gadella, T.W.J. (2010). Bright cyan fluorescent protein variants identified by fluorescence lifetime screening. Nature Methods *7*, 137–139.

Gonfloni, S., Williams, J.C., Hattula, K., Weijland, A., Wierenga, R.K., and Superti-Furga, G. (1997). The role of the linker between the SH2 domain and catalytic domain in the regulation and function of Src. The EMBO Journal *16*, 7261–7271.

Gonfloni, S., Frischknecht, F., Way, M., and Superti-Furga, G. (1999). Leucine 255 of Src couples intramolecular interactions to inhibition of catalysis. Nature Structural Biology *6*, 760–764.

Grant, D.M., Zhang, W., McGhee, E.J., Bunney, T.D., Talbot, C.B., Kumar, S., Munro, I., Dunsby, C., Neil, M. a a, Katan, M., et al. (2008). Multiplexed FRET to image multiple signaling events in live cells. Biophysical Journal *95*, L69–71.

Grizot, S., Fauré, J., Fieschi, F., Vignais, P. V, Dagher, M.C., and Pebay-Peyroula, E. (2001). Crystal structure of the Rac1-RhoGDI complex involved in nadph oxidase activation. Biochemistry *40*, 10007–10013.

Guarino, M. (2010). Src signaling in cancer invasion. Journal of Cellular Physiology *223*, 14–26.

Gulyani, A., Vitriol, E., Allen, R., Wu, J., Gremyachinskiy, D., Lewis, S., Dewar, B., Graves, L.M., Kay, B.K., Kuhlman, B., et al. (2011). A biosensor generated via high-throughput screening quantifies cell edge Src dynamics. Nature Chemical Biology *7*, 437–444.

Guo, X., Wang, M., Jiang, J., Xie, C., Peng, F., Li, X., Tian, R., and Qin, R. (2013a). Balanced Tiam1-rac1 and RhoA drives proliferation and invasion of pancreatic cancer cells. Molecular Cancer Research : MCR *11*, 230–239.

Guo, X., Wang, M., Jiang, J., Xie, C., Peng, F., Li, X., Tian, R., and Qin, R. (2013b). Balanced Tiam1-rac1 and RhoA drives proliferation and invasion of pancreatic cancer cells. Molecular Cancer Research : MCR *11*, 230–239.

Guo, X., Wang, M., Zhao, Y., Wang, X., Shen, M., Zhu, F., Shi, C., Xu, M., Li, X., Peng, F., et al. (2015). Par3 regulates invasion of pancreatic cancer cells via interaction with Tiam1. Clinical and Experimental Medicine.

Guy, C.T., Webster, M.A., Schaller, M., Parsons, T.J., Cardiff, R.D., and Muller, W.J. (1992a). Expression of the neu protooncogene in the mammary epithelium of transgenic mice induces metastatic disease. Proceedings of the National Academy of Sciences of the United States of America *89*, 10578–10582.

Guy, C.T., Cardiff, R.D., and Muller, W.J. (1992b). Induction of mammary tumors by expression of polyomavirus middle T oncogene: a transgenic mouse model for metastatic disease. Molecular and Cellular Biology *12*, 954–961.

Göppert-Mayer, M. (1931). Über Elementarakte mit zwei Quantensprüngen. Annalen Der Physik *401*, 273–294.

Ha, B.H., Morse, E.M., Turk, B.E., and Boggon, T.J. (2015). Signaling, Regulation, and Specificity of the Type II p21-activated Kinases. The Journal of Biological Chemistry *290*, 12975–12983.

Hage, B., Meinel, K., Baum, I., Giehl, K., and Menke, A. (2009). Rac1 activation inhibits E-cadherin-mediated adherens junctions via binding to IQGAP1 in pancreatic carcinoma cells. Cell Communication and Signaling : CCS *7*, 23.

Hakam, A., Fang, Q., Karl, R., and Coppola, D. (2003a). Coexpression of IGF-1R and c-Src proteins in human pancreatic ductal adenocarcinoma. Digestive Diseases and Sciences *48*, 1972–1978.

Hakam, A., Fang, Q., Karl, R., and Coppola, D. (2003b). Coexpression of IGF-1R and c-Src proteins in human pancreatic ductal adenocarcinoma. Digestive Diseases and Sciences *48*, 1972–1978.

Hall, A. (1998). Rho GTPases and the actin cytoskeleton. Science (New York, N.Y.) *279*, 509–514.

Hart, M.J., Eva, A., Evans, T., Aaronson, S.A., and Cerione, R.A. (1991). Catalysis of guanine nucleotide exchange on the CDC42Hs protein by the dbl oncogene product. Nature *354*, 311–314.

Haselmann, V., Kurz, A., Bertsch, U., Hübner, S., Olempska-Müller, M., Fritsch, J., Häsler, R., Pickl, A., Fritsche, H., Annewanter, F., et al. (2014). Nuclear death receptor TRAIL-R2 inhibits maturation of let-7 and promotes proliferation of pancreatic and other tumor cells. Gastroenterology *146*, 278–290.

Hauser, A.D., Bergom, C., Schuld, N.J., Chen, X., Lorimer, E.L., Huang, J., Mackinnon, A.C., and Williams, C.L. (2014). The SmgGDS splice variant SmgGDS-558 is a key promoter of tumor growth and RhoA signaling in breast cancer. Molecular Cancer Research : MCR *12*, 130–142.

Heid, I., Lubeseder-Martellato, C., Sipos, B., Mazur, P.K., Lesina, M., Schmid, R.M., and Siveke, J.T. (2011). Early requirement of Rac1 in a mouse model of pancreatic cancer. Gastroenterology *141*, 719–30, 730.e1–7.

Helmchen, F., and Denk, W. (2005). Deep tissue two-photon microscopy. Nature Methods *2*, 932–940.

Hermeking, H., Lengauer, C., Polyak, K., He, T.C., Zhang, L., Thiagalingam, S., Kinzler, K.W., and Vogelstein, B. (1997). 14-3-3 sigma is a p53-regulated inhibitor of G2/M progression. Molecular Cell *1*, 3–11.

Herrera Abreu, M.T., Hughes, W.E., Mele, K., Lyons, R.J., Rickwood, D., Browne, B.C., Bennett, H.L., Vallotton, P., Brummer, T., and Daly, R.J. (2011). Gab2 regulates cytoskeletal organization and migration of mammary epithelial cells by modulating RhoA activation. Molecular Biology of the Cell *22*, 105–116.

Hertzer, K.M., Donald, G.W., and Hines, O.J. (2013). CXCR2: a target for pancreatic cancer treatment? Expert Opinion on Therapeutic Targets *17*, 667–680.

Hilbig, A. (2008). Src kinase and pancreatic cancer. Recent Results in Cancer Research. Fortschritte Der Krebsforschung. Progrès Dans Les Recherches Sur Le Cancer *177*, 179–185.

Hinds, P., Finlay, C., and Levine, A.J. (1989). Mutation is required to activate the p53 gene for cooperation with the ras oncogene and transformation. Journal of Virology *63*, 739–746.

Hingorani, S.R., Petricoin, E.F., Maitra, A., Rajapakse, V., King, C., Jacobetz, M.A., Ross, S., Conrads, T.P., Veenstra, T.D., Hitt, B.A., et al. (2003). Preinvasive and invasive ductal pancreatic cancer and its early detection in the mouse. Cancer Cell *4*, 437–450.

Hingorani, S.R., Wang, L., Multani, A.S., Combs, C., Deramaudt, T.B., Hruban, R.H., Rustgi, A.K., Chang, S., and Tuveson, D. a (2005). Trp53R172H and KrasG12D cooperate to promote chromosomal instability and widely metastatic pancreatic ductal adenocarcinoma in mice. Cancer Cell *7*, 469–483.

Hjelle, B., Liu, E., and Bishop, J.M. (1988). Oncogene v-src transforms and establishes embryonic rodent fibroblasts but not diploid human fibroblasts. Proceedings of the National Academy of Sciences of the United States of America *85*, 4355–4359.

Hoffman, G.R., Nassar, N., and Cerione, R.A. (2000). Structure of the Rho family GTP-binding protein Cdc42 in complex with the multifunctional regulator RhoGDI. Cell *100*, 345–356.

Honda, H., Oda, H., Nakamoto, T., Honda, Z., Sakai, R., Suzuki, T., Saito, T., Nakamura, K., Nakao, K., Ishikawa, T., et al. (1998). Cardiovascular anomaly, impaired actin bundling and resistance to Src-induced transformation in mice lacking p130Cas. Nature Genetics *19*, 361–365.

Hruban, R.H., Wilentz, R.E., and Kern, S.E. (2000). Genetic progression in the pancreatic ducts. The American Journal of Pathology *156*, 1821–1825.

Hruban, R.H., Adsay, N.V., Albores-Saavedra, J., Anver, M.R., Biankin, A. V, Boivin, G.P., Furth, E.E., Furukawa, T., Klein, A., Klimstra, D.S., et al. (2006). Pathology of genetically engineered mouse models of pancreatic exocrine cancer: consensus report and recommendations. Cancer Research *66*, 95–106.

Hsia, D. a, Mitra, S.K., Hauck, C.R., Streblow, D.N., Nelson, J. a, Ilic, D., Huang, S., Li, E., Nemerow, G.R., Leng, J., et al. (2003). Differential regulation of cell motility and invasion by FAK. The Journal of Cell Biology *160*, 753–767.

Huveneers, S., and Danen, E.H.J. (2009). Adhesion signaling - crosstalk between integrins, Src and Rho. Journal of Cell Science *122*, 1059–1069.

Hynes, N.E., and Gattelli, A. (2011). P-Rex1, a guanine exchange factor that is overexpressed in breast cancer, is a convergence node for ErbB and CXCR4 signaling. Molecular Cell *41*, 5–7.

Inaba, K., Inaba, M., Romani, N., Aya, H., Deguchi, M., Ikehara, S., Muramatsu, S., and Steinman, R.M. (1992). Generation of large numbers of dendritic cells from mouse bone marrow cultures supplemented with granulocyte/macrophage colony-stimulating factor. The Journal of Experimental Medicine *176*, 1693–1702.

Ingrao, J.C., Johnson, R., Tor, E., Gu, Y., Litman, M., and Turner, P. V (2013). Aqueous Stability and Oral Pharmacokinetics of Meloxicam and Carprofen in Male C57BL / 6 Mice. Journal of the American Association for Laboratory Animal Science *52*, 553–559.

Innocenti, M., Gerboth, S., Rottner, K., Lai, F.P.L., Hertzog, M., Stradal, T.E.B., Frittoli, E., Didry, D., Polo, S., Disanza, A., et al. (2005). Abi1 regulates the activity of N-WASP and WAVE in distinct actin-based processes. Nature Cell Biology *7*, 969–976.

Ischenko, I., Guba, M., Yezhelyev, M., Papyan, A., Schmid, G., Green, T., Fennell, M., Jauch, K.-W., and Bruns, C.J. (2007). Effect of Src kinase inhibition on metastasis and tumor angiogenesis in human pancreatic cancer. Angiogenesis *10*, 167–182.

Isherwood, B., Timpson, P., McGhee, E.J., Anderson, K.I., Canel, M., Serrels, A., Brunton, V.G., and Carragher, N.O. (2011). Live cell in vitro and in vivo imaging applications: accelerating drug discovery. Pharmaceutics *3*, 141–170.

Ishikawa-Ankerhold, H.C., Ankerhold, R., and Drummen, G.P.C. (2012). Advanced fluorescence microscopy techniques--FRAP, FLIP, FLAP, FRET and FLIM. Molecules (Basel, Switzerland) *17*, 4047–4132.

Itoh, R.E., Kurokawa, K., Ohba, Y., Yoshizaki, H., Mochizuki, N., and Matsuda, M. (2002). Activation of rac and cdc42 video imaged by fluorescent resonance energy transfer-based single-molecule probes in the membrane of living cells. Molecular and Cellular Biology *22*, 6582–6591.

Jackson, B., Peyrollier, K., Pedersen, E., Basse, A., Karlsson, R., Wang, Z., Lefever, T., Ochsenbein, A.M., Schmidt, G., Aktories, K., et al. (2011). RhoA is dispensable for skin development, but crucial for contraction and directed migration of keratinocytes. Molecular Biology of the Cell *22*, 593–605.

Jacobetz, M. a, Chan, D.S., Neesse, A., Bapiro, T.E., Cook, N., Frese, K.K., Feig, C., Nakagawa, T., Caldwell, M.E., Zecchini, H.I., et al. (2013). Hyaluronan impairs vascular function and drug delivery in a mouse model of pancreatic cancer. Gut *62*, 112–120.

Jameson, D.M., Gratton, E., and Hall, R.D. (1984). The Measurement and Analysis of Heterogeneous Emissions by Multifrequency Phase and Modulation Fluorometry. Applied Spectroscopy Reviews *20*, 55–106.

Jamieson, T., Clarke, M., Steele, C.W., Samuel, M.S., Neumann, J., Jung, A., Huels, D., Olson, M.F., Das, S., Nibbs, R.J.B., et al. (2012). Inhibition of CXCR2 profoundly suppresses inflammation-driven and spontaneous tumorigenesis. The Journal of Clinical Investigation *122*, 3127–3144.

Janssen, A., Beerling, E., Medema, R., and Van Rheenen, J. (2013). Intravital FRET imaging of tumor cell viability and mitosis during chemotherapy. PloS One *8*, e64029.

Johansson, J., Berg, T., Kurzejamska, E., Pang, M.-F., Tabor, V., Jansson, M., Roswall, P., Pietras, K., Sund, M., Religa, P., et al. (2013). MiR-155-mediated loss of C/EBPβ shifts the TGF-β response from growth inhibition to epithelial-mesenchymal transition, invasion and metastasis in breast cancer. Oncogene *32*, 5614–5624.

Johnson, E., Seachrist, D.D., DeLeon-Rodriguez, C.M., Lozada, K.L., Miedler, J., Abdul-Karim, F.W., and Keri, R. a. (2010). HER2/ErbB2-induced breast cancer cell migration and invasion require p120 catenin activation of Rac1 and Cdc42. The Journal of Biological Chemistry *285*, 29491–29501.

Johnson, J.L., Winterwood, N., DeMali, K. a, and Stipp, C.S. (2009). Tetraspanin CD151 regulates RhoA activation and the dynamic stability of carcinoma cell-cell contacts. Journal of Cell Science *122*, 2263–2273.

Johnsson, A.-K.E., Dai, Y., Nobis, M., Baker, M.J., McGhee, E.J., Walker, S., Schwarz, J.P., Kadir, S., Morton, J.P., Myant, K.B., et al. (2014). The Rac-FRET mouse reveals tight spatiotemporal control of Rac activity in primary cells and tissues. Cell Reports *6*, 1153–1164.

Kalthoff, H., Schmiegel, W., Roeder, C., Kasche, D., Schmidt, A., Lauer, G., Thiele, H.G., Honold, G., Pantel, K., Riethmuller, G., et al. (1993). p53 and K-RAS alterations in pancreatic epithelial cell lesions. Oncogene *8*, 289–298.

Kamb, A. (2005). What's wrong with our cancer models? Nature Reviews. Drug Discovery *4*, 161–165.

Kanner, S.B., Reynolds, A.B., Vines, R.R., and Parsons, J.T. (1990). Monoclonal antibodies to individual tyrosine-phosphorylated protein substrates of oncogene-encoded tyrosine kinases. Proceedings of the National Academy of Sciences of the United States of America *87*, 3328–3332.

Karlsson, R., Pedersen, E.D., Wang, Z., and Brakebusch, C. (2009). Rho GTPase function in tumorigenesis. Biochimica Et Biophysica Acta *1796*, 91–98.

Von Karstedt, S., Conti, A., Nobis, M., Montinaro, A., Hartwig, T., Lemke, J., Legler, K., Annewanter, F., Campbell, A.D., Taraborrelli, L., et al. (2015). Cancer cell-autonomous TRAIL-R signaling promotes KRAS-driven cancer progression, invasion, and metastasis. Cancer Cell *27*, 561–573.

Katz, E., Sims, A.H., Sproul, D., Caldwell, H., Dixon, M.J., Meehan, R.R., and Harrison, D.J. (2012). Targeting of Rac GTPases blocks the spread of intact human breast cancer. Oncotarget *3*, 608–619.

Kawamura, K., Takano, K., Suetsugu, S., Kurisu, S., Yamazaki, D., Miki, H., Takenawa, T., and Endo, T. (2004). N-WASP and WAVE2 acting downstream of phosphatidylinositol 3-kinase are required for myogenic cell migration induced by hepatocyte growth factor. The Journal of Biological Chemistry *279*, 54862–54871.

Kedrin, D., Gligorijevic, B., Wyckoff, J., Verkhusha, V. V, Condeelis, J., Segall, J.E., and Van Rheenen, J. (2008). Intravital imaging of metastatic behavior through a mammary imaging window. Nature Methods *5*, 1019–1021.

Keely, P.J., Westwick, J.K., Whitehead, I.P., Der, C.J., and Parise, L. V (1997). Cdc42 and Rac1 induce integrin-mediated cell motility and invasiveness through PI(3)K. Nature *390*, 632–636.

Kelber, J. a, Reno, T., Kaushal, S., Metildi, C., Wright, T., Stoletov, K., Weems, J.M., Park, F.D., Mose, E., Wang, Y., et al. (2012). KRas induces a Src/PEAK1/ErbB2 kinase amplification loop that drives metastatic growth and therapy resistance in pancreatic cancer. Cancer Research *72*, 2554–2564.

Khosravi-Far, R., Solski, P.A., Clark, G.J., Kinch, M.S., and Der, C.J. (1995). Activation of Rac1, RhoA, and mitogen-activated protein kinases is required for Ras transformation. Molecular and Cellular Biology *15*, 6443–6453.

Kiehne, K., Herzig, K.H., and Fölsch, U.R. (2002). CCK-stimulated changes in pancreatic acinar morphology are mediated by rho. Digestion *65*, 47–55.

Kissil, J.L., Walmsley, M.J., Hanlon, L., Haigis, K.M., Bender Kim, C.F., Sweet-Cordero, A., Eckman, M.S., Tuveson, D. a, Capobianco, A.J., Tybulewicz, V.L.J., et al. (2007). Requirement for Rac1 in a K-ras induced lung cancer in the mouse. Cancer Research *67*, 8089–8094.

Kjoller, L., and Hall, A. (1999). Signaling to Rho GTPases. Experimental Cell Research *253*, 166–179.

Klarenbeek, J., Goedhart, J., Van Batenburg, A., Groenewald, D., and Jalink, K. (2015). Fourth-generation epac-based FRET sensors for cAMP feature exceptional brightness, photostability and dynamic range: characterization of dedicated sensors for FLIM, for ratiometry and with high affinity. PloS One *10*, e0122513.

Klinghoffer, R.A., Sachsenmaier, C., Cooper, J.A., and Soriano, P. (1999). Src family kinases are required for integrin but not PDGFR signal transduction. The EMBO Journal *18*, 2459–2471.

Kola, I., and Landis, J. (2004). Can the pharmaceutical industry reduce attrition rates? Nature Reviews. Drug Discovery *3*, 711–715.

Kong, W., Yang, H., He, L., Zhao, J., Coppola, D., Dalton, W.S., and Cheng, J.Q. (2008). MicroRNA-155 is regulated by the transforming growth factor beta/Smad pathway and contributes to epithelial cell plasticity by targeting RhoA. Molecular and Cellular Biology *28*, 6773–6784.

Krauthammer, M., Kong, Y., Ha, B.H., Evans, P., Bacchiocchi, A., McCusker, J.P., Cheng, E., Davis, M.J., Goh, G., Choi, M., et al. (2012). Exome sequencing identifies recurrent somatic RAC1 mutations in melanoma. Nature Genetics *44*, 1006–1014.

Kraynov, V.S., Chamberlain, C., Bokoch, G.M., Schwartz, M.A., Slabaugh, S., and Hahn, K.M. (2000). Localized Rac activation dynamics visualized in living cells. Science (New York, N.Y.) *290*, 333–337.

Kumagai, Y., Naoki, H., Nakasyo, E., Kamioka, Y., Kiyokawa, E., and Matsuda, M. (2015). Heterogeneity in ERK activity as visualized by in vivo FRET imaging of mammary tumor cells developed in MMTV-Neu mice. Oncogene *34*, 1051–1057.

Kurokawa, K., Itoh, R.E., Yoshizaki, H., Nakamura, Y.O.T., and Matsuda, M. (2004). Coactivation of Rac1 and Cdc42 at lamellipodia and membrane ruffles induced by epidermal growth factor. Molecular Biology of the Cell *15*, 1003–1010.

Kusama, T., Mukai, M., Iwasaki, T., Tatsuta, M., Matsumoto, Y., Akedo, H., Inoue, M., and Nakamura, H. (2002). 3-hydroxy-3-methylglutaryl-coenzyme a reductase inhibitors reduce human pancreatic cancer cell invasion and metastasis. Gastroenterology *122*, 308–317.

Kusama, T., Mukai, M., Endo, H., Ishikawa, O., Tatsuta, M., Nakamura, H., and Inoue, M. (2006). Inactivation of Rho GTPases by p190 RhoGAP reduces human pancreatic cancer cell invasion and metastasis. Cancer Science *97*, 848–853.

Lacoste, C., Hervé, J., Bou Nader, M., Dos Santos, A., Moniaux, N., Valogne, Y., Montjean, R., Dorseuil, O., Samuel, D., Cassio, D., et al. (2012). Iodide transporter NIS regulates cancer cell motility and invasiveness by interacting with the Rho guanine nucleotide exchange factor LARG. Cancer Research *72*, 5505–5515.

Lakowicz, J.R., Szmacinski, H., Nowaczyk, K., Berndt, K.W., and Johnson, M. (1992). Fluorescence lifetime imaging. Analytical Biochemistry *202*, 316–330.

Lamouille, S., Xu, J., and Derynck, R. (2014). Molecular mechanisms of epithelial-mesenchymal transition. Nature Reviews. Molecular Cell Biology *15*, 178–196.

Lane, J., Martin, T. a, Mansel, R.E., and Jiang, W.G. (2008). The expression and prognostic value of the guanine nucleotide exchange factors (GEFs) Trio, Vav1 and TIAM-1 in human breast cancer. International Seminars in Surgical Oncology : ISSO *5*, 23.

Lei, R., Tang, J., Zhuang, X., Deng, R., Li, G., Yu, J., Liang, Y., Xiao, J., Wang, H.-Y., Yang, Q., et al. (2014). Suppression of MIM by microRNA-182 activates RhoA and promotes breast cancer metastasis. Oncogene *33*, 1287–1296.

Li, A., Ma, Y., Yu, X., Mort, R.L., Lindsay, C.R., Stevenson, D., Strathdee, D., Insall, R.H., Chernoff, J., Snapper, S.B., et al. (2011). Rac1 drives melanoblast organization during mouse development by orchestrating pseudopod- driven motility and cell-cycle progression. Developmental Cell *21*, 722–734.

Li, Z., Chang, Z., Chiao, L.J., Kang, Y., Xia, Q., Zhu, C., Fleming, J.B., Evans, D.B., and Chiao, P.J. (2009). TrkBT1 induces liver metastasis of pancreatic cancer cells by sequestering Rho GDP dissociation inhibitor and promoting RhoA activation. Cancer Research *69*, 7851–7859.

Liggett, W.H., and Sidransky, D. (1998). Role of the p16 tumor suppressor gene in cancer. Journal of Clinical Oncology : Official Journal of the American Society of Clinical Oncology *16*, 1197–1206.

Lim, K.-H., Baines, A.T., Fiordalisi, J.J., Shipitsin, M., Feig, L. a, Cox, A.D., Der, C.J., and Counter, C.M. (2005). Activation of RalA is critical for Ras-induced tumorigenesis of human cells. Cancer Cell *7*, 533–545.

Lin, E.Y., Jones, J.G., Li, P., Zhu, L., Whitney, K.D., Muller, W.J., and Pollard, J.W. (2003). Progression to malignancy in the polyoma middle T oncoprotein mouse breast cancer model provides a reliable model for human diseases. The American Journal of Pathology *163*, 2113–2126.

Lipinski, C.A. (2001). Drug-like properties and the causes of poor solubility and poor permeability. Journal of Pharmacological and Toxicological Methods *44*, 235–249.

Liu, X., Yan, F., Yao, H., Chang, M., Qin, J., Li, Y., Wang, Y., and Pei, X. (2014). Involvement of RhoA/ROCK in insulin secretion of pancreatic β-cells in 3D culture. Cell and Tissue Research *358*, 359–369.

Liu, Y., Cheng, D.K., Sonek, G.J., Berns, M.W., and Tromberg, B.J. (1994). Microfluorometric technique for the determination of localized heating in organic particles. Applied Physics Letters *65*, 919–921.

Loeffler, M., Krüger, J.A., Niethammer, A.G., and Reisfeld, R.A. (2006). Targeting tumor-associated fibroblasts improves cancer chemotherapy by increasing intratumoral drug uptake. The Journal of Clinical Investigation *116*, 1955–1962.

Lohela, M., Casbon, A.-J., Olow, A., Bonham, L., Branstetter, D., Weng, N., Smith, J., and Werb, Z. (2014). Intravital imaging reveals distinct responses of depleting dynamic tumor-associated macrophage and dendritic cell subpopulations. Proceedings of the National Academy of Sciences of the United States of America *111*, E5086–95.

Lombardo, L.J., Lee, F.Y., Chen, P., Norris, D., Barrish, J.C., Behnia, K., Castaneda, S., Cornelius, L.A.M., Das, J., Doweyko, A.M., et al. (2004). Discovery of N-(2-chloro-6-methyl- phenyl)-2-(6-(4-(2-hydroxyethyl)- piperazin-1-yl)-2-methylpyrimidin-4- ylamino)thiazole-5-carboxamide (BMS-354825), a dual Src/Abl kinase inhibitor with potent antitumor activity in preclinical assays. Journal of Medicinal Chemistry *47*, 6658–6661.

Lucato, C.M., Halls, M.L., Ooms, L.M., Liu, H.-J., Mitchell, C. a, Whisstock, J.C., and Ellisdon, A.M. (2015). The Phosphatidylinositol (3,4,5)-Trisphosphate-dependent Rac Exchanger 1·Ras-related C3 Botulinum Toxin Substrate 1 (P-Rex1·Rac1) Complex Reveals the Basis of Rac1 Activation in Breast Cancer Cells. The Journal of Biological Chemistry *290*, 20827–20840.

Lutz, M., Kukutsch, N., and Ogilvie, A. (1999). An advanced culture method for generating large quantities of highly pure dendritic cells from mouse bone marrow. Journal of Immunological Methods *223*, 77–92.

Lutz, M.P., Esser, I.B., Flossmann-Kast, B.B., Vogelmann, R., Lührs, H., Friess, H., Büchler, M.W., and Adler, G. (1998). Overexpression and activation of the tyrosine kinase Src in human pancreatic carcinoma. Biochemical and Biophysical Research Communications *243*, 503–508.

Machacek, M., Hodgson, L., Welch, C., Elliott, H., Pertz, O., Nalbant, P., Abell, A., Johnson, G.L., Hahn, K.M., and Danuser, G. (2009). Coordination of Rho GTPase activities during cell protrusion. Nature *461*, 99–103.

Macher-Goeppinger, S., Aulmann, S., Tagscherer, K.E., Wagener, N., Haferkamp, A., Penzel, R., Brauckhoff, A., Hohenfellner, M., Sykora, J., Walczak, H., et al. (2009). Prognostic value of tumor necrosis factor-related apoptosis-inducing ligand (TRAIL) and TRAIL receptors in renal cell cancer. Clinical Cancer Research : an Official Journal of the American Association for Cancer Research *15*, 650–659.

Machesky, L.M., and Gould, K.L. (1999). The Arp2/3 complex: a multifunctional actin organizer. Current Opinion in Cell Biology *11*, 117–121.

Mack, N.A., Porter, A.P., Whalley, H.J., Schwarz, J.P., Jones, R.C., Sajid, A., Khaja, S., Bjartell, A., Anderson, K.I., and Malliri, A. (2012). β2-syntrophin and Par-3 promote an apicobasal Rac activity gradient at cell – cell junctions by differentially regulating Tiam1 activity. Nature Cell Biology *14*, 1169–1180.

Macleod, K.F., Sherry, N., Hannon, G., Beach, D., Tokino, T., Kinzler, K., Vogelstein, B., and Jacks, T. (1995). p53-dependent and independent expression of p21 during cell growth, differentiation, and DNA damage. Genes & Development *9*, 935–944.

MacMillan, C.D., Leong, H.S., Dales, D.W., Robertson, A.E., Lewis, J.D., Chambers, A.F., and Tuck, A.B. (2014). Stage of breast cancer progression influences cellular response to activation of the WNT/planar cell polarity pathway. Scientific Reports *4*, 6315.

Malaval, C., Laffargue, M., Barbaras, R., Rolland, C., Peres, C., Champagne, E., Perret, B., Tercé, F., Collet, X., and Martinez, L.O. (2009). RhoA/ROCK I signalling downstream of the P2Y13 ADP-receptor controls HDL endocytosis in human hepatocytes. Cellular Signalling *21*, 120–127.

McNiven, M. a (2013). Breaking away: matrix remodeling from the leading edge. Trends in Cell Biology *23*, 16–21.

Menke, A., Philippi, C., Vogelmann, R., Seidel, B., Lutz, M.P., Adler, G., and Wedlich, D. (2001). Down-regulation of E-cadherin gene expression by collagen type I and type III in pancreatic cancer cell lines. Cancer Research *61*, 3508–3517.

Minchinton, A.I., and Tannock, I.F. (2006). Drug penetration in solid tumours. Nature Reviews. Cancer *6*, 583–592.

Moffat, J., Grueneberg, D. a, Yang, X., Kim, S.Y., Kloepfer, A.M., Hinkle, G., Piqani, B., Eisenhaure, T.M., Luo, B., Grenier, J.K., et al. (2006). A lentiviral RNAi library for human and mouse genes applied to an arrayed viral high-content screen. Cell *124*, 1283–1298.

Mohammed, A., Janakiram, N.B., Li, Q., Madka, V., Ely, M., Lightfoot, S., Crawford, H., Steele, V.E., and Rao, C. V (2010a). The epidermal growth factor receptor inhibitor gefitinib prevents the progression of pancreatic lesions to carcinoma in a conditional LSL-KrasG12D/+ transgenic mouse model. Cancer Prevention Research *3*, 1417–1426.

Mohammed, A., Janakiram, N.B., Li, Q., Madka, V., Ely, M., Lightfoot, S., Crawford, H., Steele, V.E., and Rao, C. V (2010b). The epidermal growth factor receptor inhibitor gefitinib prevents the progression of pancreatic lesions to carcinoma in a conditional LSL-KrasG12D/+ transgenic mouse model. Cancer Prevention Research (Philadelphia, Pa.) *3*, 1417–1426.

Mohammed, A., Qian, L., Janakiram, N.B., Lightfoot, S., Steele, V.E., and Rao, C. V (2012). Atorvastatin delays progression of pancreatic lesions to carcinoma by regulating PI3/AKT signaling in p48Cre/+ LSL-KrasG12D/+ mice. International Journal of Cancer. Journal International Du Cancer *131*, 1951–1962.

Mohler, W., Millard, A.C., and Campagnola, P.J. (2003). Second harmonic generation imaging of endogenous structural proteins. Methods (San Diego, Calif.) *29*, 97–109.

Montero, J.C., Seoane, S., Ocaña, a, and Pandiella, a (2011). P-Rex1 participates in Neuregulin-ErbB signal transduction and its expression correlates with patient outcome in breast cancer. Oncogene *30*, 1059–1071.

Moore, K.A., Sethi, R., Doanes, A.M., Johnson, T.M., Pracyk, J.B., Kirby, M., Irani, K., Goldschmidt-Clermont, P.J., and Finkel, T. (1997). Rac1 is required for cell proliferation and G2/M progression. The Biochemical Journal *326*, 17–20.

Mori, S., Rönnstrand, L., Yokote, K., Engström, A., Courtneidge, S.A., Claesson-Welsh, L., and Heldin, C.H. (1993). Identification of two juxtamembrane autophosphorylation sites in the PDGF beta-receptor; involvement in the interaction with Src family tyrosine kinases. The EMBO Journal *12*, 2257–2264.

Morton, J.P., Timpson, P., Karim, S. a, Ridgway, R. a, Athineos, D., Doyle, B., Jamieson, N.B., Oien, K. a, Lowy, A.M., Brunton, V.G., et al. (2010a). Mutant p53 drives metastasis and overcomes growth arrest/senescence in pancreatic cancer. Proceedings of the National Academy of Sciences of the United States of America *107*, 246–251.

Morton, J.P., Karim, S. a, Graham, K., Timpson, P., Jamieson, N., Athineos, D., Doyle, B., McKay, C., Heung, M.-Y., Oien, K. a, et al. (2010b). Dasatinib inhibits the development of metastases in a mouse model of pancreatic ductal adenocarcinoma. Gastroenterology *139*, 292–303.

Moshfegh, Y., Bravo-Cordero, J.J., Miskolci, V., Condeelis, J., and Hodgson, L. (2014). A Trio-Rac1-Pak1 signalling axis drives invadopodia disassembly. Nature Cell Biology *16*, 574–586.

Muinonen-Martin, A.J., Susanto, O., Zhang, Q., Smethurst, E., Faller, W.J., Veltman, D.M., Kalna, G., Lindsay, C., Bennett, D.C., Sansom, O.J., et al. (2014). Melanoma cells break down LPA to establish local gradients that drive chemotactic dispersal. PLoS Biology *12*, e1001966.

Muise, A.M., Walters, T., Xu, W., Shen-Tu, G., Guo, C.-H., Fattouh, R., Lam, G.Y., Wolters, V.M., Bennitz, J., Van Limbergen, J., et al. (2011). Single nucleotide polymorphisms that increase expression of the guanosine triphosphatase RAC1 are associated with ulcerative colitis. Gastroenterology *141*, 633–641.

Mullins, R.D., and Pollard, T.D. (1999). Rho-family GTPases require the Arp2/3 complex to stimulate actin polymerization in Acanthamoeba extracts. Current Biology : CB *9*, 405–415.

Munro, J., Steeghs, K., Morrison, V., Ireland, H., and Parkinson, E.K. (2001). Human fibroblast replicative senescence can occur in the absence of extensive cell division and short telomeres. Oncogene *20*, 3541–3552.

Van Munster, E.B., and Gadella, T.W.J. (2004). phiFLIM: a new method to avoid aliasing in frequency-domain fluorescence lifetime imaging microscopy. Journal of Microscopy *213*, 29–38.

Murakoshi, H., Lee, S.-J., and Yasuda, R. (2008). Highly sensitive and quantitative FRET-FLIM imaging in single dendritic spines using improved non-radiative YFP. Brain Cell Biology *36*, 31–42.

Murga, C., Zohar, M., Teramoto, H., and Gutkind, J.S. (2002). Rac1 and RhoG promote cell survival by the activation of PI3K and Akt, independently of their ability to stimulate JNK and NF-kappaB. Oncogene *21*, 207–216.

Nakashima, M., Adachi, S., Yasuda, I., Yamauchi, T., Kawaguchi, J., Hanamatsu, T., Yoshioka, T., Okano, Y., Hirose, Y., Kozawa, O., et al. (2011). Inhibition of Rho-associated coiled-coil containing protein kinase enhances the activation of epidermal growth factor receptor in pancreatic cancer cells. Molecular Cancer *10*, 79.

Nakasone, E.S., Askautrud, H.A., Kees, T., Park, J.-H., Plaks, V., Ewald, A.J., Fein, M., Rasch, M.G., Tan, Y.-X., Qiu, J., et al. (2012). Imaging tumor-stroma interactions during chemotherapy reveals contributions of the microenvironment to resistance. Cancer Cell *21*, 488–503.

Narumiya, S., Tanji, M., and Ishizaki, T. (2009). Rho signaling, ROCK and mDia1, in transformation, metastasis and invasion. Cancer Metastasis Reviews *28*, 65–76.

Navas, C., Hernández-Porras, I., Schuhmacher, A.J., Sibilia, M., Guerra, C., and Barbacid, M. (2012). EGF receptor signaling is essential for k-ras oncogene-driven pancreatic ductal adenocarcinoma. Cancer Cell *22*, 318–330.

Nguyen, A.W., and Daugherty, P.S. (2005). Evolutionary optimization of fluorescent proteins for intracellular FRET. Nature Biotechnology *23*, 355–360.

Nimnual, A.S., Taylor, L.J., and Bar-Sagi, D. (2003). Redox-dependent downregulation of Rho by Rac. Nature Cell Biology *5*, 236–241.

Nobes, C.D., and Hall, A. (1995). Rho, rac, and cdc42 GTPases regulate the assembly of multimolecular focal complexes associated with actin stress fibers, lamellipodia, and filopodia. Cell *81*, 53–62.

Nobis, M., McGhee, E.J., Morton, J.P., Schwarz, J.P., Karim, S.A., Quinn, J., Edward, M., Campbell, A.D., Mcgarry, L.C., Evans, T.R.J., et al. (2013). Intravital FLIM-FRET Imaging Reveals Dasatinib-Induced Spatial Control of Src in Pancreatic Cancer. Cancer Research *73*, 4674–4686.

Novitskaya, V., Romanska, H., Kordek, R., Potemski, P., Kusińska, R., Parsons, M., Odintsova, E., and Berditchevski, F. (2014). Integrin α3β1-CD151 complex regulates dimerization of ErbB2 via RhoA. Oncogene *33*, 2779–2789.

Nozu, F., Tsunoda, Y., Ibitayo, A.I., Bitar, K.N., and Owyang, C. (1999). Involvement of RhoA and its interaction with protein kinase C and Src in CCK-stimulated pancreatic acini. The American Journal of Physiology *276*, G915–23.

Okada, M., and Nakagawa, H. (1989). A protein tyrosine kinase involved in regulation of pp60c-src function. The Journal of Biological Chemistry *264*, 20886–20893.

Olayioye, M.A., Neve, R.M., Lane, H.A., and Hynes, N.E. (2000). The ErbB signaling network: receptor heterodimerization in development and cancer. The EMBO Journal *19*, 3159–3167.

Olive, K.P., and Tuveson, D. a (2006). The use of targeted mouse models for preclinical testing of novel cancer therapeutics. Clinical Cancer Research : an Official Journal of the American Association for Cancer Research *12*, 5277–5287.

Olive, K.P., Jacobetz, M.A., Davidson, C.J., Gopinathan, A., McIntyre, D., Honess, D., Madhu, B., Goldgraben, M.A., Caldwell, M.E., Allard, D., et al. (2009). Inhibition of Hedgehog signaling enhances delivery of chemotherapy in a mouse model of pancreatic cancer. Science (New York, N.Y.) *324*, 1457–1461.

Olivier, M., Eeles, R., Hollstein, M., Khan, M. a, Harris, C.C., and Hainaut, P. (2002). The IARC TP53 database: new online mutation analysis and recommendations to users. Human Mutation *19*, 607–614.

Olofsson, B. (1999). Rho guanine dissociation inhibitors: pivotal molecules in cellular signalling. Cellular Signalling *11*, 545–554.

Olson, M.F., Ashworth, A., and Hall, A. (1995). An essential role for Rho, Rac, and Cdc42 GTPases in cell cycle progression through G1. Science (New York, N.Y.) *269*, 1270–1272.

Onesto, C., Shutes, A., Picard, V., Schweighoffer, F., and Der, C.J. (2008). Characterization of EHT 1864, a novel small molecule inhibitor of Rac family small GTPases. Methods in Enzymology *439*, 111–129.

Ozawa, F., Friess, H., Kleeff, J., Xu, Z.W., Zimmermann, A., Sheikh, M.S., and Büchler, M.W. (2001). Effects and expression of TRAIL and its apoptosis-promoting receptors in human pancreatic cancer. Cancer Letters *163*, 71–81.

O'Connor, D. V, and Phillips, D. (1984). Time-Correlated Single Photon Counting (London: Academic Press).

O'Connor, K., and Chen, M. (2013). Dynamic functions of RhoA in tumor cell migration and invasion. Small GTPases *4*, 141–147.

Pagler, T. a, Wang, M., Mondal, M., Murphy, A.J., Westerterp, M., Moore, K.J., Maxfield, F.R., and Tall, A.R. (2011). Deletion of ABCA1 and ABCG1 impairs macrophage migration because of increased Rac1 signaling. Circulation Research *108*, 194–200.

Papageorgis, P., and Stylianopoulos, T. (2015). Role of TGFβ in regulation of the tumor microenvironment and drug delivery (review). International Journal of Oncology *46*, 933–943.

Park, Y.M., Drazba, J. a, Vasanji, A., Egelhoff, T., Febbraio, M., and Silverstein, R.L. (2012). Oxidized LDL/CD36 interaction induces loss of cell polarity and inhibits macrophage locomotion. Molecular Biology of the Cell *23*, 3057–3068.

Pasiliao, C.C., Chang, C.-W. a, Sutherland, B.W., Valdez, S.M., Schaeffer, D., Yapp, D.T., and Ng, S.S.W. (2015). The involvement of insulin-like growth factor 2 binding protein 3 (IMP3) in pancreatic cancer cell migration, invasion, and adhesion. BMC Cancer *15*, 1–9.

Patschinsky, T., Hunter, T., Esch, F.S., Cooper, J.A., and Sefton, B.M. (1982). Analysis of the sequence of amino acids surrounding sites of tyrosine phosphorylation. Proceedings of the National Academy of Sciences of the United States of America *79*, 973–977.

Pellegata, N.S., Sessa, F., Renault, B., Bonato, M., Leone, B.E., Solcia, E., and Ranzani, G.N. (1994). K-ras and p53 gene mutations in pancreatic cancer: ductal and nonductal tumors progress through different genetic lesions. Cancer Research *54*, 1556–1560.

Pertz, O., Hodgson, L., Klemke, R.L., and Hahn, K.M. (2006). Spatiotemporal dynamics of RhoA activity in migrating cells. Nature *440*, 1069–1072.

Pham, N.-A., Magalhaes, J.M.M.M., Do, T., Schwock, J., Dhani, N., Cao, P.-J., Hill, R.P., and Hedley, D.W. (2009). Activation of Src and Src-associated signaling pathways in relation to hypoxia in human cancer xenograft models. International Journal of Cancer. Journal International Du Cancer *124*, 280–286.

Pitteri, S.J., Faca, V.M., Kelly-Spratt, K.S., Kasarda, A.E., Wang, H., Zhang, Q., Newcomb, L., Krasnoselsky, A., Paczesny, S., Choi, G., et al. (2008). Plasma proteome profiling of a mouse model of breast cancer identifies a set of up-regulated proteins in common with human breast cancer cells. Journal of Proteome Research *7*, 1481–1489.

Provenzano, P.P., and Keely, P.J. (2011). Mechanical signaling through the cytoskeleton regulates cell proliferation by coordinated focal adhesion and Rho GTPase signaling. Journal of Cell Science *124*, 1195–1205.

Provenzano, P.P., Eliceiri, K.W., and Keely, P.J. (2009). Multiphoton microscopy and fluorescence lifetime imaging microscopy (FLIM) to monitor metastasis and the tumor microenvironment. Clinical & Experimental Metastasis *26*, 357–370.

Provenzano, P.P., Cuevas, C., Chang, A.E., Goel, V.K., Von Hoff, D.D., and Hingorani, S.R. (2012). Enzymatic targeting of the stroma ablates physical barriers to treatment of pancreatic ductal adenocarcinoma. Cancer Cell *21*, 418–429.

Pustovalov, V. (1995). Initiation of explosive boiling and optical breakdown as a result of the action of laser pulses on melanosome in pigmented biotissues. Quantum Electronics *22*, 1091–1095.

Qiu, R.G., Chen, J., Kirn, D., McCormick, F., and Symons, M. (1995). An essential role for Rac in Ras transformation. Nature *374*, 457–459.

Radisky, D.C., Levy, D.D., Littlepage, L.E., Liu, H., Nelson, C.M., Fata, J.E., Leake, D., Godden, E.L., Albertson, D.G., Nieto, M.A., et al. (2005). Rac1b and reactive oxygen species mediate MMP-3-induced EMT and genomic instability. Nature *436*, 123–127.

Razidlo, G.L., Schroeder, B., Chen, J., Billadeau, D.D., and McNiven, M. a (2014). Vav1 as a central regulator of invadopodia assembly. Current Biology : CB *24*, 86–93.

Razidlo, G.L., Magnine, C., Sletten, A.C., Hurley, R.M., Almada, L.L., Fernandez-Zapico, M.E., Ji, B., and McNiven, M. a (2015a). Targeting Pancreatic Cancer Metastasis by Inhibition of Vav1, a Driver of Tumor Cell Invasion. Cancer Research *75*, 2907–2915.

Razidlo, G.L., Magnine, C., Sletten, A.C., Hurley, R.M., Almada, L.L., Fernandez-Zapico, M.E., Ji, B., and McNiven, M. a (2015b). Targeting Pancreatic Cancer Metastasis by Inhibition of Vav1, a Driver of Tumor Cell Invasion. Cancer Research *75*, 2907–2915.

Rhodes, K.R., and Miller, E.J. (1978). Physicochemical Characterization and Molecular Organization of the Collagen A and B Chains. Biochemistry *17*, 3442–3448.

Ridley, A.J. (2001). Rho family proteins: coordinating cell responses. Trends in Cell Biology *11*, 471–477.

Ridley, A.J. (2004). Rho proteins and cancer. Breast Cancer Research and Treatment *84*, 13–19.

Ridley, A.J. (2006). Rho GTPases and actin dynamics in membrane protrusions and vesicle trafficking. Trends in Cell Biology *16*, 522–529.

Ridley, A.J. (2011). Life at the leading edge. Cell *145*, 1012–1022.

Ridley, A.J., Paterson, H.F., Johnston, C.L., Diekmann, D., and Hall, A. (1992). The small GTP-binding protein rac regulates growth factor-induced membrane ruffling. Cell *70*, 401–410.

Ridley, A.J., Schwartz, M.A., Burridge, K., Firtel, R.A., Ginsberg, M.H., Borisy, G., Parsons, J.T., and Horwitz, A.R. (2003). Cell migration: integrating signals from front to back. Science *302*, 1704–1709.

Riganti, C., Pinto, H., Bolli, E., Belisario, D.C., Calogero, R. a, Bosia, A., and Cavallo, F. (2011). Atorvastatin modulates anti-proliferative and pro-proliferative signals in Her2/neu-positive mammary cancer. Biochemical Pharmacology *82*, 1079–1089.

Ritsma, L., Steller, E.J. a, Beerling, E., Loomans, C.J.M., Zomer, A., Gerlach, C., Vrisekoop, N., Seinstra, D., Van Gurp, L., Schäfer, R., et al. (2012). Intravital microscopy through an abdominal imaging window reveals a pre-micrometastasis stage during liver metastasis. Science Translational Medicine *4*, 158ra145.

Ritsma, L., Steller, E.J. a, Ellenbroek, S.I.J., Kranenburg, O., Borel Rinkes, I.H.M., and Van Rheenen, J. (2013). Surgical implantation of an abdominal imaging window for intravital microscopy. Nature Protocols *8*, 583–594.

Ritsma, L., Ellenbroek, S.I.J., Zomer, A., Snippert, H.J., De Sauvage, F.J., Simons, B.D., Clevers, H., and Van Rheenen, J. (2014). Intestinal crypt homeostasis revealed at single-stem-cell level by in vivo live imaging. Nature *507*, 362–365.

Rivat, C., Le Floch, N., Sabbah, M., Teyrol, I., Redeuilh, G., Bruyneel, E., Mareel, M., Matrisian, L.M., Crawford, H.C., Gespach, C., et al. (2003). Synergistic cooperation between the AP-1 and LEF-1 transcription factors in activation of the matrilysin promoter by the src oncogene: implications in cellular invasion. FASEB Journal : Official Publication of the Federation of American Societies for Experimental Biology *17*, 1721–1723.

Rizzo, M. a, Springer, G.H., Granada, B., and Piston, D.W. (2004). An improved cyan fluorescent protein variant useful for FRET. Nature Biotechnology *22*, 445–449.

Roh-Johnson, M., Bravo-Cordero, J.J., Patsialou, a, Sharma, V.P., Guo, P., Liu, H., Hodgson, L., and Condeelis, J. (2014). Macrophage contact induces RhoA GTPase signaling to trigger tumor cell intravasation. Oncogene *33*, 4203–4212.

Roselli, S., Kahl, R.G.S., Copeland, B.T., Naylor, M.J., Weidenhofer, J., Muller, W.J., and Ashman, L.K. (2014). Deletion of Cd151 reduces mammary tumorigenesis in the MMTV/PyMT mouse model. BMC Cancer *14*, 509.

Rosenblatt, A.E., Garcia, M.I., Lyons, L., Xie, Y., Maiorino, C., Désiré, L., Slingerland, J., and Burnstein, K.L. (2011). Inhibition of the Rho GTPase, Rac1, decreases estrogen receptor levels and is a novel therapeutic strategy in breast cancer. Endocrine-related Cancer *18*, 207–219.

Rossman, K.L., Der, C.J., and Sondek, J. (2005). GEF means go: turning on RHO GTPases with guanine nucleotide-exchange factors. Nature Reviews. Molecular Cell Biology *6*, 167–180.

Roth, S., Franken, P., Sacchetti, A., Kremer, A., Anderson, K., Sansom, O., and Fodde, R. (2012). Paneth cells in intestinal homeostasis and tissue injury. PloS One *7*, e38965.

Roura, S., Miravet, S., Piedra, J., García de Herreros, A., and Duñach, M. (1999). Regulation of E-cadherin/Catenin association by tyrosine phosphorylation. The Journal of Biological Chemistry *274*, 36734–36740.

Rous, P. (1911). A sarcoma of the fowl transmissible by an agent from the tumor cells. The Journal of Experimental Medicine *13*, 397–411.

Rubin, H. (1955). Quantitative relations between causative virus and cell in the Rous no. 1 chicken sarcoma. Virology *1*, 445–473.

Sabbatini, M.E., Bi, Y., Ji, B., Ernst, S.A., and Williams, J.A. (2010). CCK activates RhoA and Rac1 differentially through Galpha13 and Galphaq in mouse pancreatic acini. American Journal of Physiology. Cell Physiology *298*, C592–601.

Saci, A., Cantley, L.C., and Carpenter, C.L. (2011). Rac1 regulates the activity of mTORC1 and mTORC2 and controls cellular size. Molecular Cell *42*, 50–61.

Sahai, E., and Marshall, C.J. (2002). RHO-GTPases and cancer. Nature Reviews. Cancer *2*, 133–142.

Sailland, J., Tribollet, V., Forcet, C., Billon, C., Barenton, B., Carnesecchi, J., Bachmann, A., Gauthier, K.C., Yu, S., Giguère, V., et al. (2014). Estrogen-related receptor α decreases RHOA stability to induce orientated cell migration. Proceedings of the National Academy of Sciences of the United States of America *111*, 15108–15113.

Samuel, M.S., Munro, J., Bryson, S., Forrow, S., Stevenson, D., and Olson, M.F. (2009). Tissue selective expression of conditionally-regulated ROCK by gene targeting to a defined locus. Genesis (New York, N.Y. : 2000) *47*, 440–446.

Samuel, M.S., Lourenço, F.C., and Olson, M.F. (2011). K-Ras mediated murine epidermal tumorigenesis is dependent upon and associated with elevated Rac1 activity. PloS One *6*, e17143.

Sander, E.E., Ten Klooster, J.P., Van Delft, S., Van der Kammen, R.A., and Collard, J.G. (1999). Rac downregulates Rho activity: reciprocal balance between both GTPases determines cellular morphology and migratory behavior. The Journal of Cell Biology *147*, 1009–1022.

Sanders, R., Draaijer, A., Gerritsen, H.C., Houpt, P.M., and Levine, Y.K. (1995). Quantitative pH imaging in cells using confocal fluorescence lifetime imaging microscopy. Analytical Biochemistry *227*, 302–308.

Sandilands, E., Cans, C., Fincham, V.J., Brunton, V.G., Mellor, H., Prendergast, G.C., Norman, J.C., Superti-Furga, G., and Frame, M.C. (2004). RhoB and actin polymerization coordinate Src activation with endosome-mediated delivery to the membrane. Developmental Cell *7*, 855–869.

Sandilands, E., Brunton, V.G., and Frame, M.C. (2007). The membrane targeting and spatial activation of Src, Yes and Fyn is influenced by palmitoylation and distinct RhoB/RhoD endosome requirements. Journal of Cell Science *120*, 2555–2564.

Sanz-Moreno, V., Gadea, G., Ahn, J., Paterson, H., Marra, P., Pinner, S., Sahai, E., and Marshall, C.J. (2008). Rac activation and inactivation control plasticity of tumor cell movement. Cell *135*, 510–523.

Schachtner, H., Li, A., Stevenson, D., Calaminus, S.D.J., Thomas, S.G., Watson, S.P., Sixt, M., Wedlich-Soldner, R., Strathdee, D., and Machesky, L.M. (2012). Tissue inducible Lifeact expression allows visualization of actin dynamics in vivo and ex vivo. European Journal of Cell Biology *91*, 923–929.

Schechter, A.L., Stern, D.F., Vaidyanathan, L., Decker, S.J., Drebin, J.A., Greene, M.I., and Weinberg, R.A. (1984). The neu oncogene: an erb-B-related gene encoding a 185,000-Mr tumour antigen. Nature *312*, 513–516.

Schnelzer, A., Prechtel, D., Knaus, U., Dehne, K., Gerhard, M., Graeff, H., Harbeck, N., Schmitt, M., and Lengyel, E. (2000). Rac1 in human breast cancer: overexpression, mutation analysis, and characterization of a new isoform, Rac1b. Oncogene *19*, 3013–3020.

Schoenherr, R.M., Kelly-Spratt, K.S., Lin, C., Whiteaker, J.R., Liu, T., Holzman, T., Coleman, I., Feng, L.-C., Lorentzen, T.D., Krasnoselsky, A.L., et al. (2011). Proteome and transcriptome profiles of a Her2/Neu-driven mouse model of breast cancer. Proteomics. Clinical Applications *5*, 179–188.

Schutte, M., Hruban, R.H., Geradts, J., Maynard, R., Hilgers, W., Rabindran, S.K., Moskaluk, C.A., Hahn, S.A., Schwarte-Waldhoff, I., Schmiegel, W., et al. (1997). Abrogation of the Rb/p16 tumor-suppressive pathway in virtually all pancreatic carcinomas. Cancer Research *57*, 3126–3130.

Schwenk, F., Baron, U., and Rajewsky, K. (1995). A cre-transgenic mouse strain for the ubiquitous deletion of loxP-flanked gene segments including deletion in germ cells. Nucleic Acids Research *23*, 5080–5081.

Sefton, B.M., Trowbridge, I.S., Cooper, J.A., and Scolnick, E.M. (1982). The transforming proteins of Rous sarcoma virus, Harvey sarcoma virus and Abelson virus contain tightly bound lipid. Cell *31*, 465–474.

Shen, C.-H., Chen, H.-Y., Lin, M.-S., Li, F.-Y., Chang, C.-C., Kuo, M.-L., Settleman, J., and Chen, R.-H. (2008). Breast tumor kinase phosphorylates p190RhoGAP to regulate rho and ras and promote breast carcinoma growth, migration, and invasion. Cancer Research *68*, 7779–7787.

Shields, D.J., Murphy, E. a, Desgrosellier, J.S., Mielgo, a, Lau, S.K.M., Barnes, L. a, Lesperance, J., Huang, M., Schmedt, C., Tarin, D., et al. (2011). Oncogenic Ras/Src cooperativity in pancreatic neoplasia. Oncogene *30*, 2123–2134.

Shutes, A., Onesto, C., Picard, V., Leblond, B., Schweighoffer, F., and Der, C.J. (2007). Specificity and mechanism of action of EHT 1864, a novel small molecule inhibitor of Rac family small GTPases. The Journal of Biological Chemistry *282*, 35666–35678.

Singer, A.J., and Clark, R.A. (1999). Cutaneous wound healing. The New England Journal of Medicine *341*, 738–746.

Sohn, T.A., and Yeo, C.J. (2000). The molecular genetics of pancreatic ductal carcinoma: a review. Surgical Oncology *9*, 95–101.

Sosa, M.S., Lopez-Haber, C., Yang, C., Wang, H., Lemmon, M.A., Busillo, J.M., Luo, J., Benovic, J.L., Klein-Szanto, A., Yagi, H., et al. (2010). Identification of the Rac-GEF P-Rex1 as an essential mediator of ErbB signaling in breast cancer. Molecular Cell *40*, 877–892.

Squirrell, J.M., Wokosin, D.L., White, J.G., and Bavister, B.D. (1999). Long-term two-photon fluorescence imaging of mammalian embryos without compromising viability. Nature Biotechnology *17*, 763–767.

Stanley, A.C., Wong, C.X., Micaroni, M., Venturato, J., Khromykh, T., Stow, J.L., and Lacy, P. (2014). The Rho GTPase Rac1 is required for recycling endosome-mediated secretion of TNF in macrophages. Immunology and Cell Biology *92*, 275–286.

Steele, C.W., Karim, S. a, Foth, M., Rishi, L., Leach, J.D., Porter, R.J., Nixon, C., Jeffry Evans, T.R., Carter, C.R., Nibbs, R.J., et al. (2015). CXCR2 inhibition suppresses acute and chronic pancreatic inflammation. The Journal of Pathology.

Steffen, A., Rottner, K., Ehinger, J., Innocenti, M., Scita, G., Wehland, J., and Stradal, T.E.B. (2004). Sra-1 and Nap1 link Rac to actin assembly driving lamellipodia formation. The EMBO Journal *23*, 749–759.

Steffen, A., Ladwein, M., Dimchev, G. a, Hein, A., Schwenkmezger, L., Arens, S., Ladwein, K.I., Margit Holleboom, J., Schur, F., Victor Small, J., et al. (2013). Rac function is crucial for cell migration but is not required for spreading and focal adhesion formation. Journal of Cell Science *126*, 4572–4588.

Sternlicht, M.D., and Werb, Z. (2001). How matrix metalloproteinases regulate cell behavior. Annual Review of Cell and Developmental Biology *17*, 463–516.

Strumane, K., Rygiel, T., Van der Valk, M., and Collard, J.G. (2009). Tiam1-deficiency impairs mammary tumor formation in MMTV-c-neu but not in MMTV-c-myc mice. Journal of Cancer Research and Clinical Oncology *135*, 69–80.

Stryer, L. (1978). Fluorescence energy transfer as a spectroscopic ruler. Annual Review of Biochemistry *47*, 819–846.

Stryer, L., and Haugland, R.P. (1967). Energy transfer: a spectroscopic ruler. Proceedings of the National Academy of Sciences of the United States of America *58*, 719–726.

Stähle, M., Veit, C., Bachfischer, U., Schierling, K., Skripczynski, B., Hall, A., Gierschik, P., and Giehl, K. (2003). Mechanisms in LPA-induced tumor cell migration: critical role of phosphorylated ERK. Journal of Cell Science *116*, 3835–3846.

Suetsugu, S., Kurisu, S., Oikawa, T., Yamazaki, D., Oda, A., and Takenawa, T. (2006). Optimization of WAVE2 complex-induced actin polymerization by membrane-bound IRSp53, PIP(3), and Rac. The Journal of Cell Biology *173*, 571–585.

Sun, Y., Rombola, C., Jyothikumar, V., and Periasamy, A. (2013). Förster resonance energy transfer microscopy and spectroscopy for localizing protein-protein interactions in living cells. Cytometry. Part A : the Journal of the International Society for Analytical Cytology *83*, 780–793.

Takeya, T., and Hanafusa, H. (1982). DNA sequence of the viral and cellular src gene of chickens. II. Comparison of the src genes of two strains of avian sarcoma virus and of the cellular homolog. Journal of Virology *44*, 12–18.

Takeya, T., Feldman, R.A., and Hanafusa, H. (1982). DNA sequence of the viral and cellular src gene of chickens. 1. Complete nucleotide sequence of an EcoRI fragment of recovered avian sarcoma virus which codes for gp37 and pp60src. Journal of Virology *44*, 1–11.

Tang, X., Jin, R., Qu, G., Wang, X., Li, Z., Yuan, Z., Zhao, C., Siwko, S., Shi, T., Wang, P., et al. (2013). GPR116, an adhesion G-protein-coupled receptor, promotes breast cancer metastasis via the Gαq-p63RhoGEF-Rho GTPase pathway. Cancer Research *73*, 6206–6218.

Tanno, S., Mitsuuchi, Y., Altomare, D.A., Xiao, G.H., and Testa, J.R. (2001). AKT activation up-regulates insulin-like growth factor I receptor expression and promotes invasiveness of human pancreatic cancer cells. Cancer Research *61*, 589–593.

Taya, S., Inagaki, N., Sengiku, H., Makino, H., Iwamatsu, a, Urakawa, I., Nagao, K., Kataoka, S., and Kaibuchi, K. (2001). Direct interaction of insulin-like growth factor-1

receptor with leukemia-associated RhoGEF. The Journal of Cell Biology *155*, 809–820.

Tazebay, U.H., Wapnir, I.L., Levy, O., Dohan, O., Zuckier, L.S., Zhao, Q.H., Deng, H.F., Amenta, P.S., Fineberg, S., Pestell, R.G., et al. (2000). The mammary gland iodide transporter is expressed during lactation and in breast cancer. Nature Medicine *6*, 871–878.

Thayer, S.P., Di Magliano, M.P., Heiser, P.W., Nielsen, C.M., Roberts, D.J., Lauwers, G.Y., Qi, Y.P., Gysin, S., Fernández-del Castillo, C., Yajnik, V., et al. (2003). Hedgehog is an early and late mediator of pancreatic cancer tumorigenesis. Nature *425*, 851–856.

Thomas, J.W., Ellis, B., Boerner, R.J., Knight, W.B., White, G.C., and Schaller, M.D. (1998). SH2- and SH3-mediated interactions between focal adhesion kinase and Src. The Journal of Biological Chemistry *273*, 577–583.

Timpson, P., McGhee, E.J., Morton, J.P., Von Kriegsheim, A., Schwarz, J.P., Karim, S. a, Doyle, B., Quinn, J. a, Carragher, N.O., Edward, M., et al. (2011a). Spatial regulation of RhoA activity during pancreatic cancer cell invasion driven by mutant p53. Cancer Research *71*, 747–757.

Timpson, P., McGhee, E.J., Erami, Z., Nobis, M., Quinn, J. a, Edward, M., and Anderson, K.I. (2011b). Organotypic collagen I assay: a malleable platform to assess cell behaviour in a 3-dimensional context. Journal of Visualized Experiments : JoVE e3089.

Tomaskovic-Crook, E., Thompson, E.W., and Thiery, J.P. (2009). Epithelial to mesenchymal transition and breast cancer. Breast Cancer Research : BCR *11*, 213.

Toole, B.P. (2004). Hyaluronan: from extracellular glue to pericellular cue. Nature Reviews. Cancer *4*, 528–539.

Toole, B.P., and Slomiany, M.G. (2008). Hyaluronan: a constitutive regulator of chemoresistance and malignancy in cancer cells. Seminars in Cancer Biology *18*, 244–250.

Trauzold, a, Siegmund, D., Schniewind, B., Sipos, B., Egberts, J., Zorenkov, D., Emme, D., Röder, C., Kalthoff, H., and Wajant, H. (2006). TRAIL promotes metastasis of human pancreatic ductal adenocarcinoma. Oncogene *25*, 7434–7439.

Ursini-Siegel, J., Schade, B., Cardiff, R.D., and Muller, W.J. (2007). Insights from transgenic mouse models of ERBB2-induced breast cancer. Nature Reviews. Cancer *7*, 389–397.

Vargo-Gogola, T., and Rosen, J.M. (2007). Modelling breast cancer: one size does not fit all. Nature Reviews. Cancer *7*, 659–672.

Vega, F.M., and Ridley, A.J. (2008). Rho GTPases in cancer cell biology. FEBS Letters *582*, 2093–2101.

Veit, C., Genze, F., Menke, A., Hoeffert, S., Gress, T.M., Gierschik, P., and Giehl, K. (2004). Activation of phosphatidylinositol 3-kinase and extracellular signal-regulated kinase is required for glial cell line-derived neurotrophic factor-induced migration and invasion of pancreatic carcinoma cells. Cancer Research *64*, 5291–5300.

Vincent, A., Herman, J., Schulick, R., Hruban, R.H., and Goggins, M. (2011). Pancreatic cancer. Lancet *378*, 607–620.

Waldmeier, L., Meyer-Schaller, N., Diepenbruck, M., and Christofori, G. (2012). Py2T murine breast cancer cells, a versatile model of TGFβ-induced EMT in vitro and in vivo. PloS One *7*, e48651.

Wallrabe, H., and Periasamy, A. (2005). Imaging protein molecules using FRET and FLIM microscopy. Current Opinion in Biotechnology *16*, 19–27.

Wang, G.K., Hu, L., Fuller, G.N., and Zhang, W. (2006a). An interaction between insulin-like growth factor-binding protein 2 (IGFBP2) and integrin alpha5 is essential for IGFBP2-induced cell mobility. The Journal of Biological Chemistry *281*, 14085–14091.

Wang, S., Wu, Y., Hou, Y., Guan, X., Castelvetere, M.P., Oblak, J.J., Banerjee, S., Filtz, T.M., Sarkar, F.H., Chen, X., et al. (2013). CXCR2 macromolecular complex in pancreatic cancer: a potential therapeutic target in tumor growth. Translational Oncology *6*, 216–225.

Wang, S.E., Shin, I., Wu, F.Y., Friedman, D.B., and Arteaga, C.L. (2006b). HER2/Neu (ErbB2) signaling to Rac1-Pak1 is temporally and spatially modulated by transforming growth factor beta. Cancer Research *66*, 9591–9600.

Wang, S.E., Yu, Y., Criswell, T.L., Debusk, L.M., Lin, P.C., Zent, R., Johnson, D.H., Ren, X., and Arteaga, C.L. (2010a). Oncogenic mutations regulate tumor microenvironment through induction of growth factors and angiogenic mediators. Oncogene *29*, 3335–3348.

Wang, W., Wyckoff, J.B., Frohlich, V.C., Oleynikov, Y., Hüttelmaier, S., Zavadil, J., Cermak, L., Bottinger, E.P., Singer, R.H., White, J.G., et al. (2002). Single cell behavior in metastatic primary mammary tumors correlated with gene expression patterns revealed by molecular profiling. Cancer Research *62*, 6278–6288.

Wang, Y., Botvinick, E.L., Zhao, Y., Berns, M.W., Usami, S., Tsien, R.Y., and Chien, S. (2005a). Visualizing the mechanical activation of Src. Nature *434*, 1040–1045.

Wang, Y., Botvinick, E.L., Zhao, Y., Berns, M.W., Usami, S., Tsien, R.Y., and Chien, S. (2005b). Visualizing the mechanical activation of Src. Nature *434*, 1040–1045.

Wang, Z., Pedersen, E., Basse, a, Lefever, T., Peyrollier, K., Kapoor, S., Mei, Q., Karlsson, R., Chrostek-Grashoff, a, and Brakebusch, C. (2010b). Rac1 is crucial for Ras-dependent skin tumor formation by controlling Pak1-Mek-Erk hyperactivation and hyperproliferation in vivo. Oncogene *29*, 3362–3373.

Waring, M.J., Arrowsmith, J., Leach, A.R., Leeson, P.D., Mandrell, S., Owen, R.M., Pairaudeau, G., Pennie, W.D., Pickett, S.D., Wang, J., et al. (2015). An analysis of the attrition of drug candidates from four major pharmaceutical companies. Nature Reviews. Drug Discovery *14*, 475–486.

Webb, D.J., Donais, K., Whitmore, L. a, Thomas, S.M., Turner, C.E., Parsons, J.T., and Horwitz, A.F. (2004). FAK-Src signalling through paxillin, ERK and MLCK regulates adhesion disassembly. Nature Cell Biology *6*, 154–161.

Welch, H.C. (2015). Regulation and function of P-Rex family Rac-GEFs. Small GTPases *6*, 49–70.

Welch, H.C.E., Coadwell, W.J., Ellson, C.D., Ferguson, G.J., Andrews, S.R., Erdjument-Bromage, H., Tempst, P., Hawkins, P.T., and Stephens, L.R. (2002). P-Rex1, a PtdIns(3,4,5)P3- and Gbetagamma-regulated guanine-nucleotide exchange factor for Rac. Cell *108*, 809–821.

Welch, H.C.E., Condliffe, A.M., Milne, L.J., Ferguson, G.J., Hill, K., Webb, L.M.C., Okkenhaug, K., Coadwell, W.J., Andrews, S.R., Thelen, M., et al. (2005). P-Rex1 regulates neutrophil function. Current Biology : CB *15*, 1867–1873.

Wertheimer, E., Gutierrez-Uzquiza, A., Rosemblit, C., Lopez-Haber, C., Sosa, M.S., and Kazanietz, M.G. (2012). Rac signaling in breast cancer: a tale of GEFs and GAPs. Cellular Signalling *24*, 353–362.

Westwick, J.K., Lambert, Q.T., Clark, G.J., Symons, M., Van Aelst, L., Pestell, R.G., and Der, C.J. (1997). Rac regulation of transformation, gene expression, and actin organization by multiple, PAK-independent pathways. Molecular and Cellular Biology *17*, 1324–1335.

Wheeler, A.P., and Ridley, A.J. (2004). Why three Rho proteins? RhoA, RhoB, RhoC, and cell motility. Experimental Cell Research *301*, 43–49.

Wheeler, A.P., Wells, C.M., Smith, S.D., Vega, F.M., Henderson, R.B., Tybulewicz, V.L., and Ridley, A.J. (2006). Rac1 and Rac2 regulate macrophage morphology but are not essential for migration. Journal of Cell Science *119*, 2749–2757.

Wildenberg, M.E., Vos, A.C.W., Wolfkamp, S.C.S., Duijvestein, M., Verhaar, A.P., Te Velde, A. a, Van den Brink, G.R., and Hommes, D.W. (2012). Autophagy attenuates the adaptive immune response by destabilizing the immunologic synapse. Gastroenterology *142*, 1493–503.e6.

Wilentz, R.E., Iacobuzio-Donahue, C.A., Argani, P., McCarthy, D.M., Parsons, J.L., Yeo, C.J., Kern, S.E., and Hruban, R.H. (2000). Loss of expression of Dpc4 in pancreatic intraepithelial neoplasia: evidence that DPC4 inactivation occurs late in neoplastic progression. Cancer Research *60*, 2002–2006.

Worthylake, D., Rossman, K., and Sondek, J. (2000). Crystal structure of Rac1 in complex with the guanine nucleotide exchange region of Tiam1. Nature *408*, 682–688.

Worzfeld, T., Swiercz, J.M., Looso, M., Straub, B.K., Sivaraj, K.K., and Offermanns, S. (2012). ErbB-2 signals through Plexin-B1 to promote breast cancer metastasis. The Journal of Clinical Investigation *122*, 1296–1305.

Wu, C.C., Carpenter, E.S., Takeuchi, K.K., Halbrook, C.J., Peverley, L. V, Bien, H., Hall, J.C., Delgiorno, K.E., Pal, D., Song, Y., et al. (2014). PI3K Regulation of RAC1 Is Required for KRAS-Induced Pancreatic Tumorigenesis in Mice. Gastroenterology *147*, 1405–1416.

Wu, G.S., Burns, T.F., Zhan, Y., Alnemri, E.S., and El-Deiry, W.S. (1999). Molecular cloning and functional analysis of the mouse homologue of the KILLER/DR5 tumor necrosis factor-related apoptosis-inducing ligand (TRAIL) death receptor. Cancer Research *59*, 2770–2775.

Xiao, Y., Lin, V.Y., Ke, S., Lin, G.E., Lin, F.-T., and Lin, W.-C. (2014). 14-3-3τ promotes breast cancer invasion and metastasis by inhibiting RhoGDIα. Molecular and Cellular Biology *34*, 2635–2649.

Xu, K., Rajagopal, S., Klebba, I., Dong, S., Ji, Y., Liu, J., Kuperwasser, C., Garlick, J.A., Naber, S.P., and Buchsbaum, R.J. (2010). The role of fibroblast Tiam1 in tumor cell invasion and metastasis. Oncogene *29*, 6533–6542.

Xu, W., Doshi, A., Lei, M., Eck, M.J., and Harrison, S.C. (1999). Crystal structures of c-Src reveal features of its autoinhibitory mechanism. Molecular Cell *3*, 629–638.

Yamazaki, D., Kurisu, S., and Takenawa, T. (2009). Involvement of Rac and Rho signaling in cancer cell motility in 3D substrates. Oncogene *28*, 1570–1583.

Yarden, Y., and Sliwkowski, M.X. (2001). Untangling the ErbB signalling network. Nature Reviews. Molecular Cell Biology *2*, 127–137.

Yeatman, T.J. (2004). A renaissance for SRC. Nature Reviews. Cancer *4*, 470–480.

Yezhelyev, M. V, Koehl, G., Guba, M., Brabletz, T., Jauch, K., Ryan, A., Barge, A., Green, T., Fennell, M., and Bruns, C.J. (2004). Inhibition of SRC tyrosine kinase as treatment for human pancreatic cancer growing orthotopically in nude mice. Clinical Cancer Research : an Official Journal of the American Association for Cancer Research *10*, 8028–8036.

Yoshizaki, H., Ohba, Y., Kurokawa, K., Itoh, R.E., Nakamura, T., Mochizuki, N., Nagashima, K., and Matsuda, M. (2003a). Activity of Rho-family GTPases during cell division as visualized with FRET-based probes. The Journal of Cell Biology *162*, 223–232.

Yoshizaki, H., Ohba, Y., Kurokawa, K., Itoh, R.E., Nakamura, T., Mochizuki, N., Nagashima, K., and Matsuda, M. (2003b). Activity of Rho-family GTPases during cell division as visualized with FRET-based probes. The Journal of Cell Biology *162*, 223–232.

Yu, M., and Tannock, I.F. (2012). Targeting tumor architecture to favor drug penetration: a new weapon to combat chemoresistance in pancreatic cancer? Cancer Cell *21*, 327–329.

Yu, J., Zhang, L., Hwang, P.M., Rago, C., Kinzler, K.W., and Vogelstein, B. (1999). Identification and classification of p53-regulated genes. Proceedings of the National Academy of Sciences of the United States of America *96*, 14517–14522.

Zhao, X., Lu, L., Pokhriyal, N., Ma, H., Duan, L., Lin, S., Jafari, N., Band, H., and Band, V. (2009). Overexpression of RhoA induces preneoplastic transformation of primary mammary epithelial cells. Cancer Research *69*, 483–491.

Zhao, Y., Wang, Z., Jiang, Y., and Yang, C. (2011). Inactivation of Rac1 reduces Trastuzumab resistance in PTEN deficient and insulin-like growth factor I receptor overexpressing human breast cancer SKBR3 cells. Cancer Letters *313*, 54–63.

Zheng, X., Baker, H., Hancock, W.S., Fawaz, F., McCaman, M., and Pungor, E. (2006). Proteomic analysis for the assessment of different lots of fetal bovine serum as a raw material for cell culture. Part IV. Application of proteomics to the manufacture of biological drugs. Biotechnology Progress *22*, 1294–1300.

Zimmerman, N.P., Roy, I., Hauser, A.D., Wilson, J.M., Williams, C.L., and Dwinell, M.B. (2015). Cyclic AMP regulates the migration and invasion potential of human pancreatic cancer cells. Molecular Carcinogenesis *54*, 203–215.

Zipfel, W.R., Williams, R.M., and Webb, W.W. (2003a). Nonlinear magic: multiphoton microscopy in the biosciences. Nature Biotechnology *21*, 1369–1377.

Zipfel, W.R., Williams, R.M., Christie, R., Nikitin, A.Y., Hyman, B.T., and Webb, W.W. (2003b). Live tissue intrinsic emission microscopy using multiphoton-excited native fluorescence and second harmonic generation. Proceedings of the National Academy of Sciences of the United States of America *100*, 7075–7080.

Zomer, A., Ellenbroek, S.I.J., Ritsma, L., Beerling, E., Vrisekoop, N., and Van Rheenen, J. (2013). Intravital imaging of cancer stem cell plasticity in mammary tumors. Stem Cells (Dayton, Ohio) *31*, 602–606.

Zuo, Y., Berdeaux, R., and Frost, J. a (2014). The RhoGEF Net1 is required for normal mammary gland development. Molecular Endocrinology (Baltimore, Md.) *28*, 1948–1960.